Evaluation of the performance of photocatalytic systems for the treatment of indoor air in medical environments

Henrietta Essie Whyte

UNIVERSITE BRETAGNE SCIENCES LOIRE POUR L'INGENIEUR

IMT Atlantique
Bretagne-Pays de la Loire
École Mines-Télécom

THESE DE DOCTORAT DE

L'ÉCOLE NATIONALE SUPERIEURE MINES-TELECOM ATLANTIQUE
BRETAGNE PAYS DE LA LOIRE - IMT ATLANTIQUE
COMUE UNIVERSITE BRETAGNE LOIRE

ECOLE DOCTORALE N° 602
Sciences pour l'Ingénieur
Spécialité : « *Génie des procédés et bioprocédés*»

Par

« Henrietta Essie WHYTE»

« Evaluation of the performance of photocatalytic systems for the treatment of indoor air in medical environments »

Thèse présentée et soutenue à « IMT Atlantique», le « 7 Décembre 2018 »
Unité de recherche : GEPEA UMR CNRS 6144
Thèse N° : 2018IMTA0112

Rapporteurs avant soutenance :

Caroline ANDRIANTSIFERANA	Maitre de conférences, HDR, Université Paul Sabatier
Thierry PIGOT	Professeur, Université de Pau

Composition du Jury :

Président	: Evelyne GONZE	Professeur, Université de Savoie
Examinateurs	: Caroline ANDRIANTSIFERANA	Maitre de conférences, HDR, Université Paul Sabatier
	Thierry PIGOT	Professeur, Université de Pau
Dir. de thèse	: Valérie HEQUET	Professeur, IMT Atlantique
Co-dir. de thèse	: Albert SUBRENAT	Enseignant chercheur, HDR, IMT Atlantique
Co-encadrant	: Cécile RAILLARD	Maitre de conférences, Université de Nantes

Invité(s)
Pascal MISMAQUE Chef d'entreprise, ATA Medical

THIS WORK IS DEDICATED TO MY PARENTS HENRY AND ESSIE, MY BROTHER HENRY JNR AND TO CHRISTINE CINIER

ACKNOWLEDGEMENTS

My greatest appreciation goes to God who endowed me with enough wisdom and grace to complete this PhD.

I would like to thank IMT Atlantique and ATA Medical for the financial support provided during the course of this PhD.

My special and profound thanks go to my supervisors Pr. Valérie HEQUET, Dr. Cécile RAILLARD and Dr. Albert SUBRENAT for their guidance, support, advice and help without which this work would not have been completed. Most importantly I would like to thank them for their immense patience, I appreciate this greatly.

I would also like to thank Pr. Yves ANDRES the head of the department and Pr. Laurence LE COQ the head of research for their hospitality and for allowing me to work in excellent conditions throughout these three years. Thank you Yves for also agreeing to present my poster at IAQ conference 2018.

I thank Mr. Pascal MISMAQUE the president of ATA medical for his help in diverse ways during the course of this work.

I would also like to thank Dr. Caroline ANDRIANTSIFERANA and Pr. Thierry PIGOT for accepting to review my work and to Pr. Evelyn GONZE for agreeing to be a member of the jury.

All the experimental work could not have been done without the invaluable help of the technical team for this I am very grateful to Eric CHEVREL, Patrick BRION, Francois-Xavier BLANCHET, Yvan GOURIOU and Katell CHAILLOU. I would also like to thank Eric DUMONT for his help with the modelisation.

These 3 years were particularly pleasant, interesting and eventful thanks to the other PhD and post doctoral students and friends. So I thank Jenny, Ana-Maria, Chantal, Victor, Agustina, Guillaume, Mouna, Hend, Marwaa, Manel, Ronke, Zipporah, Thibault, Kevin, Rachid, Sylvester , Mexi, Manuel, Getnet and Walid.

I would also like to thank my parents and my brother whose love, care, support and advice saw me through these three years.

Lastly, my heartfelt thanks go to Mathieu Cinier who provided me with immense support and encouragement whenever I had doubts.

Henrietta Essie Whyte

CONTENTS

LIST OF FIGURES

LIST OF TABLES

NOMENCLATURE

a	:	Absorption coefficient	(m^{-1})
Q	:	Air flow rate	($m^3.h^{-1}$)
A	:	Area	(m^2)
C	:	Concentration	(ppm)
ρ	:	Density	($kg.m^{-3}$)
s	:	Direction of photon	(m)
μ	:	Dynamic viscosity	($kg.m^{-1}.s^{-1}$)
P_c	:	Electric power consumption	(kW)
g	:	Gravitational force	($m.s^{-2}$)
C_0	:	Initial concentration	(ppm)
E	:	Irradiance	($W.m^{-2}$)
k	:	Kinetic constant	(h^{-1})
I	:	Light intensity	($mW.cm^{-2}$)
I	:	Light intensity	($W.m^{-2}$)
T	:	Local temperature	(K)
m	:	Mass	(g)
e	:	Media thickness	(m)
ϕ_i^{mod}	:	Modal pore size	(μm)
MV	:	Molar volume	($L.mol^{-1}$)
MW	:	Molecular weight	($g.mol^{-1}$)
S_M	:	Momentum sink term	(-)
k	:	Permeability	(m^2)
Φ	:	Phase function	(-)
Re_p	:	Pore Reynolds number	(-)
d_p	:	Pore size	(μm)
v_p	:	Pore velocity	($m.s^{-1}$)
ε	:	Porosity	(-)
P	:	Pressure	(Pa)
ΔP	:	Pressure drop	(Pa)
n	:	Reaction order	(-)
r	:	Reaction rate	($ppm.min^{-1}$)
n	:	Refractive index	(-)

τ_R	:	Residence time	(min)
σ	:	Scattering coefficient	(m^{-1})
s'	:	Scattering direction	(m)
Ω'	:	Scattering solid angle	(sr)
E	:	Short-circuit factor	(-)
α	:	Single-pass removal efficiency	(-)
α_i	:	Slope attenuation coefficient of porosity curve	(-)
Ω	:	Solid angle	(sr)
σ_{SB}	:	Stefan-Boltzmann constant	($W.m^{-2}K^{-4}$)
τ	:	Stress tensor	($kg.m^{-1}.s^{-2}$)
t	:	Time	(min)
v	:	Velocity	($m.s^{-1}$)
V	:	Volume	(m^3)

ABBREVIATIONS

ACH	:	Air Change per Hour
ACROSS	:	Automatic Clean Room Sampler
AICHA	:	Air Intérieur et Pollution Chimiques dans les Hôpitaux
ANSES	:	Agence Nationale de Sécurité Sanitaire de l'alimentation, de l'environnement et du Travail
ANSM	:	Agence Nationale de Sécurité du Médicament et des produits de santé
ASHRAE	:	American Society of Heating, Refrigerating and Air-Conditioning Engineers
ASPEC	:	Association pour la Prévention et l'Etude de la contamination
BRI	:	Building Related Illnesses
CADR	:	Clean Air Delivery Rate
CDC	:	Center for Disease Control and Prevention
CLIN	:	Comité de Lutte contre les Infections Nosocomiales
FID	:	Flame Ionization Detection
GC	:	Gas Chromatography
HEPA	:	High Efficiency Particulate Air
HPLC	:	High Performance Liquid Chromatography
HRI	:	Health Related Index
HVAC	:	Heating, Ventilation And Air Conditioning
IAQ:	:	Indoor Air Quality
JOSHA	:	Japanese Occupational Safety and Health Association
MS	:	Mass Spectrometry
NIOSH	:	National Institute of Occupational Safety and Health
OCE	:	Operating Cost Effectiveness
OEL	:	Occupational Exposure Limits
OQAI	:	Observatoire de la Qualité de l'air Intérieur
OSHA	:	Occupational Safety and Health Association
PCO	:	Photocatalytic Oxidation
QAIHOSP	:	Qualité de l'air Intérieur dans les Hôpitaux
REL	:	Recommended Exposure Limit
RH	:	Relative Humidity
SBS	:	Sick Building Syndrome
SF2H	:	Société Française d'Hygiène Hospitalière

TD	:	Thermal Desorption
TVOC	:	Total Volatile Organic Compound
TWA	:	Time Weighted Average
UV	:	Ultra Violet
UVT	:	UV Transmittance
VOC	:	Volatile Organic Compound

SCIENTIFIC PRODUCTION

Publications in Scientific Journals

- Whyte H.E., Raillard C., Subrenat A., Héquet V.,*"Photocatalytic oxidation of isoflurane, an anesthetic gas: the influence of operating parameters"* Chem. Eng. J. 352 (2018) 441–449. doi:10.1016/j.cej.2018.07.059.

- Whyte H.E., Raillard C., Subrenat A., Héquet V.,*" Influence of operating parameters on the single-pass photocatalytic removal efficiency of acrylonitrile" (submitted)*

- Whyte H.E., Raillard C., Subrenat A., Héquet V.*, "Influence of environmental parameters on the photocatalytic oxidation efficiency of acrylonitrile and isoflurane; two operating room pollutants" (Under preparation)*

- Whyte H.E., Raillard C., Subrenat A., Héquet V.*,"The influence of change of media geometry on the photocatalytic degradation of acrylonitrile: Experimental and CFD analysis" (Under preparation)*

Communication at International Conferences

- Whyte H.E., Raillard C., Subrenat A., Héquet V.*, "Photocatalytic oxidation for indoor air quality in hospital operating rooms: Study of isoflurane degradation" Oral Presentation* - The 2nd International Conference on New Photocatalytic Materials for Environment, Energy and Sustainability (NPM 2), Ljubljana, Slovenia 2-6 July 2017

- Raillard C., Whyte H.E., Maroga Mboula V., Héquet V., Thévenet F., Locoge N., *"Indoor Air Purification by a Commercialized Photocatalytic Oxidation Stand-alone Device: Efficiency and Safety" - Oral Presentation* -The 2nd International Conference on New Photocatalytic Materials for Environment, Energy and Sustainability (NPM 2), Ljubljana, Slovenia 2-6 July 2017

- Whyte H.E., Raillard C., Subrenat A., Héquet V.*, "Influence of operating parameters on the single-pass removal efficiency during the photocatalytic degradation of acrylonitrile"- Oral and Poster Presentation* – The 10th European meeting on Solar Chemistry and Photocatalysis: Environmental Applications (SPEA10), Almería, Spain, 4 – 8 June 2018.

- Raillard C., Whyte H.E., Maroga Mboula V., Thévenet F., Locoge N., Héquet V., *"Photocatalytic oxidation of several mixtures of indoor air pollutants by a commercialized stand-alone device" - Poster Presentation* -– The 10th European meeting on Solar Chemistry and Photocatalysis: Environmental Applications (SPEA10), Almería, Spain, 4 – 8 June 2018.

- Whyte H.E., Raillard C., Subrenat A., Héquet V.,Andrés Y., *"Photocatalytic oxidation of acrylonitrile: a study of the influence of operating parameters" -Poster Presentation* – The 15th Conference of the International Society of Indoor Air Quality & Climate (ISIAQ), Philadelphia, PA, USA ,22- 27 July 2018

RESUME EN FRANCAIS

La qualité de l'air intérieur (QAI) fait actuellement l'objet d'une attention particulière et constitue une préoccupation majeure des pouvoirs publics dans nombre de pays. Nous passons, en effet, plus de 80%, en moyenne, de notre temps à l'intérieur. De plus, il est généralement admis qu'une mauvaise QAI peut conduire à une dégradation de l'état de santé des occupants par le biais du syndrome des bâtiments malsains (Sick Building Syndrome) ou de maladies liées à l'air respiré dans les bâtiments (Building Related Illnesses) avec des degrés de gravité variés. L'Organisation Mondiale de la Santé (OMS) estime que la pollution de l'air intérieur provoque environ 3,8 millions de décès prématurés par an dans le monde. En France, l'Agence Nationale de SEcurité sanitaire de l'alimentation, de l'environnement et du travail (ANSES) estime que les coûts socio-économiques liés aux effets de la qualité de l'air intérieur sur la santé humaine s'élèvent à environ 19 milliards d'euros par an. De nombreuses organisations nationales et internationales ont alors vu le jour afin d'assurer la surveillance de la qualité de l'air intérieur. En France, l'Observatoire de la Qualité de l'Air Intérieur (OQAI) a été créé pour mieux connaître la pollution intérieure, ses origines et ses dangers. Depuis sa création, en 2010, les études se sont concentrées sur la qualité de l'air intérieur des maisons, bureaux et écoles. Certains lieux, tels que les hôpitaux, ont, eux, été rarement investigués. Pourtant, la qualité de l'air dans les hôpitaux mérite attention en raison de la complexité des lieux et des activités qui y sont menées ainsi que de la vulnérabilité des personnes qui y séjournent. Un contrôle inadéquat de la QAI à l'hôpital peut provoquer les maladies chez les patients et les soignants. Deux projets récents financés par l'ANSES, AICHA (Air intérieur et pollution chimique dans les hôpitaux) et QAIHOSP (Qualité de l'air intérieur dans les hôpitaux), ont été menés en 2010 et 2013 respectivement, avec pour objectif de fournir des connaissances qualitatives et quantitatives sur les polluants présents dans certains hôpitaux en France. Alors que le projet AICHA se concentrait seulement sur la présence de contaminants chimiques, QAIHOSP a étudié plus largement les contaminants chimiques, microbiologiques et particulaires. Les résultats de ces études ont montré que l'air intérieur des hôpitaux contient un mélange complexe de composés chimiques, physiques et microbiologiques. Les auteurs de ces études concluent également que l'exposition continue des occupants à ces polluants peut nuire à leur santé. Afin de limiter le niveau de pollution en milieu hospitalier, plusieurs agences nationales donnent des recommandations pour le contrôle de la qualité de l'air intérieur en fonction des taux de renouvellement d'air. Aux États-Unis, la norme de référence ASHRAE 170-2017 est issue des travaux de l'American Society of Heating, Refrigerating and Air-Conditioning Engineers (ASHRAE). En France, c'est la norme NFS 90-351, basée sur les recommandations de l'Association pour la Prévention et l'étude de la contamination (ASPEC), qui est appliquée. Actuellement, les dispositifs de traitement d'air, qu'ils soient autonomes ou inclus dans les systèmes de ventilation, sont de plus en plus utilisés comme moyen complémentaire d'amélioration de la QAI. Ces dispositifs de traitement utilisent des technologies telles que la filtration, l'adsorption, le plasma froid ou l'oxydation photocatalytique, seules ou combinées. En milieu hospitalier, la préoccupation principale concerne la réduction des contaminants de nature microbiologique en raison du risque d'infections nosocomiales. Par conséquent, l'efficacité de ces dispositifs ne repose généralement que sur l'élimination des micro-organismes. Cependant, comme les résultats issus des projets AICHA et QAIHOSP montrent que les hôpitaux contiennent également des contaminants chimiques dont certains sont spécifiques à l'environnement médical, il est nécessaire d'étudier le devenir de ces polluants chimiques lorsqu'ils traversent ces dispositifs de traitement. Parmi les technologies de traitement, l'oxydation photocatalytique est considérée comme une méthode économique, peut consommatrice d'énergie et capable de dégrader une large gamme de polluants chimiques. Ces dernières années, de plus en plus de systèmes de traitement utilisant l'oxydation photocatalytiques sont apparus sur le marché et

pourraient potentiellement être utilisés dans les salles d'opération des hôpitaux. il est donc nécessaire d'étudier le devenir de ces polluants chimiques lorsqu'ils traversent un dispositif PCO. C'est cette technologie qui est étudiée lors de ce travail. La thèse vise à évaluer l'efficacité des dispositifs dans l'élimination de certains polluants chimiques spécifiques présents dans les hôpitaux, ainsi qu'à donner des recommandations quant à l'utilisation de cette technologie dans les milieux hospitaliers.

Dans le premier chapitre, la synthèse d'une revue bibliographique est présentée. Elle a été réalisée afin de fournir un état des lieux des polluants chimiques présents dans les hôpitaux et de déterminer ceux qui pourraient être intéressants à étudier de par leur fréquence d'apparition ou leurs niveaux de concentration dans ces milieux. Le choix des molécules cibles a été limité aux composés rencontrés dans les blocs opératoires (BO). Dans les BO, la pollution de l'air provient de trois sources principales : les gaz anesthésiques, la fumée chirurgicale et les agents désinfectants. Sur cette base, deux polluants cibles, l'isoflurane et l'acrylonitrile, ont été choisis. Ils appartiennent à deux des principaux types de composés gazeux présents dans les BO : les gaz anesthésiants (isoflurane) et les gaz contenus dans les fumées chirurgicales (acrylonitrile). Ils proviennent également de deux familles chimiques différentes ; ce qui permet de comparer leurs comportements de dégradation par procédé photocatalytique. En outre, ce sont des molécules complexes qui peuvent être source d'intermédiaires réactionnels. Ensuite, dans ce chapitre, le principe de la photocatalyse en milieu gazeux est d'abord présenté puis les principaux paramètres opératoires et environnementaux susceptibles d'influencer l'efficacité des procédés d'oxydation photocatalytique sont détaillés. Cette partie permet d'identifier les paramètres clés à faire varier pour étudier, comprendre et analyser les performances du système de traitement photocatalytique mis en œuvre dans ce travail. Enfin, ce premier chapitre vise également à établir les objectifs de la thèse :

- Effectuer une évaluation paramétrique de la dégradation de l'isoflurane et de l'acrylonitrile en étudiant l'influence de la vitesse de l'air, de l'intensité lumineuse, de la géométrie des matériaux photocatalytiques, de la concentration initiale en polluants, de la présence de co-polluants chimiques (le protoxyde d'azote et l'acide acétique), de la présence de particules (ou bioaérosols) et de l'humidité relative.
- Effectuer des simulations numériques afin de mieux comprendre l'influence du changement de géométrie sur la dégradation des molécules cibles par procédé d'oxydation photocatalytique.
- Évaluer l'innocuité de la dégradation de l'isoflurane et de l'acrylonitrile par oxydation photocatalytique hétérogène en identifiant les éventuels intermédiaires réactionnels formés et émis dans la phase gazeuse.

Dans le deuxième chapitre, le matériel et les méthodes utilisés sont décrits. Les essais ont été réalisés sur un banc expérimental de 420 L, fonctionnant en boucle fermée. Ce banc inclut un module dans lequel sont disposés le média photocatalytique fibreux non tissé et deux tubes fluorescents UVC de 18 W (série Phillips PL-L). L'air à traiter circule dans le réacteur avec un débit pouvant aller de 28 à 300 $Nm^3.h^{-1}$ grâce à un ventilateur à vitesse variable. Une chambre de tranquillisation dans laquelle un nid d'abeille est installé permet une homogénéisation de l'air ainsi que l'injection et l'échantillonnage des composés d'intérêt. L'évolution dans le temps de la concentration des composés permet de réaliser des cinétiques de dégradation qui sont ensuite analysées. Au cours de la cinétique de dégradation, les échantillons d'air sont prélevés sur des cartouches CarboPack B et DNPH et sont analysés via

un appareillage de thermodésorption couplé a une chromatographie gazeuse et une détection par spectrométrie de masse et ionisation de flamme (TD/GC/MS/FID) ainsi qu'une chromatographie liquide avec détecteur UV (HPLC-UV). Le média photocatalytique utilisé est un média commercial produit par Saint-Gobain Quartz (QUARTZEL®). Ce média non tissé (feutre) est constitué de fibres de SiO_2 revêtues de TiO_2 déposé par un procédé sol-gel. Il a une épaisseur moyenne de 17.5 ± 1.5 mm et une surface spécifique BET de 112 ± 1 $m^2.g^{-1}$. D'autres caractéristiques telles que la porosité, la perméabilité, le facteur de résistance inertielle et la transmittance UV ont été déterminées pour servir lors de la simulation numérique. Celles-ci sont résumées dans le tableau ci-dessous.

Caractéristiques	**Valeur**
Porosité	0,875
Permeabilité (m^2)	1,45 $x10^{-8}$
Facteur de résistance inertielle (m^{-1})	823
Transmittance UV (%)	0,6

Table 1: Caractéristiques du média photocatalytique

Afin d'extraire les indicateurs de performance permettant d'évaluer l'influence des paramètres sur la dégradation phocatalytique, un modèle développé par Dumont et Héquet est utilisé. La modèle décrit une relation de premier ordre de décroissance de la concentration en fonction du temps dans un réacteur multi-passage et permet le calcul du taux d'abattement par passage. Le modèle est donné comme suit:

$$\mathbf{C} = \boldsymbol{C_0}\ \mathbf{exp}\left\{-\frac{\boldsymbol{t}}{\boldsymbol{\tau_R}}\left|[\mathbf{1}-\mathbf{exp}(-\boldsymbol{\alpha})]\right.\right\}$$

où le terme α est le taux d'abattement par passage et représente la fraction du débit total traité pendant le temps τ_R (temps de résidence dans le réacteur). C est la concentration du polluant considéré au temps t et C_0 est sa concentration initiale.

Les gammes quantitatives choisies pour certains paramètres sont résumées dans le tableau ci-dessous.

Paramètre	**Valeur**
Vitesse ($m.s^{-1}$)	0,5 – 1,5
Intensité lumineuse ($mW.cm^{-2}$)	1,0 – 4,5
Concentration initiale (ppm)	0,5 - 10
Humidité relative (%)	20 - 80

Table 2 : Conditions opératoires expérimentales pour l'oxydation photocatalytique de l'isoflurane et de l'acrylonitrile

Les valeurs de la vitesse et de l'intensité lumineuse ont été choisies en fonction des conditions de fonctionnement généralement utilisées par un purificateur d'air commercial. La concentration des polluants dans le bloc opératoire varie en fonction des activités et peut aller de plusieurs ppb à quelques dizaines de ppm. La concentration initiale serait donc étudiée dans une plage de 0,5 à 10 ppm. L'humidité relative recommandée par plusieurs agences nationales pour une salle d'opération typique est de 30 à 60 % selon le type de chirurgie à

effectuer. Comme la revue de la littérature a montré que les niveaux pouvaient être supérieurs ou inférieurs à cet intervalle, il a été décidé d'étudier l'humidité relative de 20 à 80 %.

Dans le troisième chapitre, les essais de dégradation de l'acrylonitrile et de l'isoflurane sont présentés. Une étude des profils des courbes de dégradation de l'acrylonitrile et de l'isoflurane montre que l'acrylonitrile est plus rapidement (60 minutes) dégradé que l'isoflurane (600 minutes). L'isoflurane est une molécule halogénée pour laquelle les mécanismes de dégradation sont plus complexes ; ce qui peut expliquer que la dégradation est plus lente que pour l'acrylonitrile. Il est également observé que la dégradation de l'acrylonitrile peut être représentée par une cinétique apparente du premier ordre tandis que la dégradation de l'isoflurane se fait en deux étapes. Au cours de la première phase, la dégradation est lente et peu efficace. Elle peut être attribuée à d'éventuelles réactions de l'isoflurane avec les radicaux hydroxyles OH°. Au cours de la seconde phase, la dégradation s'accélère grâce à un mécanisme supposé de réaction en chaîne incluant les radicaux chlores Cl°, similaire à celui de dégradation photocatalytique du trichloréthylène décrit dans la littérature. Cette seconde phase de dégradation est représentée par une cinétique de décroissance de premier ordre apparent. Le modèle développé par Dumont et Héquet est alors appliqué aux cinétiques de dégradation des deux polluants et permet de calculer un indicateur, le taux d'abattement par tour α, pour l'acrylonitrile et deux indicateurs, la période d'induction τ_i (correspondant à la durée de la première étape de la cinétique) et, le taux d'abattement par tour α, pour l'isoflurane. L'influence de la vitesse de passage de l'air, de l'intensité lumineuse, de la géométrie du média, de la présence de co-polluants et de particules (bioaérosols) ainsi que de l'humidité relative influant sur ces indicateurs de performance est présentée. Les résultats montrent que l'influence des paramètres est similaire quel que soit le composé considéré. Lorsque la vitesse augmente de 0,5 $m.s^{-1}$ à 1,5 $m.s^{-1}$, le α diminue de 0,04 à 0,007 pour l'acrylonitrile tandis que pour l'isoflurane, le α diminue de 0,0023 à 0,00048 et le τ_i passe de 45 minutes à 225 minutes. La diminution de la vitesse de l'air de 1.5 $m.s^{-1}$ à 0.5$m.s^{-1}$ entraîne un temps de contact plus long, ce qui conduit à des périodes d'induction plus courtes pour l'isoflurane et à des taux d'abattement par passage α plus élevés. L'augmentation de l'intensité lumineuse de 1 $mW.cm^{-2}$ à 4.5 $mW.cm^{-2}$ conduit à une diminution de τ_i 250 minutes à 45 minutes et à une augmentation de α de 0,0012 à 0,0023 pour l'isoflurane et à une augmentation de α de 0,0052 à 0,012 pour l'acrylonitrile. Il est observé que la relation entre l'intensité lumineuse et le taux d'abattement par tour suit un régime d'ordre 0,5 pour les deux composés. Cela signifie que pour la gamme d'intensités lumineuses étudiées, la recombinaison électron-trou est dominante. En conséquence, un accroissement supplémentaire de l'intensité lumineuse n'améliorerait pas de manière significative les taux d'abattement par tour, mais imposerait des coûts énergétiques inutiles. Lorsque la concentration initiale est augmentée de 0,5 ppm à 10 ppm, le taux d'abattement par tour pour l'acrylonitrile diminue de 0,032 à 0,006, tandis que pour l'isoflurane, la période d'induction augmente de 130 minutes à 600 minutes et le taux d'abattement par le passage diminue de 0,0008 à 0,0003. L'augmentation des concentrations initiales en acrylonitrile et en isoflurane de 0,5 ppm à 10 ppm entraîne une diminution d'efficacité de dégradation attribuable à une limitation du nombre d'espèces actives pouvant oxyder les polluants. Lorsque l'humidité relative a été augmentée de 20 % à 80 % les α ont été diminués de 50 % et 27 % respectivement pour l'acrylonitrile et l'isoflurane et le τ_i a augmenté de 79 %. L'adsorption compétitive entre le polluant à dégrader et les molécules d'eau explique qu'une augmentation de l'humidité relative conduit à inhiber la dégradation des deux composés cibles. La présence d'autres polluants gazeux diminuent également la dégradation des composés cibles en raison de la compétition pour l'adsorption sur les sites actifs. Il a également été montré que, dans la présence de particules sur la surface du média photocatalytique, le α était 0,7 fois inférieur et 0,8 fois inférieur pour l'acrylonitrile et l'isoflurane respectivement, tandis que le τ_i était

augmenté de 1,3. Cela est dû au fait que les particules peuvent bloquer les sites actifs et colmater le média ce qui diminue l'efficacité de la dégradation des composés cibles. Les résultats de l'évaluation de l'influence des paramètres opératoires et environnementaux ont montré que pour améliorer la performance de la dégradation photocatalytique pour l'élimination de l'acrylonitrile et de l'isoflurane, il est préférable de travailler à faibles vitesses car cela augmente le temps de contact entre les polluants et les espèces actives. Des intensités lumineuses plus élevées donnent de meilleures performances mais, pour le système étudié, une intensité lumineuse au-delà de 5 $mW.cm^{-2}$ engendrerait un coût énergétique important à mettre en balance avec une efficacité de dégradation plus mitigée. Dans le bloc opératoire les niveaux de l'humidité relative recommandés se situent entre 30 et 60 %, donc il est préférable de ne pas opérer au-delà de 60 %. L'introduction de filtres en amont du média photocatalytique est souhaitable pour réduire la charge de particules reçue sur le support. Le procédé présente une efficacité accrue lorsque le niveau de concentration reste peu élevé (0,5 ppm pour l'isoflurane et l'acrylonitrile). Cependant, étant donné que les concentrations de polluants (cibles et co-polluants) varient avec le temps, le système de traitement photocatalytique devrait comporter plusieurs modules photocatlytiques en séries ou en parallèle afin de maximiser l'efficacité d'élimination des polluants. Cela serait également bénéfique pour réduire les concentrations en intermédiaires réactionnels éventuellement émis en phase gazeuse et les maintenir à des niveaux qui ne posent pas de risques pour la santé. Les composés intermédiaires identifiés lors de la dégradation de l'isoflurane comprennent le pentafluoropropanal, le chlorodifluoroacétaldéhyde, le formaldéhyde, l'acétaldéhyde, l'acide formique et l'acide acétique. Les concentrations mesurées de ces produits en phase gazeuse restent en-deçà des limites susceptibles de présenter un risque avéré pour la santé. Dans le cas de l'acrylonitrile, aucun intermédiaire n'a été identifié. Cependant l'analyse du taux de minéralisation en fonction du taux de conversion a montré que l'acrylonitrile était transformé en produits intermédiaires avant d'être complètement minéralisé. Il a donc été conclu que les méthodes d'échantillonnage et d'analyse n'étaient probablement pas appropriées pour permettre leur piégeage et leur détection de façon exhaustive. Enfin, l'influence du changement de géométrie des médias photocatalytiques a été étudiée. Des expériences dans des conditions de référence à la fois pour l'acrylonitrile et l'isoflurane ont été réalisées avec une configuration de média plan et une configuration de média plissé. L'objectif expérimental était ici de mettre en évidence l'influence du temps de contact pour une intensité lumineuse moyenne reçue sur le support maintenue constante dans les deux configurations. Les résultats ont montré que les le taux d'abattement par tour pour les deux composés étaient 2,3 fois plus élevés pour la configuration plissée que pour la configuration plane. Cette augmentation peut être imputable à l'augmentation de la quantité de photocatalyseur lorsque le média est plissé car la surface de média utilisée est supérieure par rapport à la configuration dans laquelle le média est plan. Pour éliminer l'influence de l'augmentation de la quantité de catalyseur, les taux d'abattement par tour ont été corrigés en les divisant par les surfaces de média respectives des configurations plane et plissée. Les résultats ont montré que la configuration du média plissé améliorait encore la dégradation de 27 % par rapport à la géométrie plane. Cette augmentation d'efficacité peut être attribuée à un temps de contact plus long et également à une meilleure distribution de l'irradiance dans le cas de la géométrie plissée. En effet, dans la littérature, certains auteurs sont en accord avec le fait que le temps de contact puisse augmenter dans les médias plissés, mais certains avancent l'hypothèse d'une diminution de la vitesse de passage de l'air dans le média tandis que d'autres évoquent un allongement du chemin parcouru par les molécules dans le média. Les deux hypothèses sont difficiles à évaluer expérimentalement. En outre, même si l'intensité lumineuse reçue est la même pour les deux supports, la répartition de l'éclairement sur et dans les médias peut également influer sur l'efficacité. Afin de mieux comprendre le rôle de la géométrie du média dans l'amélioration des rendements d'élimination, des simulations numériques ont semblé

nécessaires pour étudier le comportement du flux d'air et de l'éclairement dans le réacteur photocatalytique pour les deux configurations.

Dans le quatrième chapitre, des simulations numériques de l'écoulement d'air et du rayonnement dans le pilote, pour les deux configurations de média photocatalytique (plane et plissée) ont été effectuées en utilisant le logiciel ANSYS 14.5. Les résultats des simulations ont montré que la longueur du trajet parcouru par l'air dans le support était égale à l'épaisseur du média photocatalytique et restait donc identique quelle que soit la configuration considérée. Cependant, la vitesse de l'air à travers le média a été estimée, par les simulations, être 43 % inférieure dans le cas du média plissé par rapport au cas du média plan. Par conséquent, le temps de contact des molécules à dégrader avec le photocatalyseur est plus long dans le cas du support plissé que dans le cas du support plan. Les calculs ont permis de mettre en évidence que le temps de contact était augmenté de 76 % pour la configuration plissée par rapport à la configuration plane. Cette valeur est supérieure à l'augmentation de l'efficacité de dégradation entre média plan et média plissée observée grâce à l'indicateur de performance α obtenu expérimentalement. Cela peut être imputé à une distribution différente de l'irradiance entre les deux configurations testées. En effet, les simulations numériques ont également permis d'observer que la distribution de l'irradiance était plus hétérogène sur le support plissé que sur le support plan. Ainsi, sur la base de l'analyse de la répartition de l'éclairement sur le média et des profils d'écoulement dans le module photocatalytique, deux hypothèses ont pu être proposées pour expliquer les différence d'efficacité de dégradation obtenue expérimentalement : premièrement, la surface efficace du média plissé peut être réduite en raison de la présence d'une zone sombre importante (18 %) autour des plis et, en second lieu, l'hétérogénéité plus élevée de la distribution de la vitesse et de l'irradiance pourraient entraver l'effet du temps de contact et entraîner une réduction de l'efficacité globale attendue de la configuration plissée. L'approche de simulations numériques qui a été développée et utilisée pour la configuration expérimentale a été appliquée à une unité commerciale pour aider à étudier l'amélioration du système en proposant une configuration plissée. Bien qu'il n'ait pas été possible d'obtenir une confirmation expérimentale, les simulations ont montré qu'en modifiant uniquement la géométrie du média de plan à plissée l'efficacité de dégradation du système pouvait être améliorée car il y avait une augmentation de la quantité de catalyseur, du temps de contact et de l'irradiance moyenne reçue dans le média.

En conclusion, ces travaux contribuent à l'amélioration des connaissances sur l'influence des paramètres opératoires et environnementaux lors de la dégradation photocatalytique de deux composés qui n'ont jamais ou rarement été étudiés : l'isoflurane et l'acrylonitrile. Il a été démontré comment il était possible d'améliorer les performances de systèmes photocatalytiques dans des conditions spécifiques qui correspondent à des environnements hospitaliers. La simulation numérique constitue un outil utile pour une compréhension plus fine des mécanismes et pour mettre en évidence le comportement de l'écoulement et de l'irradiance dans un média photocatalytique.

Au regard de ces résultats de thèse, plusieurs perspectives peuvent être envisagées:

- Il serait nécessaire d'étudier la performance pour un système de traitement photocatalytique comportant comporter plusieurs modules photocatalytiques en séries ou en parallèle. Cela va contribuer à fournir des réponses en premier part sur l'efficacité d'un tel système sur l'élimination des polluants et, d'autre part, sur l'influence qu'il aurait sur les intermédiaires trouvés à la sortie du système de traitement.

- Des études devraient être menées sur l'effet de la combinaison de plusieurs techniques de traitement de l'air, telle que la filtration avec l'oxydation photocatalytique, sur l'efficacité d'élimination des polluants. Comme l'air intérieur contient des particules dont on a démontré qu'elles diminuaient l'efficacité de l'oxydation photocatalytique, l'utilisation de techniques de prétraitement comme la filtration pourrait améliorer l'efficacité.

- L'innocuité de l'oxydation photocatalytique est importante pour caractériser complètement son efficacité. La sécurité peut être assurée en identifiant et en quantifiant les intermédiaires formés pendant la dégradation. Des travaux supplémentaires devraient être menés sur l'identification et la quantification des composés intermédiaires en utilisant des processus d'échantillonnage et d'analyse plus sensibles.

- Un modèle de la dynamique des fluides computationnelle plus rigoureuse couplant la modélisation de la vitesse, du champ de rayonnement et de la réaction cinétique devrait être développé pour aider à concevoir et à optimiser les réacteurs photocatalytiques. La modélisation pourrait être plus économique car le réacteur peut être facilement modifié pour optimiser l'hydrodynamique et le champ de rayonnement du système sans nécessiter différentes configurations de réacteurs pour déterminer la géométrie la plus efficace.

GENERAL INTRODUCTION

Indoor air quality (IAQ) is receiving significant attention and is currently a major public concern as it is observed that people generally spend more than 80 % of their time indoors. Poor IAQ has been known to cause outbreaks of Sick Building Syndrome (SBS) or Building Related Illnesses (BRI) with varying degrees of severity examples of which include skin and eye irritations, eye infections, headaches, fatigue, nausea, asthma, cancer, etc. The World Health Organization (WHO) estimates that air pollution causes approximately 4.3 million premature deaths per year worldwide. In France, the Agence nationale de sécurité sanitaire de l'alimentation, de l'environnement et du travail (ANSES) estimates that the socio-economic costs associated with the effects of indoor air quality on human health is about 19 billion euros per year.

Indoor air pollution is therefore a great preoccupation of many national and international organizations. These organizations are tasked with the surveillance of indoor air quality. In France for example, the Observatoire de la qualité de l'air intérieur (OQAI) was created to provide better knowledge of indoor pollution, its origins and its dangers. However, since its creation in 2001, the indoor environments mostly studied have been homes, offices and schools. Whilst some indoor environments like the hospital had been rarely studied. The air quality in hospitals deserves a lot more attention because of the complexities and vulnerabilities of the occupants. Consequently improper control of hospital IAQ may cause hospital-acquired (nosocomial) infections and occupational diseases.

It is for this reason that two projects AICHA (Air intérieur et pollution chimiques dans les hôpitaux) and QAIHOSP (Qualité de l'air intérieur dans les hôpitaux) were created in 2010 and 2013 respectively and financed by ANSES. These projects were undertaken to provide some quantitative and qualitative knowledge on the pollutants that were present in some hospitals in France. While AICHA focused on the presence of chemical contaminants, QAIHOSP studied chemical and microbiological contaminants and particulate matter. Their results showed that hospital indoor air contained a complex mixture of chemical, physical and microbiological compounds. They also concluded that the continuous exposure of occupants to these pollutants could be detrimental to their health.

In order to limit the level of pollution in hospital environments, several national agencies, recommend regulations for indoor air quality control based on ventilation rates. In the US the reference guideline is ASHRAE 170-2017 adopted from the work of The American Society of Heating, Refrigerating and Air-Conditioning Engineers (ASHRAE) whilst in France it is the

standard NFS 90-351 based on the recommendations of the Association pour la Prévention et l'Etude de la Contamination (ASPEC). Currently, air treatment devices whether stand-alone or included in the main ventilation systems are becoming increasingly popular for use as complementary means to improve IAQ. ASHRAE states that in recent years, more and more air cleaning devices are advertised in the market for the removal of indoor pollutants. The Center for Disease Control and Prevention (CDC) and the Société Française d'Hygiène Hospitalière (SF2H) recognize these devices as supplementary means of treating the air and also improving ventilation in medical environments in the US and France respectively.
The treatment devices use technologies that can be divided in two categories:

- Trapping and separation techniques: These include filtration and adsorption where pollutants are transferred unto a filter or a sorbent material. Filtration is used to remove particulate matter whilst adsorption targets gaseous pollutants. Consequently they are effective for certain pollutants but less for others. Additionally, they do not eliminate the pollutants but only transfer them to another phase and subsequently additional disposal or handling steps are required.

- Destruction and oxidation techniques: These techniques include plasma treatment, UV germicidal irradiation (UVGI), ozonation and photocatalytic oxidation (PCO). Plasma treatment involves oxidizing pollutants by means of cold plasma at a very high voltage between two electrodes. This technique is effective but it can lead to ozone production and the formation of toxic by-products. UVGI is mostly used for the destruction of bioaerosls using UV light. However it is also capable of degrading some gaseous pollutants. It has the disadvantage of producing intermediates that may be toxic including ozone. Ozonation involves using ozone an oxidizing agent for the destruction of volatile organic compounds (VOCs) and microbial agents. However it can lead to the exposure of ozone. For photocatalytic oxidation, pollutants are oxidized at ambient temperature and under atmospheric pressure using a catalyst activated by light. This technique leads to the transformation of pollutants into innocuous final products. However depending on the type of pollutants and conditions it could also lead to the formation of toxic by-products.

When it comes to air treatment in the hospital however, the major concern is with the reduction of microbiological pollutants rather than chemical pollutants due to the risk of nosocomial infections. Consequently, the efficiency of these devices is usually based on the

microbiological pollutant removal. However, since studies such as AICHA and QAIHOSP show that hospitals contains several chemical contaminants some of which are specific to the medical environment, it is necessary that the fate of these chemical pollutants when they pass through these treatment devices is studied.

Among these treatment technologies, photocatalytic oxidation (PCO) is seen as an economic and energy efficient method capable of degrading a wide range of chemical pollutants and is therefore chosen for this work.

The PhD work therefore aims to evaluate the efficiency of PCO devices in removing some specific chemical pollutants found in hospitals and subsequently to investigate whether PCO is a safe technology for the occupants of the hospital.

The PhD work was financed by ATA Medical and the IMT Atlantique. ATA medical is a French company that has expertise in providing air treatment solutions to various sectors including the medical sector. The research work was carried out in the Department of energetic systems and environment, part of the Génie des procédés, environnement et agro-alimentaire (GEPEA) laboratory located in IMT Atlantique campus in Nantes. The laboratory has a research platform called SAFEAIR which has expertise in indoor air treatment and has made several scientific contributions to PCO for air treatment and is furnished with specific equipments necessary for the study of indoor air treatment by photocatalytic oxidation.

This manuscript consists of four chapters each of which provides information to help achieve the main objective.

- The first chapter recapitulates the state of the art on the indoor air quality in the hospitals detailing principally the chemical pollutants that are present and how some are chosen for this study. Then a preview of the existing knowledge of the photocatalytic degradation process including the principles, the reactors that are available, the parameters influencing its efficiency and the performance evaluation factors are presented. Based on this review and some of these parameters that are important for this study are retained. Finally the experimental objectives of this PhD work are listed.

- In the second chapter, the experimental materials and methods that are utilized to achieve the objectives are described. The photocatalytic reactor in which the

degradations are carried out is presented. Next, the sampling and analytical devices are explained. Then the model that enables the calculation of the performance indicators is described and then, the experimental methodology is given.

- The third chapter deals with the photocatalytic degradation of the target pollutants. Firstly, a parametric evaluation to study the influence that air velocity, light intensity, relative humidity, presence of particles (bioaerosols) and presence of chemical co-pollutants will have on the degradation efficiency of the target compounds is presented. Then, the investigation of intermediates formed during the degradation is done to assess the safety of the process. Thirdly, the mineralization rates obtained during the degradation are also discussed. In the last section of this chapter the influence of two different media geometries is presented. Experimental results from the degradation of isoflurane and acrylonitrile using a pleated media configuration are compared to those obtained using plane media geometry under similar experimental conditions.

- Complementary to the last section of the third chapter, the fourth chapter focuses on using numerical simulations to examine how a change in media geometry affects the behavior of air flow and light irradiance. This is done with the aim of better understanding the role of the media geometry in improving the removal efficiencies of the target compounds.

Finally, the general conclusion summarizes the main results achieved from the work presented in this manuscript as well as some recommendations regarding PCO use in hospital environments.

CHAPTER I: MANAGEMENT OF INDOOR AIR QUALITY IN MEDICAL ENVIRONMENTS

I.1 Introduction

This work is concerned with the study of using photocatalytic oxidation (PCO) to remove chemical pollutants that are specific to medical environments. This chapter through a review of literature defines a reference frame about the research topic. In detail, the first section (I.2) discusses the indoor air quality generally in hospitals and then specifically in operating rooms (ORs). It aims to provide information on the sources of pollutants and the methods employed to ensure a good indoor air quality. The second section (I.3) discusses photocatalytic oxidation and its use as an air treatment process by looking at its principles and the factors that influence the efficiency of PCO. The different photocatalytic reactors and the performance indicators are also detailed in this section. All of this is done with the objective to identify target compounds as well as the operating parameters that will influence the effectiveness of PCO to remove these target compounds. Finally the experimental objectives of the PhD work are presented.

I.2 Indoor air quality in hospitals

The air quality in hospitals plays an important role on the health of both patients and hospital staff and consequently improper control of hospital indoor air quality (IAQ) may cause hospital-acquired (nosocomial) infections and occupational diseases [1]. Indoor air quality is even more critical in the hospitals than in most other building environments, because of the increased susceptibility of the patients [2].

Unlike other closed indoor environments like residential and commercial buildings, hospitals are composed of a diversity of facilities and occupants and thus the indoor air requirements differ from one facility to the other. Consequently, there is the need to set specific requirements for ventilation, temperature and humidity for the various facilities. For example, facilities such as intensive care units and laboratories will require stricter demands compared to facilities such as meeting rooms. This therefore makes the hospital a complex environment.

In order to reach adequate indoor air, one important feature is the heating, ventilation and air conditioning (HVAC) systems. Ventilation has the function of supplying filtered air from outside (or recycled filtered room air) to dilute pollutant concentrations. The dilution effect is controlled by the ventilation rate which is expressed as air change per hour (ACH).

The ACH (h^{-1}) is defined as the volumetric air flow through the facility divided by the volume of the facility [3]. In most developed countries, national organizations and agencies provide guidelines based on these ventilation rates. These guidelines may vary depending on the country.

In the US, the reference guideline for ventilation requirements in hospitals is provided in ASHRAE 170-2017 [4] which is based on the recommendations of the American Society of Heating, Refrigerating and Air-Conditioning Engineers (ASHRAE). Whilst in France the NFS 90-351 [5] is the document providing guidelines for indoor air quality in the hospitals. This guideline is based on the recommandations of Association pour la Prévention et l'Etude de la Contamination (ASPEC). The ventilation requirements for some hospital facilities according to these two guidelines are summarized in Table 1.

Facility	**Minimum ACH (h^{-1})**	
	ASHRAE 170-2017 [4]	**NFS – 90-351 [5]**
Halls	4	-
Consultation room	6	10
Laboratories	6	15

Table 1 : Ventilation requirements in hospital facilities in France and in the US

Indoor pollutants that could be present in the hospital are principally of three types; biological pollutants, chemical pollutants and particulate matter and their levels are influenced by outdoor and indoor emissions [6]. Due to nosocomial infections however, the main focus when it comes to IAQ is microbiological pollutants. It has been reported that 5% of all patients who go to the hospital get nosocomial infections whilst they are there [7]. In the USA it is estimated that over 100,000 people die each year from hospital infections and 25,000 die in Italy every year [6].

The principal mission of the hospital is to prevent airborne infection and transmission. Consequently, in addition to the ventilation requirements; strict hygiene standards are adhered to, to reduce the microbiological risk of contamination. This is done through the implementation of rigorous cleaning standards. Depending on the degree of infectious risk, hospitals are classified into different zones and the cleaning requirements (frequency of cleaning and products used) necessary to ensure the prevention of nosocomial diseases is influenced by the zone [8,9]. In France, the Comité de Lutte contre les Infections Nosocomiales (CLIN) developed a program which classifies the hospital into four zones.

Table 2 shows the various facilities that are categorized in the zones as well as the products used and the frequency of cleaning.

Zone	Facilities	Cleaning times	Products used
Zone 1 (Low risk)	Halls, offices, elevators, meeting and training rooms, staff restaurant	Twice a week	Detergent
Zone 2 (Moderate risk)	Consultation rooms, laundry rooms	At least twice daily	Detergent + disinfectant
Zone 3 (High risk)	Patient wards, endoscopy rooms, laboratories, sterilization rooms	After each use	Detergent + disinfectant
Zone 4 (Very High risk)	Operating blocks, obstetric unit, virology and bacteriology laboratories	Before and after each use	Detergent + disinfectant

Table 2 : Classification of hospital premises into risk zones by CLIN, France [8]

Chemical pollution unlike biological contamination remains rarely studied and information on the chemical quality of the air in hospitals is limited. However, many activities and uses specific to health facilities are potential sources of chemical pollutants which may lead to a change in the air quality. These activities can be concentrated in specific premises like laboratories, sterilization rooms, operating rooms or be common to all premises [10].

I.2.1 Sources of chemical pollutants in hospitals

The presence of chemical pollutants in the hospital could be attributed to both outdoor sources and indoor sources.

I.2.1.1 Outdoor sources of pollution

Indoor air in a hospital is subject to pollution from outdoor air. The outdoor pollutants are normally physico-chemical (particles and gases) caused by human activities such as transportation. In urban area with dense populations, automobile exhaust gas is the major air pollutant, resulting in high pollutant concentrations. These are mainly carbon oxides, nitrogen and sulfur oxides, ozone and volatile organic compounds (VOCs). The transfer of outdoor pollutants into the hospital environments is also linked to factors such as the location of these hospitals and the placement of the air intake for ventilation.

Chen *et al.*[11] compared the levels of nitrogen dioxide (NO_2) and ozone (O_3) in two Taiwanese hospitals. One of them was located close to a major road and thus would be impacted by traffic whilst the second hospital was located at a distance from traffic. Their results showed that NO_2 and O_3 were significantly higher in the hospital close to traffic (average concentrations: 54.1 ppb versus 32.7 ppb for NO_2 and 15.0 ppb versus 9.7 ppb for O_3). They therefore highlighted the influence of local traffic pollution levels on the indoor pollution in the hospitals.

I.2.1.2 Indoor sources of pollution

Within the hospital itself, chemical pollutants could be produced from architectural components, interior coverings (paints), building materials and even electronic devices. In addition, certain specific activities performed within the hospital can also cause pollution.

The Danish Technological Institute conducted a large study of the substances emitted by electrical and electronic equipments [12]. The study highlighted that the following predominant pollutants, toluene, trimethylbenzene, styrene, xylene, benzene, dibutylphthalate, were emitted by computer equipment, TV and phones. They estimated concentrations for these pollutants to range between 0.03 and 0.5 ppm. Formaldehyde is also a common indoor pollutant as it is present in many everyday products such as insulating foam, glues, varnishes, inks, resins, paper [13]. Phthalates, which are widely used in the manufacture of PVC, were measured in indoor air of 120 apartments [14]. The presence of all these substances and devices in the hospital could mean that these pollutants are likely to be found in the hospital indoor air environment.

In 2010, the French agency ANSES funded the AICHA project with the aim to provide some knowledge on the chemical pollutants that could be present in a hospital due to indoor pollution sources. In the project, the work undertaken by Bessonneau *et al.* [10] was done in a hospital in Rennes. They studied six sampling sites; reception hall, nursing care, post-anesthesia care unit, parasitology-mycology laboratory and flexible endoscope disinfection unit and measured more than 40 volatile organic compounds (VOCs) including aliphatic, aromatic and halogenated hydrocarbons, aldehydes, alcohols, ketones, ethers and terpenes. Their results showed that the main compounds found in indoor air were alcohols (ethanol at 0.5 ppm) and isopropanol at 0.02 ppm) ethers (ether at 0.03 ppm) and ketones (acetone at 0.01 ppm). They observed that the concentration levels of these compounds varied depending on the activities performed in the sites. For example they found that the high levels

of alcohols were present in the sampling sites was due to the cleaning and alcohol based products that were used in all sites to reduce nosocomial infections. Qualitative analysis of the air samples in the post-anesthesia care unit also led to the identification of anesthetic gases; sevoflurane and desflurane. They concluded that the continuous exposure of the occupants to these compounds could have negative effects on their health.

The AICHA project although very insightful studied only one hospital and generalized the results for all hospitals. Thus in 2013 the QAIHOSP project was developed to study the chemical contamination in two hospitals in Rennes and Nancy. 7 sampling sites were studied, that is; reception hall, patient ward, post-anesthesia care unit, laboratory, disinfection unit, nurses care, and operating rooms. According to preliminary results presented by Baures *et al*. [15], 47 compounds were identified including aliphatic, aromatic and halogenated hydrocarbons, aldehydes, alcohols, ketones, ethers, terpenes and phthalates. Concentrations of the pollutants were found to be in the same order of magnitude in both hospitals. They also observed that the chemical compounds with the highest concentration were those that were emitted as a result of specific activities performed in the sampling sites.

In order to access the exposure of workers to disinfecting agents, Koda *et al.* [16] measured the airborne concentrations of formaldehyde and gluteraldehyde in the pathology units and in endoscopy services of two Japanese hospitals. The average concentrations found ranged between 0.3 and 2.3 ppm and between 0.1 and 0.8 ppm for formaldehyde and gluteraldehyde respectively. These values were reported to be higher than the Japanese occupational safety and health association (JOSHA) of 0.5 ppm and 0.05 ppm for formaldehyde and gluteraldehyde respectively. They also reported that the continuous exposure to these compounds could lead to skin and eye irritations, acute and chronic respiratory diseases and cancer.

Tokigawa *et al*. [17] also studied eight volatile organic compounds (VOCs) levels in nineteen rooms of a new hospital in Japan with the aim of examining the association between the pollutants and health effects. The VOCs studied included formaldehyde, toluene, ethylbenzene, hexane, m,p-xylene and o-xylene, ethyl acetate and butyl acetate. Among these, the most prevalent were formaldehyde (0.003 – 0.006 ppm) and toluene (0.04 - 0.4 ppm). The Total VOC (TVOC) level was 1 ppm which was higher than the JOSHA guideline of 0.5 ppm. Their results also showed that symptoms of deterioration in the skin, eye, ear, throat,

chest, central nervous system, autonomic system, musculoskeletal system, and digestive system among employees were associated mainly with the high TVOC concentration levels.

Dascalakis *et al.* [18] measured the concentrations of anesthetic gases and disinfecting agents in 17 operating rooms, within ten Greek hospitals. Anesthetic gases (isoflurane and sevoflurane) were found at concentrations ranging from non-detectable to 1.3 ppm. They were below the US Occupational Safety and Health association (OSHA) guideline of 2 ppm. The disinfecting agents (formaldehyde and gluteraldehyde) were found non-detectable to 1.7 ppm. They were above the OSHA guideline of 0.8 ppm and 0.2 ppm for formaldehyde and gluteraldehyde respectively.

I.2.1.3 Conclusion on the chemical pollutants present in hospitals

Based on the work performed by some authors in the literature some conclusions on chemical pollutants found in the hospital can be made. Firstly, occupants of the hospital (workers and patients) are exposed to a wide variety of compounds which could have negative effects on their health. Secondly, the chemical pollutants found in hospitals could be classified into two groups; those that are found in hospitals but can be found in other indoor environments and those that can be found in hospitals due to the specific activities. These are summarized in Table 3.

Compounds specific to hospital environments	Common indoor compounds (not specific to hospital environments)
Gluteraldehyde [16,18] Peracetic acid [10] Ethanol [10] Isopropanol [10] Isoflurane [18] Desflurane [10] Sevoflurane [10,18]	Formaldehyde [16,18] Phtalates [12,15] Benzene, toluene, xylene, styrene [10,17] Nitrogen dioxide [11]

Table 3: Summary of some chemical pollutants identified in hospitals

Due to the fact that the pollutants varied from one facility to another based on the specific activities performed, it would be necessary for this study to limit the search for target compounds to one facility. For the purpose of this work, the operating room (OR) was chosen. In the section that follows the IAQ in the ORs is going to be discussed.

I.2.2 Indoor air quality in operating rooms

In the hospital, the operating room requires careful control of its environment and thus is among the most demanding hospital facility. Therefore, systems serving them need to be designed in order to minimize the concentration of chemical compounds and microorganisms.

I.2.2.1 Pollutants found in operating rooms

The indoor air of an operating room contains different chemical pollutants like waste medical gases used for anesthesia, disinfection and sterilizing substances and surgical smoke. The presence of these substances is known to have adverse health effects on and lead to discomfort of OR personnel. Therefore occupational exposure to these should be limited [18].

Anesthetic gases

General anesthesia is a state of unconsciousness following the administration of drugs. Anesthetic substances are given to the patient to control and depress the central nervous system in order to provide the patient with an experience that is free of pain during a surgical procedure [19]. There are two induction methods that are usually employed; intravenous injection and inhalation. Intravenous injection consists of the administration of anesthetic molecules by the venous or intramuscular route whilst inhalation anesthesia involves the administration of an anesthetic gas mixture using a face mask or breathing tube affixed to the mouth of the patient.

Inhalation anesthesia is known to be the main source of anesthetic gases in operating room air. Anesthetic gases escape into indoor air through leaks in the patient breathing circuit, during installation and disconnection of the system and also when patient exhales [20]. Inhaled anesthetic agents are categorized into two classes of chemicals: nitrous oxide (N_2O) and volatile halogenated agents. N_2O is supplied in a gas form whilst the halogenated agents are supplied as a liquid and then vaporized by an anesthesia machine into a gaseous state before it is delivered to the patient [21].

The three most commonly used volatile halogenated agents worldwide are isoflurane, desflurane and sevoflurane. Depending on the surgical procedure, they can be either delivered alone or in combination with N_2O [22]. According to the OSHA, anesthetic gases pose a hazard to hospital workers such as anesthesiologists, surgeons, operating room technicians and dentists because exposure to these compounds could cause nausea, dizziness, headaches, fatigue, and irritability, miscarriages, birth defects, liver and kidney disease [23].

The National Institute of Occupational Safety and Health (NIOSH) have 8-hr time weighted average (TWA) recommended occupational exposure limits (OEL) at 25 ppm for nitrous oxide, 2 ppm for halogenated anesthetic gases without N_2O and 0.5 ppm for halogenated anesthetic gases with N_2O.

Significant improvements have been made over the years to control anesthetic gas pollution in operating rooms. These have been accomplished through the use and improved design of scavenging systems, installation of more effective general ventilation systems, and increased attention to equipment maintenance and leak detection as well as to careful anesthetic practice. However, occupational exposure to waste anesthetic gases still occurs [24].

Dascalakis *et al.* [18] measured the concentrations of anesthetic gases; isoflurane and sevoflurane in 17 operating rooms, within ten Greek hospitals. Anesthetic gases (isoflurane and sevoflurane) were found at concentrations ranging from non-detectable to 1.3 ppm. Sitarek *et al.* [25] found isoflurane concentrations to range between 0.4 and 12 ppm when they measured the concentrations of isoflurane in a Polish hospital OR. Crea and Tkaczuk [26] in studying Australian ORs measured isoflurane levels between 0.001 and 3.6 ppm. Jafari *et al.* [27] found the average isoflurane and sevoflurane concentrations in an Iranian OR to be 1.14 and 0.005 ppm respectively. Hoerauf *et al.* [28] studied the concentration of nitrous oxide in an Austrian OR and found average levels of 12.8 ppm whilst Chang *et al.* [29] found average levels of 85 ppm in a Taiwanese hospital OR and Passeron *et al.* [30] measured average levels of 31 ppm in a French hospital OR.

These studies show that concentrations of anesthetic gases like nitrous oxide and isoflurane in the operating rooms can exceed the recommended occupational exposure limits. Consequently, continuous exposure to these gases can lead to negative health effects for OR occupants.

Sterilants

Surgical procedures involve the contact of a medical device or surgical instrument with a patient's sterile tissue and a risk of all surgeries is the introduction of pathogens that can lead to infection. Sterilization is therefore essential to ensure that medical and surgical instruments do not transmit infectious pathogens to patients [31–33]. Sterilization is the complete removal or destruction of all types of life form on a surface and is achieved in the

hospitals by physical or chemical processes. Depending on the characteristics of the devices to be sterilized, sterilization is classified into three types; High temperature sterilization, low temperature sterilization and liquid immersion [34]. These processes are adopted worldwide.

For heat-tolerant equipments, high temperature sterilization methods like the use of steam and dry heat are employed. Equipments are exposed to steam or dry heat at temperatures ranging between 121°C and 160°C for several minutes (3-120 minutes). For heat sensitive instruments, they are typically sterilized by low temperature methods and liquid immersion. Low temperature sterilization involves exposing the equipments to ethylene oxide gas treatment and hydrogen peroxide gas plasma at low temperatures ranging from 35°C to 63°C for several hours (1-15 hrs). Finally, sterilization by liquid immersion involves dipping the equipments in liquid solutions consisting of peracetic acid and hydrogen peroxide for several hours. [34–39].

For the sterilization methods that involve chemicals like ethylene oxide and peracetic acid, aeration or rinsing step is needed after the sterilization process in order to remove residuals of the chemicals from the surgical instruments. Consequently if this is not properly done, it leads to the introduction of these substances into OR air [40]. The occupational exposure limit set by NIOSH for 8-hr TWA is 0.6 ppm for peracetic acid, and 1 ppm for hydrogen peroxide and ethylene oxide respectively.

Wesołowski and Sitarek [41] measured levels of ethylene oxide in the ORs of 13 polish hospitals located in Lodz. The average concentration ranged from 0.006 to 3.4 ppm Whilst Pacenti *et al.* [42] also measured average peracetic acid levels of 0.07 ppm in a the OR of a regional hospital in Florence, Italy.

Exposure to these chemicals may lead to acute health effects including respiratory and eye irritation, vomiting and diarrhea, while chronic health effects include altered behavior, anemia, secondary respiratory infections, skin sensitization, miscarriages, reproductive problems and possibly cancer [18,43,44]. In recent decades, due to its possible mutagenic, reproductive, neurologic and carcinogenic hazard to workers, strict regulations concerning the use of ethylene oxide are being implemented. In France, the Agence nationale de sécurité du médicament et des produits de santé (ANSM) is advocating for the use of alternatives such hydrogen peroxide and peracetic acid [45].

According to the literature, it has been shown that the presence of these compounds could be anticipated in operating rooms and they could negatively impact the health of the OR personnel and patients.

Surgical smoke

Electrosurgery, laser tissue ablation and ultrasonic scalpel dissection are techniques that are used by in order to cut, coagulate, desiccate or vaporize biological tissue. These devices are frequently used during surgical operations to help surgeons make precise cuts and prevent blood loss [46]. The disadvantage of such techniques though is that they produce smoke referred to as surgical smoke.

Surgeons and operating theatre personnel are routinely exposed to pollution from the surgical smoke which hinders the vision of the surgeon and produces an unpleasant odor. It has been known to consist of 95% water vapor and 5% blood and particulate matter (tissue particles, viruses and bacteria) and chemical compounds [47].

The aerodynamic sizes of particles vary significantly, depending on the type of procedure, pathology of target tissue, type of energy imparted, power levels used, and the scope of surgery (cutting, coagulation, or ablation) [48]. An electrosurgery creates the particles whose size is < 0.1 μm and a laser tissue ablation does larger particles (< 0.3 μm). But the largest particles are generated using an ultrasonic scalpel (0.35-6.5 μm) [49]. Their presence exposes surgical staff to the risk of infection. In addition, the exposure is associated with an increased risk of respiratory diseases and strokes [50].

Gianella *et al.* [51] in studying the smoke produced during laparoscopic surgery found concentrations of methane, ethane and ethylene to be in a range of 0.1-34 ppm, 0.1-2 ppm and 5 -10 ppm respectively. Moot *et al.* [52] found that the smoke produced during a surgical procedure contained acetylene, butadiene, 1-decene and 2-propylene nitrile in concentrations of 2.3-7.5 ppm, 0.2-0.7 ppm, 0.3-1.4 ppm and 0.018-0.4 ppm respectively. These results are summarized in Table 4.

Compound	Range (ppm)
Acetylene	2.3-7.5 [52]
Butadiene	0.2-0.7 [52]
1-decene	0.3-1.4 [52]
Ethane	0.1-2.0 [51]
Ethylene	5.0 -10 [51]
Methane	0.1-34 [51]
2-propylene nitrile	0.018-0.4 [52]

Table 4 : Concentrations of compounds found in surgical smoke

In a review, Barrett and Garber [53] listed about 40 compounds that had been found to be present in surgical smoke during surgical procedures. These compounds are summarized in Table 5.

Compounds found in surgical smoke categorized under chemical families		
Hydrocarbons	**Nitriles**	**Phenols**
Acetylene	*Acetonitrile*	*Creosol*
Alkyl benzene	*Acrylonitrile*	*4-methyl phenol*
Benzene	*Benzonitrile*	*Phenol*
Butadiene	*3-butenenitrile*	
Butene	*2-propylene nitrile*	**Miscellaneous**
1-decene	*Pyridine*	*Carbon dioxide*
2,3-dihydro indene		*Hexadecanoic acid*
Ethane	**Amines**	*Methyl pyrazine*
Ethene	*Indole*	
Ethylene	*6-methyl indole*	
Ethyl benzene	*Pyrrole*	
Ethynyl benzene	*Aldehydes*	
Isobutene	*Acrolein*	
Methane	*Benzaldehyde*	
Propene	*Formaldehyde*	
Styrene	*Furfural*	
Toluene	*3-methyl butenal*	
1-undecene	*2-methyl propanol*	
Xylene		

Table 5 : Compounds identified in surgical smoke [53]

The chemicals that are found to be present in the greatest quantity in the surgical smoke are hydrocarbons, nitriles and amines [54,55]. Of these compounds, acrylonitrile is one of the most concerning as it has been classified as a hazardous compound by US EPA. Its short-term exposure is known to cause eye irritation, nausea, vomiting, headache, sneezing,

weakness, and light-headedness. It has also been reported that its long-term exposure raises the incidence of cancer. Moreover, it has also been documented that its repeated or prolonged exposure to skin may irritate the skin and trigger the occurrence of dermatitis [55,56]. The occupational exposure limit for acrylonitrile set by NIOSH for 8-hr TWA is 2 ppm. Barrett and Garber [53] stated that OR personnel are exposed to acrylonitrile concentrations ranging between 1and 1.6 ppm.

Surgical staff and patients are continuously exposed to surgical smoke which contains compounds that could negatively impact the health of OR occupants. Therefore it will be beneficial if these compounds can be removed from the air.

I.2.2.2 Ventilation in the OR

The indoor environmental quality (IEQ) in an OR is determined by the level of indoor air pollutants and other characteristics, including the air temperature, relative humidity and air velocity [4]. The air in an OR must be aseptic, at constant and reasonable temperature and humidity and have relatively low velocity to avoid drafts and swirls that will disrupt the surgical procedure and re-circulate microbes [57]. As previously discussed in section I.2.2.1, patients and OR personnel can be exposed to a wide range of pollutants, therefore maintaining a high quality of air is also essential for protecting both the patient and OR personnel from surgical infections and occupational diseases.

ORs are usually equipped with heating, ventilation and air conditioning (HVAC) systems whose fundamental role is to maintain temperature and humidity at acceptable levels and keep the concentrations of particulates, microbes and gaseous contaminants at low levels.

Maintaining proper temperature and humidity levels is essential for occupants comfort. The guidelines recommended by several national agencies state that indoor OR temperature must be kept within 18 - 26°C to ensure comfortable conditions (Table 6). They also recommend that the overall humidity levels should also be maintained at an acceptable range (30 – 60 %). Low humidity can cause favor blood coagulation whilst high moisture content will promote the growth of bacteria and also cause discomfort for OR occupants. The average reported by some authors in the literature is 50 % however they have also reported high levels of 80 % [58,59].

Country	T(°C)	Relative Humidity (%)	Minimum ACH (h^{-1})	Source
USA	17-26	30-60	20	ASHRAE 170-2017 [4]
Germany	22-26	50-60	20	DIN 1946-4 [60]
France	19-26	45-55	25	NFS – 90-351[5]
Canada	18-23	30-60	20	CSA Z317.13-17 [61]

Table 6 : Operating room recommended indoor conditions

In the operating theatre, the specific features of the airflow are air distribution, room pressurization (infiltration barrier), ventilation (dilution), and filtration (contaminant removal) [62].

The main types of air distribution systems used in an OR are: non-unidirectional flow and unidirectional-flow. Non-unidirectional flow involves the whole environment and is based on diffuse and turbulent streams of filtered air with the aim of creating mixed ventilation in the whole operating room (Figure 1). The concentration of airborne contaminants is controlled by means of dilution which increases the effectiveness of air. However, it has the disadvantage of speeding up microbial dispersion [63]. This type of airflow is generally considered enough for general surgery operating rooms [64].

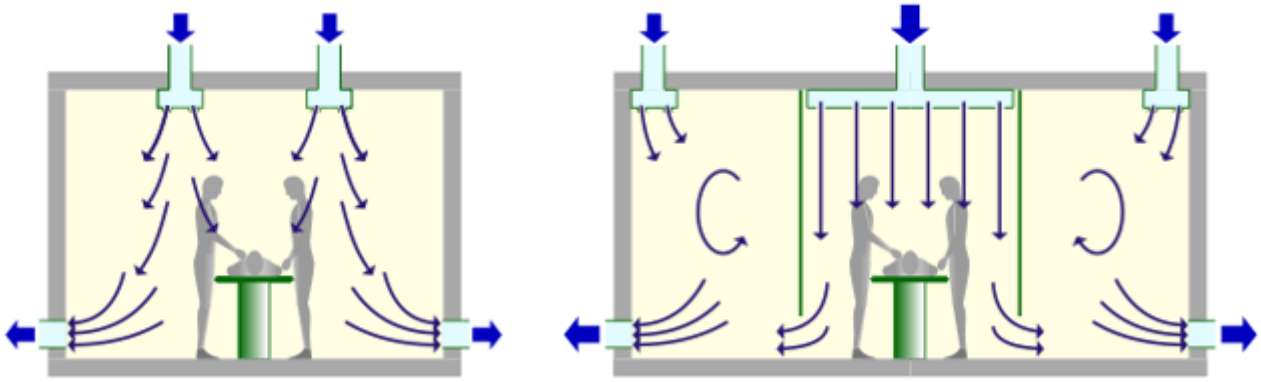

Figure 1 : Non-unidirectional-flow distribution in an operating room [65]

The unidirectional-flow system (Figure 2) attempts to avoid turbulence and instead strives to direct a linear stream of filtered air to the surgical field. The system delivers air from the ceiling, with a downward movement over the operating table to several exhaust inlets located on opposite walls [66]. It constitutes the best option for an operating theatre, in

terms of contamination control, because it results in the smallest percentage of particles impacting the surgical site [67].

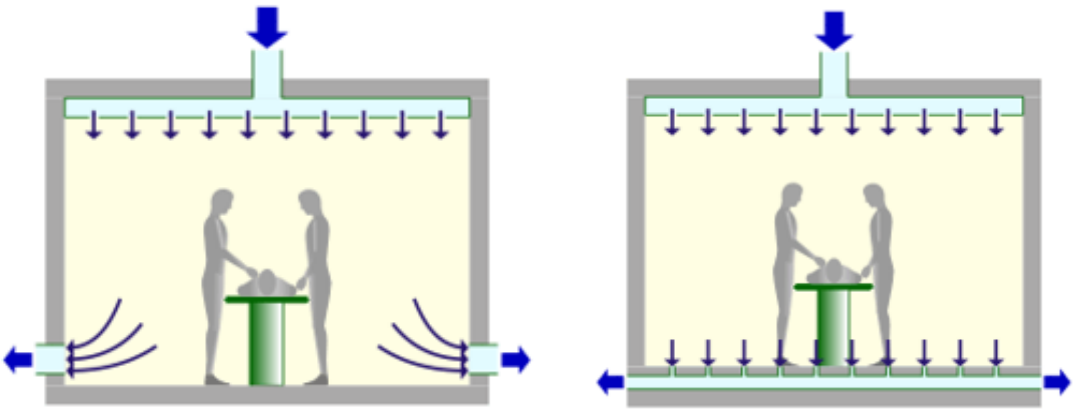

Figure 2 : Unidirectional-flow distribution in an operating room [65]

With regards to the room pressurization, air must be maintained at positive pressure. The OR should have higher pressure than adjoining rooms and corridors so that air flows from and not into the OR. This prevents the infiltration of contaminated air into the OR [4].

For a critical room such as an OR, it should be supplied with ventilation rates between 20-25 ACH. Recommended ventilation rates may vary between countries as shown in Table 6. Conventionally, ORs are ventilated with 100% outdoor air but some guidelines allow for about 30% of re-circulated air [4,61].

The extracted outdoor air first passes through some filters before it is brought into the OR. In France, the guideline NFS 90-351 recommends three stages of filtration; a low efficiency filter to remove particles with diameters greater than 10 µm, medium efficiency filter to remove particles with diameters greater than 1µm and a High Efficiency Particulate Air (HEPA) filter which has a collection efficiency of 99.97% for particles with diameters greater than 0.3 µm.

Due to their demanding indoor conditions, operating theatres constitute the most expensive sector of the healthcare establishment mandating an efficient management reaching 33-50% of the total cost [57]. Increased ventilation rates are great to reduce contaminant levels but they result in increased energy consumption necessary to condition (heat, cool, humidify, dehumidify) the air. Additionally, the filters installed in typical HVACs are targeted for particulate matter control and as such may not be very efficient at removing some indoor chemical pollutants [68].

As a result of these drawbacks associated with the conventional ventilation systems, the implementation of air treatment technologies whether as standalone or as part of the existing HVAC system (in-duct) is becoming popular as a complementary means of improving IAQ. ASHRAE states that in recent years, more and more air cleaning devices are advertised in the market for the removal of indoor pollutants generally in indoor environments [69]. In hospitals, The US Center for Disease Control and Prevention (CDC) and the Société Française d'Hygiène Hospitalière (SF2H) recognize these treatment devices as supplementary means of treating the air and also improving ventilation in ORs [40,70]. These devices control chemical pollutants and allow air quality levels to be maintained with reduced outdoor air supply and concomitant energy savings [71–73].

The treatment technologies that are used by these devices include filtration, adsorption, cold plasma, ultraviolet germicidal irradiation (UVGI), ozonation and photocatalytic oxidation (PCO). Filtration and adsorption transfer the pollutants unto a filter or a sorbent material. Filtration is used to remove particulate matter whilst adsorption targets gaseous pollutants. These techniques can be very effective for certain pollutants but less for others. Additionally, they do not eliminate the pollutants but only transfer them to another phase and subsequently additional disposal or handling steps are required [74]. Cold plasma treatment involves the oxidation of pollutants by means of non thermal plasma produced at a very high voltage between two electrodes. UVGI is mostly used for the destruction of bioaerosls using UV light. However it is also capable of degrading some gaseous pollutants. It has the disadvantage of producing intermediates that may be toxic including ozone [75]. Ozonation involves using ozone an oxidizing agent for the destruction of VOCs and microbial pollutants. However , it can lead to the exposure of ozone and other toxic intermediates [69]. Cold plasma is very efficient at removing particulate matter and biological and chemical pollutants. However, it has poor energy efficiency, especially for the treatment of chemical pollutants at low concentrations. Additionally, it could lead to ozone production and the formation of other toxic by-products [76]. Photocatalytic oxidation involves the oxidation of pollutants (microbiological and chemical) using a catalyst that is activated by UV light. The appeal of this technology is the prospect of complete mineralization of a broad range of VOCs to environmentally harmless compounds such as CO_2 and H_2O at room temperature and atmospheric pressure. It is also well suited for contaminated air with low pollutant concentrations. However depending on the type of pollutants and conditions it could also lead

to the formation of toxic by-products [77]. In addition to the mineralization of many gaseous compounds, photocatalysis has also a proven bactericidal effect [78].

Some studies have been conducted to evaluate the efficiency of these technologies when placed in ORs. Bergeron *et al.* [79] evaluated the performance of a mobile air-treatment unit using cold plasma reactors for lowering the airborne levels of *Aspergillus fumigates* in an OR. Their results indicated that the treatment unit could rapidly reduce the levels of airborne *Aspergillus fumigates* and consequently concluded that it could significantly lower the risk of nosocomial infections. Similarly Schoenleber *et al.* [80] also investigated the ability of a mobile cold plasma treatment device to control the aerobiocontamination in an OR. Their results showed that aerobiocontaminant levels were decreased by a factor of 2.5 in the presence of the device and concluded that the implementation of their device in the OR significantly improved the IAQ. Cram *et al.* [81] examined the airborne microbial killing efficiency of a photocatalytic reactor placed in an OR and found that the airborne microbes were reduced by an average of 25% . They therefore concluded that implementation of their unit would lead to a reduction in nosocomial infections as a result of the reduction in levels of airborne microbes.

I.2.2.3 Conclusions on IAQ in ORs

The literature review on the IAQ in ORs showed that the occupants could be exposed to a variety of chemical pollutants that are grouped under three main sources; anesthetic gases, sterilants and surgical smoke. Although there is not a lot of information about the concentrations, the levels that were measured by some authors showed that these pollutants could be present at concentrations higher than their recommended levels. Also, constant exposure of occupants to these compounds could lead to several negative health effects thus it would be beneficial to remove these specific compounds form the air.

The conventional method of diluting air using HVAC is not always efficient for removing some of these specific compounds and thus air treatment technologies (adsorption, UVGI, ozonation, cold plasma and PCO) are used as complementary methods to ensure good air quality. Very few studies exist in the literature on the efficiency of these technologies for indoor air treatment in ORs and these studies evaluate the efficiency of some of these air treatment technologies based on microbial pollutant removal. However, since the air in the OR also contains some specific chemical pollutants, it is necessary to also investigate their possible removal by these treatment technologies. Among these technologies, PCO has been

gaining a lot of attention as it is an economic and energy efficient method capable of degrading a wide variety of VOCs into innocuous final products like CO_2 and H_2O. Additionally as the SAFEAIR platform has a renowned expertise in air treatment with PCO, the decision was made to evaluate the performance of PCO for improving air quality in ORs.

I.3 Photocatalytic Oxidation (PCO)

PCO is a heterogeneous catalytic process. Heterogeneous catalysis indicates that the catalytic substance and reagents are in several phases. In photocatalysis, catalytic substance is solid and reactant is liquid or gaseous. Photocatalysis differs from the catalysis by the fact that it is necessary to apply electromagnetic radiation on the solid catalyst or photocatalyst for it to become active [82,83].

Over the past twenty years PCO has been greatly studied as a means of indoor air purification. It has been demonstrated that it has the ability to degrade a broad spectrum of VOCs to final products such as carbon dioxide, water and mineral acids. Additionally PCO can work at ambient temperature, atmospheric pressure and uses inexpensive catalysts [74,84–89].

Many semiconductors have been examined as candidate photocatalysts, such as ZnO, ZrO_2, SnO_2, CeO_2, WO_3, Fe_2O_3, Al_2O_3 and TiO_2 [90,91]. Among these photocatalysts, TiO_2 is most widely used due to its properties such as excellent catalytic performance, high chemical stability, optical stability and low cost [92,93]. Thus it has been extensively studied and developed. These properties of TiO_2 depend on its crystal structure, phase and particle size. The two industrially useful crystalline forms of TiO_2 are anatase and rutile; generally anatase particles perform better than rutile due to its higher band gap value. Consequently, the photocatalysts that are used consist either of pure anatase or of a mixture of anatase and rutile that is predominantly anatase [94–96].

I.3.1 Principles of PCO

For there to be a catalytic reaction, it is necessary that, initially, the target chemical species to be treated are adsorbed on the surface of the catalyst. Thus the heterogeneous catalytic processes can be decomposed in seven elemental processes that occur in series and takes place at the solid-gas phase interface. These processes shown in Figure 3 are:

1. Advection of pollutants (movement in airflow),

2. External diffusion or mass transfer of reactant species from the main flow to the exterior surface of the catalyst,
3. Molecular diffusion of the reactants from the catalysts exterior face into its interior pore structure,
4. Adsorption onto interior catalysts surface,
5. Chemical reaction on the catalyst surface,
6. Desorption of the reaction products from the catalyst surface,
7. Mass transfer of products from catalysts pores to external surface and finally to main flow by diffusion.

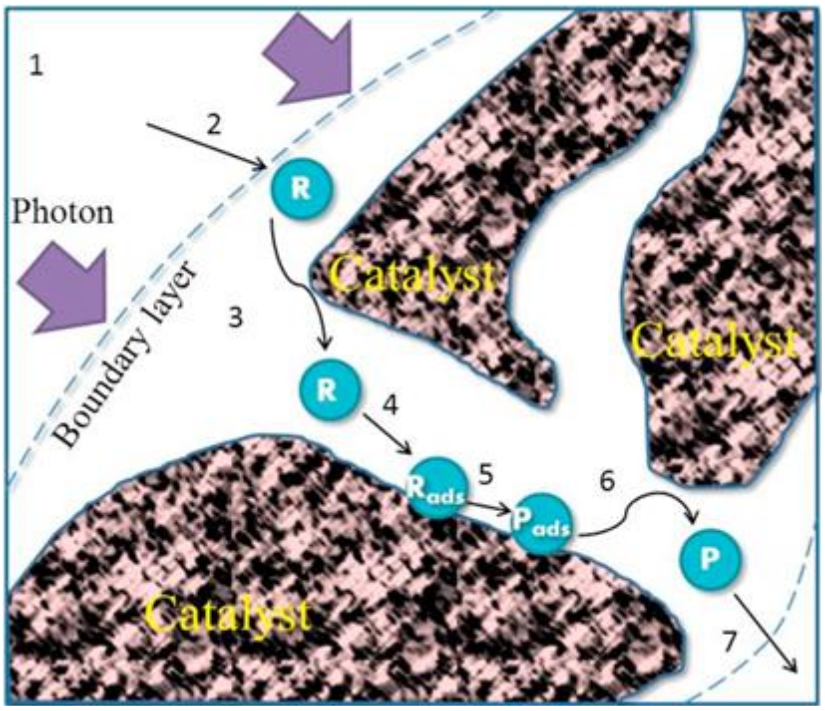

Figure 3: Schematic representation of heterogeneous catalytic reaction steps [95]

In PCO, the chemical reaction is based on the activation of the semiconductor. Semiconductors unlike metals possess a band gap instead of free electrons which prevents electron transfer. When the semiconductor is illuminated by photons, electrons are transferred from the valence band (VB) to the conduction band (CB) if the photon energy (h_v) is greater than the band-gap energy (E_g). The excitation and movement of electrons (e^-) from the conduction band creates holes (h^+) in the valence band. The minimum required excitation energy is associated with the lattice structures of semiconductors. For example, the octahedron in anatase crystals of TiO_2 is significantly distorted than that in rutile crystals of

TiO_2, which results in different mass densities and electronic band structures (3.2 eV for the anatase structure and 3.0 eV for the rutile structure) between the two forms [95].

After excitation, these highly reactive electron and hole pairs undergo a diversity of fates [97]. Figure 4 shows the possible pathways of electrons and holes induced by the photo excitation of the catalyst.

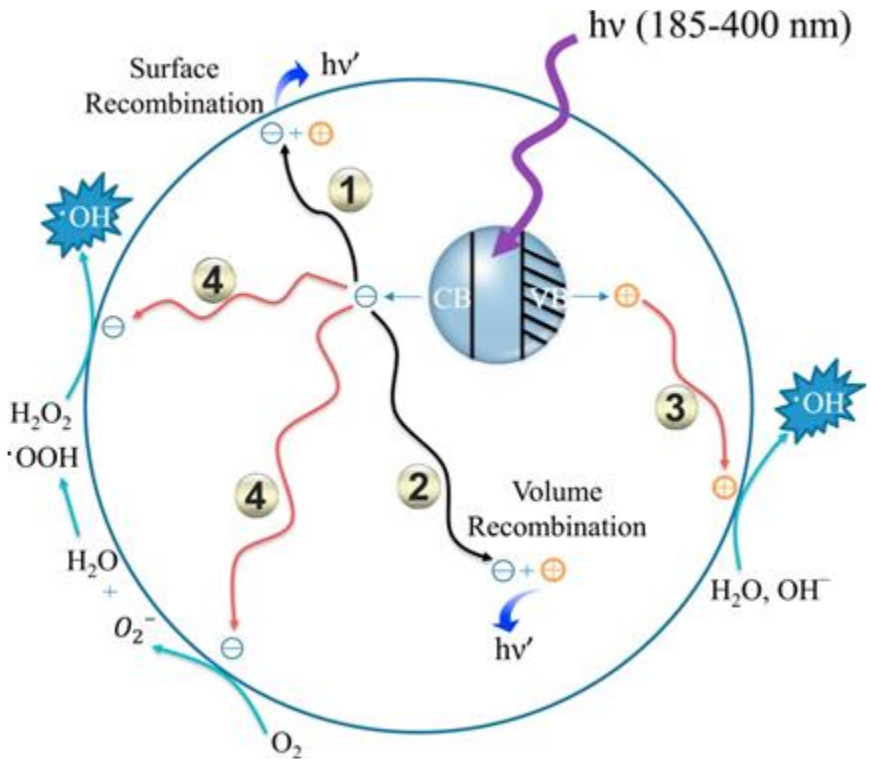

Figure 4 : Schematic representation of the photocatalytic mechanism induced by the photo-excitation of the catalyst [95]

An important step for an efficient heterogeneous photocatalytic reaction is the migration of the electrons and holes to the catalyst surface where the target VOCs are adsorbed. The positive holes move to the surface and react with OH^- dissociated from adsorbed water (pathway 3) to generate hydroxyl radicals (OH°), which are the key reactive species that oxidize the adsorbed VOCs into final products such as CO_2, H_2O and mineral acids. The electrons also partake in reduction reactions with adsorbed oxygen leading to the production of super anion O_2^- (pathway 4) which can be involved in further reactions to produce OH°. The PCO reactions could however be interfered by the recombination of the electrons and holes with the release of heat, which is an unfavorable process involved in the PCO reaction. The recombination can happen on the surface (pathway 1) or within the

semiconductor particle volume (pathway 2) [96]. The possible reaction pathways are described in the following equations:

$TiO_2 + h\nu \rightarrow h_{VB}^+ , e_{CB}^-$ **Equation 1**

$h_{VB}^+ + e_{CB}^- \rightarrow$ recombination /heat **Equation 2**

$h_{VB}^+ + H_2O_{(ads)} \rightarrow OH° + H^+$ **Equation 3**

$OH^- + h_{VB}^+ \rightarrow OH°$ **Equation 4**

$O_{2(ads)} + e_{CB}^- \rightarrow O_2^-°$ **Equation 5**

$O_2^-° + h_{VB}^+ \rightarrow O_{2(ads)}$ **Equation 6**

$O_2^-° + H^+ \rightarrow OOH°$ **Equation 7**

$OOH° + H^+ + e_{CB}^- \rightarrow H_2O_{2(ads)}$ **Equation 8**

$H_2O_{2(ads)} + e_{CB}^- \rightarrow OH° + OH^-$ **Equation 9**

$H_2O_{2(ads)} + O_2^- \rightarrow OH° + OH^- + O_{2(ads)}$ **Equation 10**

$H_2O_{2(ads)} + h\nu \rightarrow 2\ OH°$ **Equation 11**

I.3.2 Photocatalytic reactors used for the study of gas phase PCO

In general, the photocatalytic performance for gas phase degradation of pollutants greatly depends on the design of the photocatalytic reactor. In the literature the principal reactors that have been reported include plate, annular, fluidized and monolith reactors. Each reactor geometry and design has its relevance. They present different mass transfer rates, reaction surface area and accessibility to UV light. Simplified representations of these reactors are shown in Figure 5.

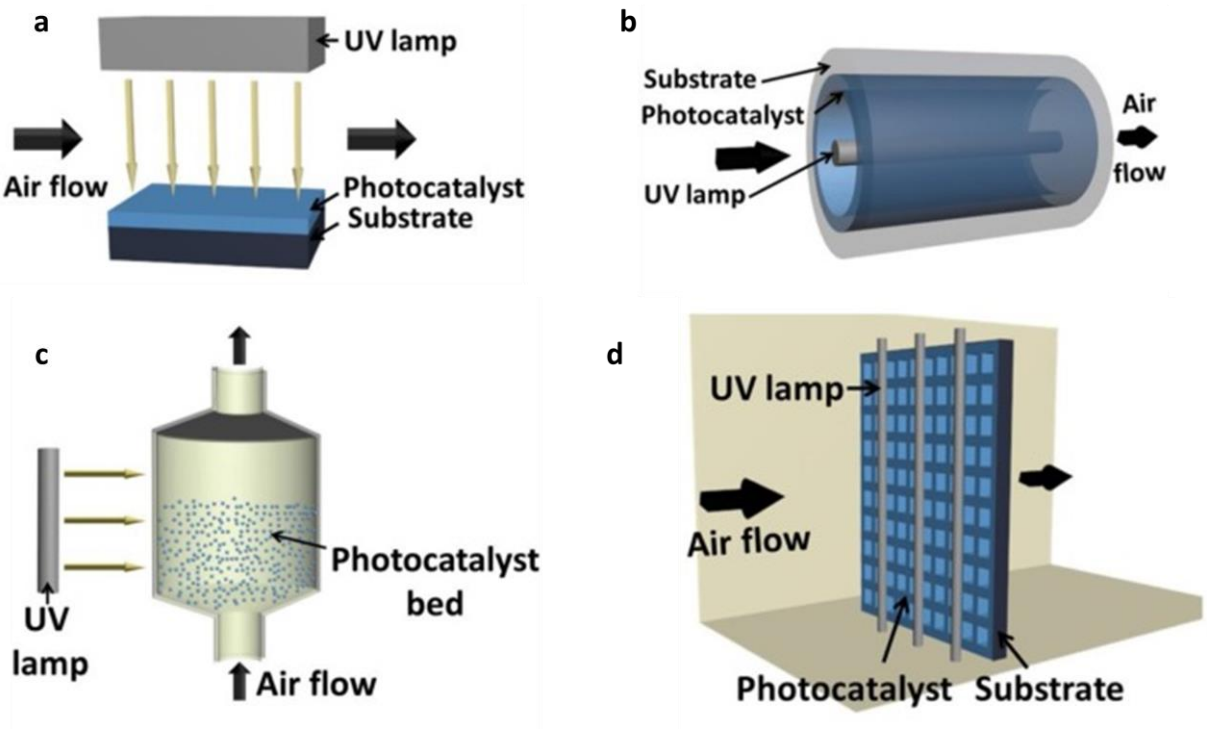

Figure 5 : Schematic representation of (a) plate, (b) annular, (c) fluidized bed and (d) monolith reactors [99]

Plate type reactors have the UV lamp placed parallel to the plate with the photocatalyst coated on plate surface. For the annular type reactors the UV lamps are enclosed by a cylinder and the photocatalyst is coated on the inner wall of the cylinder. Both of these reactors have a simple geometry and low pressure drop but have low mass transfer rate and low reaction surface area and good accessibility to light [85]. Though they are not designed for high air throughput, they are important in the determination of kinetic parameters [100]. In the fluidized bed reactors, gas flows through a photocatalyst bed and the UV lamps are placed outside the reactor. They allow high gas-feed rate, low pressure drop and high mass transfer rate but tend to suffer from loss of catalyst in entrained air, consequently catalyst replacement is needed or additional equipment are needed to separate and return the entrained catalyst to the reactor. The penetration of UV light is also restricted by the catalyst [101]. Monolith type reactors have the photocatalyst usually coated on a substrate with the UV lamps placed in front of the substrate. They have a high reaction area and intermediate convective mass transfer rate. However, the light intensity quickly declines through the monoliths [102].

Of the four reactor types described above the most commonly found in commercial air purification units is the monolith configuration because it provides high photocatalyst surface to volume ratio and is compact which allows it to be easily put in a standalone unit or

incorporated in the HVAC systems [103]. The photocatalysts used are usually in the form of monolithic filters or fibers which are referred to as photocatalytic media. The typical media geometry often utilized is a plane one in which the lamps are placed in front of the photocatalytic media and air is forced to move through the photocatalyst. However, for the media to be effective it must (i) have a high surface area to allow contact with as large a volume of reactants as possible, (ii) allow a better utilization of the light and (ii) allow a longer contact time between the reactants the photocatalyst [104]. Hence, modified reactor designs which include several photocatalytic media geometries like pleated configuration also exist to offer better conditions for photocatalytic reactions.

Indeed, Destaillats *et al*.[105] showed that the contact time was a critical parameter to be considered while investigating the performance of photocatalytic reactors under realistic conditions (i.e., gas mixtures and low pollutant concentrations). They suggested that the use of a pleated media could improve reactor performance by increasing the residence time in media and extending the contact time of pollutants in the photocatalytic media.

In this work, the photocatalytic reactor that is used is similar to a monolith reactor and is thus representative of available commercial units. The reactor design also allows the study of the influence of different photocatalytic media geometries. This could bring into evidence whether or not the change in media geometry improves the PCO efficiency.

I.3.3 Parameters influencing PCO efficiency

The effectiveness of the photocatalytic oxidation process is dependent on certain parameters. In order to optimize the performance of PCO, it is necessary to study how these parameters affect the photocatalytic degradation process. These parameters and their effects on PCO have been greatly studied in the literature [74,84,85,87,103]. These parameters can be categorized in two types; process parameters related to the reactor design (eg. air velocity, light intensity) and environmental parameters related to the characteristic of the air to be treated (e.g initial concentration, relative humidity, and presence of co-pollutants). The effects of the main parameters important for this work are described in the following sub sections.

I.3.3.1 Air velocity

In the literature, the effect of air velocity has been studied greatly for single pass reactors and its influence on the photocatalytic reaction is due to two processes, (i) the mass transfer and (ii) the contact time whose effects are antagonistic [104–106].

The mass transfer entails the transport of VOCs from the gas phase onto the photocatalyst surface. As the velocity increases, the number of molecules that are transported to the photocatalyst surface also increases. It therefore stands to reason that, an increase in the velocity tends to improve the mass transfer co-efficient between the air and the photocatalyst surface. This results in more pollutants being transferred to the surface to react with active species which consequently increases the degradation rate [109,110]. However, once the velocity reaches a certain value, the effect of mass transfer becomes negligible. In the meantime, when increasing the velocity, the residence time of the pollutants in the media is reduced thus the contact time between the pollutants and the photocatalyst decreases leading to a reduction in degradation rates [105,111,112]. In investigating the degradation of 5 VOCs, Yu *et al.* [113] showed that the degradation rate of these compounds were increased when the air flow rates were increased (0 - 600 $ml.min^{-1}$) attributed to the effect of mass transfer whilst on the other hand Ginestet *et al*. [114] found the degradation rate of toluene to be decreased in half when airflow rate increased from 40 $m^3.h^{-1}$ to 80 $m^3.h^{-1}$ which they attributed to the reduction of the contact time between the pollutants and the photocatalytic media.

The Reynolds number has been described as a good indicator to set an appropriate regime to determine mass transfer limitations. It has been demonstrated by Obee that with a Reynolds number over 500 the photocatalytic reaction is less influenced by mass transfer [115]. Most of the time, the Reynolds number is sufficiently high enough to neglect the effect of mass transfer.

In multi-pass reactors, in addition to the effect of contact time, another effect (also linked to the velocity), the number of passes of the pollutant through the media, comes into play. When the velocity within the media is increased, the contact time decreases but then the number of passes of the pollutant through the media increases. The superposition of these two effects subsequently makes it difficult to highlight the influence of velocity on the reaction rate. Consequently, the global effect of the velocity on the degradation remains the same irrespective of the velocity. This was evidenced by Dumont *et al.* [116] and Batault *et al.*

[117] when they degraded toluene in a multi pass reactor. Subsequently, it seems that in order to highlight the influence of velocity, it will be necessary to study or evaluate the single-pass removal efficiency.

I.3.3.2 Light intensity

Light intensity is one of the main parameters that influences the photocatalytic degradation and therefore plays a crucial role on the degradation rate. For a given wavelength, an increase in the light intensity leads to higher generation of the electron-hole pairs (e^-/h^+). Thus the degradation rate usually increases with higher light intensity [112].

The relationship between the light intensity and the photocatalytic degradation is described in the literature by a power law:

$$r = kI^n$$ **Equation 12**

Where *r* is the reaction rate, *k*, kinetic constant, *I* is the light intensity and *n* is the order of the reaction and takes values between 0 and 1.

At low light intensity, the production of electron-hole pairs is low and so they are rapidly consumed by the chemical reactions resulting in a linear increase in the reaction rate (n = 1). At medium- high light intensity, rate of formation of electron-hole pairs is higher than their consumption leading to recombination of the charges resulting half order increase in the reaction rate (n = 0.5). At very high light intensity, the electron-hole recombination is so fast that the reaction rate no longer depends on the light intensity and reaches a plateau (n = 0) [82,118]. A schematic representation of the order regimes is shown in Figure 6.

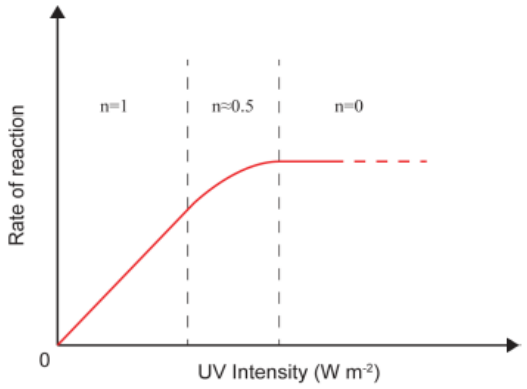

Figure 6 : Photocatalytic reaction rate and order regimes related to light intensity [119]

Yang *et al.* [120] studied the degradation of formaldehyde in a single-pass photocatalytic reactor equipped with UV-C lamps and TiO_2-coated foam nickel. They observed that when the light intensity increased from 0.15 to 0.25 $mW.cm^{-2}$, the reaction rate of formaldehyde increased linearly (n = 1) due to the rapid consumption of the electron hole pairs. When the light intensity was greater than 0.25 $mW.cm^{-2}$, the increase of the reaction rate followed a half order regime (n = 0.5) which they attributed to electron–hole recombination.

It should be mentioned that even though increment in the light intensity leads to higher degradation rate, excessive light intensity diminishes quantum efficiency and imposes unnecessary energy costs [121].

I.3.3.3 Initial concentration

With respect to different classes of VOCs and broad ranges of concentrations, it is generally agreed that an increase in the initial concentration leads lower removal efficiency and lower mineralization rates [94,122,123]. The impact of higher VOC concentration on PCO reactions can be analyzed from different aspects. As the concentration increases, the limitation of active sites lead to competitive adsorption thus, the ratio of active species to pollutant molecules decreases and consequently, more VOCs can leave the media without undergoing degradation [108]. Moreover, high amount of intermediates possibly generated during PCO reactions can occupy the active sites, impeding the degradation progress [124].

Mo *et al*. [94] found that the removal efficiency of toluene dropped by 30% when toluene concentration was increased from 1 to 4 ppm. They attributed this to the competitive adsorption effect between the toluene molecules. Similarly, Vildozo *et al.* [125] showed that increasing the inlet concentration of 2-propanol from 100 to 700 ppb significantly lowered the mineralization rate from ca. 90% to 63%. On the other hand Sleiman *et al.* [106], did not note any significant influence of inlet concentration (20 - 400 ppb) on the conversion and mineralization rates of toluene. They explained that at this range of toluene concentrations, the PCO is not limited by the number of active sites on TiO_2 and no competitive adsorption effect between the by-products and toluene occurs.

I.3.3.4 Relative humidity (RH)

Water vapor is known to play a dual role in PCO as on one hand it provides a promotive effect because adsorbed water molecules are oxidized to hydroxyl radicals which improve the PCO reactions and on the other hand, it has an inhibitive effect because excessive water competes with target VOCs for the same surface on the photocatalyst [85,87]. In the absence of water vapor, the photocatalytic degradation of some pollutants may be retarded but, excessive water vapor on the catalyst surface may lead to the decrease in reaction rate because water can occupy the active sites of the reactants on the surface [126–128]. Taking into consideration the opposing effects of RH, there could be an optimal value of RH before which efficiency ascends with RH and after which the inhibiting effect of competitive adsorption dominates and the efficiency descends with RH [112].

Luo and Ollis [129] studied the effect of water vapor on toluene and found that: (a) no toluene photodegradation occurred in the total absence of water in the toluene–air mixture, , (b) toluene oxidation rate increased by water concentration up to about 6%, (c) toluene oxidation rate began to decrease when water concentration increased to more than 15%, and toluene degradation was inhibited at 60% water concentration. The degree of the inhibition effect is determined by the affinity of the pollutants with the surface of the catalysts relative to water. Raillard *et al.*[130] reported that the PCO of acetone and 2-butanone was obviously inhibited by water vapor but that the effect of water vapor on the oxidation of acetone was much greater than on 2-butanone. They stated it also depended on the type of photocatalysts and the level of hyrophilicity of the PCO media.

I.3.3.5 Presence of other pollutants

The composition of indoor air is a multi-component one and contains several chemical pollutants and particulate matter (dust and bio-aerosols) [131–134]. The characteristics of these compounds can be quite different. This brings a challenge to the purification process of pollutant mixtures. Therefore, it is important to understand the interaction mechanisms of different pollutants during PCO.

It has been observed that the presence of these chemical pollutants can affect the conversion of a target VOC. On one hand, the presence of other pollutants contributes to the reduction of the adsorption of target VOCs. If several chemical compounds are degraded simultaneously, they will compete for adsorption on the catalyst surface in a way that depends

upon their affinity for sorption, and their concentrations. Consequently, the degradation rate of the target compound in a mixture may be lower than when this compound is treated alone [135–138]. Additionally, the presence of some intermediate compounds may also disrupt the degradation of the target compounds as they may compete for active sites on the catalyst surface. The higher the concentration of these chemicals is, the higher the yield of intermediates and thus the lower the adsorption of target VOCs [85,112,139]. On the other hand the presence of some chemical pollutants can promote the yield of reactive radicals such as Cl° which may in turn enhance the removal of co-existing pollutants [85].

The presence of particles (dust and bio-aerosols) could also potentially impact the degradation of target VOCs. In a study to determine the collection efficiency of QUARTZEL® PCO media for different size particles and for different loading rates (Figure 7), Hequet *et al.* [140] showed that depending on the particle size and loading rate, this media could trap some particles which could subsequently affect the photocatalytic degradation of VOCs

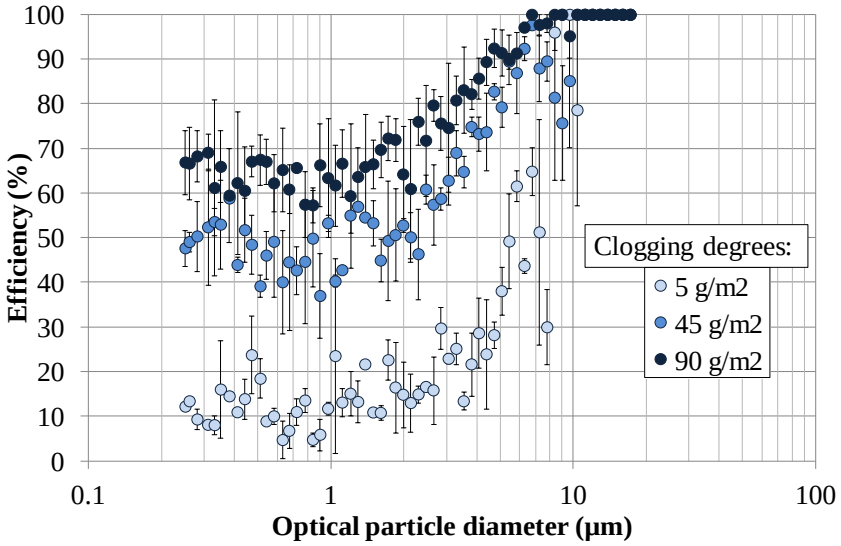

Figure 7 : Collection efficiency of QUARTZEL® PCO media as a function of particle diameter and loading rate [140]

I.3.3.6 Choice of influencing parameters

The parameters that have been previously discussed in section I.3.3 are important parameters that are necessary to evaluate the performance of a PCO reactor in degrading target pollutants. In this work, three process parameters (air velocity, light intensity and

change in media geometry) and four environmental parameters (initial pollutant concentration, presence of particles (bioaerosols), presence of chemical co-pollutants and relative humidity) are chosen.

The air velocity and light intensity are important process parameters which when studied help to give recommendations on their appropriate operating ranges to provide better degradation efficiency. Additionally, the study of the light intensity may provide some knowledge on the light intensity levels that would possibly avoid unnecessary energy costs.

The environmental parameters are studied to provide information on the performance of the PCO reactor under real conditions. As seen in section I.2.2, the concentrations of the chemical pollutants may vary in the OR thus studying the initial concentration in a range that is representative of real conditions provides information on the degradation efficiency when the concentrations are varied. Additionally it was also seen in this section that the OR is polluted by a variety of chemical pollutants thus it would also be necessary to provide information on how the presence of co-pollutants affects the degradation efficiency of the target compounds. In this study nitrous oxide and acetic acid were chosen to study the effect of co-pollutants on the degradation efficiency of the target pollutants. Nitrous oxide is an anesthetic pollutant typically found in ORs. Acetic acid however is a derivative of peracetic acid (sterilant) and was chosen to represent peracetic acid as the latter was not stable enough to allow its use. Based on the literature review it was shown that surgical smoke contains particles (tissue and microbial) which could be trapped by the photocatalytic media. There is a lack of information about how the presence of particles would influence the degradation process of VOCs thus their influence on the degradation efficiency of the target compounds is also studied. The relative humidity varies within the OR depending on the type of surgery that is to be performed thus a study of the influence of change in relative humidity is necessary to know how the degradation is affected in real OR humidity conditions.

Finally, the influence of the change in media geometry is also studied. According to Destaillats *et al*. [105], changing the media geometry (for example from plane to pleated) so that the developed surface is increased is a way to improve the degradation performance. They suggested that the improvement could be attributed to an increase in TiO_2 content, contact time and better irradiance distribution. However, experimentally confirming the influence of contact time and irradiance distribution could be difficult. In this work, the influence of geometry of the media is studied by comparing the degradation efficiency of the

target compounds using two geometries; plane and pleated. Additionally, numerical simulations are performed to better understand the role of the media geometry on PCO efficiency with regards to the contact time and irradiance distribution.

I.3.4 Performance evaluation of PCO

The performance of PCO systems is studied in order to evaluate the impact of the operating parameters and also to highlight the efficiency of the process to enable comparison with other treatment processes. In the literature, some performance indicators that have been used to enable the characterization of the effectiveness of PCO are described below.

Single-pass removal efficiency is a performance indicator that quantifies the fraction of the total flow that is treated as the air flows through the reactor. Single-pass efficiency can be calculated as follows:

$$\boldsymbol{\alpha = 1 - \frac{C}{C_0}} \qquad \textbf{Equation 13}$$

Where α is the single-pass removal efficiency, C_0 is the initial concentration of pollutant entering the reactor (ppm) and C is the final concentration of the pollutant leaving the reactor (ppm).

The Clean Air Delivery Rate (CADR), another performance indicator is a measure which characterizes the air cleaning capacity of a PCO reactor [141]. It is defined as the clean air volume that is delivered by the treatment system. The CADR ($m^3.h^{-1}$) for single-pass gaseous contaminant removal can be computed as:

$$\boldsymbol{CADR = \alpha QE} \qquad \textbf{Equation 14}$$

where α is the single-pass removal efficiency, Q is the air flow rate passing through the photocatalytic reactor ($m^3.h^{-1}$) and E is a short-circuit factor which equals 1 under well-mixed conditions. E is calculated as C_{in}/C_{avg} where C_{in} is the inlet concentration and C_{avg} is the average concentration in the reactor. In France, the CADR has been recommended in the AFNOR standard XP B44-013, as one of the performance indicators for the evaluation of photocatalytic prototypes and commercial devices. Costarramone *et al.* [142] compared the efficiency of several commercial photocatalytic air-purifiers in a large closed chamber at the ppb level under controlled conditions representative of indoor air. The comparison of efficiency was done using the CADR according to AFNOR XP B44-013. Based on their

work, they were able to recommend that the most efficient device was the one with high CADR and no by-product.

In a closed reactor, the kinetic constant which describes the reaction rate can also be used as an indicator. For a first order decay the kinetic rate constant can be calculated from:

$$\boldsymbol{C = C_o \exp(-k_{app} t)} \qquad \textbf{Equation 15}$$

where k_{app} is the kinetic constant (h^{-1}) and t is the time (h).

In terms of the energetic performance of the PCO reactor, the Operating Cost Effectiveness (OCE), also called the energy efficiency index is the indicator that is used [143,144]. Operating cost effectiveness can be found as follows:

$$\boldsymbol{OCE = \frac{CADR}{P_c}} \qquad \textbf{Equation 16}$$

where OCE is expressed in $m^3.h^{-1}kW^{-1}$ and P_c is the electric power consumption of the photocatalytic reactor (kW).

PCO is known to transform a wide range of pollutants into final products such H_2O, CO_2 and mineral acids. However, this reaction is not immediate. Most PCO reactions are stepwise which means they take several intermediate steps to form the final reaction products, and during these steps, various intermediates are formed. These unintended intermediates can be toxic or irritating and maybe more harmful to human health than their precursors. Consequently the safety of the PCO process becomes questionable and in addition, some of these intermediates poison the active sites on the photocatalyst resulting in deactivation of catalysts [84,85,145]. Ethanol photodegradation is known to produce formaldehyde and acetaldehyde which are toxic and carcinogenic [146,147]. In the case of toluene, benzaldehyde, benzoic acid, benzyl alcohol, benzene have been found to be the reaction intermediates [106,148,149]. It has been noted that the intermediates of chlorinated VOCs during PCO could be more toxic and hazardous than those of other VOCs [103]. For example, phosgene ($COCl_2$), dichloroacetyl chloride (DCAC) and trichloroacetyl chloride (TCAC), chloroform ($CHCl_3$), carbon tetrachloride (CCl_4), and carbon monoxide (CO) were observed in PCO process trichloroethylene (TCE) [150,151]. The safety of the PCO process with regards to the intermediates that are formed is therefore a necessary indicator to evaluate its

performance. The health related index (HRI) is the indicator that describes the potential health risks associated with the generation of intermediates [85]. It is defined as:

$$\boldsymbol{HRI_i = \frac{C_i}{REL_i}} \qquad \textbf{Equation 17}$$

Where C_i is the concentration of compound i and REL_i is the recommended exposure limit of compound i. It requires that the sum of all HRI not exceed the value of 1.

I.4 Choice of performance indicators

Commercial air purification units that are available on the market mostly operate under single-pass configuration in which a volume of air passes through the reactor once for treatment. Thus in order to evaluate the performance of photocatalytic oxidation in a way that is representative, the single-pass removal efficiency is chosen as the indicator. This choice of the single-pass removal efficiency is necessary to also highlight the influence of air velocity.

Additionally, as PCO is known to produce intermediate compounds whose toxicity could be higher than the precursor compounds, the health related index (HRI) was also chosen to help investigate the safety of PCO during the degradation of the target compounds.

I.5 Choice of target compounds

In order to evaluate the performance of PCO as an air treatment technology in the OR it is necessary to select some target compounds.

The target compounds that were chosen to be studied in this work are isoflurane ($C_3F_5H_2ClO$) and acrylonitrile (C_3H_3N). These two compounds were chosen generally because they belong to two of the main pollutants types that are specifically found in ORs; anesthetic gases (isoflurane) and surgical smoke (acrylonitrile). The fact that they belonged to two different chemical families would also allow the evaluation of the behavior of two different compounds towards degradation by PCO. Additionally, they are complex compounds and thus could potentially be important sources of intermediates.

The PCO of isoflurane has not been studied in the literature thus studying it is necessary to provide some knowledge on the effectiveness of PCO for its removal. In addition

it is a chlorinated compound capable of forming Cl° which may form some toxic intermediates. Thus it would be necessary to verify whether or not the PCO of isoflurane led to the formation of toxic intermediates.

The PCO of acrylonitrile has rarely been studied in the literature although it is classified as a hazardous pollutant. Moreover, these previous studies were however done at concentrations that were higher than what could potentially be found in ORs. It is necessary to have some information on the degradation of acrylonitrile at low concentrations representative of OR indoor air.

I.6 Conclusion on the literature review and objectives of this work

This chapter enabled the provision of the state of the art on the indoor air quality in hospitals. Just like any other indoor environment, the hospitals are polluted by both microbiological and chemical compounds. In hospitals, the main focus when it comes to indoor air quality was microbiological pollution because of the risk of nosocomial infections. However, due to the variety of activities that are undertaken in the various facilities in the hospitals, occupants (workers and patients) are exposed to a wide variety of chemical compounds which could have negative effects on their health.

In this work, the study for the choice of target compounds was limited to the OR. In the ORs, occupants could be exposed to waste anesthetic gases, residual sterilants and surgical smoke. Constant exposure to these compounds could lead to several negative health effects.

The conventional way of assuring good indoor air quality is through ventilation which aims at reducing the levels of pollutants by dilution with outside air. Due to drawbacks such as high energy costs and inability of installed filters to treat chemical pollutants it becomes necessary to employ air treatment techniques such as adsorption, UVGI, cold plasma and photocatalytic oxidation. PCO is an economical and energy efficient technology that could be used to degrade a variety of chemical pollutant and could potentially be used in the ORs. However, the studies that exist to evaluate the performance of these PCO devices in hospital environments are based solely on their ability to reduce microbial load. Consequently there is no information on the fate of these typical OR chemical pollutants when they were present in the air treated by these PCO devices.

In this chapter, the principles and influencing parameters of PCO were also detailed. It was shown that its performance is dependent on several parameters. The knowledge acquired from the study of the parameters would be necessary to help understand and validate the experimental results in this work.

The general aim of this PhD work is therefore to evaluate the capability of PCO for degrading specific chemical pollutants found in the OR by investigating the degradation efficiency and safety. To achieve this, the objectives of this PhD work are:

1) Perform a parametric evaluation on the degradation of isoflurane and acrylonitrile by studying the influence of air velocity, light intensity, the change in media geometry, initial pollutant concentration, presence of chemical co-pollutants, presence of particles (bioaerosols) and relative humidity on their degradation efficiencies.

2) Perform numerical simulations to better understand the role that the change in geometry has on the PCO performance during the degradation of the target molecules.

3) Evaluate the safety of the use of PCO for the degradation of isoflurane and acrylonitrile through the identification of possible intermediates formed during their degradation.

I.7 References

[1] C.-C. Jung, P.-C. Wu, C.-H. Tseng, H.-J. Su, Indoor air quality varies with ventilation types and working areas in hospitals, Build. Environ. 85 (2015) 190–195.

[2] M.P. Bivolarova, A.K. Melikov, C. Mizutani, K. Kajiwara, Z.D. Bolashikov, Bed-integrated local exhaust ventilation system combined with local air cleaning for improved IAQ in hospital patient rooms, Build. Environ. 100 (2016) 10–18. doi:10.1016/J.BUILDENV.2016.02.006.

[3] Centers for Disease Control and Prevention, Guidelines for Preventing the Transmission of Mycobacterium tuberculosis in Health-Care Settings, 2005, (2005).

[4] ASHRAE, ASHRAE 170-2017-Ventilation of Health Care Facilities, (2017). https://www.techstreet.com/ashrae/standards/ashrae-170-2017?product_id=1999079&ashrae_auth_token=12ce7b1d-2e2e-472b-b689-8065208f2e36 (accessed April 18, 2018).

[5] AFNOR, NF S90-351 - Health care institutions - Controlled environment areas - Requirements for airborne contamination control, (2013). https://www.boutique.afnor.org/norme/nf-s90-351/etablissements-de-sante-zones-a-environnement-maitrise-exigences-relatives-a-la-maitrise-de-la-contamination-aeroportee/article/809391/fa168416 (accessed April 18, 2018).

[6] S. Capolongo, G. Settimo, M. Gola, Indoor air quality in healthcare facilities, n.d.

[7] A. Berrube, D. Cavereau, L. Mosqueron, La Qualité de l'air interieur dans les hopitaux, Air Pur. 80 (2011) 31–38.

[8] Centre de Coordination de la Lutte contre les Infections Nosocomiales (CCLIN), Classification des locaux selon le risque infectieux. | Base documentaire | BDSP, 2004. (n.d.). http://www.bdsp.ehesp.fr/Base/309976/ (accessed May 3, 2018).

[9] Victoria State Government, Cleaning standards for Victorian health facilities, 2011. (n.d.). https://www2.health.vic.gov.au/about/publications/researchandreports/Cleaning-standards-for-Victorian-health-facilities-2011-August (accessed May 3, 2018).

[10] V. Bessonneau, L. Mosqueron, A. Berrubé, G. Mukensturm, S. Buffet-Bataillon, J.-P. Gangneux, O. Thomas, VOC Contamination in Hospital, from Stationary Sampling of a Large Panel of Compounds, in View of Healthcare Workers and Patients Exposure Assessment, PLoS One. 8 (2013). doi:10.1371/journal.pone.0055535.

[11] H.-W. Chen, C.-Y. Chuang, H.-T. Lin, Indoor Air Distribution of Nitrogen Dioxide and Ozone in Urban Hospitals, Bull. Environ. Contam. Toxicol. 83 (2009) 147–150. doi:10.1007/s00128-009-9631-x.

[12] The Danish Technological Institute, Emission and evaluation of chemical substances from selected electricaland electronic products - part 2, (2005).

[13] INERIS, Exposition de la population française au bruit de fond du formaldéhyde et risques sanitaires associés. Rapport final. | Base documentaire | BDSP, (2004).

[14] R.A. Rudel, D.E. Camann, J.D. Spengler, L.R. Korn, J.G. Brody, Phthalates, Alkylphenols, Pesticides, Polybrominated Diphenyl Ethers, and Other Endocrine-Disrupting Compounds in Indoor Air and Dust, Environ. Sci. Technol. 37 (2003) 4543–4553. doi:10.1021/es0264596.

[15] E. Baurès, O. Blanchard, M. Fabien, E. Surget, P. Le Cann, A. Rivier, J.P. Gangneux, A. Florentin, La qualité de l'air intérieur dans les hôpitaux, Les Cah. La Rech. Santé, Environnement, Trav. (2016) 50–51. https://hal-anses.archives-ouvertes.fr/anses-01766347 (accessed July 12, 2018).

[16] S. Koda, S. Kumagai, H. Ohara, Environmental monitoring and assessment of short-term exposures to hazardous chemicals of a sterilization process in hospital working environments, Acta Med. Okayama. 53 (1999) 217–223.

[17] T. Takigawa, T. Horike, Y. Ohashi, H. Kataoka, D.-H. Wang, S. Kira, Were volatile

organic compounds the inducing factors for subjective symptoms of employees working in newly constructed hospitals?, Environ. Toxicol. 19 (2004) 280–290. doi:10.1002/tox.20035.

[18] E.G. Dascalaki, A. Lagoudi, C.A. Balaras, A.G. Gaglia, Air quality in hospital operating rooms, Build. Environ. 43 (2008) 1945–1952. doi:10.1016/j.buildenv.2007.11.015.

[19] E.N. Brown, R. Lydic, N.D. Schiff, General anesthesia, sleep, and coma., N. Engl. J. Med. 363 (2010) 2638–50. doi:10.1056/NEJMra0808281.

[20] NIOSH, Waste Anesthetic gases: Occupational Hazards in Hospitals, 2007. https://www.cdc.gov/niosh/docs/2007-151/pdfs/2007-151.pdf (accessed April 30, 2018).

[21] OSHA, Anesthetic Gases: Guidelines for Workplace Exposures, (2000). file:///Z:/HWHYTE/THESE/PAPERS/Anesthetic gases/Papers/Anesthetic Gases Guidelines for Workplace Exposures.htm (accessed April 30, 2018).

[22] J.S. Yasny, J. White, Environmental Implications of Anesthetic Gases, Anesth. Prog. 59 (2012) 154–158. doi:10.2344/0003-3006-59.4.154.

[23] NIOSH, Waste Anesthetic Gases–Occupational Hazards in Hospitals, (2007).

[24] Occupational Safety & Health Administration, Anesthetic Gases: Guidelines for Workplace Exposures, (2000).

[25] K. Sitarek, W. Wesołowski, M. Kucharska, G. Celichowski, Concentrations of anaesthetic gases in hospital operating theatres, Int. J. Occup. Med. Environ. Health. 13 (2000) 61–66.

[26] J. Crea, M. Tkaczuk, Follow-up study of anaesthetic pollution in hospital operating theatres, veterinary and dental surgeries, The Authors, Adelaide, 1997.

[27] A. Jafari, R. Bargeshadi, F. Jafari, I. Mohebbi, M. Hajaghazadeh, Environmental and biological measurements of isoflurane and sevoflurane in operating room personnel, Int. Arch. Occup. Environ. Health. 91 (2018) 349–359. doi:10.1007/s00420-017-1287-y.

[28] K. Hoerauf, M. Lierz, G. Wiesner, K. Schroegendorfer, P. Lierz, A. Spacek, L. Brunnberg, M. Nüsse, Genetic damage in operating room personnel exposed to isoflurane and nitrous oxide., Occup. Environ. Med. 56 (1999) 433–437. doi:10.1136/oem.56.7.433.

[29] W.P. Chang, C.W. Kau, S.S. Hseu, Exposure of anesthesiologists to nitrous oxide during pediatric anesthesia., Ind. Health. 35 (1997) 112–8. http://www.ncbi.nlm.nih.gov/pubmed/9009509 (accessed July 23, 2018).

[30] J. Passeron, A. Guilleux, M. Guillemot, E. Langlois, F. Pillière, Protoxyde d'azote lors de l'utilisation du MEOPA en milieu de soins : toxicité, situations d'exposition, données métrologiques, pistes de prévention et rôle du médecin du travail - Article de revue - INRS, Références En Santé Au Trav. (2016).

[31] D.H. Spach, F.E. Silverstein, W.E. Stamm, Transmission of infection by gastrointestinal endoscopy and bronchoscopy., Ann. Intern. Med. 118 (1993) 117–28. http://www.ncbi.nlm.nih.gov/pubmed/8416308 (accessed May 1, 2018).

[32] D.J. Weber, W.A. Rutala, Lessons From Outbreaks Associated With Bronchoscopy, Infect. Control Hosp. Epidemiol. 22 (2001) 403–408. doi:10.1086/501924.

[33] H. Meyers, B.A. BrownElliott, D. Moore, J. Curry, C. Truong, Y. Zhang, R.J. Wallace, Jr., An Outbreak of *Mycobacterium chelonae* Infection Following Liposuction, Clin. Infect. Dis. 34 (2002) 1500–1507. doi:10.1086/340399.

[34] W.A. Rutala, D.J. Weber, Infection control: the role of disinfection and sterilization, J. Hosp. Infect. 43 (1999) S43–S55. doi:10.1016/S0195-6701(99)90065-8.

[35] W.A. Rutala, D.J. Weber, Guideline for disinfection and sterilization in healthcare

facilities, 2008, 2008. https://stacks.cdc.gov/view/cdc/11560 (accessed May 1, 2018).
[36] G.C.C. Mendes, T.R.S. Brandão, C.L.M. Silva, Ethylene oxide sterilization of medical devices: A review, Am. J. Infect. Control. 35 (2007) 574–581. doi:10.1016/J.AJIC.2006.10.014.
[37] A.J. Wilson, S. Nayak, Disinfection, sterilization and disposables, Anaesth. Intensive Care Med. 17 (2016) 475–479. doi:10.1016/J.MPAIC.2016.07.002.
[38] W.A. Rutala, D.J. Weber, Disinfection and sterilization: An overview, Am. J. Infect. Control. 41 (2013) S2–S5. doi:10.1016/J.AJIC.2012.11.005.
[39] W.A. Rutala, D.J. Weber, Clinical effectiveness of low-temperature sterilization technologies, Infect. Control Hosp. Epidemiol. 19 (1998) 798–804.
[40] Center for Disease Control and Prevention, Guidelines for Environmental Infection Control in Health-Care Facilities: Recommendations of CDC and the Healthcare Infection Control Practices Advisory Committee (HICPAC), 2013.
[41] W. Wesołowski, K. Sitarek, Occupational exposure to ethylene oxide of hospital staff., Int. J. Occup. Med. Environ. Health. 12 (1999) 59–65. http://www.ncbi.nlm.nih.gov/pubmed/10360085 (accessed May 1, 2018).
[42] M. Pacenti, S. Dugheri, P. Boccalon, G. Arcangeli, P. Dolara, V. Cupelli, Air monitoring and assessment of occupational exposure to peracetic acid in a hospital environment., Ind. Health. 48 (2010) 217–21. http://www.ncbi.nlm.nih.gov/pubmed/20424354 (accessed May 1, 2018).
[43] K. Yahata, K. Fujishiro, H. Hori, T. Higashi, An Investigation of Symptoms in Ethylene Oxide Sterilization Workers in Hospitals, J. Occup. Health. 43 (2001) 180–184. doi:10.1539/joh.43.180.
[44] National Research Council (US) Committee on Acute Exposure Guideline Levels, Peracetic Acid Acute Exposure Guideline Levels, in: Acute Expo. Guidel. Levels Sel. Airborne Chem. Vol. 8., National Academies Press (US), Washignton Dc, 2010. https://www.ncbi.nlm.nih.gov/books/NBK220001/ (accessed May 1, 2018).
[45] Agence nationale de sécurité du médicament et des produits de Santé, Dispositifs médicaux stérilisés à l'oxyde d'éthylène et utilisés dans les services de néonatalogie et pédiatrie : Rappel de la réglementation aux fabricants - Point d'Information - ANSM : Agence nationale de sécurité du médicament et des produits de santé, (n.d.). http://ansm.sante.fr/S-informer/Points-d-information-Points-d-information/Dispositifs-medicaux-sterilises-a-l-oxyde-d-ethylene-et-utilises-dans-les-services-de-neonatalogie-et-pediatrie-Rappel-de-la-reglementation-aux-fabricants-Point-d-Information (accessed July 23, 2018).
[46] K. Ball, Surgical smoke: is it safe to breathe?, 18 (1996) 16–21. https://www.scopus.com/record/display.uri?eid=2-s2.0-0030228375&origin=inward&txGid=a556e357f5a992904fcab940b271a5fb (accessed May 1, 2018).
[47] J.K.-M. Fan, F.S.-Y. Chan, K.-M. Chu, Surgical Smoke, Asian J. Surg. 32 (2009) 253–257. doi:10.1016/S1015-9584(09)60403-6.
[48] E. Alp, D. Bijl, R.P. Bleichrodt, B. Hansson, A. Voss, Surgical smoke and infection control, J. Hosp. Infect. 62 (2006) 1–5. doi:10.1016/j.jhin.2005.01.014.
[49] K.J. Weld, S. Dryer, C.D. Ames, K. Cho, C. Hogan, M. Lee, P. Biswas, J. Landman, Analysis of Surgical Smoke Produced by Various Energy-Based Instruments and Effect on Laparoscopic Visibility, J. Endourol. 21 (2007) 347–351. doi:10.1089/end.2006.9994.
[50] J.-G. DesCôteaux, P. Picard, É.C. Poulin, M. Baril, Preliminary study of electrocautery smoke particles produced in vitro and during laparoscopic procedures, Surg. Endosc. 10 (1996) 152–158. doi:10.1007/BF00188362.

[51] M. Gianella, D. Hahnloser, J.M. Rey, M.W. Sigrist, Quantitative Chemical Analysis of Surgical Smoke Generated During Laparoscopic Surgery With a Vessel-Sealing Device, Surg. Innov. 21 (2014) 170–179. doi:10.1177/1553350613492025.

[52] A.R. Moot, K.M. Ledingham, P.F. Wilson, S.T. Senthilmohan, D.R. Lewis, J. Roake, R. Allardyce, Composition of volatile organic compounds in diathermy plume as detected by selected ion flow tube mass spectrometry, ANZ J. Surg. 77 (2007) 20–23. doi:10.1111/j.1445-2197.2006.03827.x.

[53] W.L. Barrett, S.M. Garber, Surgical smoke: a review of the literature, Surg. Endosc. Other Interv. Tech. 17 (2003) 979–987. doi:10.1007/s00464-002-8584-5.

[54] O.S. Al Sahaf, I. Vega-Carrascal, F.O. Cunningham, J.P. McGrath, F.J. Bloomfield, Chemical composition of smoke produced by high-frequency electrosurgery, Ir. J. Med. Sci. 176 (2007) 229–232. doi:10.1007/s11845-007-0068-0.

[55] D.S. Hill, J.K. O'Neill, R.J. Powell, D.W. Oliver, Surgical smoke - a health hazard in the operating theatre: a study to quantify exposure and a survey of the use of smoke extractor systems in UK plastic surgery units, J. Plast. Reconstr. Aesthetic Surg. JPRAS. 65 (2012) 911–916. doi:10.1016/j.bjps.2012.02.012.

[56] N. Mowbray, J. Ansell, N. Warren, P. Wall, J. Torkington, Is surgical smoke harmful to theater staff? a systematic review, Surg. Endosc. 27 (2013) 3100–3107. doi:10.1007/s00464-013-2940-5.

[57] C.A. Balaras, E. Dascalaki, A. Gaglia, HVAC and indoor thermal conditions in hospital operating rooms, Energy Build. 39 (2007) 454–470. doi:10.1016/j.enbuild.2006.09.004.

[58] E.G. Dascalaki, A.G. Gaglia, C.A. Balaras, A. Lagoudi, Indoor environmental quality in Hellenic hospital operating rooms, Energy Build. 41 (2009) 551–560. doi:10.1016/J.ENBUILD.2008.11.023.

[59] K.. Wong, H.. Kamar, N. Kamsah, H. Tan, M.. deris, Real-Time Measurements of Relative Humidity and Temperature in Hospital Operating Room, Int. J. Mech. Prod. Eng. 5 (2017) 92–95. http://ijmpe.iraj.in/paper_detail.php?paper_id=9530&name=Real-Time_Measurements_of_Relative_Humidity_and_Temperature_in_Hospital_Operating_Room (accessed May 10, 2018).

[60] German Institute for Standardization, DIN 1946-4 : Ventilation and air conditioning - Part 4: VAC systems in buildings and rooms used in the health care sector, 2008. (n.d.). https://global.ihs.com/doc_detail.cfm?document_name=DIN 1946-4 (accessed May 2, 2018).

[61] Canadian Standards Association, CAN/CSA-Z317.2-15 Special requirements for heating, ventilation, and air- conditioning (HVAC) systems in health care facilities, (2015). http://shop.csa.ca/en/canada/health-care-facility-engineering/cancsa-z3172-15/invt/27013482015 (accessed April 18, 2018).

[62] T.. Chow, X.. Yang, Ventilation performance in operating theatres against airborne infection: review of research activities and practical guidance, J. Hosp. Infect. 56 (2004) 85–92. doi:10.1016/j.jhin.2003.09.020.

[63] T.T. Chow, X.Y. Yang, Ventilation performance in the operating theatre against airborne infection: numerical study on an ultra-clean system, J. Hosp. Infect. 59 (2005) 138–147. doi:10.1016/j.jhin.2004.09.006.

[64] A.M. Spagnolo, G. Ottria, D. Amicizia, F. Perdelli, M.L. Cristina, Operating theatre quality and prevention of surgical site infections., J. Prev. Med. Hyg. 54 (2013) 131–7. http://www.ncbi.nlm.nih.gov/pubmed/24783890 (accessed May 2, 2018).

[65] Energie plus, La norme NF S 90-351: établissement de santé: salles propres et environnements maîtrisés et apparentés, (n.d.). https://www.energieplus-

lesite.be/index.php?id=11810#c1857+c1858+c1861+c1862+c1863 © Architecture et Climat - Faculté d'architecture, d'ingénierie architecturale, d'urbanisme (LOCI) – Université catholique de Louvain (Belgique) (accessed July 23, 2018).

[66] F. Memarzadeh, J. Jiang, Effect of operation room geometry and ventilation system parameter variations on the protection of the surgical site, (2010).

[67] and A.-C.E. American Society of Heating, Refrigerating, Chapter 7: Health care facilities, in: ASHRAE Handb. HVAC Appl., 2007.

[68] L. Zhong, J.J. Brancho, S. Batterman, B.M. Bartlett, C. Godwin, Experimental and modeling study of visible light responsive photocatalytic oxidation (PCO) materials for toluene degradation, Appl. Catal. B Environ. 216 (2017) 122–132. doi:10.1016/J.APCATB.2017.05.047.

[69] W. Chen, J.J. Zhang, Z. Zhibin, Performance of Air Cleaners for Removing Multi-Volatile Organic Compounds in Indoor Air, ASHRAE Trans. 111 (2005) 1101–1114. https://www.researchgate.net/publication/275344400 (accessed May 28, 2018).

[70] Société Franciase d'Hygiène Hospitalière, Qualité de l'air au bloc opératoire et autres secteurs interventionnels, 2015.

[71] F. Batault, F. Thevenet, V. Hequet, C. Raillard, L. Le Coq, N. Locoge, Acetaldehyde and acetic acid adsorption on TiO_2 under dry and humid conditions, Chem. Eng. J. 264 (2015) 197–210. doi:10.1016/J.CEJ.2014.10.089.

[72] M. Perraud, M.C. Nicolle, E. Chiarello, F. Tissot Guerraz, J.C. Cetre, M. Sepetjan, Air filtration and prevention of aspergillary pneumopathies. Preliminary comparative study of two mobile units for bacteriological air purification with recycling, Nouv. Rev. Fr. Hematol. 34 (1992) 295–299.

[73] R.A. Rosenbaum, J.S. Benyo, R.E. O'Connor, B.A. Passarello, D.R. Williams, B.D. Humphrey, R.W. Ross, J.M. Berry, J.G. Krebs, Use of a portable forced air system to convert existing hospital space into a mass casualty isolation area, Ann. Emerg. Med. 44 (2004) 628–634. doi:10.1016/j.annemergmed.2004.03.012.

[74] J. Zhao, X. Yang, Photocatalytic oxidation for indoor air purification: a literature review, Build. Environ. 38 (2003) 645–654. doi:10.1016/S0360-1323(02)00212-3.

[75] C. Wang, J.-Y. Xi, H.-Y. Hu, Y. Yao, Advantages of combined UV photodegradation and biofiltration processes to treat gaseous chlorobenzene, J. Hazard. Mater. 171 (2009) 1120–1125. doi:10.1016/J.JHAZMAT.2009.06.129.

[76] A. Luengas, A. Barona, C. Hort, G. Gallastegui, V. Platel, A. Elias, A review of indoor air treatment technologies, Rev. Environ. Sci. Bio/Technology. 14 (2015) 499–522. doi:10.1007/s11157-015-9363-9.

[77] W.A. Jacoby, D.M. Blake, J.A. Penned, J.E. Boulter, L.M. Vargo, M.C. George, S.K. Dolberg, Heterogeneous Photocatalysis for Control of Volatile Organic Compounds in Indoor Air, J. Air Waste Manage. Assoc. 46 (1996) 891–898. doi:10.1080/10473289.1996.10467525.

[78] J.-H. Kim, G. Seo, D.-L. Cho, B.-C. Choi, J.-B. Kim, H.-J. Park, M.-W. Kim, S.-J. Song, G.-J. Kim, S. Kato, Development of air purification device through application of thin-film photocatalyst, Catal. Today. 111 (2006) 271–274. doi:10.1016/J.CATTOD.2005.10.058.

[79] V. Bergeron, G. Reboux, J.L. Poirot, N. Laudinet, Decreasing Airborne Contamination Levels in High-Risk Hospital Areas Using a Novel Mobile Air-Treatment Unit, Infect. Control Hosp. Epidemiol. 28 (2007) 1181–1186. doi:10.1086/520733.

[80] T. Schoenleber, H. Gbaguidi Haore, L. Jeunet, D. Talon, Évaluation d'un dispositif mobile de décontamination pour la maîtrise de l'air au bloc opératoire., Hygienes. 15 (2007) 158–164.

[81] N. Cram, N. Shipman, J. Quarles, Reducing Airborne Microbes in the Surgical

Operating Theater & Other Clinical Settings: A Study Utilizing the AiroCide TM System, (2011). http://industrial.airocide.com/healthcare/case-studies/operating-rooms-study/Default.aspx (accessed July 24, 2018).

[82] J.-M. Herrmann, Heterogeneous photocatalysis: State of the art and present applications, Top. Catal. 34 (2005) 49–65. doi:10.1007/s11244-005-3788-2.

[83] K.I. Zamaraev, Photocatalysis: State of the art and perspectives, Stud. Surf. Sci. Catal. 101 (1996) 35–50. doi:10.1016/S0167-2991(96)80213-8.

[84] L. Lin, Y. Chai, B. Zhao, W. Wei, D. He, B. He, Q. Tang, Photocatalytic oxidation for degradation of VOCs, Open J. Inorg. Chem. 03 (2013) 14–25. doi:10.4236/ojic.2013.31003.

[85] J. Mo, Y. Zhang, Q. Xu, J.J. Lamson, R. Zhao, Photocatalytic purification of volatile organic compounds in indoor air: A literature review, Atmos. Environ. 43 (2009) 2229–2246. https://www.sciencedirect.com/science/article/pii/S135223100900065X#sec4 (accessed April 23, 2018).

[86] M. Zeng, Y. Li, M. Mao, J. Bai, L. Ren, X. Zhao, Synergetic Effect between Photocatalysis on TiO_2 and Thermocatalysis on CeO_2 for Gas-Phase Oxidation of Benzene on TiO_2 /CeO_2 Nanocomposites, ACS Catal. 5 (2015) 3278–3286. doi:10.1021/acscatal.5b00292.

[87] A.H. Mamaghani, F. Haghighat, C.-S.S. Lee, Photocatalytic oxidation technology for indoor environment air purification: The state-of-the-art, Appl. Catal. B Environ. 203 (2017) 247–269. doi:10.1016/J.APCATB.2016.10.037.

[88] E. Kabir, K.-H. Kim, A Review of Some Representative Techniques for Controlling the Indoor Volatile Organic Compounds, Asian J. Atmos. Environ. 6 (2012) 137–146. doi:10.5572/ajae.2012.6.3.137.

[89] J. Peral, X. Domènech, D.F. Ollis, Heterogeneous Photocatalysis for Purification, Decontamination and Deodorization of Air, J. Chem. Technol. Biotechnol. 70 (1997) 117–140. doi:10.1002/(SICI)1097-4660(199710)70:2<117::AID-JCTB746>3.0.CO;2-F.

[90] M.R. Hoffmann, S.T. Martin, W. Choi, D.W. Bahnemann, Environmental Applications of Semiconductor Photocatalysis, Chem. Rev. 95 (1995) 69–96. doi:10.1021/cr00033a004.

[91] R. Thiruvenkatachari, S. Vigneswaran, I.S. Moon, A review on UV/TiO_2 photocatalytic oxidation process (Journal Review), Korean J. Chem. Eng. 25 (2008) 64–72. doi:10.1007/s11814-008-0011-8.

[92] D.F. Ollis, Photocatalytic purification and remediation of contaminated air and water, Comptes Rendus l'Académie Des Sci. - Ser. IIC - Chem. 3 (2000) 405–411. doi:10.1016/S1387-1609(00)01169-5.

[93] A. Fujishima, X. Zhang, Titanium dioxide photocatalysis: present situation and future approaches, Comptes Rendus Chim. 9 (2006) 750–760. doi:10.1016/J.CRCI.2005.02.055.

[94] J. Mo, Y. Zhang, Q. Xu, R. Yang, Effect of TiO_2/adsorbent hybrid photocatalysts for toluene decomposition in gas phase, J. Hazard. Mater. 168 (2009) 276–281. doi:10.1016/J.JHAZMAT.2009.02.033.

[95] L. Zhong, F. Haghighat, Photocatalytic air cleaners and materials technologies – Abilities and limitations, Build. Environ. 91 (2015) 191–203. doi:10.1016/J.BUILDENV.2015.01.033.

[96] M. Lim, Y. Zhou, L. Wang, V. Rudolph, G.Q. (Max) Lu, Development and potential of new generation photocatalytic systems for air pollution abatement: an overview, Asia-Pacific J. Chem. Eng. 4 (2009) 387–402. doi:10.1002/apj.321.

[97] Y. Nosaka, M.A. Fox, Kinetics for electron transfer from laser-pulse irradiated colloidal semiconductors to adsorbed methylviologen: dependence of the quantum yield on incident pulse width, J. Phys. Chem. 92 (1988) 1893–1897. doi:10.1021/j100318a039.

[98] A.L. Linsebigler, G. Lu, J.T. Yates, Photocatalysis on TiO_2 Surfaces: Principles, Mechanisms, and Selected Results, Chem. Rev. 95 (1995) 735–758. doi:10.1021/cr00035a013.

[99] H. Ren, P. Koshy, W.-F. Chen, S. Qi, C.C. Sorrell, Photocatalytic materials and technologies for air purification, J. Hazard. Mater. 325 (2017) 340–366. doi:10.1016/j.jhazmat.2016.08.072.

[100] J. Mo, Y. Zhang, R. Yang, Novel insight into VOC removal performance of photocatalytic oxidation reactors, Indoor Air. 15 (2005) 291–300. doi:10.1111/j.1600-0668.2005.00374.x.

[101] L.A. Dibble, G.B. Raupp, Fluidized-bed photocatalytic oxidation of trichloroethylene in contaminated air streams, Environ. Sci. Technol. 26 (1992) 492–495. doi:10.1021/es00027a006.

[102] M.M. Hossain, G.B. Raupp, S.O. Hay, T.N. Obee, Three-dimensional developing flow model for photocatalytic monolith reactors, AIChE J. 45 (1999) 1309–1321. doi:10.1002/aic.690450615.

[103] Y. Boyjoo, H. Sun, J. Liu, V.K. Pareek, S. Wang, A review on photocatalysis for air treatment: From catalyst development to reactor design, Chem. Eng. J. 310 (2017) 537–559. doi:10.1016/J.CEJ.2016.06.090.

[104] M. Birnie, S. Riffat, M. Gillott, Photocatalytic reactors: design for effective air purification, Int. J. Low-Carbon Technol. 1 (2006) 47–58. doi:10.1093/ijlct/1.1.47.

[105] H. Destaillats, M. Sleiman, D.P. Sullivan, C. Jacquiod, J. Sablayrolles, L. Molins, Key parameters influencing the performance of photocatalytic oxidation (PCO) air purification under realistic indoor conditions, Appl. Catal. B Environ. 128 (2012) 159–170. doi:10.1016/j.apcatb.2012.03.014.

[106] M. Sleiman, P. Conchon, C. Ferronato, J.-M. Chovelon, Photocatalytic oxidation of toluene at indoor air levels (ppbv): Towards a better assessment of conversion, reaction intermediates and mineralization, Appl. Catal. B Environ. 86 (2009) 159–165.

[107] D. Farhanian, F. Haghighat, C.-S.S. Lee, N. Lakdawala, Impact of design parameters on the performance of ultraviolet photocatalytic oxidation air cleaner, Build. Environ. 66 (2013) 148–157.

[108] F.V.S.S. Lopes, R.A.R.R. Monteiro, A.M.T.T. Silva, G. V. Silva, J.L. Faria, A.M. Mendes, V.J.P.P. Vilar, R.A.R.R. Boaventura, Insights into UV-TiO_2 photocatalytic degradation of PCE for air decontamination systems, Chem. Eng. J. (2012) 244–257. https://www.sciencedirect.com/science/article/pii/S1385894712009813 (accessed May 7, 2018).

[109] K.-H. Wang, H.-H. Tsai, Y.-H. Hsieh, The kinetics of photocatalytic degradation of trichloroethylene in gas phase over TiO_2 supported on glass bead, Appl. Catal. B Environ. 17 (1998) 313–320. doi:10.1016/S0926-3373(97)00099-4.

[110] H. Yu, K. Zhang, C. Rossi, Experimental Study of the Photocatalytic Degradation of Formaldehyde in Indoor Air using a Nano-particulate Titanium Dioxide Photocatalyst, Indoor Built Environ. 16 (2007) 529–537. doi:10.1177/1420326X07083513.

[111] N. Quici, M.L. Vera, H. Choi, G.L. Puma, D.D. Dionysiou, M.I. Litter, H. Destaillats, Effect of key parameters on the photocatalytic oxidation of toluene at low concentrations in air under 254+185nm UV irradiation, Appl. Catal. B Environ. 95 (2010) 312–319. doi:10.1016/j.apcatb.2010.01.009.

[112] L. Zhong, F. Haghighat, P. Blondeau, J. Kozinski, Modeling and physical

interpretation of photocatalytic oxidation efficiency in indoor air applications, Build. Environ. 45 (2010) 2689–2697.

[113] K.-P. Yu, G.W.M. Lee, W.-M. Huang, C. Wu, S. Yang, The correlation between photocatalytic oxidation performance and chemical/physical properties of indoor volatile organic compounds, Atmos. Environ. 40 (2006) 375–385. doi:10.1016/J.ATMOSENV.2005.09.045.

[114] A. Ginestet, D. Pugnet, J. Rowley, K. Bull, H. Yeomans, Development of a new photocatalytic oxidation air filter for aircraft cabin, Indoor Air. 15 (2005) 326–334. doi:10.1111/j.1600-0668.2005.00369.x.

[115] T.N. Obee, Photooxidation of Sub-Parts-per-Million Toluene and Formaldehyde Levels on Titania Using a Glass-Plate Reactor, Environ. Sci. Technol. 30 (1996) 3578–3584. doi:10.1021/es9602713.

[116] E. Dumont, V. Héquet, Determination of the Clean Air Delivery Rate (CADR) of Photocatalytic Oxidation (PCO) Purifiers for Indoor Air Pollutants Using a Closed-Loop Reactor. Part I: Theoretical Considerations, Molecules. 22 (2017). doi:10.3390/molecules22030407.

[117] F. Batault, V. Héquet, C. Raillard, F. Thévenet, N. Locoge, L. Le Coq, How chemical and physical mechanisms enable the influence of the operating conditions in a photocatalytic indoor air treatment device to be modeled, Chem. Eng. J. 307 (2017) 766–775. doi:10.1016/j.cej.2016.08.118.

[118] D.F. Ollis, E. Pelizzetti, N. Serpone, Photocatalyzed destruction of water contaminants, Environ. Sci. Technol. 25 (1991) 1522–1529. doi:10.1021/es00021a001.

[119] M. Vezzoli, Intrinsic kinetics of titania photocatalysis : simplified models for their investigation, Queensland University of Technology, 2012. https://eprints.qut.edu.au/51574/ (accessed July 25, 2018).

[120] L. Yang, Z. Liu, Study on light intensity in the process of photocatalytic degradation of indoor gaseous formaldehyde for saving energy, Energy Convers. Manag. 48 (2007) 882–889. doi:10.1016/J.ENCONMAN.2006.08.023.

[121] W. Wang, Y. Ku, Photocatalytic degradation of gaseous benzene in air streams by using an optical fiber photoreactor, J. Photochem. Photobiol. A Chem. 159 (2003) 47–59. doi:10.1016/S1010-6030(03)00111-4.

[122] A. Bouzaza, C. Vallet, A. Laplanche, Photocatalytic degradation of some VOCs in the gas phase using an annular flow reactor: Determination of the contribution of mass transfer and chemical reaction steps in the photodegradation process, J. Photochem. Photobiol. A Chem. 177 (2006) 212–217. doi:10.1016/J.JPHOTOCHEM.2005.05.027.

[123] P.-A. Deveau, F. Arsac, P.-X. Thivel, C. Ferronato, F. Delpech, J.-M. Chovelon, P. Kaluzny, C. Monnet, Different methods in TiO2 photodegradation mechanism studies: Gaseous and TiO_2-adsorbed phases, J. Hazard. Mater. 144 (2007) 692–697. doi:10.1016/J.JHAZMAT.2007.01.097.

[124] L. Zhong, F. Haghighat, C.-S. Lee, N. Lakdawala, Performance of ultraviolet photocatalytic oxidation for indoor air applications: Systematic experimental evaluation, J. Hazard. Mater. 261 (2013) 130–138.

[125] D. Vildozo, C. Ferronato, M. Sleiman, J.-M. Chovelon, Photocatalytic treatment of indoor air: Optimization of 2-propanol removal using a response surface methodology (RSM), Appl. Catal. B Environ. 94 (2010) 303–310. doi:10.1016/J.APCATB.2009.11.020.

[126] N. Bouazza, M.A. Lillo-Ródenas, A. Linares-Solano, Photocatalytic activity of TiO_2-based materials for the oxidation of propene and benzene at low concentration in presence of humidity, Appl. Catal. B Environ. 84 (2008) 691–698. doi:10.1016/J.APCATB.2008.06.002.

[127] H. Einaga, S. Futamura, T. Ibusuki, Heterogeneous photocatalytic oxidation of benzene, toluene, cyclohexene and cyclohexane in humidified air: comparison of decomposition behavior on photoirradiated TiO_2 catalyst, Appl. Catal. B Environ. 38 (2002) 215–225. doi:10.1016/S0926-3373(02)00056-5.

[128] T. Guo, Z. Bai, C. Wu, T. Zhu, Influence of relative humidity on the photocatalytic oxidation (PCO) of toluene by TiO_2 loaded on activated carbon fibers: PCO rate and intermediates accumulation, Appl. Catal. B Environ. 79 (2008) 171–178. doi:10.1016/J.APCATB.2007.09.033.

[129] Y. Luo, D.F. Ollis, Heterogeneous Photocatalytic Oxidation of Trichloroethylene and Toluene Mixtures in Air: Kinetic Promotion and Inhibition, Time-Dependent Catalyst Activity, J. Catal. 163 (1996) 1–11.

[130] C. Raillard, V. Héquet, P. Le Cloirec, J. Legrand, Kinetic study of ketones photocatalytic oxidation in gas phase using TiO_2-containing paper: effect of water vapor, J. Photochem. Photobiol. A Chem. 163 (2004) 425–431.

[131] C.R. Angle, Indoor air pollutants., Adv. Pediatr. 35 (1988) 239–80. http://www.ncbi.nlm.nih.gov/pubmed/3055860 (accessed May 8, 2018).

[132] US EPA, Introduction to Indoor Air Quality, (n.d.). https://www.epa.gov/indoor-air-quality-iaq/introduction-indoor-air-quality (accessed May 8, 2018).

[133] J.M. Samet, M.C. Marbury, J.D. Spengler, Health Effects and Sources of Indoor Air Pollution. Part II, Am. Rev. Respir. Dis. 137 (1988) 221–242. doi:10.1164/ajrccm/137.1.221.

[134] K. Koistinen, D. Kotzias, S. Kephalopoulos, C. Schlitt, P. Carrer, M. Jantunen, S. Kirchner, J. McLaughlin, L. Mølhave, E.O. Fernandes, B. Seifert, The INDEX project: executive summary of a European Union project on indoor air pollutants, Allergy. 63 (2008) 810–819. doi:10.1111/j.1398-9995.2008.01740.x.

[135] F. Moulis, J. Krýsa, Photocatalytic degradation of several VOCs (n-hexane, n-butyl acetate and toluene) on TiO_2 layer in a closed-loop reactor, Catal. Today. 209 (2013) 153–158. doi:10.1016/J.CATTOD.2012.10.017.

[136] C.H.H. Ao, S.C.C. Lee, J.Z.Z. Yu, J.H.H. Xu, Photodegradation of formaldehyde by photocatalyst TiO_2: effects on the presences of NO, SO_2 and VOCs, Appl. Catal. B Environ. 54 (2004) 41–50.

[137] O. Debono, V. Héquet, L. Le Coq, N. Locoge, F. Thévenet, VOC ternary mixture effect on ppb level photocatalytic oxidation: Removal kinetic, reaction intermediates and mineralization, Appl. Catal. B Environ. 218 (2017) 359–369. doi:10.1016/j.apcatb.2017.06.070.

[138] D. Vildozo, R. Portela, C. Ferronato, J.-M. Chovelon, Photocatalytic oxidation of 2-propanol/toluene binary mixtures at indoor air concentration levels, Appl. Catal. B Environ. 107 (2011) 347–354. doi:10.1016/J.APCATB.2011.07.035.

[139] C.S. Turchi, D.F. Ollis, Mixed reactant photocatalysis: Intermediates and mutual rate inhibition, J. Catal. 119 (1989) 483–496. doi:10.1016/0021-9517(89)90176-0.

[140] V. Hequet, P. Bruno, C. Hort, V. Platel, J.-F.J.. Petit, K. Morisseau, L. Le Coq, Y. Andres, Microorganisms spores inactivation by photocatalysis in air handling unit, in: Indoor Air, Ghent, Belgium, 2016. https://www.isiaq.org/docs/Papers/Paper157.pdf (accessed May 8, 2018).

[141] R.J. Shaughnessy, R.G. Sextro, What Is an Effective Portable Air Cleaning Device? A Review, J. Occup. Environ. Hyg. 3 (2006) 169–181. doi:10.1080/15459620600580129.

[142] N. Costarramone, B. Kartheuser, C. Pecheyran, T. Pigot, S. Lacombe, Efficiency and harmfulness of air-purifying photocatalytic commercial devices: From standardized chamber tests to nanoparticles release, Catal. Today. 252 (2015) 35–40. doi:10.1016/J.CATTOD.2015.01.008.

[143] Ü. Palmiste, H. Voll, Gas-phase optical fiber photocatalytic reactors for indoor air application: a preliminary study on performance indicators, IOP Conf. Ser. Mater. Sci. Eng. 251 (2017) 012055. doi:10.1088/1757-899X/251/1/012055.

[144] K.-C. Noh, S.-J. Yook, Evaluation of clean air delivery rates and operating cost effectiveness for room air cleaner and ventilation system in a small lecture room, Energy Build. 119 (2016) 111–118. doi:10.1016/J.ENBUILD.2016.03.027.

[145] O. Debono, Oxydation photocatalytique de composés organiques volatils et suivi de leurs intermédiaires réactionnels : étude en réacteurs statique et dynamique à des concentrations typiques de l'air intérieur, Nantes, Ecole des Mines, 2011. http://www.theses.fr/2011EMNA0005 (accessed April 3, 2018).

[146] D.S. Muggli, J.T. McCue, J.L. Falconer, Mechanism of the Photocatalytic Oxidation of Ethanol on TiO2, J. Catal. 173 (1998) 470–483. doi:10.1006/JCAT.1997.1946.

[147] M.R. Nimlos, E.J. Wolfrum, M.L. Brewer, J.A. Fennell, G. Bintner, Gas-Phase Heterogeneous Photocatalytic Oxidation of Ethanol: Pathways and Kinetic Modeling, (1996). doi:10.1021/ES9602298.

[148] O. Debono, F. Thévenet, P. Gravejat, V. Héquet, C. Raillard, L. Lecoq, N. Locoge, Toluene photocatalytic oxidation at ppbv levels: Kinetic investigation and carbon balance determination, Appl. Catal. B Environ. 106 (2011) 600–608. doi:10.1016/J.APCATB.2011.06.021.

[149] F. Tang, X. Yang, A "deactivation" kinetic model for predicting the performance of photocatalytic degradation of indoor toluene, o-xylene, and benzene, Build. Environ. 56 (2012) 329–334. doi:10.1016/J.BUILDENV.2012.04.001.

[150] W.A. Jacoby, M.R. Nimlos, D.M. Blake, R.D. Noble, C.A. Koval, Products, Intermediates, Mass Balances, and Reaction Pathways for the Oxidation of Trichloroethylene in Air via Heterogeneous Photocatalysis, Environ. Sci. Technol. 28 (1994) 1661–1668. doi:10.1021/es00058a018.

[151] M. Mohseni, Gas phase trichloroethylene (TCE) photooxidation and byproduct formation: photolysis vs. titania/silica based photocatalysis, Chemosphere. 59 (2005) 335–342. doi:10.1016/J.CHEMOSPHERE.2004.10.054.

CHAPTER II: EXPERIMENTAL MATERIALS AND METHODS

II.1 Introduction

In Chapter I, two experimental objectives were defined; firstly to study the influence of key parameters including air velocity, light intensity, the change in media geometry, initial pollutant concentration, presence of chemical co-pollutants, presence of particles (bioaerosols) and relative humidity on the degradation of selected target compounds and secondly to investigate the formation of intermediates during the degradation of these target compounds. Isoflurane (anesthetic gas) and acrylonitrile (compound present in surgical smoke) were chosen as the target compounds whilst nitrous oxide and acetic acid were chosen as co-pollutants.

This chapter therefore presents the materials and methods that were implemented to achieve the fixed experimental objectives. The setup used, has been developed in the laboratory of the Département Systèmes Energétiques et Environnement (DSEE) of the IMT Atlantique under the SAFEAIR platform.

Firstly, the experimental device that is used in this work is presented. The setup is divided into three sections: (i) the pollutant generation system (ii) the multi-pass photocatalytic reactor (iii) the sampling and analytical equipment and setup. Then, the experimental method is presented. In this part, the strategy that is used to perform experiments and the operating conditions used are discussed. Additionally, the model that is used to treat the experimental data in order to calculate the performance indicator is also presented.

II.2 Experimental devices

II.2.1 Pollutant generation system

The pollutant generation system allows the production of air with controlled pollutant concentrations and relative humidity. The generation is done by diluting concentrated vapors of the pollutants with humid air zero; air that is free from Volatile Organic Compounds (VOCs).

II.2.1.1 Humid air zero generation

The system allowing the generation of humid air zero is shown in Figure 8. The process starts by taking compressed air from the laboratory network. Then because the compressed air may contain VOCs, it is passed through a Claind AZ 2020 generator which

makes it possible to eliminate VOCs present in the air by oxidation on a platinum-palladium catalyst at 250°C. The achieved air quality corresponds to a total VOC concentration of less than 100 ppt. The air then passes through a filter to remove any particulate matter.

The air taken from the laboratory network contains about 400 ppm of CO_2 which must be reduced in order to detect CO_2 during the photocatalytic degradation. To do this, the air is passed through an NDC-300, F-DGS scrubber which uses a pressure swing adsorption (PSA) process to extract CO_2 and humidity from the air. The CO_2 concentration at the system outlet is about 15 ppm. The generated air zero is then humidified by splitting it into two flows with one part bubbled through water at room temperature (20 ± 2°C). The desired humidity is achieved by adjusting the flow rates of the humidified and dry air with the aid of mass flow controllers (MFC). The humid zero air is then mixed with the pollutants to dilute them before injection into the photocatalytic reactor.

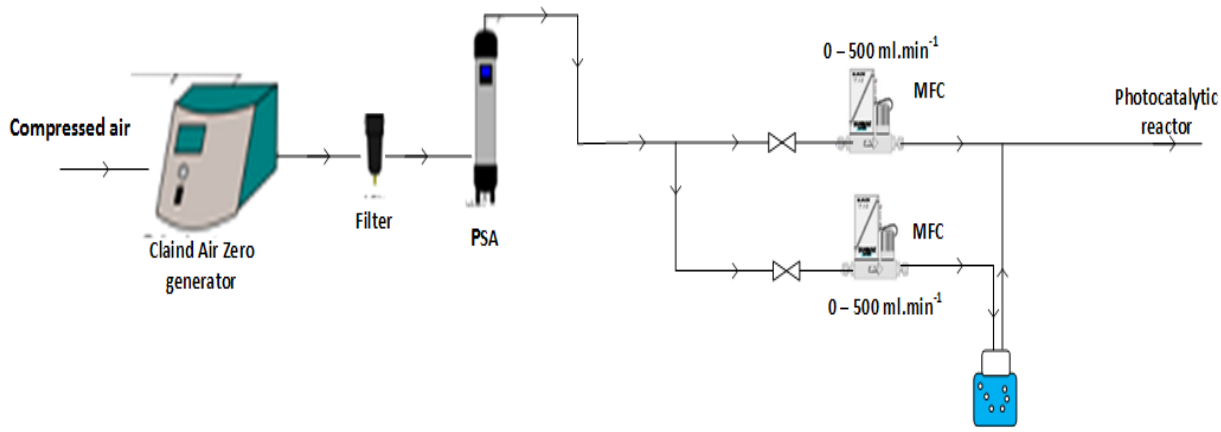

Figure 8 : Schematic representation of humid air zero generation system

II.2.1.2 Pollutant generation techniques

Two different techniques of pollutant generation are used to fill the pilot: (i) the use of certified commercial cylinders and (ii) the generation in a dropping funnel under vacuum. The first technique was used for the generation of isoflurane, acrylonitrile and nitrous oxide. They were supplied by Linde Gas, Air products and Air Liquide respectively. The characteristics of each cylinder are given in Table 7.

VOC	Concentration (ppm)	Pressure (bar)	Balancing gas
Isoflurane	154 ± 4	150	N_2
Acrylonitrile	149 ± 5	150	N_2
Nitrous oxide	500 ± 10	150	N_2

Table 7 : Characteristics of certified gas cylinders used for the generation of pollutants in the photocatalytic reactor

The desired pollutant concentrations were achieved by diluting the concentrations from certified gas cylinders with humid air zero. The flow rates of each channel were set by mass flow controllers (MFC). This made it possible to modify the concentration of the pollutant in the generated air. The MFC of the moist and dry air channels have maximum flow rates of 500 mL.min^{-1} whilst that of the pollutant gas cylinder has maximum flow rates of 50 mL.min^{-1} each. The generation system is represented in Figure 9.

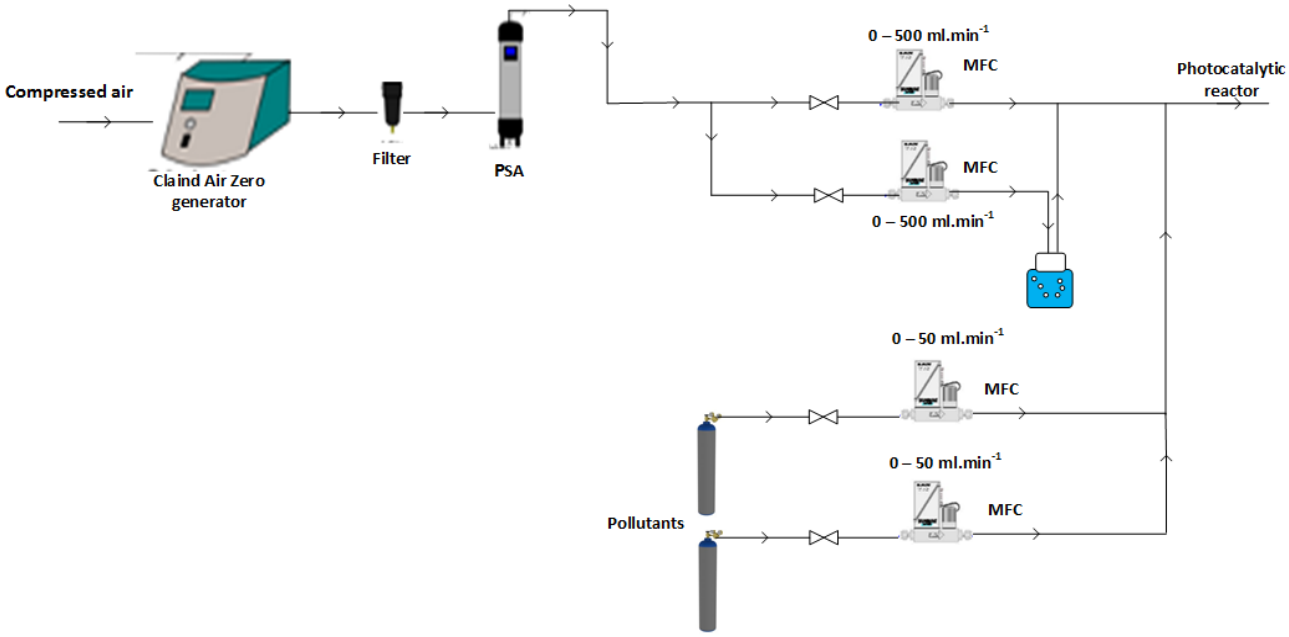

Figure 9 : Schematic representation of the system used for the generation of pollutants in certified gas cylinders

For acetic acid (AA), the gas vapor was generated in a dropping funnel under vacuum before injection into the photocatalytic reactor. AA liquid has a low vapor pressure of 1.5 kPa at 20 °C [1] consequently this vacuum method is needed to improve its volatilization. A volume of analytical grade (99.95%) liquid acetic acid supplied by Sigma Aldrich was injected into a 285 mL pyrex dropping funnel. The concentration in the dropping funnel is calculated from the volume of injected liquid, its density and its mass. A vacuum of less than 300 mbar is then created in the dropping funnel by sucking the air using a vacuum pump. The

purpose of this step is to promote the vaporization of acetic acid. The funnel is then heated at 50 °C to help complete the vaporization process. After some minutes of heating and cooling to room temperature, the funnel is re-pressurized with ambient air by rapidly opening and closing its valve. Finally, a fraction of the volume generated is taken using a 10 mL gas syringe and injected into the photocatalytic reactor.

The concentration of acetic acid introduced into the reactor is calculated from the amount in the dropping funnel, the volume of the dropping funnel and the amount taken from the funnel and injected into the photocatalytic reactor. These calculations make it possible to determine the volume of liquid acetic acid injected into the dropping funnel and the volume of vapor injected into the photocatalytic reactor based on the concentration needed in the photocatalytic reactor.

II.2.2 Multi-pass photocatalytic reactor

II.2.2.1 General description

The photocatalytic experiments were carried out in a 420L closed-loop reactor operating in recirculating mode (Figure 10). This reactor was designed during the PhD of Audrey Maudhuit [2] and has also been used by Olivier Debono [3] and Frederic Batault [4] during their PhD studies. This reactor permits a better representation of PCO systems developed in dynamic mode and is realistic regarding air treatment apparatus working as standalone devices or implanted in HVAC systems.

The reactor is constituted of two steel chambers connected by flexible steel pipes. The first chamber is a 20 cm x 20 cm square section and 80 cm long canalization which houses the photocatalytic module. The second is a 250 L tranquilization chamber where the pollutants are introduced and where sampling is also done. A structure of parallel channels arranged in a honeycomb is placed at the inlet of the tranquilization chamber in order to distribute the air flow throughout its width and to prevent the formation of stagnation zones.

A variable speed fan is used to control the air flow within the reactor and allows a flow rate from 28 to 300 $Nm^3.h^{-1}$. The control of the flow rates is achieved with the aid of the National Instrument Labview software. To measure the flow rate, the pressure difference on either side of a calibrated diaphragm is measured by a differential pressure sensor. The reactor is also equipped with thermo-hygrometers that keep track of the temperature and relative humidity during experiments.

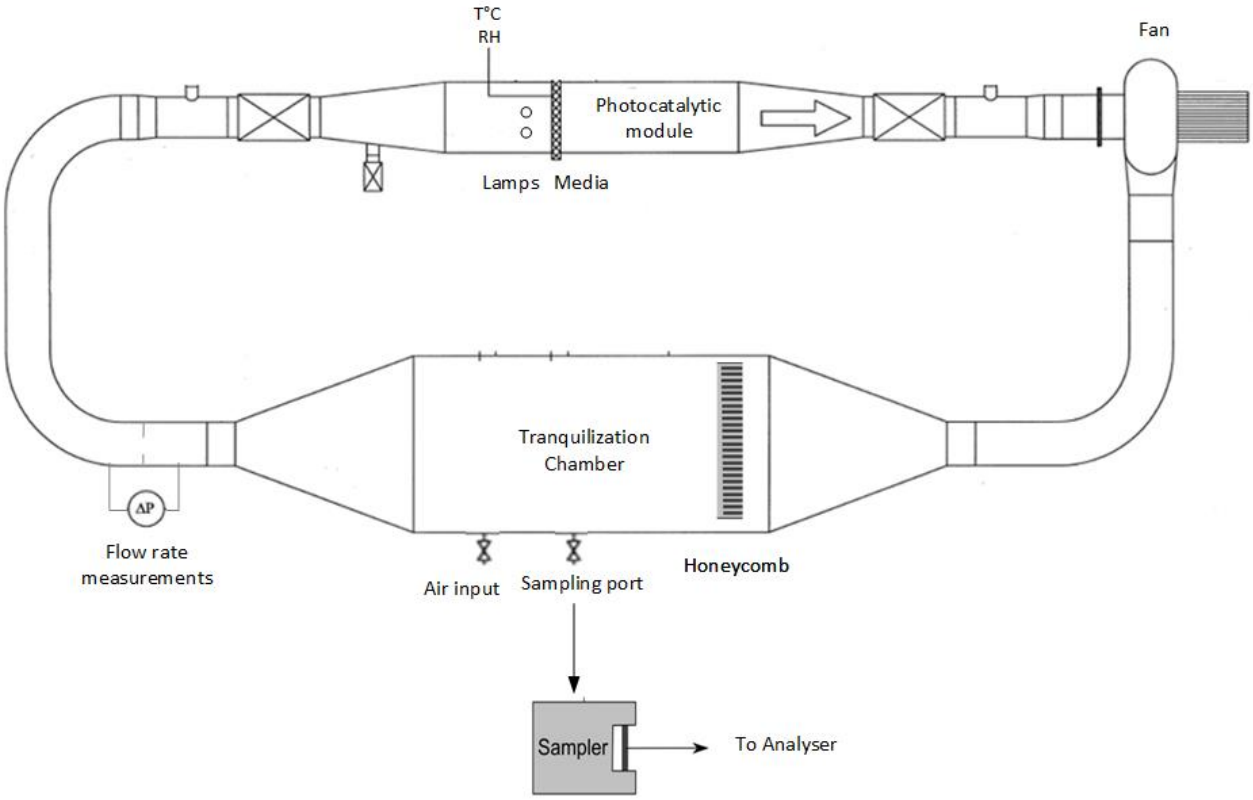

Figure 10 : Schematic representation of the closed-loop photocatalytic reactor

II.2.2.2 Photocatalytic module

The photocatalytic module is the part of the reactor where the photocatalytic media and the lamps are housed.

The photocatalytic media is irradiated by two Philips TUV PL-L 18W lamps. These lamps emit light principally at a wavelength of 254 nm (UVC) as shown in Figure 11. The light intensity received by the media surface is measured with a Fisher VLX-3W radiometer (Vilber Lourmat) equipped with a calibrated CX-254 nm sensor. The sensor has a cell capture with a $1cm^2$ surface that allows the measure of light intensity at a fixed wave length range of

254 nm and an accuracy of ± 5%. The measurement range of the radiometer is 0 - 250 $mW.cm^{-2}$.

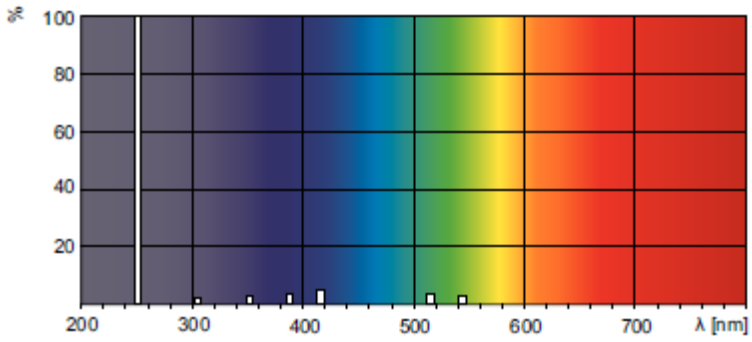

Figure 11 : Photometric data of lamps provided by Philips

During the measurements, the radiometer sensor is positioned such that the distance between the cell capture and the lamp is the same as the distance between the media surface and the lamps during experiments. The desired average light intensity needed for experiments is achieved by means of a variable voltage supply which is adjusted to modify the power of the lamps. The average values obtained represent the mean value of several points taken across the media surface. Figure 12 shows the measurement points taken across the plane media. The area was divided evenly into 80 lattices of 2 cm x 2 cm.

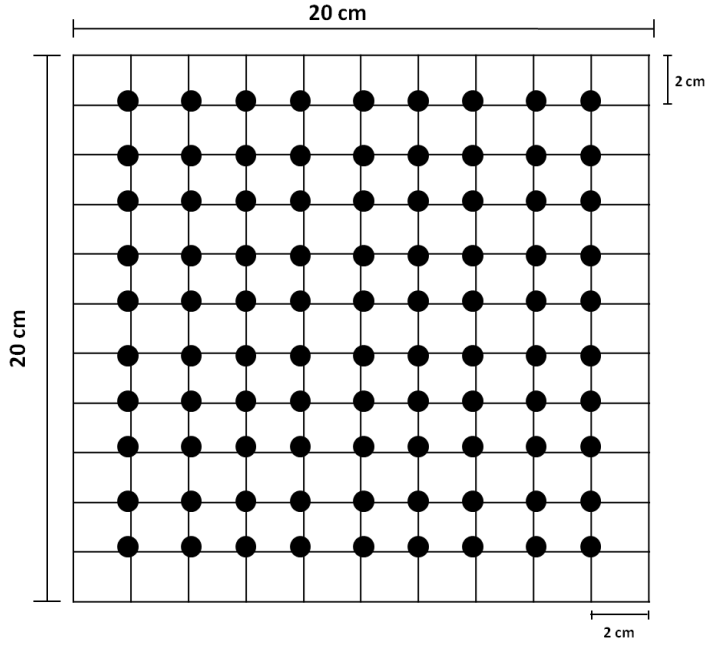

Figure 12 : Grid showing points for the measurement of irradiance

II.2.2.2.1 Media characterization

The photocatalytic media used is the commercial QUARTZEL® PCO supplied by Saint Gobain Quartz. It consists of quartz fibers coated with TiO_2 deposited through a sol-gel method and pressed into a felt with average thickness of 17.5 mm (Figure 13). A characterization of the media was done to give information on its properties and the results are discussed in the following sub-sections.

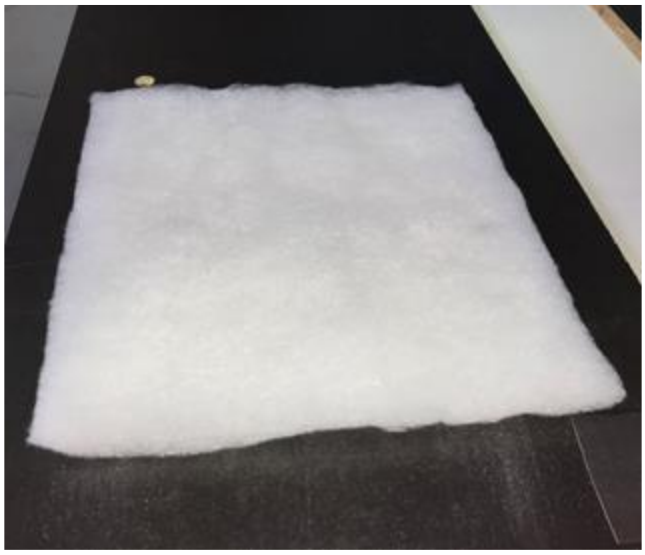

Figure 13 : Photograph of the photocatalytic media

Scanning Electron Microscopy (SEM)

The arrangements of the fibers as well as their thickness were determined by using a JOEL JSM 5800LV Scanning Electron microscope to analyze the surface images of the media. Figure 14 a-d show the scanning electron micrographs of the photocatalytic media. The SiO_2 fibers are long and interconnected and form a complex mesh as shown in Figures 14 a and b. This complexity offers a tortuous path for air flow and increases the probability of pollutants to be trapped and degraded. The SEM image (Figure 14 d) shows the variation in thickness of the coated fibers to be in the range 10 µm - 20 µm.

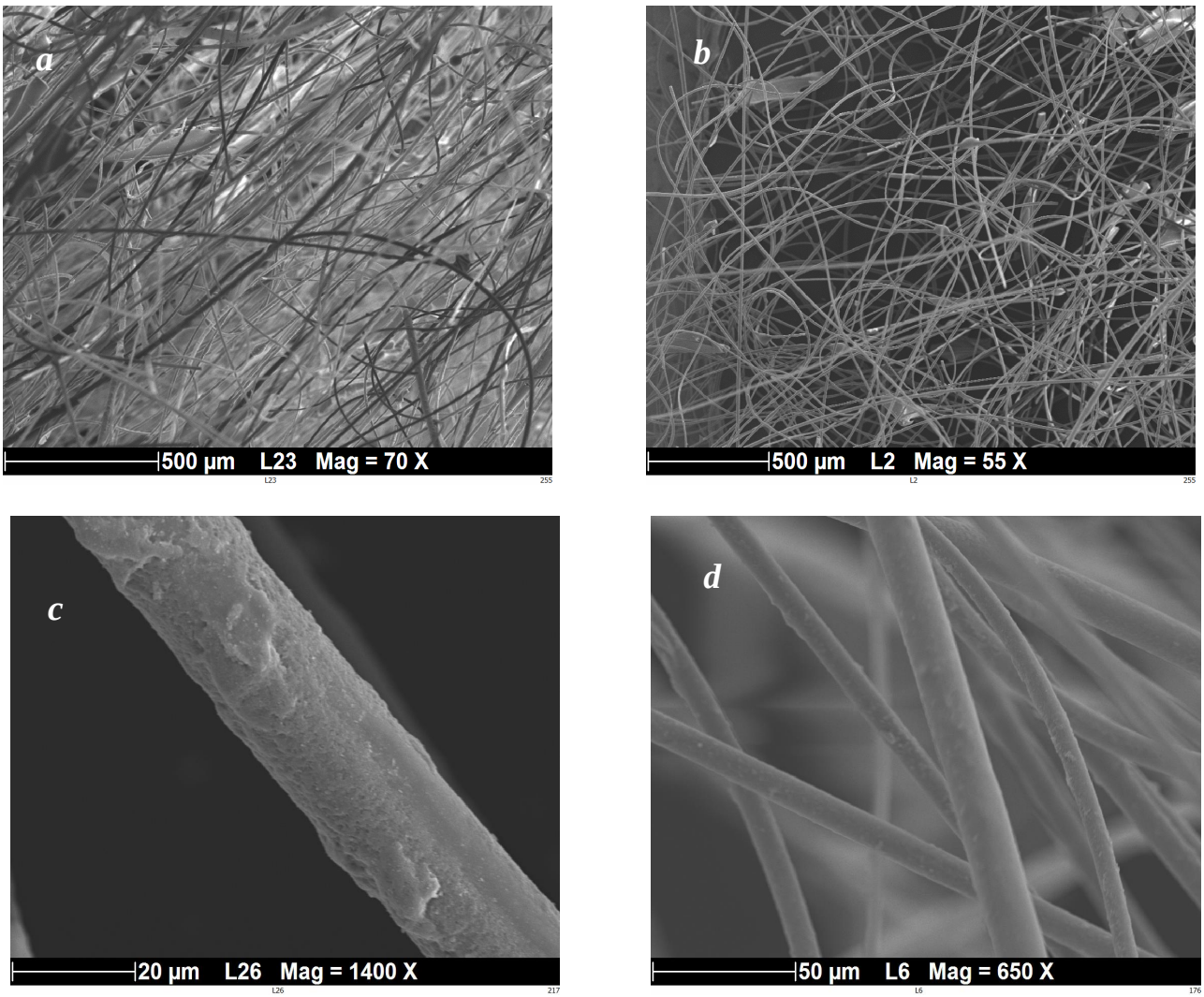

Figure 14 : Scanning electron micrographs of (a) arrangement of fibers (b) arrangement of fibers (c) fiber coated with TiO_2 (d) different sized fibers

BET Specific Surface area

The BET specific surface area of the photocatalytic media was determined from a nitrogen adsorption/desorption isotherm at 77 K using a Micrometrics ASAP 2020 analyzer. Prior to the analysis, the media with average weight of 140 mg was degassed at 110 °C for 24 hours. Table 8 shows the specific surface area and the total pore volume.

Material	S_{BET} ($m^2.g^{-1}$)	Pore Volume ($cm^3.g^{-1}$)
Photocatalytic media	112 ± 1	0.091 ± 0.005

Table 8 : Results from nitrogen adsorption/desorption analysis

The specific surface area is known to influence the efficiency of the photocatalyst. Hajaghazadeh *et al*. [5] studied the performance of P25, from Evonik and PC series, another common commercial photocatalyst from Cristal Global Companies for the degradation of methyl ethyl ketone. The commercial photocatalyst powders were supported on glass beads. They observed a conversion rate of *PC50 < P25 < PC500*. Monteiro *et al*. [6] also studied the degradation of PCE and n-decane on transparent cellulose acetate monolithic structures coated with PC500 and P25 powders. They observed that PC500 showed higher conversion of both pollutants in comparison with P25. Taranto *et al.* [7], using fibrous SiO_2 tissue coated with PC500 and P25, also found that PC500 performed better than P25 during the degradation of methanol. The authors attributed the better performance of PC500 compared to P25 and PC50 to its higher specific surface area as shown in Table 9. As the surface area is increased, the number of active sites and the pollutant adsorption capacity are increased consequently leading to a better photocatalytic activity.

Reference	S_{BET} ($m^2.g^{-1}$)		
	P25	**PC50**	**PC500**
Hajaghazadeh *et al*. [5]	47	45	240
Monteiro *et al*. [6]	50	-	345
Taranto *et al.* [7]	52	-	317

Table 9 : Comparison of surface areas of commercial photocatalysts

The media that is used in this study (Quartzel® PCO) has a high enough surface area of 112 $m^2.g^{-1}$. Thus greater number of active sites and high pollutant adsorption can be envisaged. It is however important to note that a specific surface that is too high may diminish efficiency of the media by encouraging recombination of electrons and hole pairs.

Porosity

The total porosity of the media is obtained by mercury porosimetry using Micrometrics Autopore IV 9500. It allows to work between 0 and 60,000 psia of pressure. 0.013 g of sample was put into a penetrometer which is filled with mercury at a starting pressure of 0.2 and gradually increased until 30,000 psia. The experiments were repeated two times. Table 10 shows the results obtained from mercury porosimetry experiments. The total porosity is measured at 87.5 % and the average pore size is 339 µm.

Material	Porosity (%)	Average pore size (µm)
Photocatalytic media	87.5 ± 0.7	339.1 ± 10.5

Table 10 : Results from mercury porosimetry

For a fibrous media, two levels of porosity can be determined: the surface roughness or rugosity and the media internal porosity. Mercury porosimetry also helps to plot the porosity distribution curve as a function of the pore diameter in order to determine the share of the internal porosity and surface roughness of the media by applying the Le Coq model [8]. This model makes it possible to distinguish the different levels of pore sizes constituting a material. The model is based on the following equation which represents the porosity distribution as a function of the pore size:

$$\varepsilon(\phi_j) = \sum_{i=1}^{k} \frac{\varepsilon_i^{\max}}{\left(\phi_j / \phi_i^{\mathrm{mod}}\right)^{\alpha_i} + 1} \qquad \textbf{Equation 18}$$

where $\varepsilon_i^{\max}$ is the maximum porosity,

ϕ_i^{mod} is the modal pore size (µm),

α_i is the slope attenuation coefficient at the cumulative porosity curve inflection point for the pore size distribution *i*.

The model is set to converge as much as possible with experimental points from mercury porosimetry. The porosity distribution curve and the Le Coq model fitting the experimental points are given in Figure 15. It is seen that the media contains pores between 100 µm and 1000 µm. The two observed peaks are linked to the internal porosity and surface rugosity with modal diameters of 150 µm and 686 µm respectively.

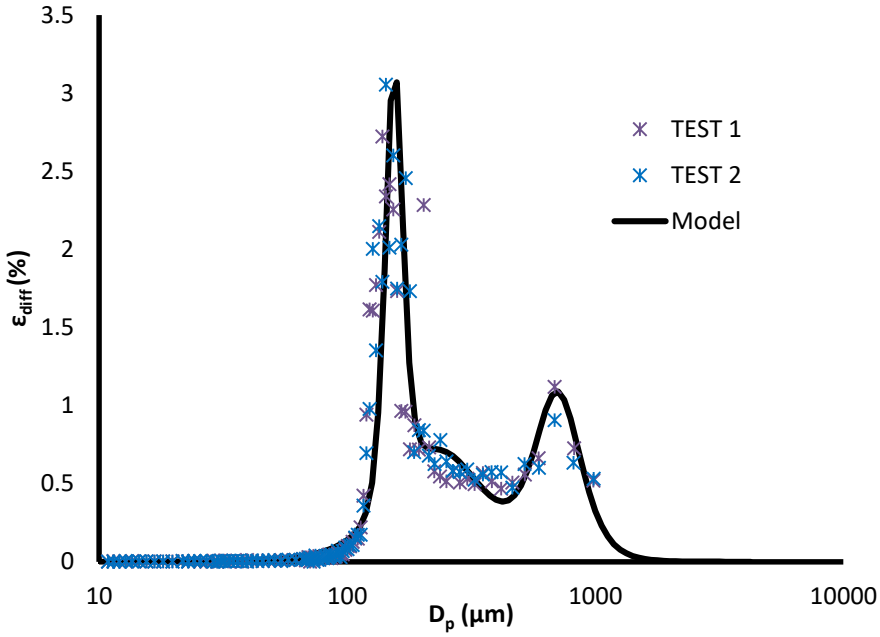

Figure 15 : Experimental mercury porosimetry points fitted to Le Coq Model

Permeability

The permeability of the media was calculated based on the measurement of pressure drop as a function of velocity using a laboratory experimental bench. This test bed is shown in Figure 16.

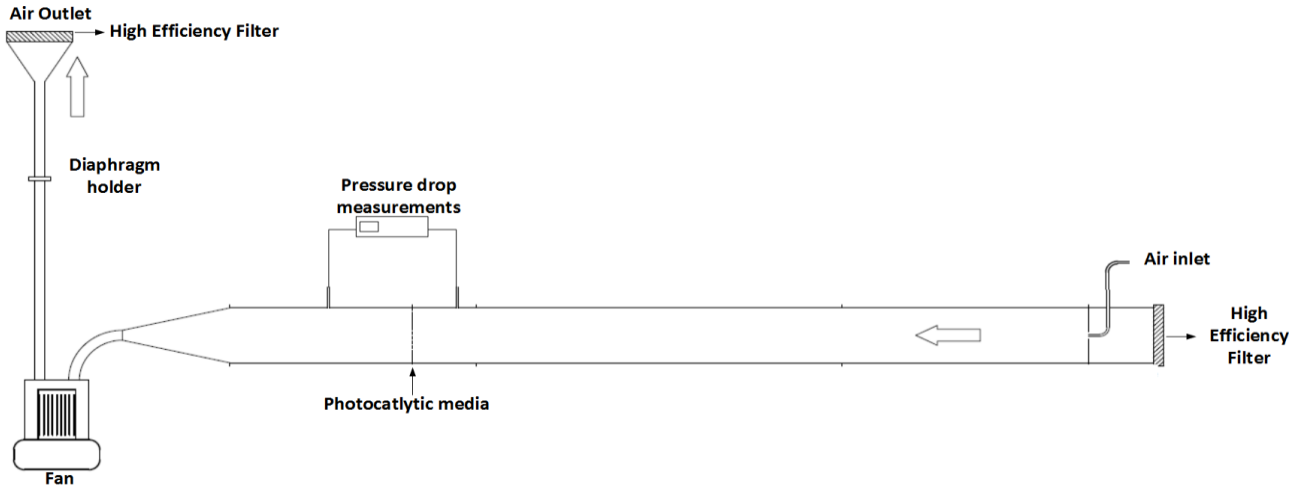

Figure 16 : A schematic representation of laboratory experimental bench used for pressure drop versus velocity measurements

The experimental bench is equipped with a centrifugal fan which is used to control the flow of air. Diaphragms with several diameters were used to control the velocity of air. The

reactor has a media holder where the tested media is fixed. Pressure drop measurements were made with differential pressure sensors placed 60 cm upstream and 30 cm downstream of the media. The measurements are carried out for a velocity range of 0.1 $m.s^{-1}$ to 2 $m.s^{-1}$. The results are shown in Figure 17.

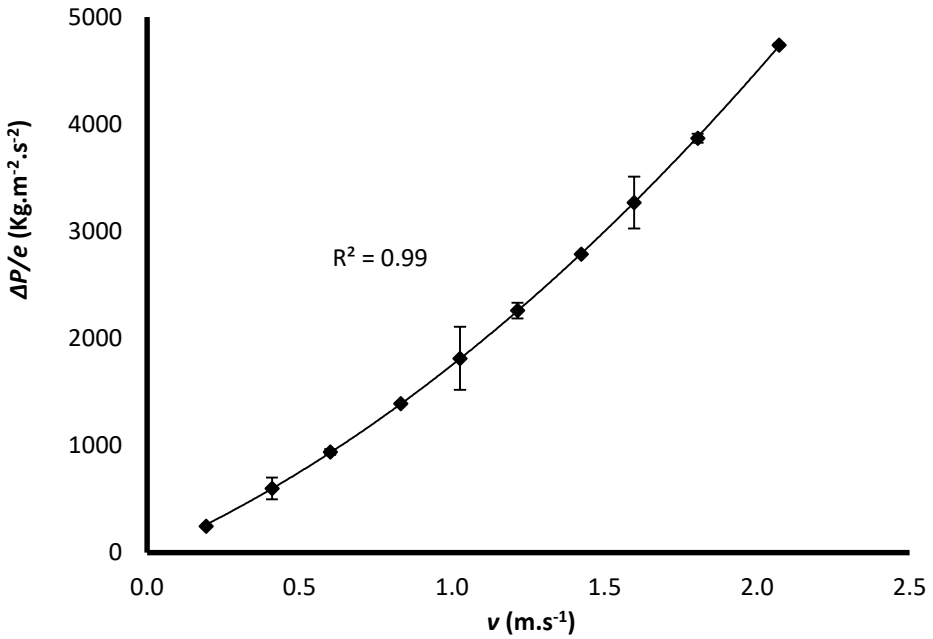

Figure 17 : Dependence of pressure drop on the velocity for the photocatalytic media

Permeability can be calculated using models that have been developed based on the flow regime through the pores of the media and which establish a relationship between velocity and pressure drop. The pore Reynolds number (Re_p) is used to determine the flow regime and is based on the mean pore velocity ($\overline{v_p}$) and the mean pore size ($\overline{d_p}$:)

$$\mathrm{Re}_p = \frac{\rho \overline{v_p}\,\overline{d_p}}{\mu} \qquad \textbf{Equation 19}$$

Where μ is the dynamic viscosity of the fluid ($kg.m^{-1}.s^{-1}$) and ρ the density ($kg.m^{-3}$).

According to the Reynolds number, four flow regimes can be identified within the pores [9]:

- $Re_p < 1$: Creeping regime. The viscous forces dominate the inertia forces and the pressure drop is linked linearly to the velocity.

- $1\text{-}10 < Re_p < 150$: Inertial flow regime. Steady non-linear laminar flow begins between Re_p of 1 and 10. Boundary layers are more pronounced but when Re_p increases, the

thickness of the boundary layer decreases. This indicates the dominance of the inertial forces over the viscous forces.

- $150 < Re_p < 300$: Unsteady laminar flow regime: Oscillations with frequencies of the order of 1 Hz and amplitudes of the order of one tenth of the particle diameter are observed. The laminar wake instability may be responsible for the transition from laminar steady flows to unsteady flows.

- $Re_p > 300$: Unsteady and turbulent flow regime.

The pore Reynolds number for the media used in this study considering the velocity range of 0.1 to 2 $m.s^{-1}$ was found to be 3 to 55 respectively. This puts the regime in the laminar non-linear range.

Darcy's law is the most common and widely used empirical model for the correlation of pressure drop and velocity [10]. It describes the flow of a fluid through a porous medium as a linear relationship between the pressure gradient and the fluid velocity. The law was formulated by Henry Darcy based on the results of experiments on the flow of water through beds of sand.

The law may be stated as:

$$Q = \frac{kA}{\mu}\frac{(\Delta P)}{e} \qquad \textbf{Equation 20}$$

Q is volumetric flow rate ($m^3.s^{-1}$),
A is the flow area (m^2),
ΔP is the pressure drop (Pa),
e is the flow path length (m),
k is the permeability (m^2) of the porous media

Permeability (k) is a property of the structure of the porous media and it is entirely independent of the nature of the fluid. The permeability k is considered to characterize the dynamic properties of a porous media with respect to flow of fluids though it.
Darcy's law is therefore stated as:

$$\frac{\Delta P}{e} = \frac{\mu}{k} v \qquad \textbf{Equation 21}$$

Where v is the velocity ($m.s^{-1}$).

Darcy's law assumes laminar or viscous flow and experimentally is represented by linear curve. However, it has been observed that when the flow velocity increases, the inertial effects start dominating the flow and the relationship is non-linear. To account for the increased pressure drop, a second order or quadratic velocity term is added. The modified Darcy equation is written as:

$$\frac{\Delta P}{e} = \frac{\mu}{k} v + \frac{1}{2} C \rho v^2 \qquad \textbf{Equation 22}$$

where C is the inertial resitance factor (m^{-1}).

Using the regression model from experimental results and the modified Darcy equation (Equation 22), the permeability is calculated as $1.45 \times 10^{-8} \pm 4.05 \times 10^{-10}$ m^2 and the inertial resistance factor is calculated as 823 ± 106.8 m^{-1}. The experiments were repeated twice. The flow through the media also generates a low pressure drop of about 83 ± 2 Pa at 2 $m.s^{-1}$ which is beneficial in terms of energy demand.

UV Transmittance (UVT)

The measurement of the transmission of UV-Visible light through the photocatalytic media was made using UV-Vis spectrophotometer (UV-1800, Shimadzu) within the wavelength range of 190 to 900 nm. The media was placed in a quartz cell and the intensity of transmitted light was measured by a sensor and compared to that of air as a reference material. The results obtained from the experiment are shown in Figure 18. It can be observed that the transmittance was measured as 0.6 % from 200 nm to about 300 nm but increased to about 1.4 % when the wavelength was increased to 900 nm. The UVT at 254 nm which is the wavelength used in this study was therefore measured at 0.6 %.

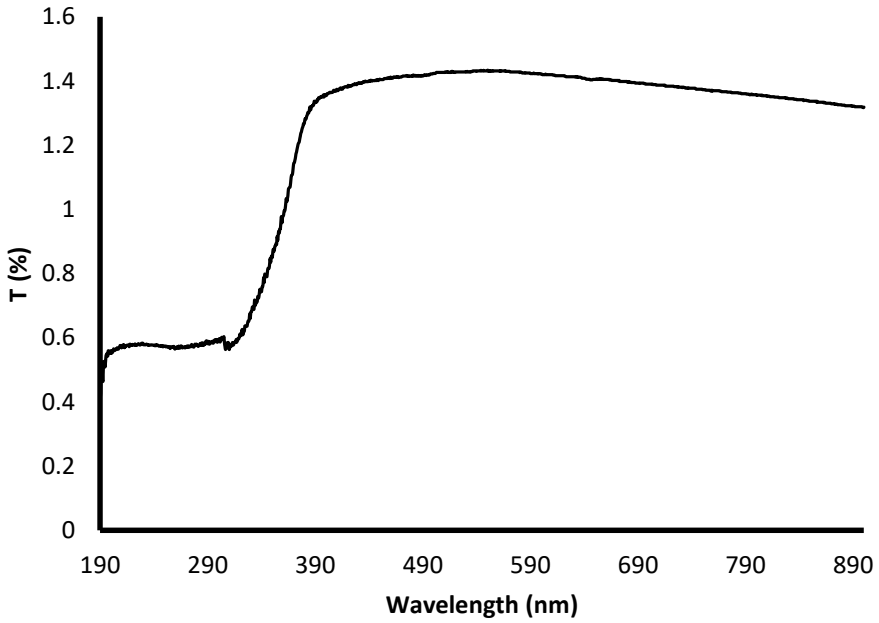

Figure 18 : Transmittance of the photocatalytic media with respect to wavelength

Conclusions on media characterization

The SEM and BET analysis of the media allowed to make conclusions that complexity of the fiber arrangements offered a tortuous path for air flow that would increase the probability of pollutants to be trapped and degraded and also that high number of active sites and high pollutant adsorption can be envisaged due to the high surface area. The media porosity, permeability, inertial resistance and UVT are characteristics that are necessary as inputs for the numerical simulation that will be discussed in chapter IV. These are summarized in Table 11.

Media property	**Value**
Porosity	0.875
Permeability (m^2)	1.45×10^{-8}
Inertial resitance factor (m^{-1})	823
UV transmittance (%)	0.6

Table 11 : Characteristics of the photocatalytic media

II.2.2.3 Media geometry configurations

In this study, two media geometry configurations are used; a plane configuration and a pleated configuration. In both cases, the media is placed so that the air was forced to flow through it at each pass.

For the plane configuration, as the name suggests the photocatalytic media has a plane surface and is placed perpendicularly to the flow. The surface of the media is 0.04 m^2. In the case of the pleated configuration, the photocatalytic media is folded into four pleats creating two triangles at 60°. The developed media surface is 0.072 m^2. For both configurations, the media is put in stainless grill support in order to keep the media in place during the experiments.

The position and arrangement of the media and lamps within the photocatalytic module is shown in Figure 19 for each configuration. The lamps in the plane configuration are placed horizontally and are also 3 cm from the media whilst for the pleated configuration; they are placed vertically and are 3 cm from the middle of the pleats. This choice of lamp position for the pleated configuration would allow a better symmetry in terms of the irradiance received on the surface of the media.

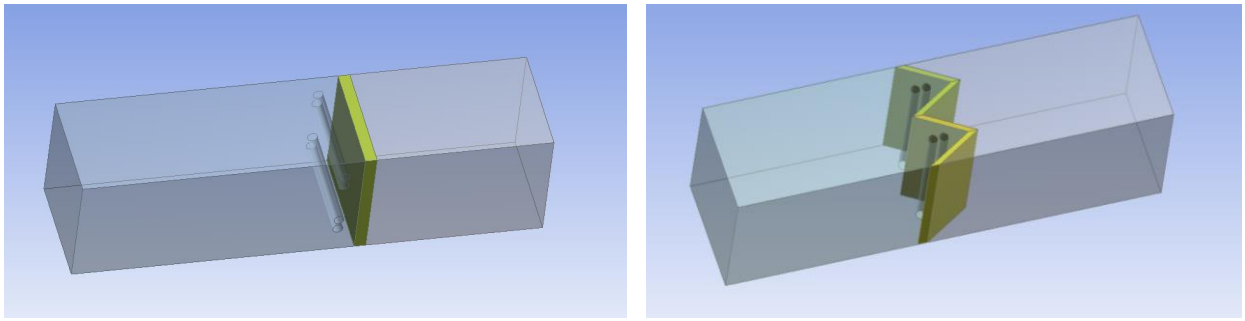

Figure 19 : Representation of the photocatalytic module showing position and arrangement of lamps and plane (left) and pleated (right) media configuration

II.2.3 Sampling and analytical methods

The sampling and analytical methods and devices that were used in this work allowed the detection and quantification of the two main target pollutants and also the identification of possible intermediates and are detailed below.

II.2.3.1 Sampling

The Automatic Clean Room Sampler (ACROSS), supplied by Tera Environnement, was used to sample air onto adsorbent cartridges. It is shown in Figure 20. It has four sampling ramps, each having six cartridge slots. It is equipped with a pump and MFC which allow the collection of samples with determined flow rates ranging between 10 and 540 $mL.min^{-1}$. It can also be programmed to perform sampling sequences. Trapping the pollutants in the cartridges allows to pre-concentrate them in order to improve their detection sensibility to the analytical devices.

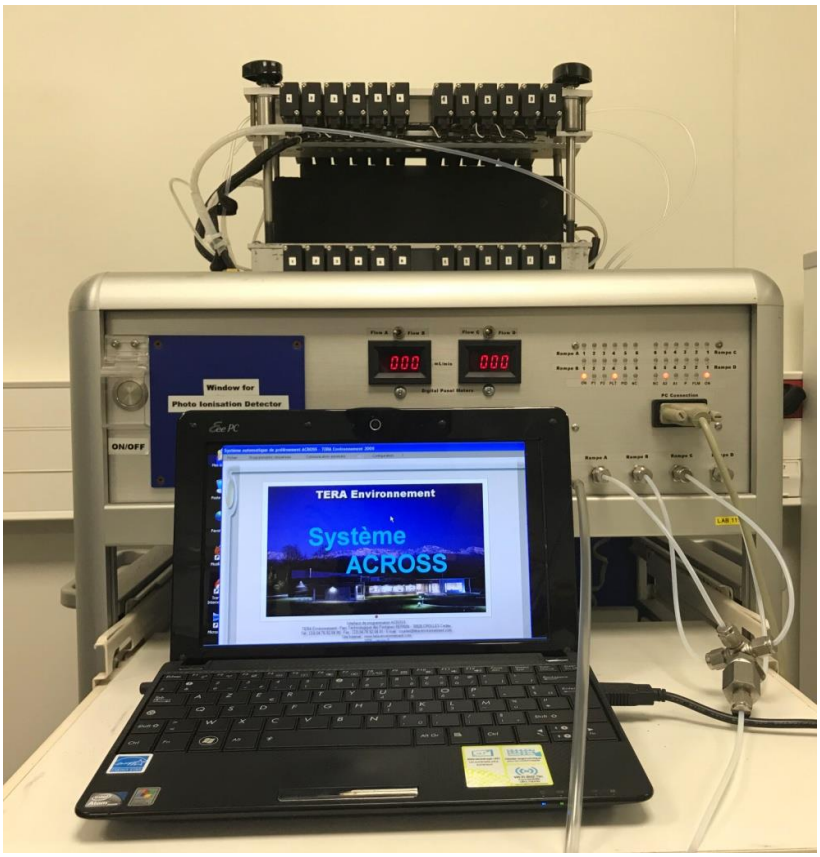

Figure 20 : ACROSS System for sampling

In this work, sampling was done on two different adsorbent cartridges:

- Volatile carbonyl samples, specifically acetaldehyde and formaldehyde were sampled onto 2,4- dinitrophenylhydrazine (DNPH) catridges prepared by Supelco. The DNPH catridge was used because it is the reference adsorbent for carbonyl compound sampling [11,12]. The sampling was done for 4 min at 500 $mL.min^{-1}$.

- VOC samples were collected onto stainless steel tubes packed with Carbopack B (Perkin Elmer) at a flow rate of 200 $mL.min^{-1}$ for 2.5 minutes. Carbopack B is a graphitized carbon black adsorbent that is pure, non specific and hydrophobic. It was chosen because it allows accurate samples to be taken despite high humidity levels and also because they captured a wide range of compounds C_4 –C_{14} [13]. Prior to each use the CarboPack B cartridges were cleaned by heating at 280°C using RTA (Régénérateur Thermique des Adsorbants) provided by Tera Environnement.

II.2.3.2 Thermal Desorption/Gas Chromatography/Flame Ionization Detection -Mass Spectrometry (TD/GC/FID-MS)

A TD/GC/FID/MS system is used to identify and measure the concentrations of a large range of VOCs in the pilot, whether target compounds (isoflurane and acrylonitrile) or their possible intermediates. After pre-concentration on Carbopack B catridges, the compounds are desorbed using a thermo-desorber (Turbomatrix 300, Perkin Elmer) by heating at 250 °C. VOCs were driven by helium to a trap at a flowrate of 20 $mL.min^{-1}$. This trap contains a multi-bed adsorbent of Carbopack C 80/100 (22.3 mg), Carbopack B 60/80 (38.8 mg) and Carbopack X 60/80 (22.9 mg) and is cooled to -30 °C.

By passing through this trap, the VOCs are refocused on the adsorbent beds. They are then desorbed from the trap at a flash temperature of 250 °C. They are then conducted in a transfer line heated to 250 °C into the column. The column used is Rxi-624Sil MS manufactured by Restek. This is a moderately polar column, which improves the separation of polar compounds and has a high selectivity for a wide range of VOCs. After elution in the column, the flow is divided into two equal parts by a flow divider. Half of the flow goes to a Flame Ionization Detector (FID) whilst the other half goes to the Mass Spectrometer (MS). The MS (Turbo Mass Gold, Perkin Elmer) allows the identification of the compounds whilst the FID in the GC (AutoSystem XL, Perkin Elmer) allows their quantification. A schematic representation of the TD/GC/FID-MS system is shown in Figure 21.

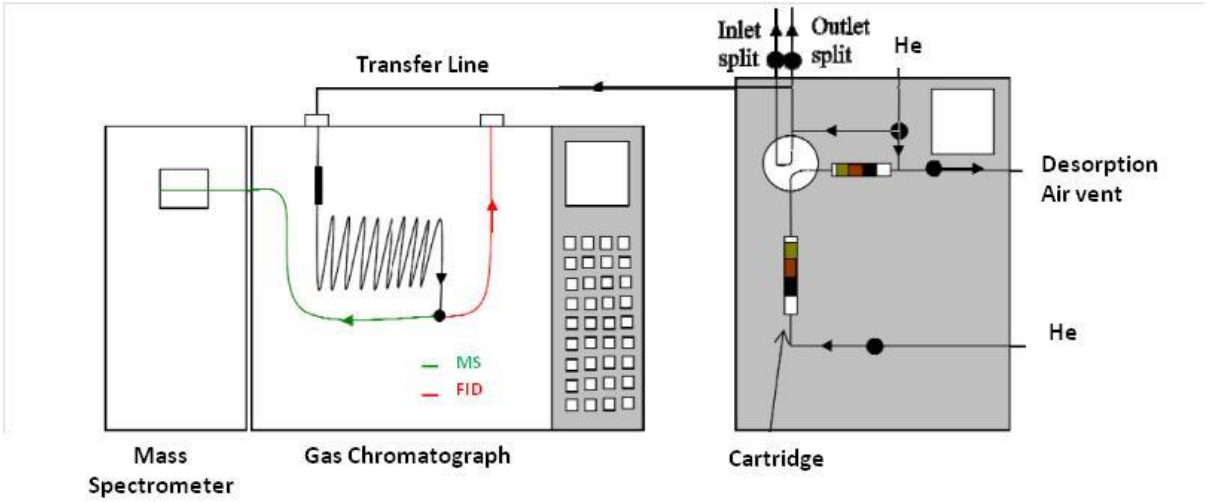

Figure 21 : Schematic representation of the TD/GC/FID-MS system

The parameters of the TD/GC/FID-MS system used in this work are summarized in Table 12.

Sampling	
Adsorbent cartridge	Carbopack B
Temperature (°C)	Ambient
Volume (mL)	500
Flow rate ($mL.min^{-1}$)	200
Cartridge Desorption	
Time (min)	10
Flow rate ($mL.min^{-1}$)	20
Temperature (°C)	250
Trap Desorption	
Flow rate ($mL.min^{-1}$)	20
Refocusing temperature (°C)	-30
Trap desorption temperature (°C)	250
Trap hold (min)	10
Injection	
Mode	Splitless
Heating rate (°C/s)	40
Temperature (°C)	250
GC	
Mode	Constant pressure
Pressure (bar)	20
Column flow rate ($mL.min^{-1}$)	3
Detectors	FID/MS
Column	
Name	Rxi-624Sil MS
Nature	6% cyanopropylphenyl 94% dimethyl arylene polysiloxane
Length (m)	60
Diameter (µm)	350
Film thickness (µm)	1.8
FID	
Temperature (°C)	250
Fuel	H_2
Flow rate ($mL.min^{-1}$)	45
Oxidizer	Air
Flow rate ($mL.min^{-1}$)	450
MS Detection	
Source temperature (°C)	200
Electron Energy (eV)	70
Scan range (m/z)	20-200
GC/MS Analysis	
Oven temperature program	35 °C (5 min), 15 $°C.min^{-1}$ to 150 °C (2 min), 20 $°C.min^{-1}$ to 250 °C (5 min)

Table 12 : Operational parameters of the TD/GC/FID-MS analytical system

GC/FID-MS calibration of the target compounds is performed by generating five concentrations between 0.15 ppm and 12 ppm. The generation of the standard calibration concentrations is done using the pollutant generation system described in section II.2.1. However in this case, the photocatalytic media is absent from the photocatalytic module (Figure 22). The air zero generated is humidified by bubbling it through water at ambient room temperature. Relative humidity is controlled by mixing dry and moist air zero. The calibration concentration needed is obtained by modifying the flow rates of each channel.

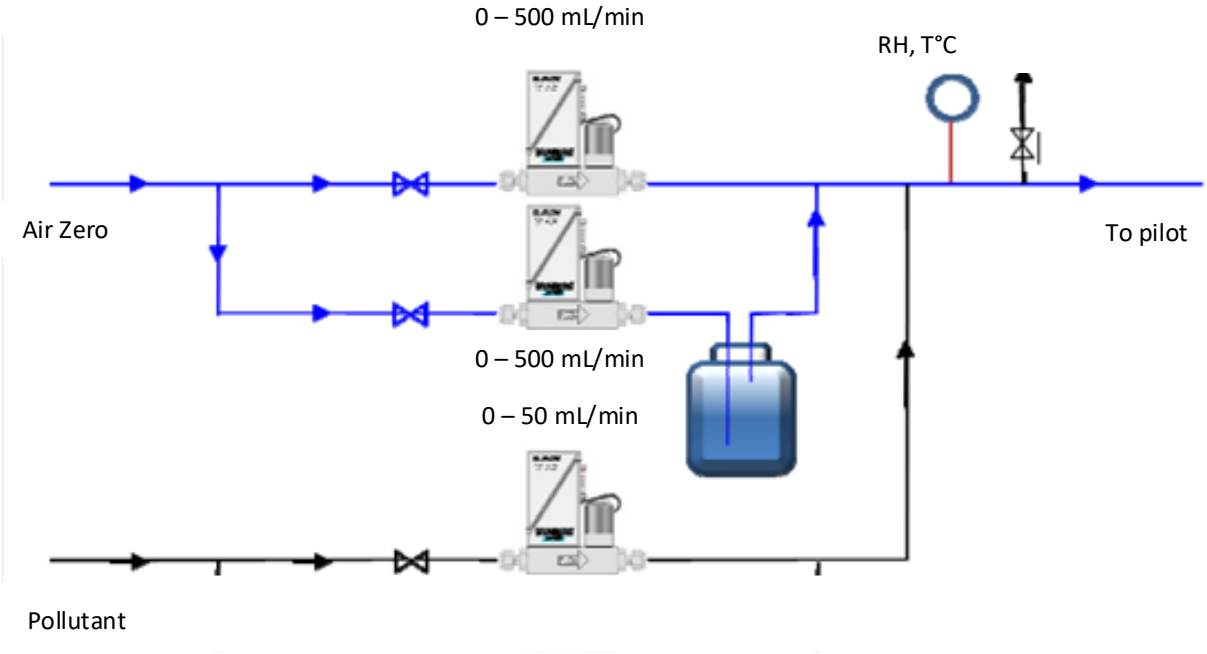

Figure 22 : Pollutant generation system for calibration

The results of this calibration are collated in Table 13. In this table, the response coefficient (k) of each compound, the correlation coefficient (R^2) corresponding to this response coefficient as well as the detection limit (LOD) are given. The detection limit was calculated by multiplying the background noise by 3.

Compound	t_R (min)	k (u.a.ppm^{-1})	R^2	LOD (ppm)
Isoflurane	11.2	5.75×10^5	0.95	0.100
Acrylonitrile	12.8	4.72×10^6	0.98	0.075

Table 13 : Calibration results for target compounds using GC/FID-MS

II.2.3.3 High performance liquid chromatography (HPLC) analysis

In order to analyze the volatile carbonyls, specifically formaldehyde and acetaldehyde, which could be potential intermediates compounds, HPLC analysis is done. The DNPH cartridges containing the air samples are first desorbed with 3 ml of acetonitrile. The eluate is then filtered and 25 µL of this eluate is injected into the HPLC Agilent 1260 Infinity device. The injected sample is driven by a solvent stream (mobile phase) through the column at a flow rate of 1 $mLmin^{-1}$. The mobile phase consists of acetonitrile, ultrapure water and formic acid (0.2%). The column used is ZORBAX Eclipse Plus C18 column with 4.6 mm diameter and length of 100 mm and 3.5 µm film thickness. It consists of octadecyl silane chemically bonded to porous silica micro-particles, which give the column an apolar character. After separation in the chromatographic column, the compounds are detected by means of a UV detector. UV detection is done at 360 nm. A general schematic representation is shown in Figure 23.

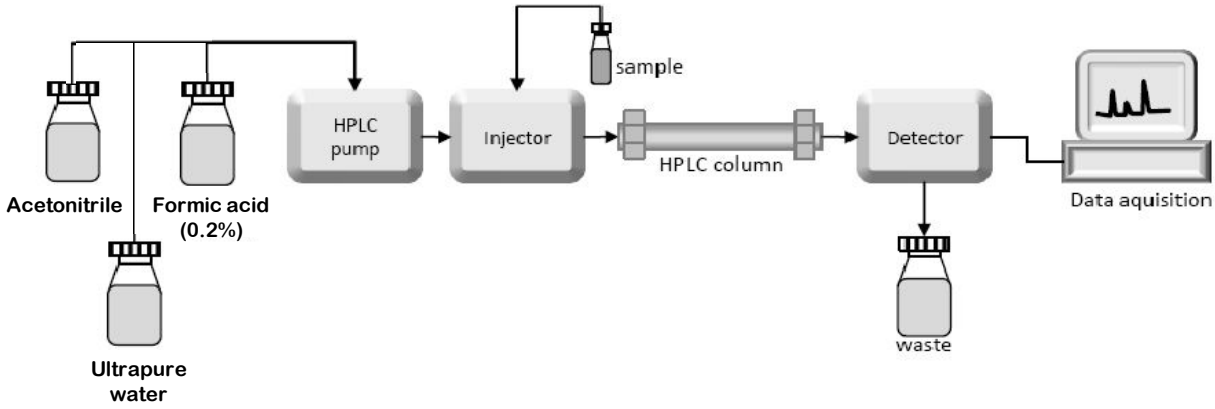

Figure 23 : Schematic representation of HPLC analytical process [14]

The calibration of these two compounds is done by generating concentrations between 0.07 and 3 ppm from certified gas cylinders. The cylinders are provided by Air Products (Acetaldehyde) and Air Liquide (Formaldehyde). Their concentrations in the cylinders are 28 ppm and 30 ppm respectively. The generation system used was the same as for the calibration of the target compounds. The results of the calibration are presented in Table 14.

Compound	t_R (min)	k (u.a.ppm^{-1})	R^2	LOD (ppm)
Formaldehyde	3.9	234.3	0.94	0.01
Acetaldehyde	5.5	71.7	0.80	0.01

Table 14 : Formaldehyde and acetaldehyde HPLC calibration results

II.2.3.4 Analysis of CO_2

The concentration of CO_2 in the reactor is measured with an Ecotech EC 9820T infra-red spectrometer. The infra-red radiation is emitted in a broad spectrum by a heating resistor. The beam passes through a gas cell where the analyzed CO_2 absorbs part of the radiation. The cell has an optical length of five meters thanks to mirrors in the cell which ensure that the beam passes through the gas several times. At the cell output, the beam passes through an optic filter with a bandwidth of 4.5 µm. The bandwidth is chosen by the manufacturer to ensure good sensitivity and low interference, especially by water. A lead selenide detector cooled to -20 °C converts the intensity of the beam into an electrical signal. A correlation wheel is placed between the source and the cell. In this way, the beam passes alternately through a chamber containing CO_2 and another containing nitrogen. The subtraction of the signals corresponding to the crossing of the two chambers eliminates the absorption of infrared radiation by molecules other than CO_2.

After passing through the Ecotech EC 9820T levels of CO_2 entering the reactor is measured at about 15 ppm. However, it is observed that during the homogenization of the pilot there was an entry of CO_2 into the photocatalytic reactor. The CO_2 entry rate in the pilot was estimated at an average of 100 ppb. min^{-1} as shown in Figure 24. For degradation tests, the incoming CO_2 is subtracted from the measured CO_2 to estimate CO_2 from the mineralization of the compounds.

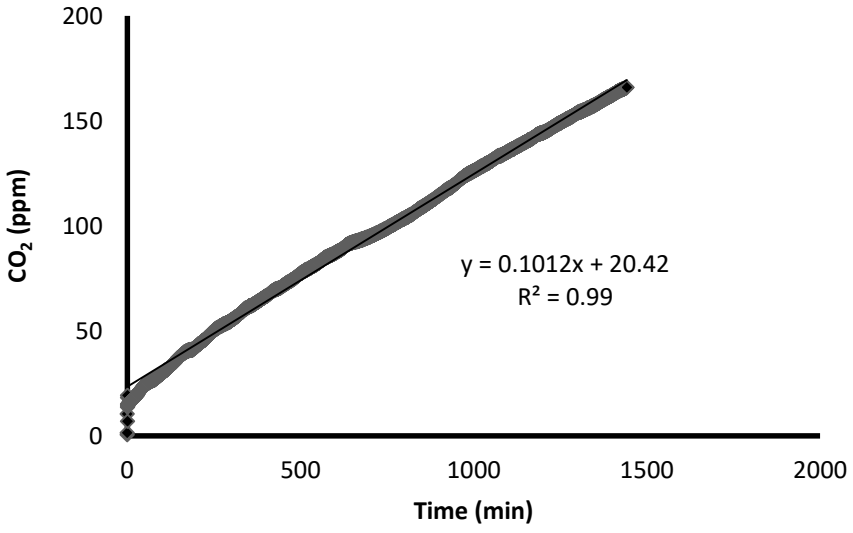

Figure 24 : Estimation of the quantity of CO_2 entering the reactor with time

II.2.4 Protocol for a photocatalytic degradation in the multi-pass reactor

Prior to each experiment, the reactor was cleaned to remove any VOCs that may be present. The UV lamps were switched on for about 5 hours to remove any organic trace present in the media while flushing with humid zero air. The pollutants (isoflurane, acrylonitrile and nitrous oxide) are then introduced into the reactor up to about 24 hours and then the inlet and outlet of the reactor are closed to homogenize the pollutants (24 hours). In the case of acetic acid, it is injected into the pilot after the 24 hr homogenization period of the target compounds and is allowed 1 hr of homogenization.

The final step is the photocatalytic degradation which involves switching on the lamps. Prior to that however, samples were collected in order to ascertain the initial concentrations of the pollutants in the pilot. During the reaction, samples were collected at regular intervals (depending on the reaction time) and then analyzed with appropriate equipment. The standard protocol for a photocatalytic degradation of the pollutants in the multi-pass photocatalytic reactor is summarized in Figure 25.

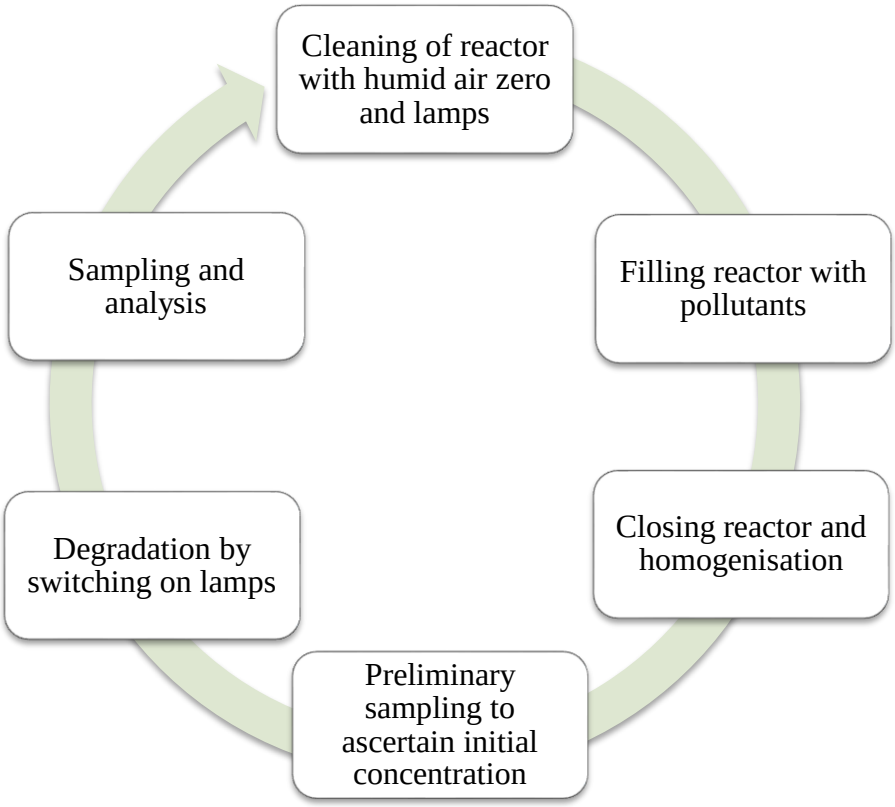

Figure 25 : Protocol used during photocatalytic degradation experiments

II.2.5 Validation of the multi-pass rector

II.2.5.1 Reactor leak tests

To verify the air tightness of the photocatalytic reactor, macro leaks were found by injecting methane into the pilot and passing a methane detector all around the pilot. The leaks that were detected were clogged. A second test was performed to quantify the micro leaks. The quantification was done by measuring the concentration of the pollutant over a course of 10 hours at several flow rates. It was observed that leak rate increased from 0.1 to 2.3% per hour when velocities were increased from 0.5 $m.s^{-1}$ to 1.5 $m.s^{-1}$ respectively (Figure 26). This led to the conclusion that the leak was derived from the rotor of the pilot fan and could not be further reduced.

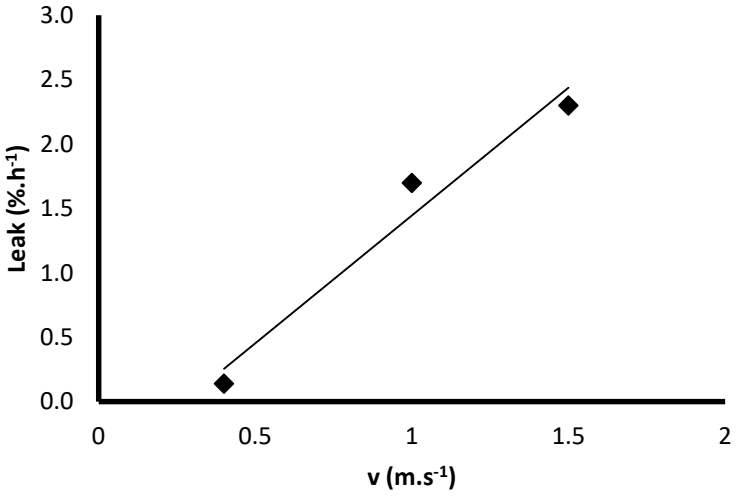

Figure 26 : Leak rate measured at different velocities

II.2.5.2 Photolysis and adsorption onto the photocatalytic media

Photolysis and adsorption are processes that could also potentially remove pollutants from the air stream and if their influence is not measured the photocatalytic removal rate could be overestimated. In order to determine whether or not the effect of these two processes can be neglected; two preliminary experiments were carried out. The pollutant concentrations were followed in the first instance with no media but with the lamps tuned on to study the possible influence of photolysis and in the second instance with the media and the lamps turned off to study the possible influence of adsorption.

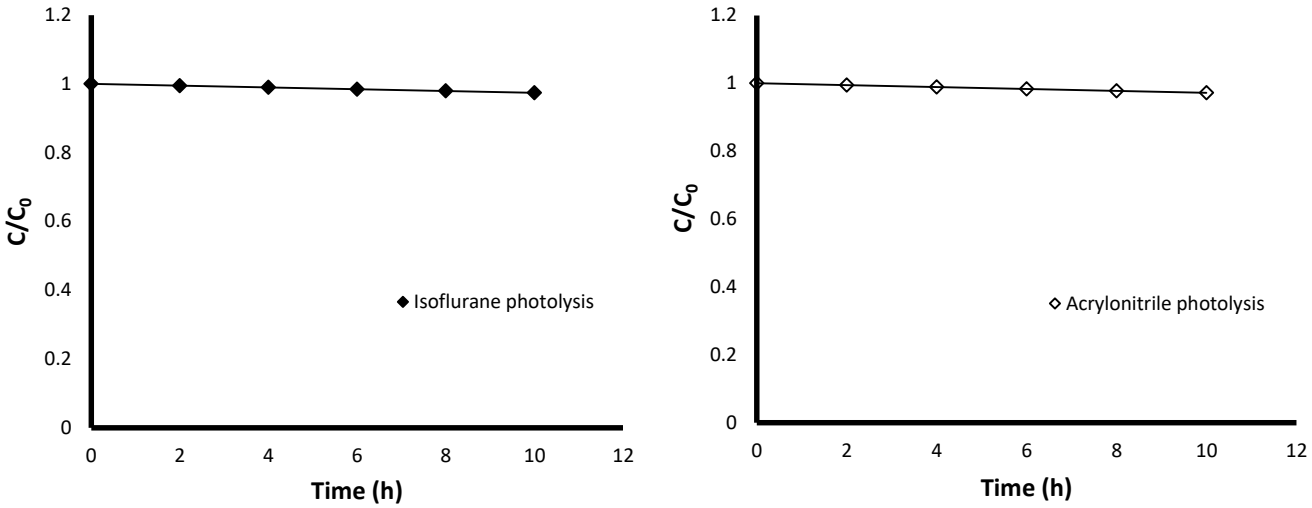

Figure 27 : Photolysis of target compounds (C_0 = 10 ppm; v = 1 m.s^{-1}; I = 4.5 mW.cm^{-2})

The removal rates were calculated at 0.1 and 0.3% per hour for adsorption and photolysis respectively and thus it was concluded that no significant loss of isoflurane and acrylonitrile was observed when illuminated without the media or when exposed to the media without illumination (Figure 27 and 28).

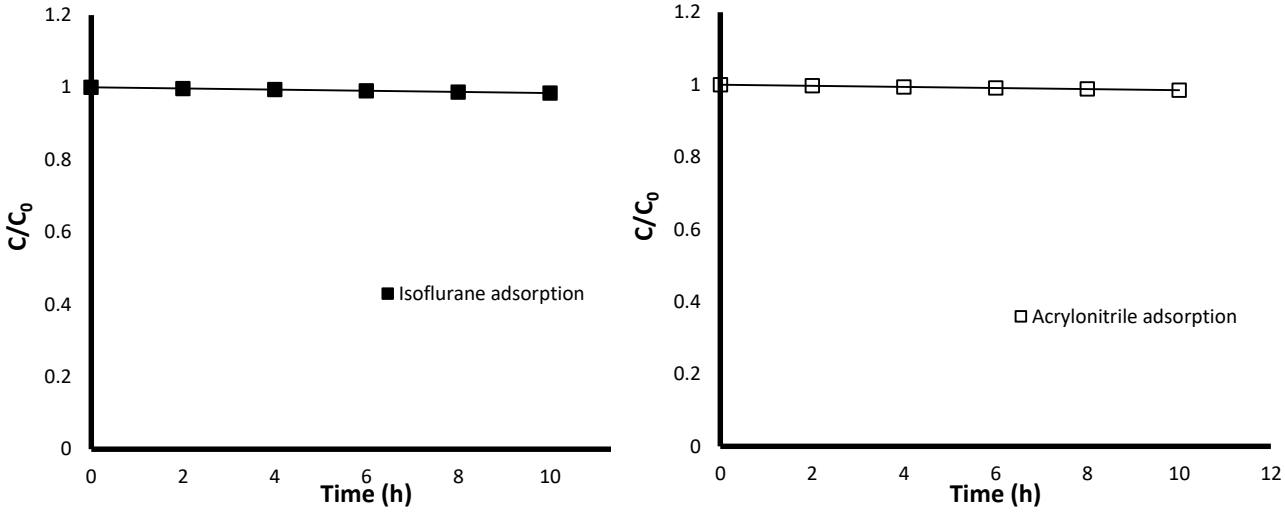

Figure 28 : Adsorption of target compounds (C_0 = 10 ppm; v = 1 m.s^{-1})

II.3 Loading of media surface with particles

The effect that the presence of particles (bio-aerosols) may have on the photocatalytic degradation efficiency was studied by clogging the media surface with micronized rice. The micronized rice particles were chosen to simulate the presence of particles. The micronized rice is white rice grains that have been finely ground with an average aerodynamic diameter of 0.5 µm and thus was a good representation of particles that could be collected on the photocatalytic media. The rice particles were generated within a laboratory test bed shown in Figure 29. A Palas RBG 1000 particle generator with a turning brush was used to disperse the particles onto the media. This generator contained cylindrical tank (diameter: 10 mm, height: 7 cm) where the particles were put. With a piston, the particles were conveyed to the brush which, whiles rotating, dispersed them. Compressed air was used to feed the generator, and allowed the particles to be conveyed onto the media that had been placed in the test bed.

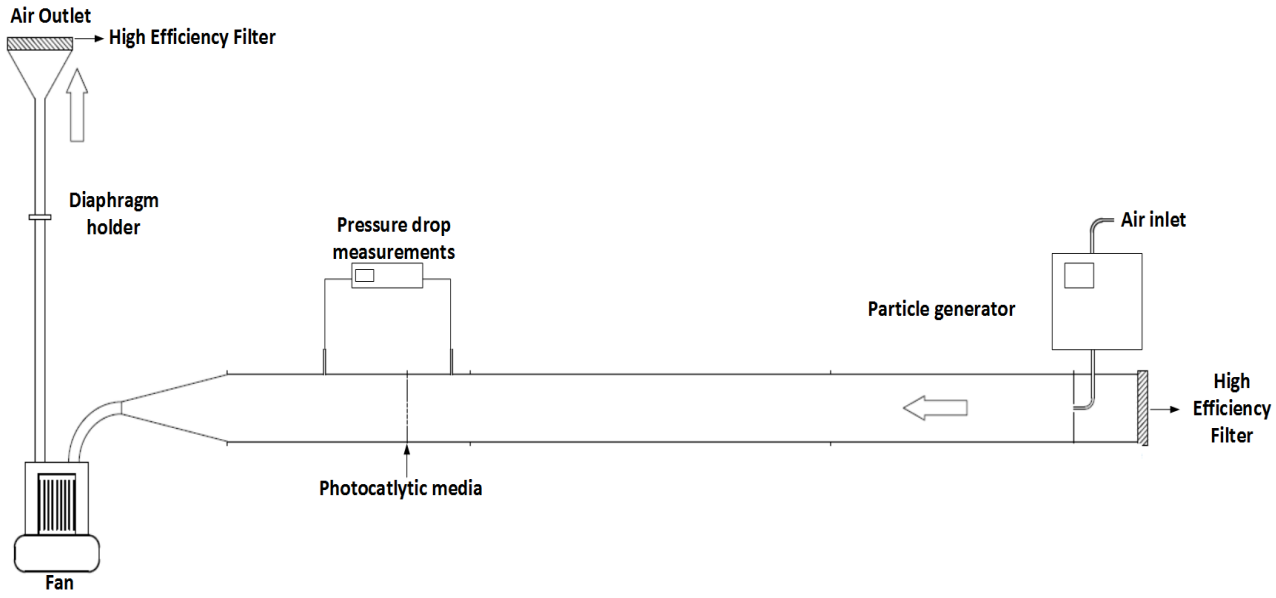

Figure 29 : Schematic representation of test bed used to load photocatalytic media with micronized rice

The generated particles were oven-dried overnight at 50 °C. A generation time of about 45 minutes allowed a loading rate of 0.002 $g.m^{-2}$. The operating conditions of the test bed and the generator are shown in Table 15.

Parameter	Value
Ascension speed of piston ($mm.h^{-1}$)	100
Turning brush speed ($turn.min^{-1}$)	1203
Test bed nominal flow rate ($m^3.h^{-1}$)	48
Test bed velocity ($m.s^{-1}$)	0.15

Table 15 : Operational parameters of Palas RBG 1000 particle generator

II.4 Experimental Method

The objective of this part is to describe the experimental strategy that is used to achieve the objectives and also the tool that is used for analyzing the results.

II.4.1 Experimental strategy

The experimental objective of this study is to perform a parametric evaluation of the effects of air velocity, light intensity, initial pollutant concentration, presence of chemical co-pollutants, presence of particles (bioaerosols), relative humidity and the change in media geometry on the photocatalytic degradation of isoflurane and acrylonitrile. In order to achieve this objective, the experimental strategy employed in this work was divided into two parts.

In the first part, the influence of the parameters on the degradation of isoflurane and acrylonitrile was determined using the plane media configuration. The parameters are divided into process parameters and environmental parameters. These parameters were all studied under conditions that were relevant to or representative of actual applications.

Two process parameters; air velocity (v) and light intensity (I) are studied within the ranges of 0.5-1.5 $m.s^{-1}$ and 1- 4.5 $mW.cm^{-2}$ respectively. These ranges were chosen based on the operating conditions typically used by commercial air purifiers.

The environmental parameters include the initial concentration, the relative humidity (RH), the presence of bio-aerosols and the presence of co-pollutants. As described in Chapter I, the concentration of the pollutants in the OR varies depending on the activities and could range from several ppb to some tens of ppm. The initial concentration is therefore studied at a range of 0.5-10 ppm. The RH recommended by several national agencies for a typical OR is

30-60% depending on the type of surgery to be performed. As the literature review showed that levels could be higher or lower than this range, the decision was made to study RH from 20 to 80%. The experimental conditions described are summarized in Table 16.

Experimental Parameter	Value
Air velocity ($m.s^{-1}$)	0.5 - 1.5
Light intensity ($mW.cm^{-2}$)	1.0 - 4.5
Initial concentration (ppm)	0.5 - 10
Relative humidity (%)	20 - 80

Table 16 : Experimental operating conditions for the PCO of isoflurane and acrylonitrile

The influence of the presence of particles (bio-aerosols) and the presence of co-pollutants is then studied. Experiments with the particles loaded onto the media are carried out and compared to experiments without the particles under the same operating conditions. The effect of the co-pollutants (nitrous oxide and acetic acid) is studied in a binary mixture with the target compounds firstly at equi-molar concentrations and then with co-pollutants at higher concentration levels. In order to determine the influence of the parameters, all other parameters are kept constant whilst the parameter of interest is varied.

In the second part, an experiment is carried out with the pleated media configuration under similar operating conditions as a reference experiment chosen for the plane media configuration. The purpose is to highlight the possible influence that the change in media geometry would have on the degradation efficiency of the target pollutants.

II.4.2 Model used for the calculation of the performance indicator

In this work the single pass removal efficiency is chosen as the quantitative descriptor to evaluate the performance of the reactor and the influence of the operational parameters. For single-pass reactors, the removal efficiency is usually calculated as

$$\alpha = 1 - \frac{C}{C_0} \qquad \textbf{Equation 23}$$

where α is the single-pass removal efficiency, C_0 is the initial concentration of pollutant entering the rector (ppm) and C is the final concentration of the pollutant leaving the reactor (ppm). The reactor used in this study however, is a multi-pass one which provides the concentration decay profile of the pollutant and does not directly give information on the single-pass removal efficiency. Thus, to be able to determine this descriptor from this type of reactor, mathematical models are needed to enable the extraction of the single-pass removal efficiency.

The model that is used in this study was developed by Dumont and Héquet [15] and has been extensively described in their paper [15]. The model was developed based on the same multi-pass reactor that is used in this study. The model is based on the one proposed by Walker and Wragg [16] for concentration-time relationships established for recirculating electrochemical reactor systems. The closed-loop reactor operating in recirculation mode was modeled by associating equations related to two ideal reactors: a perfectly mixed reservoir with a volume V_R and a plug flow system corresponding to the PCO module with a volume V_P. Considering that the volume of the PCO module is small in relation to the volume of the reservoir, the concentration-time relationship was given as:

$$\mathbf{C} = \boldsymbol{C_0}\,\mathbf{exp}\left\{-\frac{\boldsymbol{t}}{\boldsymbol{\tau_R}}\left|[\mathbf{1}-\mathbf{exp}(-\boldsymbol{\alpha})]\right.\right\} \qquad \textbf{Equation 24}$$

In this equation, the term α is the single-pass removal efficiency and represents the fraction of the total flow treated during the time τ_R (residence time in the reactor). C is the pollutant concentration at time t and C_0 is the initial pollutant concentration.

The experimental C/C_0 measurements can be fitted with the model (Equation 24) by numerical resolutions using Excel® solver. The procedure is based on the least-squares method, which minimizes the Sum of Squared Residuals (SSR) between experimental and predicted values.

$$\boldsymbol{SSR} = \sum_{\boldsymbol{i=1}}^{\boldsymbol{n}}\left\{\left(\frac{\boldsymbol{C}}{\boldsymbol{C_0}}\right)^{\boldsymbol{exp}} - \left(\frac{\boldsymbol{C}}{\boldsymbol{C_0}}\right)^{\boldsymbol{model}}\right\}^{\mathbf{2}} \qquad \textbf{Equation 25}$$

II.5 Conclusion of chapter II

In this chapter, the multi-pass photocatalytic reactor which is used for the degradation experiments is described. The sampling and analytical devices and techniques that allowed the identification and quantification of the target compounds and their possible by-products are also detailed. The photocatalytic media that is used was also characterized and certain properties like the porosity, permeability, inertial resistance factor and the UV Transmittance were determined. These characteristics are necessary as inputs for the numerical simulations that are described in chapter IV. Finally, the experimental strategy, the operational conditions and the model that are used for the determination of the performance indicator were also presented.

In chapter III, the results obtained with these experimental devices and methods and treated with the mathematical model are presented and interpreted in order to answer the research questions.

II.6 References

[1] National Center for Biotechnology Information, Acetic acid, PubChem Compd. Database. (n.d.). https://pubchem.ncbi.nlm.nih.gov/compound/176#section=Top (accessed July 31, 2018).

[2] A. Maudhuit, Purification de l'air intérieur-Elimination des micro-polluants par procédé photocatalytique, Ecole des Mines de Nantes, 2010.

[3] O. Debono, Oxydation photocatalytique de composés organiques volatils et suivi de leurs intermédiaires réactionnels : étude en réacteurs statique et dynamique à des concentrations typiques de l'air intérieur, Nantes, Ecole des Mines, 2011.

[4] F. Batault, Influence de l'adsorption et des paramètres opératoires sur le traitement photocatalytique de composés organiques volatils en mélange dans les conditions de l'air intérieur, Mines Doai et L'Université de Lille 1, 2014.

[5] M. Hajaghazadeh, V. Vaiano, D. Sannino, H. Kakooei, R. Sotudeh-Gharebagh, P. Ciambelli, Heterogeneous photocatalytic oxidation of methyl ethyl ketone under UV-A light in an LED-fluidized bed reactor, Catal. Today. 230 (2014) 79–84. doi:10.1016/j.cattod.2013.08.020.

[6] R.A.R. Monteiro, S.M. Miranda, C. Rodrigues-Silva, J.L. Faria, A.M.T. Silva, R.A.R. Boaventura, V.J.P. Vilar, Gas phase oxidation of n-decane and PCE by photocatalysis using an annular photoreactor packed with a monolithic catalytic bed coated with P25 and PC500, Appl. Catal. B Environ. 165 (2015) 306–315. doi:10.1016/J.APCATB.2014.10.026.

[7] J. Taranto, D. Frochot, P. Pichat, Photocatalytic Treatment of Air: Comparison of Various TiO_2, Coating Methods, and Supports Using Methanol or *n* -Octane as Test Pollutant, Ind. Eng. Chem. Res. 48 (2009) 6229–6236. doi:10.1021/ie900014f.

[8] L. Le Coq, Influence on permeability of the structural parameters of heterogeneous porous media, Environ. Technol. 29 (2008) 141–149. doi:10.1080/09593330802028477.

[9] R.W. Johnson, Handbook of Fluid Dynamics, Second Edition, CRC Press, 2016.

[10] K. Yazdchi, S. Luding, Towards unified drag laws for inertial flow through fibrous materials, Chem. Eng. J. 207–208 (2012) 35–48.

[11] T. Zhang, G. Jiang, Quantitative Analysis of Carbonyl-DNPH Derivatives by UHPLC–UV, (n.d.). http://www.chromatographyonline.com/quantitative-analysis-carbonyl-dnph-derivatives-uhplc-uv (accessed July 31, 2018).

[12] E. Cirera-Domènech, R. Estrada-Tejedor, F. Broto-Puig, J. Teixidó, M. Gassiot-Matas, L. Comellas, J.L. Lliberia, A. Méndez, S. Paz-Estivill, M.R. Delgado-Ortiz, Quantitative structure–retention relationships applied to liquid chromatography gradient elution method for the determination of carbonyl-2,4-dinitrophenylhydrazone compounds, J. Chromatogr. A. 1276 (2013) 65–77. doi:10.1016/J.CHROMA.2012.12.027.

[13] V. Camel, M. Caude, Trace enrichment methods for the determination of organic pollutants in ambient air, J. Chromatogr. A. 710 (1995) 3–19. doi:10.1016/0021-9673(95)00080-7.

[14] Indian Council of Agricultural Research, HPLC instrument details, (n.d.). http://14.139.58.69/icar_teldir/services/home/service_detail?name_instru=High performance liquid chromatography (HPLC)&unique_num=78&xdidz=205&p=../institute/instrument_image&d=services_inti&c=services_chargeinti&xdybz=institute_committee&qptsu=.. 2017 DKMA, ICAR (accessed July 31, 2018).

[15] É. Dumont, V. Héquet, Determination of the Clean Air Delivery Rate (CADR) of

Photocatalytic Oxidation (PCO) Purifiers for Indoor Air Pollutants Using a Closed-Loop Reactor. Part I: Theoretical Considerations, Molecules. 22 (2017). doi:10.3390/molecules22030407.

[16] A.T.S. Walker, A.A. Wragg, The modelling of concentration—time relationships in recirculating electrochemical reactor systems, Electrochim. Acta. 22 (1977) 1129–1134. doi:10.1016/0013-4686(77)80051-0.

CHAPTER III: PHOTOCATALYTIC DEGRADATION OF TARGET COMPOUNDS FROM MEDICAL ENVIRONMENTS

III.1 Introduction

Air treatment devices that use photocatalytic oxidation can potentially be used in the operating rooms (ORs) to improve the quality of air by degrading both microbiological and chemical pollutants. However in the ORs, the efficiency of these systems is based on their ability to reduce the microbiological load whilst their performance with respect to the removal of chemical pollutants is rarely looked at. It is therefore necessary that the fate of these compounds specific to the operating room is investigated.

The aim of this work is to evaluate the performance of PCO in degrading isoflurane and acrylonitrile, two pollutants that are typically found in hospital operating rooms, under conditions that are relevant to and representative of actual applications. Therefore this chapter presents the results of a parametric evaluation of the air velocity, light intensity, the change in media geometry, initial pollutant concentration, presence of chemical co-pollutants, presence of particles (bioaerosols) and relative humidity on the degradation efficiency of acrylonitrile and isoflurane. The study of the influence of the parameters aims to firstly extend the existing knowledge of their influence on PCO onto isoflurane and acrylonitrile and secondly to help improve the efficiency of the system and finally to highlight the performance of PCO in real OR conditions.

The first section of this chapter is dedicated to the experimental results obtained from the use of the plane media geometry. This media geometry has a square shape with a surface area of 0.04 m^2. It is placed perpendicularly to the flow. The lamps are placed horizontally and are also 3 cm from the media surface. Firstly, the degradation profiles of the target compounds are presented. Then to enable the calculation of the performance indicators (single-pass removal efficiency and induction period), the model developed by Dumont and Héquet is applied to the experimental points. The influence of the parameters on the performance indicators is then discussed. Finally the possible intermediate compounds and mineralization rates obtained are also presented and discussed as they provide information on the safety of the use of PCO.

The second section of this chapter deals with studying the effect of the change in media geometry on the degradation efficiency of isoflurane and acrylonitrile. The results of experiments performed with the pleated media are presented and compared to experiments made with the plane geometry under similar conditions. For the pleated media configuration,

the photocatalytic media is folded into four pleats creating two triangles at 60° with developed media surface of 0.072 m^2 as shown in Figure 19 in Chapter II. The lamps are placed vertically and are 3 cm from the middle of the pleats. The objective of this is to highlight the possible influence that the change in media geometry would have on the degradation efficiency of acrylonitrile and isoflurane.

III.2 Degradation profiles of target compounds

In this section the degradation profiles of the target compounds were observed to provide information on their behavior during PCO. For each of the compounds, the experiments were performed under reference experimental conditions which will be detailed in the sub sections. The reactor was filled with the compounds and their concentrations were left to stabilize before degradation was done. The multi-pass photocatalytic reactor enables to follow the concentration of a compound with respect to time.

III.2.1 Acrylonitrile degradation profile

To obtain the degradation profile of acrylonitrile, the reference experimental condition used was C_0 = 2 ppm, v = 1 $m.s^{-1}$ and I = 4.5 $mW.m^{-2}$ and RH = 50 %. Figure 30 shows the degradation profile of acrylonitrile. It is observed that the complete degradation of acrylonitrile was achieved after 60 minutes. The degradation profile is characterized by a mono-exponential decay curve which is representative of an apparent first order decay as shown in Figure 30. By fitting the experimental points to the mono-exponential equation [$C/C_0 = \exp(-k_{app}\, t)$], the model fit almost perfectly to the experimental points as indicated by coefficient of determination (R^2 = 0.98) in Table 17. This profile is similar to what has been described for some compounds like toluene and decane which were previously studied with the same closed loop reactor [1–4].

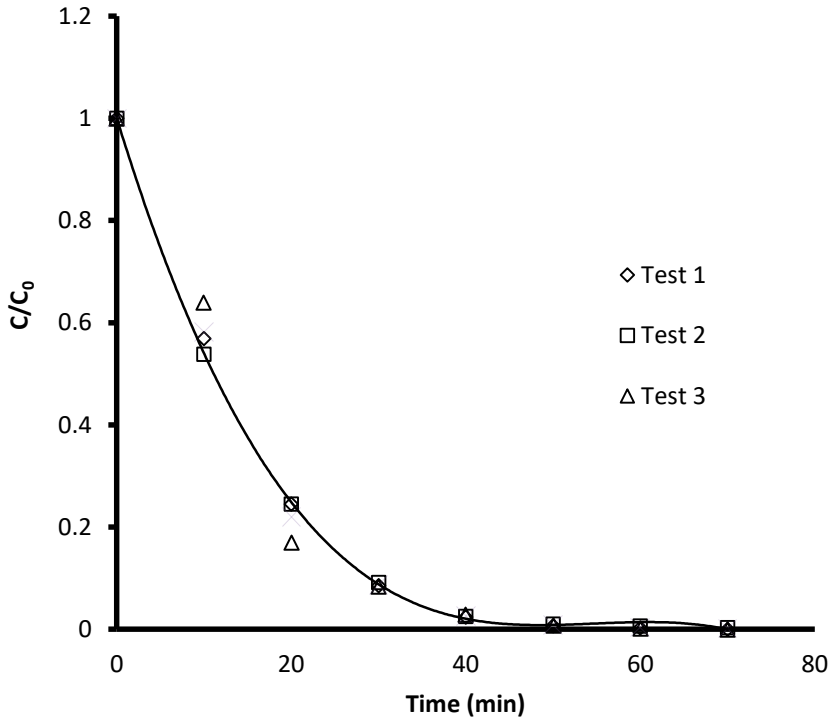

Figure 30 : Degradation profile of acrylonitrile under the reference experimental conditions of C_0 = 2 ppm; v = 1 m.s^{-1}; I = 4.5 mW.cm^{-2}; RH = 50 %

The reference experiments were performed three times to access the repeatability. The calculation of the first order constants (k_{app}) calculated from the mono-exponential equation were quite similar (Table 17) indicating the repeatability of the experiments.

Test	k_{app} (min^{-1})	R^2
1	0.0954	0.98
2	0.0960	0.98
3	0.0956	0.98
Average ± Std	0.0957 ± 0.0003	

Table 17 : First order constants and coefficient of determination calculated from first order equation for the three references acrylonitrile experiments (C_0 = 2 ppm; v = 1 m.s^{-1}; I = 4.5 mW.cm^{-2}; RH = 50 %)

III.2.2 Isoflurane degradation profile

In order to describe the behaviour of isoflurane, its degradation profile was obtained. The reference experiment was performed under the conditions of C_0 = 0.5 ppm; v = 1 m.s^{-1}; I = 4.5 mW.cm^{-2} and RH = 50 %. The degradation profile of isoflurane is presented in Figure

31. It can be observed that, under the experimental conditions, the complete degradation of isofluane is achieved at about 600 minutes of irradiation. The reference experiments were performed three times to access the repeatability and the results show that the experiments were repeatable (Figure 31).

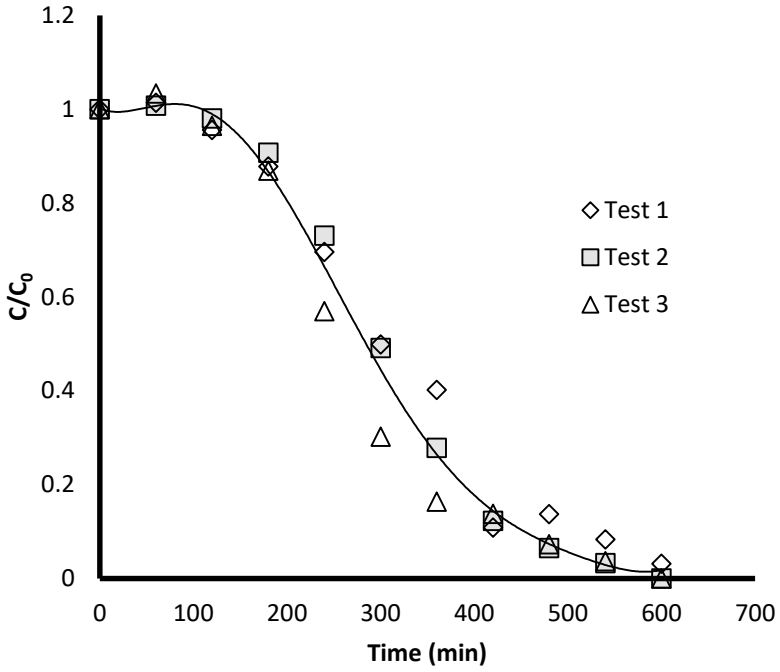

Figure 31 : Degradation profile of isoflurane under the reference experimental conditions of C_0 = 0.5 ppm; v = 1 m.s^{-1}; I = 4.5 mW.cm^{-2}; RH = 50 %

It can also be seen that the degradation curve can be divided into two distinct phases: the first phase where the degradation occurs slowly and a second phase where the degradation accelerates. Additionally, the second phase seemed to follow an exponential decay profile.

The shape of the concentration profile of isoflurane is not common in comparison to that of some compounds like toluene, decane and acrylonitrile. This unique shape has been described in very few similar instances for the photocatalytic degradation of some other chlorinated compounds like trichloroethylene (TCE) [4–8] and perchloroethylene (PCE) [9,10]. These authors observed this profile albeit the difference in experimental devices and conditions. For example Guo-Min *et al.* [6] also observed a similar profile during the degradation of TCE at 4000 ppm in a cylindrical stainless steel photoreactor which had a quartz window with the P25-Degussa TiO_2 powder uniformly coated onto the inner surface of the quartz window. Héquet *et al.* [11] observed this two phase profile when they studied the degradation of 0.8 ppm of TCE in the same reactor as the one used in this study but with

Ahlstrom photocatalytic paper. For PCE, the two stage degradation was observed by Fukami *et al*. [9] when they used a 0.8 L Pyrex reactor with the TiO_2 photocatalyst sprayed inside it to degrade 1000 ppm of PCE.

In the literature, the gas-phase PCO of TCE has been extensively studied with regards to the kinetic reaction mechanism [12–14]. It is agreed by these authors that TCE undergoes a chain reaction mechanism that involves both OH° and Cl°. The process of PCO begins when TiO_2 is illuminated with UV-light resulting in band-gap photo excitation and the generation of electron–hole pairs. The production of electron-hole pairs leads to subsequent reactions that generate hydroxyl radicals which then react with TCE. The reaction continues with the generation of Cl°. The Cl° formed ensure the continous attack of TCE by propagating a chain reaction. This propagation plays a key role in increasing the degradation rate of TCE. Based on this, a hypothesis is therefore made that isoflurane may undergo a similar reaction mechanism. That is to say that the first phase could probably correspond to isoflurane reactions with OH° resulting in the formation of Cl°. The second phase could probably be attributed to the reactions of isoflurane with Cl° leading to a possible chain propagation reaction.

III.2.3 Conclusions on degradation behavior of target compounds

Experiments were performed at selected reference conditions in order to investigate the behavior of the target compounds during their degradation by PCO. It was observed that because the target compounds belonged to different chemical families, their nature influenced their degradation differently.

First of all, acrylonitrile was degraded faster than isoflurane. Isoflurane is a halogenated compound whilst acrylonitrile is a nitrile compound with a vinyl group. According to Hodgson *et al.* [15] , the degradation efficiency follows the order : alcohols and glycol ethers > aldehydes, ketones and terpene hydrocarbons > aromatic and alkane hydrocarbons > halogenated hydrocarbons. They attributed this to the sorption capabilities of the expected type of attractive force between each compound and the photocatalyst surface. Indeed for sorption, the efficiency increases with the decrease in the vapor pressure [16]. According to the data base of the National Center for Biotechnology Information, the vapor pressure of acrylonitrile and isoflurane at 20°C is 11 kPa [17] and 32 kPa [18] respectively

making isoflurane more volatile than acrylonitrile. Conclusively, it could be assumed that acrylonitrile was better adsorbed onto the photocatalytic media surface than isoflurane. This could be one of the reasons that explain the better degradation efficiency of acrylonitrile.

Second of all, their degradation profiles were different. Whilst acrylonitrile followed a single phase exponential decay, isoflurane's degradation on the other hand followed a two phase degradation. In the first phase, the degradation is slow but accelerates in the second phase. Based on the similarities of the degradation curve to what some authors have observed for TCE, a hypothesis is made that isoflurane may undergo a similar reaction mechanism as TCE. That is to say that the first phase could probably correspond to isoflurane reactions with OH° resulting in the formation of Cl°. The second phase could probably be attributed to the reactions of isoflurane with Cl° leading to a possible chain propagation reaction.

III.3 Determination of indicators for the evaluation of the influence of the operating parameters

As previously mentioned in chapter II, to evaluate the influence of the parameters, the descriptor that was chosen was the single-pass removal efficiency. This indicator can be calculated or extracted from the degradation profiles by employing the model that describes the first order decay relationship of concentration vs. time in a multi-pass reactor developed by Dumont and Héquet and explained in their paper [19]. The model has been successfully applied to the mono-exponential (first order) decay profile of toluene to calculate the single pass removal efficiency [20] and is given as:

$$\mathbf{C} = \boldsymbol{C_0}\ \mathbf{exp}\left\{-\frac{\boldsymbol{t}}{\boldsymbol{\tau_R}}\left|[\mathbf{1}-\mathbf{exp}(-\boldsymbol{\alpha})]\right.\right\} \qquad \textbf{Equation 26}$$

In this equation, the term α is the single-pass removal efficiency and represents the fraction of the total flow treated during the time τ_R (residence time in the reactor). *C* is the pollutant concentration at time *t* and C_0 is the initial pollutant concentration. Numerical resolutions were carried out using Excel® Solver which is based on the least-square method.

To be able to study the influence of the parameters on the performance indicator, the parameter of interest was varied whilst all others were kept constant. Due to the duration of each experiment and the number of experiments that needed to be done, the coefficient of variation on the performance indicators for the reference experiments was calculated and

reported for all the set of experiments. The coefficient of variation on the reference experiment was calculated as follows:

$$\delta = \frac{\sigma}{\bar{x}} * 100 \qquad \textbf{Equation 27}$$

Where δ is the coefficient of variation, σ is the standard deviation and $\bar{x}$ is the average value of the performance indicator calculated from the three reference experiments.

III.3.1 Acrylonitrile single-pass removal calculation

The experimental points of the reference acrylonitrile experiment were fitted to the model and the results are shown in Figure 32. The experimental points were shown to fit satisfactorily to the model based on the coefficient of determination (R^2) of 0.99. The single pass removal efficiency (α) was then calculated as 0.01203 ± 0.00011. This indicated that in one pass, 1.2 % of acrylonitrile would be eliminated from the total flow that passed through the media.

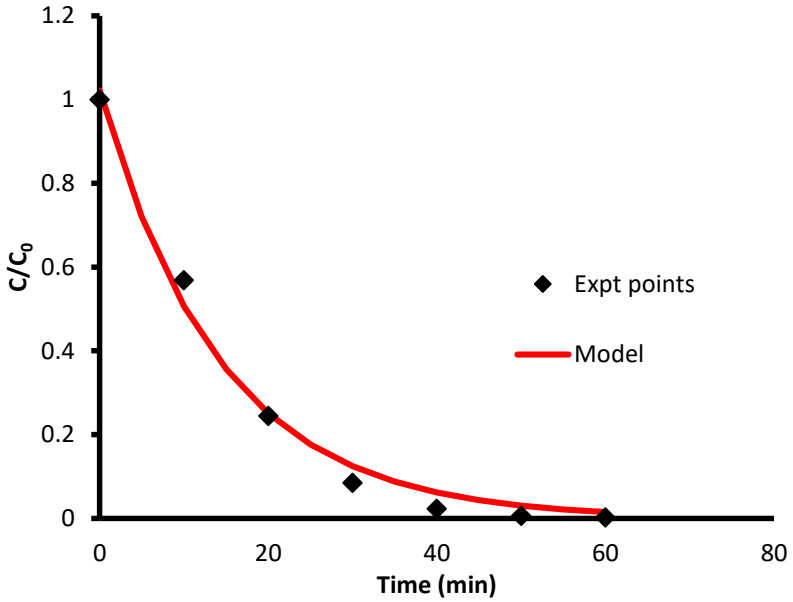

Figure 32 : Experimental degradation curve of acrylonitrile fitted to Dumont and Héquet model (C_0 = 2 ppm; v = 1 m.s^{-1}; I = 4.5 mW.cm^{-2}; RH = 50 %)

The results of the analysis of the experiments performed to study the influence of the parameters on acrylonitrile degradation are given in Table 18.

Experimental Conditions					Experimental Results	
Exp	**C_0 (ppm)**	**v (m.s^{-1})**	**I (mW.cm^{-2})**	**Varying parameter**	**α (10^{-2})**	**R^2**
1	2	1	4.5	Reference experiment	1.20	0.99
2	2	1	4.5	Reference experiment	1.22	0.99
3	2	1	4.5	Reference experiment	1.22	0.97
4	2	0.5	4.5	Velocity	4.07	0.99
5	2	0.75	4.5	Velocity	2.26	0.99
6	2	1.25	4.5	Velocity	0.92	0.97
7	2	1.5	4.5	Velocity	0.75	0.98
8	2	1	1	Light intensity	0.52	0.99
9	2	1	2	Light intensity	0.68	0.99
10	2	1	3	Light intensity	0.82	0.99
11	2	1	4	Light intensity	1.04	0.99
12	0.5	1	4.5	Initial concentration	3.16	0.99
13	10	1	4.5	Initial concentration	0.66	0.99
14	2	1	4.5	Acetic acid 2 ppm	0.96	0.98
15	2	1	4.5	Nitrous oxide 2 ppm	1.12	0.98
16	2	1	4.5	Nitrous oxide 25 ppm	0.64	0.97
17	2	1	4.5	RH 20 %	1.97	0.99
18	2	1	4.5	RH 80 %	0.98	0.99
19	2	1	4.5	Particles (bioaerosols)	0.93	0.98

Table 18 : Experimental conditions and experimental results for acrylonitrile using the Dumont and Héquet model

The coefficient of variation calculated on the single pass removal efficiency for the acrylonitrile experiments based on the mean and standard deviation of the thrice repeated reference experiment was calculated as 1 %.

III.3.2 Determination of isoflurane indicators

As previously discussed, isoflurane has a two-stage degradation profile and subsequently, two different descriptors would have to be used to evaluate the influence of the parameters. As isoflurane did not follow a mono-exponential decay profile over the entire degradation period, the model cannot be applied to the entire degradation profile. However, as the second phase can be represented by a first order decay, the model was applied only to the second phase. The choice of the number of points to fit to the model in order to calculate the single pass removal efficiency (α) was based on a coefficient of determination (R^2) above 0.9. In so doing, the model enabled the calculation of the single-pass removal efficiency for the second phase. Additionally, by applying the model to the second phase it provided an idea of the duration of the first phase which is the period where the model did not fit the experimental points because the first phase cannot be represented by a first order decay. Consequently the induction period (τ_i), which is the duration of the first phase was chosen as the descriptor for phase one.

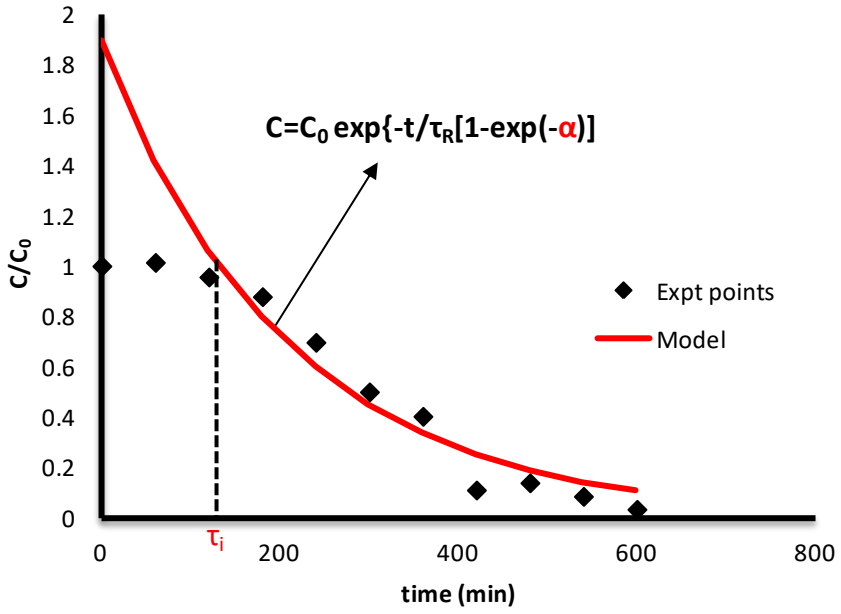

Figure 33: Experimental degradation curve of isoflurane fitted to Dumont and Héquet model (C_0 = 0.5 ppm; v = 1 m.s^{-1}; I = 4.5 mW.cm^{-2}; RH = 50 %)

Figure 33 shows the experimental concentration decay curve of the reference experiment fitted to the model (Equation 31). As it can be observed in Figure 33, from irradiation time of about 130 minutes the model described the experimental values quite satisfactorily (R^2 = 0.94) but did not fit the values from t = 0 to t = 130 minutes. By modeling the second phase with the Dumont and Héquet model it was then possible to determine the

induction period (τ_i) as 137 ± 6 min and calculate the α for the second phase as $(8.2 \pm 0.8)x10^{-4}$. The results of the analysis of experiments performed to study the influence of the parameters on isoflurane degradation are given in Table 19.

	Experimental Conditions				Experimental Results		
Exp	**C_0 (ppm)**	**v ($m.s^{-1}$)**	**I ($mW.cm^{-2}$)**	**Varying parameter**	**τ_i (min)**	**α (10^{-4})**	**R^2**
1	0.5	1	4.5	Reference experiment	130	8.22	0.94
2	0.5	1	4.5	Reference experiment	140	8.77	0.93
3	0.5	1	4.5	Reference experiment	142	8.79	0.94
4	0.5	0.5	4.5	Velocity	45	23.20	0.98
5	0.5	0.75	4.5	Velocity	75	11.37	0.95
6	0.5	1.25	4.5	Velocity	205	6.27	0.91
7	0.5	1.5	4.5	Velocity	225	4.88	0.91
8	0.5	0.5	1	Light intensity	250	12.80	0.92
9	0.5	0.5	2	Light intensity	200	17.50	0.91
10	0.5	0.5	3	Light intensity	130	18.60	0.91
11	0.5	0.5	4	Light intensity	90	19.90	0.94
12	2	1	4.5	Initial concentration	300	4.90	0.96
13	10	1	4.5	Initial concentration	600	3.16	0.96
14	0.5	1	4.5	Acetic acid 0.5 ppm	160	8.16	0.93
15	0.5	1	4.5	Nitrous oxide 0.5 ppm	170	7.05	0.92
16	0.5	1	4.5	Nitrous oxide 6ppm	200	2.96	0.95
17	0.5	1	4.5	RH 20 %	95	10.26	0.98
18	0.5	1	4.5	RH 80 %	170	7.45	0.92
19	0.5	1	4.5	Particles (bioaerosols)	171	7.35	0.95

Table 19 : Experimental conditions and experimental results for isoflurane using the Dumont and Héquet model

The coefficient of variation on α and τ_i was calculated as 9 % and 5 % respectively based on the repetition of the reference experiment.

III.4 Influence of the operating parameters

The objective of this section is to investigate how varying the parameters influences the performance of PCO during the degradation of the target compounds. The parameters that were studied can be classified into two categories: the process parameters and the environmental parameters. The process parameters, air velocity and light intensity, are two factors that can be controlled on the photocatalytic reactor whilst the environmental parameters cannot be controlled. Studying the influence that varying these parameters have on the degradation efficiency helps to also highlight how the PCO degradation efficiency is affected in real OR applications and also to provide some recommendations on how to improve the degradation efficiency of the target compounds.

III.4.1 Influence of air velocity (v)

In this work, the velocity is studied in order to determine the sensitivity of PCO performance to a change in velocity and to provide some recommendation to improve the PCO performance. To study the influence of air velocity, experiments were carried out at velocities ranging from 0.5 to 1.5 $m.s^{-1}$. This range was chosen based on the operating conditions typically used by a commercial air purifier that was studied.

The influence of velocity on the degradation efficiency can be different depending on the mode of operation of the photocatlytic reactor. That is to say whether the reactor operates under single-pass or multi-pass.

For single-pass reactors, the effect of air velocity is known to present a dual antagonistic effect [21]. As the velocity increases the mass transfer improves but the contact time between the pollutant and the photocatalytic media decreases. Some authors have observed a positive effect of the increase in velocities on the photocatalytic degradation of pollutants due to improvement in mass transfer [22,23] whilst others have observed negative effect of increasing velocities attributed to insufficient contact time [24–26]. Depending on the range of velocities studied, a transition between the effects can also be observed. For example, Yang *et al.* [27] studied the degradation of formaldehyde using a single pass tubular foam-nickel PCO reactor with the TiO_2 powder immobilized on porous nickel substrate. They observed that the removal efficiencies increased when velocities were increased from 0.47 to 0.66 $m.s^{-1}$, whilst removal efficiencies decreased when velocities ranged from 0.66 to

0.94 $m.s^{-1.}$ They explained this by the fact that when velocities were increased from low values (0.47 $m.s^{-1}$) there was an enhancement in the mass transfer rate leading to an increase in removal efficiencies. However, once the air velocity reached 0.66 $m.s^{-1}$, the removal efficiencies declined due to a reduction in contact time between the pollutants and the photocatalytic media. At this stage, the process was no longer controlled by the mass transfer but by the surface reaction.

The Reynolds number has been described as a good indicator to set an appropriate regime to determine mass transfer limitations. Obee [28] demonstrated when he studied the degradation of 0.7 ppm of toluene in a TiO_2-coated glass-plate reactor that with a Reynolds number over 500 the photocatalytic reaction was less influenced by mass transfer. In the present work, the velocities studied provide a Reynolds number that range from 6500 to 19800. This means that the mass transfer is not a limiting factor.

In multi-pass reactors, the velocity brings into play an additional phenomenon which is the number of passes of the pollutant through the media. However, since the Reynolds number in the multi-pass reactor is sufficiently high enough, the effect of mass transfer can be neglected. Therefore, when the velocity within the media is increased, the contact time decreases but then the number of passes of the pollutant through the media increases. The superposition of these two effects subsequently makes it difficult to highlight the influence of velocity on the reaction rate. Consequently, the global effect of the velocity on the degradation remains the same irrespective of the velocity. In studying the degradation of toluene in a multi-pass reactor, Batault *et al.* [29] observed that the velocity had no influence on the kinetic constant due to the superposition of the contact time and number of passes.

In this study however, the air velocity was shown to have an influence on the entire kinetic curve of both isoflurane and acrylonitrile even though operating in a multi-pass system as shown in Figure 34 and Figure 35 respectively.

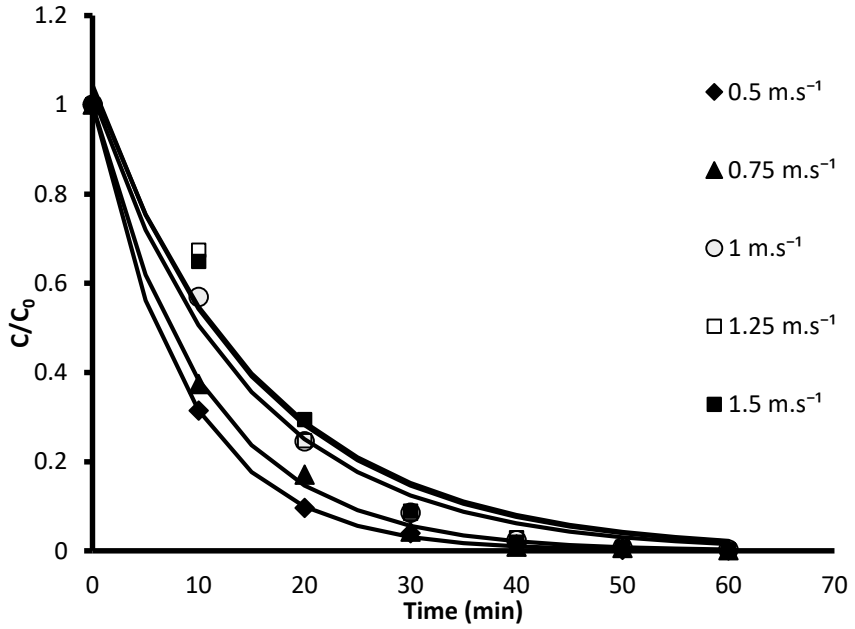

Figure 34 : Degradation curves of acrylonitrile velocity experiments fitted to model to obtain α (C_0 = 2 ppm; I = 4.5 mW.cm^{-2}; RH = 50 %)

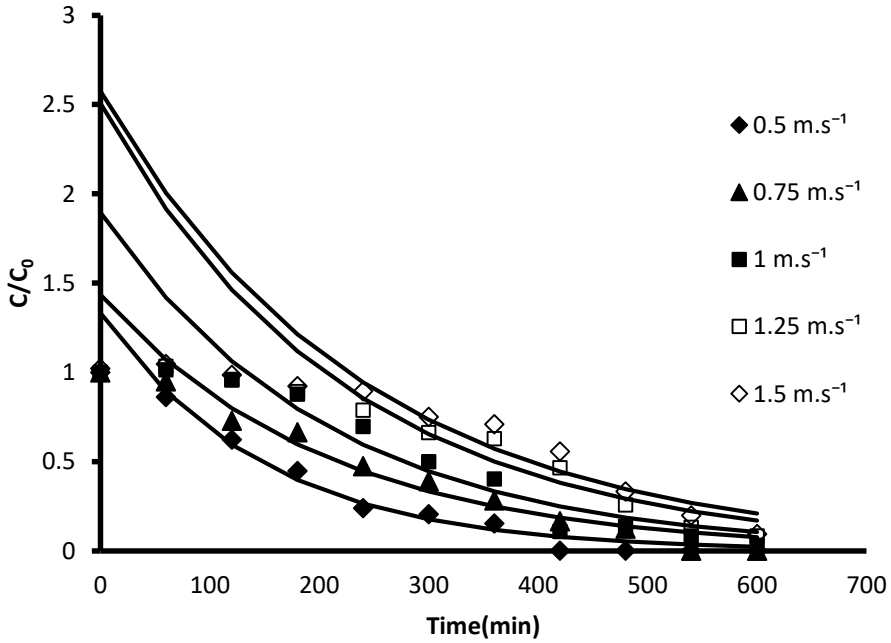

Figure 35 : Degradation curves of isoflurane velocity experiments fitted to model to obtain τ_i and α (C_0 = 0.5 ppm; I = 4.5 mW.cm^{-2}; RH = 50 %)

An assumption is made that there is competition created between the velocity of the molecules through the media and the amount of time needed for molecules to react with active species created by the media. Thus, increasing the velocity tends to not favor the occurrence of the chemical reaction. This would in turn emphasize the influence of air

velocity on the kinetic degradation. In order to clearly bring into evidence the influence of the velocity on the degradation of isoflurane and acrylonitrile, the single-pass removal efficiency is chosen as one of the descriptors. The results obtained for isoflurane and acrylonitrile experiments are discussed below.

For acrylonitrile, C_0 and I were maintained at 2 ppm and 4.5 mW.cm^{-2} respectively whilst for isoflurane they were maintained at 0.5 ppm and 4.5 mW.cm^{-2}. The results are first presented for acrylonitrile and then for isoflurane. Figure 36 shows the dependency of α on air velocity during acrylonitrile degradation. As the velocity is increased from 0.5 to 1.5 m.s^{-1}, the α decreases from 0.04 to 0.007.

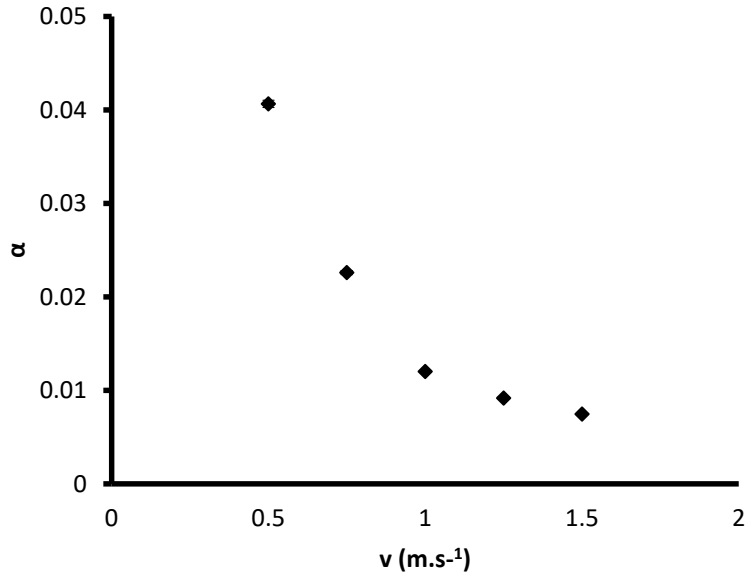

Figure 36 : Influence of air velocity on the single-pass photocatalytic removal efficiency of acrylonitrile at experimental conditions of C_0 = 2 ppm; I = 4.5 mW.cm^{-2}; RH = 50 %

For isoflurane an increase in the air velocity had a negative influence on both the induction period (τ_i) and the single-pass removal efficiency in that the single-pass removal efficiency (α) was decreased from 0.0023 to 0.00048 whilst the induction period was increased from 45 to 225 minutes as shown in Figure 37.

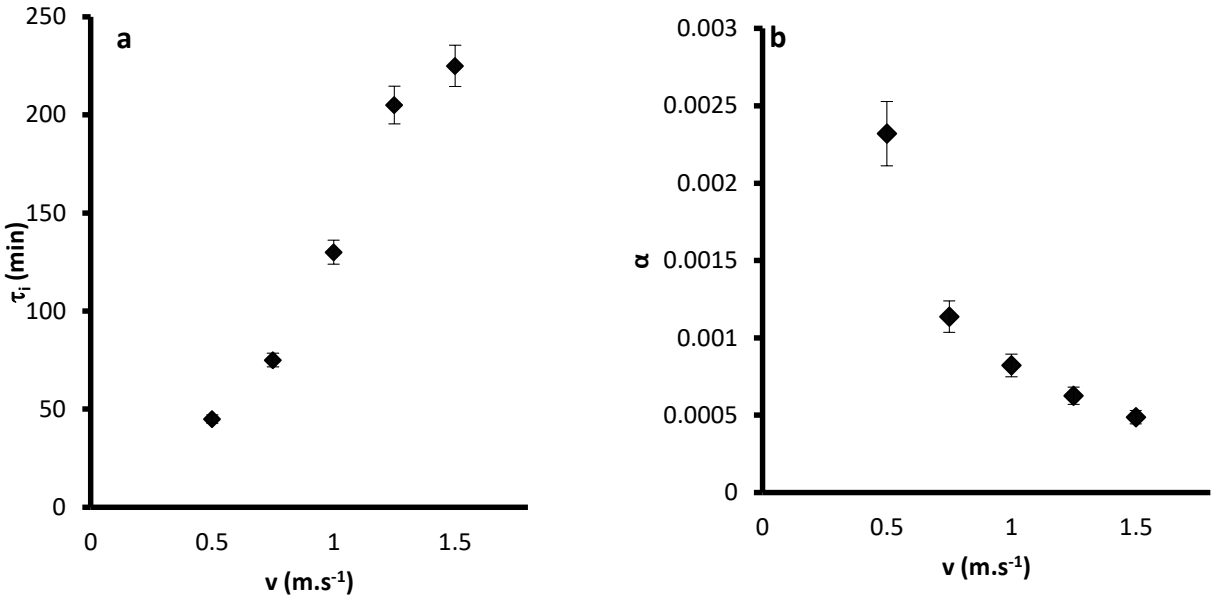

Figure 37 : Effect of air velocity on (a) the length of the induction time (b) the single-pass removal efficiency determined during isoflurane degradation at experimental conditions of C_0 = 0.5 ppm; I = 4.5 mW.cm^{-2}; RH = 50 %

The trend of decreasing removal efficiency due to increase in velocity observed for these two compounds is in accordance with with what some authors observed in the literature. Zhong *et al.* [26] studied the degradation of 8 VOCs (ethanol, 1-butanol, hexane, octane, acetone, MEK, toluene and p-xylene) at 0.5 ppm in a single-pass reactor fitted with a commercial media consisting of TiO_2 coated on glass fibers. They observed that when the velocities were increased from 0.12 to 0.76 m.s^{-1}, the removal efficiencies of all the compounds decreased. Similarly, Ginestet *et al*. [30] found that the single-pass removal efficiencies of ethanol, toluene and acetone decreased in half when airflow rate increased from 40 m^3.h^{-1} to 80 m^3.h^{-1}. They performed the studies in a PCO device that was equipped with a plane photocatalytic media made up of a porous substrate coated with TiO_2 powder. These authors concluded that by increasing the velocity, the residence time of the pollutants within the media was decreased consequently leading to shorter contact time between the molecules and the photocatalytic media which then led to a decrease in the removal efficiencies.

For both isoflurane and acrylonitrile, decreasing the air velocity causes an increase in the single-pass removal efficiencies. This could be attributed to the fact that lowering the air velocity potentially increases the residence time of the molecules in the media so that the molecules have enough time to be adsorbed on the surface of the media and thus have a better

chance to participate in reactions with the active species and be degraded. In the case of isoflurane, as the velocities are increased, the molecules are not given enough time to react with the OH° which would allow for the production of enough Cl° to initiate the second phase and thus the induction period takes longer.

The influence of the contact time on α for both compounds was then evaluated. In this study, the contact time is defined as the contact length between the air and the photocatalytic media divided by the velocity. However since the contact length is fixed but not known the inverse of the velocity was used to assess the role of the contact time on the single-pass removal efficiency. Figure 38 clearly shows that α increases with 1/v. The relationship was also observed to be exponential which was in accordance with what some authors had described for single pass reactors. Quici *et al.* [25] who studied the degradation of toluene in a tubular-flow reactor coated with TiO_2 and Hogdson *et al.* [15] who studied the degradation of 27 VOCs in PCO reactor equipped with a TiO_2 coated aluminum honeycomb monoliths reported the evolution of removal efficiency in function of the contact time showed an exponential increase.

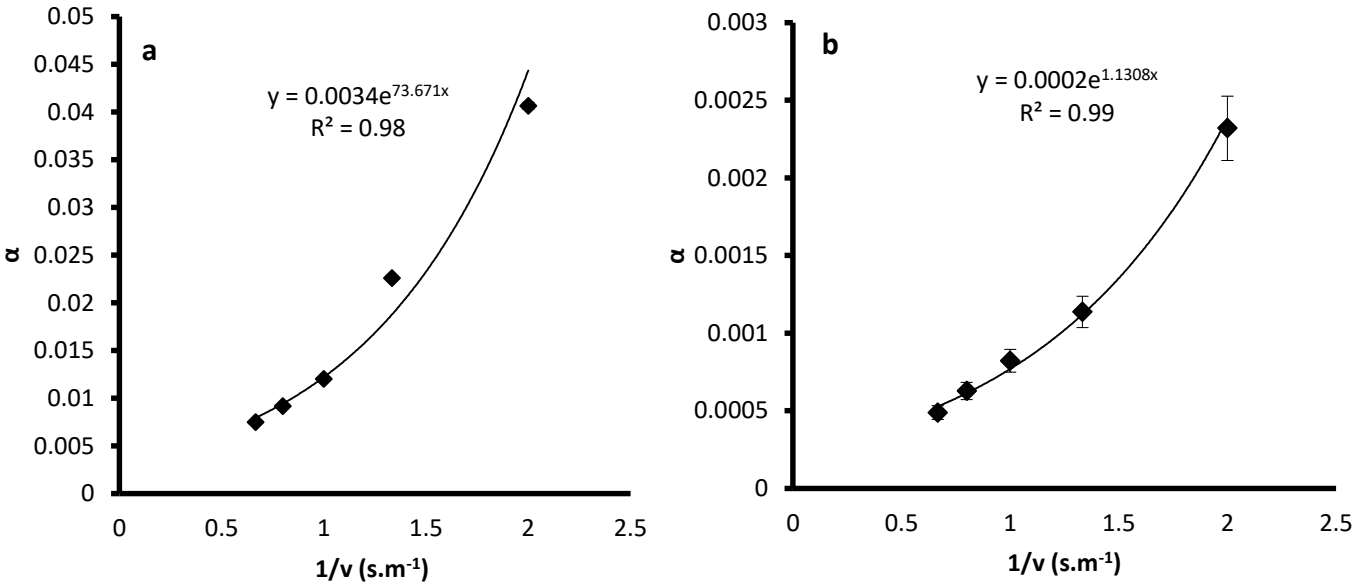

Figure 38 : Single-pass removal efficiency vs 1/v for (a) acrylonitrile (b) isoflurane

The study of the influence of velocity on the degradation of acrylonitrile and isoflurane showed that increasing the contact time between the molecules and the photocatalytic media is an important factor in improving the efficiency of the degradation

system. Consequently, it can be said that, to be able to improve the effectiveness of removal, shorter induction times and high single pass removal efficiencies are needed for isoflurane whilst high single pass removal efficiencies are needed for acrylonitrile. This can be achieved at lower velocities.

III.4.2 Influence of light intensity (I)

During PCO, the light intensity plays a crucial role on the degradation of pollutants as UV light generates photons that activate the photocatalyst to create the electron-hole pairs that in turn leads to the photocatalytic oxidation of the pollutants [32].

In photocatalysis, the influence of light intensity varies as a power function, I^n where n approaches 1 at very low intensities and approaches 0 at very high intensities. According to what is commonly agreed in the literature, depending on the range of light intensities studied, the order "n" can transition into 3 regimes [33,34]. At low light intensity, the production of electron-hole pairs is low and so they are rapidly consumed by the chemical reactions resulting in a linear increase in the reaction rate (n = 1). At medium- high light intensity, rate of formation of electron-hole pairs is higher than their consumption leading to recombination of the charges resulting half order increase in the reaction rate (n = 0.5). At very high light intensity, the electron-hole recombination is so fast that the degradation efficiency no longer depends on the light intensity and reaches a plateau (n = 0). Yu *et al*. [23] studied the degradation of formaldehyde (1 ppm) on a polytetrafluoroethylene (PTFE) filter coated with TiO_2 and placed in a closed-loop photocatalytic reactor at light intensity range of 0.05 to 0.25 $mW.cm^{-2}$. They reported an increase in the first order and concluded that the electron hole pairs were consumed rapidly during the degradation of formaldehyde. Lim and Kim [35] who studied the degradation of trichloroethylene (212 ppm) in a fluidized bed reactor however, reported a transition of regimes from first order to half-order when light intensities were increased from 0.25 to 9 $mW.cm^{-2}$. They observed that observed that when the light intensity increased from 0.25 to 2 $mW.cm^{-2}$, the degradation efficiency of TCE increased linearly (n=1) due to the rapid consumption of the electron hole pairs. When the light intensity was increased from 2 to 9 $mW.cm^{-2}$, the degradation efficiency followed a half order regime (n = 0.5) which they attributed to faster electron-hole recombination.

It should be mentioned that an increment in the light intensity leads to higher degradation rate, however excessive light intensity diminishes the quantum efficiency due to electron-hole recombination. When electron-hole pairs created by the photons recombine, these photons are not utilized effectively. In this way, increasing the light intensity causes much more energy waste instead of much more degradation of VOCs consequently imposing unnecessary energy costs [36].

Based on the operating conditions typically used by commercial devices, the range to be studied in this work was 1-4.5 $mW.cm^{-2}$. The objective of studying the influence of light intensity on the degradation of acrylonitrile and isoflurane was to be able to see if this range was appropriate for their degradation and if it was necessary to recommend higher intensities.

Figure 39 shows the influence of the light intensity on the α during acrylonitrile degradation. The initial concentration and velocity were fixed at 2 ppm and 1 $m.s^{-1}$ respectively. From the graph, it can be seen that the α increases from 0.005 to 0.12 when the light intensity increases from 1 to 4.5 $mW.cm^{-2}$. It can also be observed that the relationship between I and α is well explained by the power trend and has an order n = 0.5.

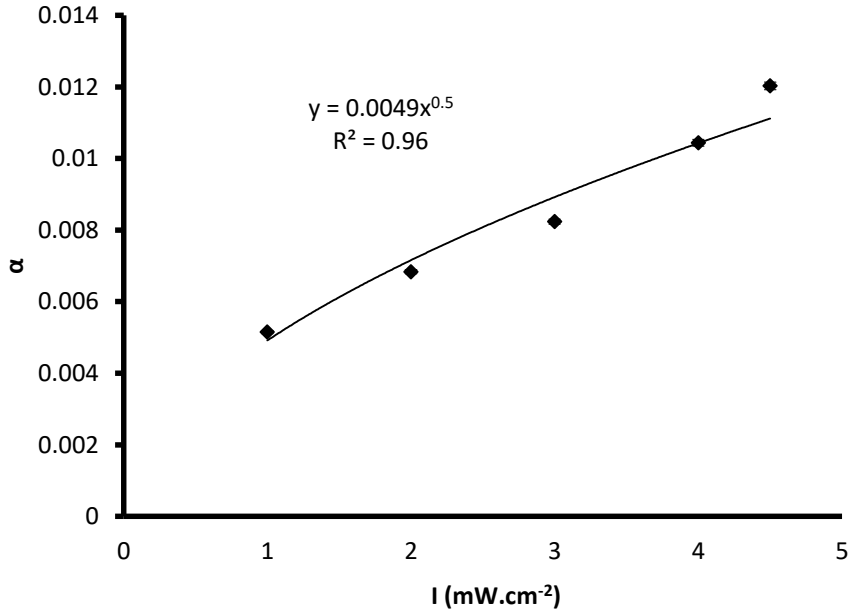

Figure 39: Effect of light intensity the single pass removal efficiency determined during acrylonitrile degradation (C_0 = 2 ppm; v = 1 $m.s^{-1}$; RH = 50 %)

Figure 40a shows the influence of light intensity on τ_i whilst Figure 40b shows the influence of light intensity on α. The graphs show that the induction period decreased whilst the single-pass removal efficiency increased when the light intensity was increased. It can also be observed that the relationship between I and α is well explained by the power trend and has an order n = 0.4. Based on Figure 40a it could be concluded that the decreasing in the induction period is because higher intensities allow higher generation of OH° which are needed to oxidize isoflurane to produce enough Cl° to initiate the acceleration of the degradation. It can also be observed that the induction period could be reduced to 0 when light intensities reach above 5 mW.cm^{-2}.

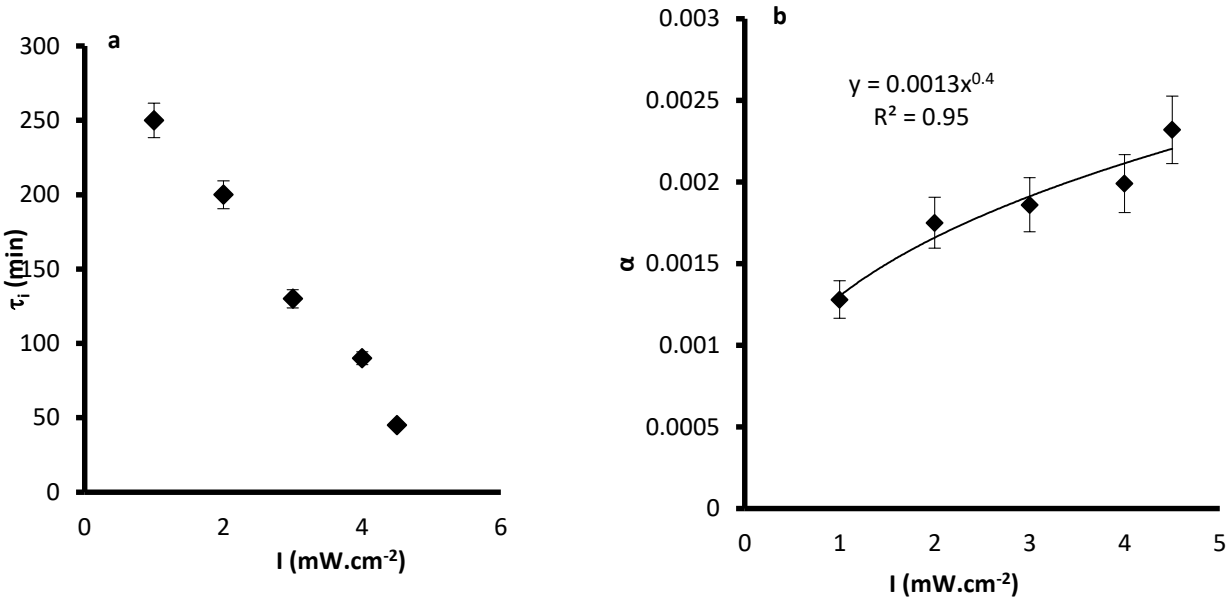

Figure 40: Effect of light intensity on (a) the length of the induction time (b) the single pass removal efficiency determined during isoflurane degradation (C_0 = 0.5 ppm; v = 0.5 m.s^{-1}; RH = 50 %)

The relationship between the single-pass removal efficiency and light intensity was non-linear and was well described by a power function. The power exponent was calculated as 0.5 for acylonitrile and 0.4 for isoflurane. This result is similar to what Raillard *et al*. [37] reported when they studied the degradation of toluene in a closed loop reactor at similar light intensities of 1 to 4 mW.cm^{-2}. This half-order relationship indicates that over the range of light intensities studied, the reactions were dominated by the electron-hole recombination effect. As previously mentioned, the efficiency increases with the light intensity since more hydroxyl radicals are generated. However, the recombination of the electron-hole pairs at high light intensity inhibits the rate of electron transfer and thus increasing the light intensity would not significantly improve or influence the removal efficiencies but would only impose unnecessary energy costs.

According to our results, for the range of light intensities studied, higher light intensities provide better degradation performance as it guarantees shorter induction periods for isoflurane and better removal efficiencies for both compounds. However, due to reduction in quantum efficiency as a result of the domination of electron-hole recombination, increasing the light intensity above 5 $mW.cm^{-2}$ would not significantly improve the removal efficiencies but would only impose unnecessary energy costs.

III.4.3 Influence of initial concentration (C_0)

As discussed in Chapter I, the concentration of the pollutants in the OR varies depending on the activities performed and could range from several ppb to some tens of ppm. For this reason, the initial concentrations of acrylonitrile and isoflurane were therefore studied from 0.5 to 10 ppm. This would provide some knowledge on the performance of PCO in degrading these compounds under possible OR concentrations.

Acrylonitrile experiments were conducted at fixed velocity and light intensity of 1 $m.s^{-1}$ and 4.5 $mW.cm^{-2}$ respectively. The results of the influence of concentration on the single-pass removal efficiencies are presented in Figure 41. From the graph it can be observed that α decreases from 0.03 to 0.006 when the concentrations are increased from 0.5 ppm to 10 ppm.

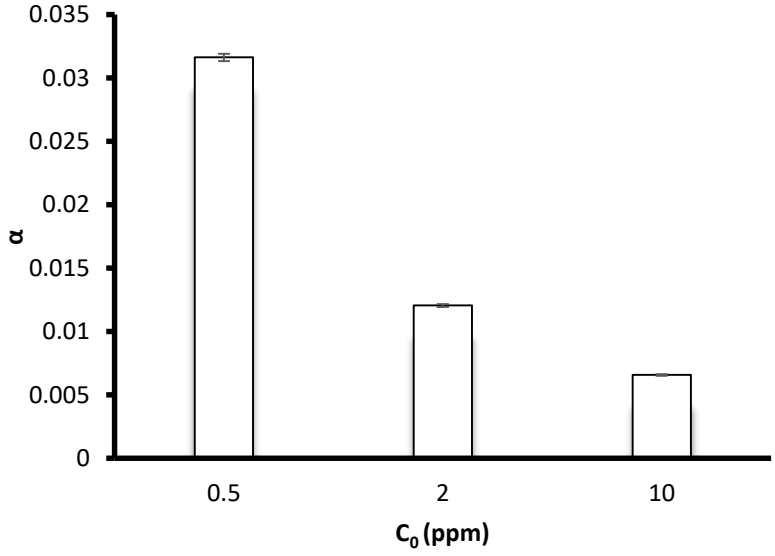

Figure 41: Effect of initial concentration on the single pass removal efficiency determined during acrylonitrile degradation (v = 1 $m.s^{-1}$; I = 4.5 $mW.cm^{-2}$; RH = 50 %)

Figure 42a depicts the dependence of the induction period on the initial concentration whilst Figure 42b shows the effect of the initial concentration on the removal efficiencies for isoflurane degradation. Isoflurane experiments were conducted at fixed velocity and light

intensity of 1 $m.s^{-1}$ and 4.5 $mW.cm^{-2}$ respectively. It can be observed that increasing the initial concentration negatively impacts the degradation of isoflurane as the inductions periods increase and the single-pass removal efficiencies decrease.

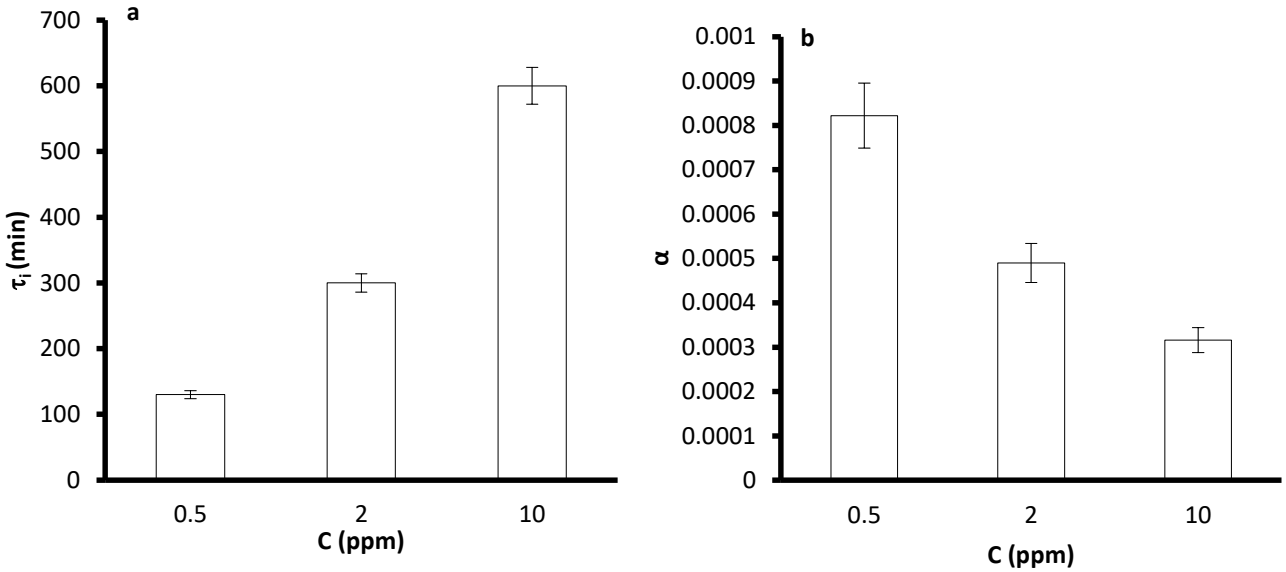

Figure 42: Effect of initial concentration on (a) the length of the induction time (b) the single pass removal efficiency determined during isoflurane degradation (v = 1 $m.s^{-1}$; I = 4.5 $mW.cm^{-2}$; RH = 50 %).

From literature, the pollutant initial concentration plays an important role on the performance of photocatalytic oxidation. For various classes and concentration ranges of VOCs, higher concentrations generally result in lower removal efficiencies [21,38]. This can be explained from two perspectives. Firstly, due to the fixed active sites on the photocatalytic media surface the amount of molecules effectively participating in the photocatalytic reaction is not enhanced in the same ratio as an increase of the inlet concentration resulting in a decrease of removal efficiency [21,39]. Secondly, there could be the interference of intermediates as higher amounts of intermediates generated during PCO reactions could occupy part of the active sites and impede the degradation progress [40,41]. Zhong *et al*. [41] studied the degradation of eight VOCs using a media made up of TiO_2 coated on fiber glass fibers placed in a open-loop PCO reactor. They found that the removal efficiency of all eight VOCs decreased when the initial concentrations were increased from 0.25 to 1 ppm. They attributed this behavior to the limited adsorption capacity of the fixed active sites at the catalyst surface. The amount of active sites compared to pollutant molecules decreases and consequently the removal efficiency is decreased.

For both acrylonitrile and isoflurane the trend of decreasing removal efficiencies for increasing initial concentration observed could be attributed to the phenomena of competitive

adsorption and catalyst saturation. Due to the limited number of active sites on the media, an increase in concentration leads to competition between molecules for chance to be adsorbed onto the active sites and degraded consequently more molecules pass through the media without undergoing degradation. This is in accordance with what Jafarikojour *et al*. [42] observed for toluene degradation at concentration range of 20 to 100 ppm.

For isoflurane, the induction period is seen to increase significantly when the inlet concentrations are increased. This can be explained by the fact that as the concentration of isoflurane increases, more OH° are required to oxidize the higher number of molecules in order to initiate Cl° generation thus longer induction periods occurs until sufficient concentration of Cl° are formed to initiate the acceleration of the reaction.

In this work, the range of concentrations studied show that a better removal of the pollutants will be achieved at lower concentrations. This is due to the fact that at higher pollutant concentrations, the number of active sites on the media is a limiting factor for efficient degradation. However as the concentrations of the pollutants vary in the OR, in order to maximize the performance of PCO it can be recommended that the unit have multiple photocatalytic banks (photocatalytic media and UV lamps). These would give the polluted air a chance to pass through several irradiated photocatalysts before it exits the unit consequently increasing the degradation efficiency.

III.4.4 Influence of Relative Humidity (RH)

In the operating rooms, the humidity levels in ORs should range between 30 and 60 % as recommended by national guidelines such as NFS 90-351 [46] and ASHRAE 170-2017 [47] for France and the US respectively. However levels measured could be outside this range. Wong *et al*. [48] measured levels of 80 % in a Malaysian OR. As a result of this, in the present study, the influence of RH on the degradation process of the two target compounds were studied from 20 % to 80 % at 20°C which gave moisture content of 4657 - 18893 ppm. This would provide representative information on how different RH levels encountered in the ORs affect the performance of PCO during the degradation of isoflurane and acrylonitrile.

For the acrylonitrile experiments, velocity and light intensity were fixed at 1 $m.s^{-1}$ and 4.5 $mW.cm^{-2}$ whilst initial concentration was maintained at 2 ppm. Figure 43 shows the influence of RH on acrylonitrile degradation. It can be observed that the single-pass removal efficiency decreases when the RH is increased from 20 % to 80 %.

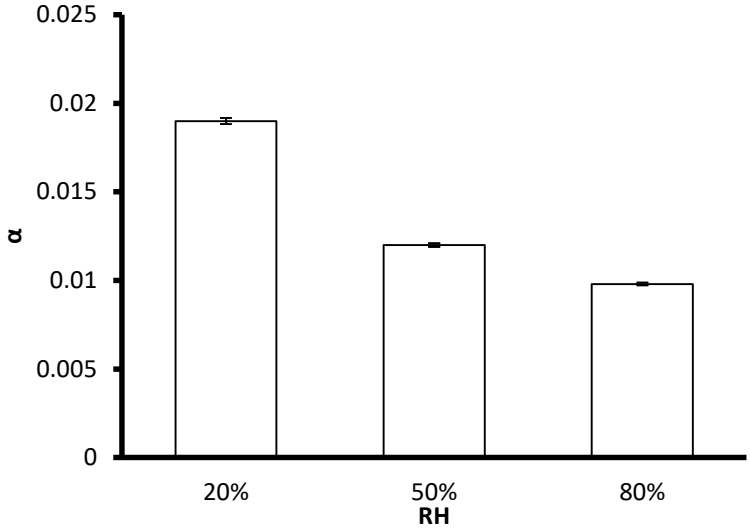

Figure 43 : Influence of relative humidity on the single-pass removal efficiency determined during acrylonitrile degradation. (C_0 = 2 ppm; v = 1 m.s^{-1}; I = 4.5 mW.cm^{-2})

The results for the influence of RH on the degradation of isoflurane are shown in Figure 44. The results of the experimental study show that as the relative humidity is increased from 20 % to 80 %; (i) isoflurane induction periods are increased; (ii) the single-pass removal efficiency is decreased.

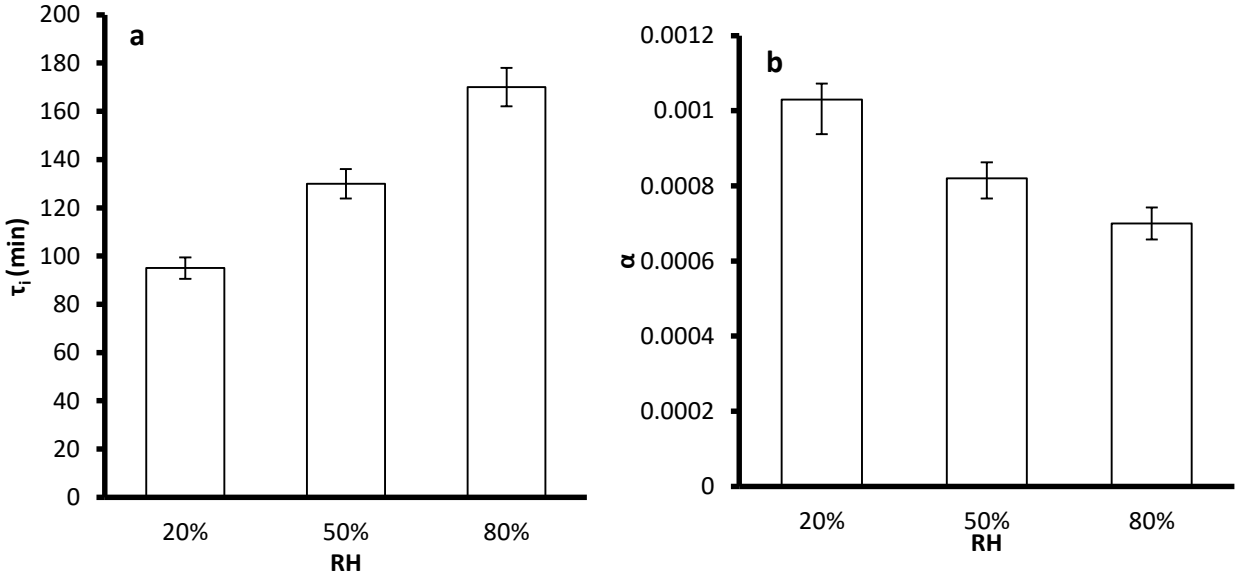

Figure 44 : Influence of relative humidity on (a) the length of the induction time (b) the single pass removal efficiency determined during isoflurane degradation. (C_0 = 0.5 ppm; v = 1 m.s^{-1}; I = 4.5 mW.cm^{-2})

In the literature, the role of water vapor in the photocatalytic oxidation process has been described as a dual one [21,43,44]. On one hand adsorbed water molecules are oxidized into OH° which are necessary for the progress of the reaction whilst on the other hand excessive amounts of water creates a competition with the pollutants for adsorption onto

active sites which inhibits the degradation. When varying humidity, some studies have shown that both effects can be predominant, depending on the humidity range studied whilst other studies have reported that only one of these effects is visible. For example, Mo *et al.* [45] studied the influence of relative humidity in a range of 0 -70 % on the degradation of toluene (0.7 ppm) in a stainless steel plate-type UV-PCO reactor with two glass plates coated with Degussa P25 placed in the reactor. They showed that the removal efficiency of toluene increased from 0 to 35 % due to the promotion of the degradation by the formation of OH° and decreased from 35 % to 70 % as a result of competitive adsorption between the toluene molecules and the water molecules. On the contrary, Zhong *et al.* [41] demonstrated a continuous decrease in removal efficiency when they degraded ethanol (0.5ppm) at RH range 10 % to 60 % in an open-loop PCO reactor equipped with TiO_2 coated fiber glass media. They attributed their results to the competition for adsorption between ethanol and water molecules.

The results from this study show that increasing the relative humidity decreases the degradation efficiency of both compounds. This observation can be interpreted as the competition for adsorption between the pollutants and water molecules. As the amount of water molecules increases, they occupy the active sites which in turn decreases the chance the pollutants have to react with the active species resulting in lower removal efficiencies [49]. In addition to this, water molecules may form layers on the photocatalyst surface and therefore, in order to react, VOCs must first be absorbed into the water film and then penetrate towards the catalyst surface which also subsequently decrease the degradation efficiency [50,51]. This inhibition effect was also observed by Raillard *et al*. [49] when they studied the influence of RH (0 – 30 %) on the photocatalytic degradation of two ketones: acetone and 2-butanone. The experiments were performed in a 12-L Pyrex-glass batch reactor with TiO_2 deposited on cellulose substrates. Similarly, Krichevskaya *et al*. [52] observed a decrease in the removal efficiency of acrylonitrile (40 ppm) when RH was increased from 0 % to 66 % in an annular reactor coated with Degussa (P25) TiO_2 powder. These authors attributed the inhibition to the effect of competitive adsorption between the pollutant molecules and water.

For the induction period of isoflurane, the increase in the induction periods during increase in RH could also be attributed to the competition between isoflurane molecules and water molecules for adsorption onto active sites. As the RH increases, they prevent isoflurane

molecules from reacting with active species thus longer induction periods occur until sufficient concentration of Cl° are formed to initiate the acceleration of the reaction.

At 20 % RH the moisture content at 20°C is 4657 ppm this increases to 11725 ppm at 50 % RH and 18893 ppm at 80 % RH. These concentrations are quite high relative to the pollutant concentrations of 0.5 ppm and 2 ppm for isoflurane and acrylonitrile respectively. The percentage decrease in the single-pass removal efficiency from 20 % to 50 % RH was 36 % and 20 % for acrylonitrile and isoflurane respectively whilst the percentage decrease from 50 % to 80 % was 18 % and 14 % for acrylonitrile and isoflurane respectively. This shows that although the degradation of both compounds is impeded by the increase in RH, the influence was more pronounced when the RH was increased from 20 % to 50 % than from 50 % to 80 %. This could be explained by the fact that at 50 % RH the surface already had abundant water and that increasing the concentration of water probably led to a saturation effect thus the removal efficiency was not drastically decreased when the RH was increased to 80 %.

Relative humidity has a significant influence on the degradation of isoflurane and acrylonitrile. Under the experimental conditions studied, PCO performance during the degradation of both isoflurane and acrylonitrile is better at lower relative humidity. According to several national regulations, RH between 30 % and 60 % is recommended in ORs and at these levels water vapor exists in large excess compared to pollutant concentrations (usually ppb to several tens of ppm) and thus competitive adsorption which inhibits PCO performance can be deemed as the dominating process. Under this condition, it would be advisable not to operate above RH of 60 %.

III.4.5 Presence of co-pollutants

Single compound photocatalytic oxidation studies are convenient for understanding the kinetics of degradation of a compound but in the real case, the indoor air stream usually contains several contaminants.

As seen in Chapter I, the OR is polluted by a variety of chemical pollutants such as waste anesthetic gases, sterilants and compounds present in surgical smoke. It is reasonable to assume that the coexistence of these compounds may have an influence on the degradation rate of isoflurane and acrylonitrile thus it would also be necessary to provide information on

how the presence of co-pollutants will affect the degradation efficiency of the target compounds.

In this study nitrous oxide and acetic acid were chosen to study the effect of co-pollutants on the degradation efficiency of the target pollutants. Nitrous oxide is an anesthetic pollutant typically found in ORs. Acetic acid however is a derivative of peracetic acid (sterilant) and was chosen to represent peracetic acid as the latter was not stable enough to allow its use.

In this work, a series of experiments conducted at different binary mixture configurations of nitrous oxide and acetic acid with acrylonitrile and isoflurane were made. As the co-pollutants may vary in concentration, the experiments were performed in two ways. Firstly degradation was performed at equi-molar concentrations of the co-pollutants and the target pollutants. Then the experiments were conducted with the co-pollutant at a higher concentration. Since the reference concentration of isoflurane and acrylonitrile are different, the higher concentration of the co-pollutant was chosen so that the molar ratios between the reference concentrations and co-pollutant concentration were the same for both isoflurane and acrylonitrile experiments. The compositions of these mixtures are described in Table 20.

Mixture Name	Composition
A1	2 ppm acrylonitrile + 2 ppm acetic acid
N1	2 ppm acrylonitrile + 2 ppm nitrous oxide
N2	2 ppm acrylonitrile + 25 ppm nitrous oxide
A2	0.5 ppm isoflurane + 0.5 ppm acetic acid
N3	0.5 ppm isoflurane + 0.5 ppm nitrous oxide
N4	0.5 ppm isoflurane + 6 ppm nitrous oxide

Table 20 : Binary mixture compositions

Figure 45 shows the experimental results for the binary mixtures compared to single compound experiments for acrylonitrile. The velocity and light intensity were fixed at 1 $m.s^{-1}$ and 4.5 $mW.cm^{-2}$ respectively.

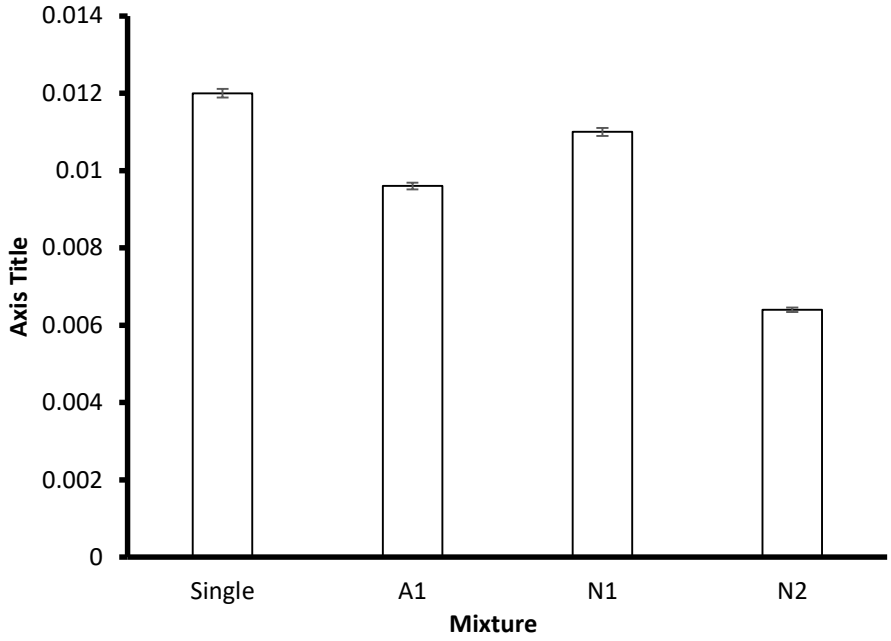

Figure 45 : Influence of presence of co-pollutants on the single pass removal efficiency determined during acrylonitrile degradation (C_0 = 2 ppm; v = 1 m.s^{-1}; I = 4.5 mW.cm^{-2}; RH = 50 %)

Acrylonitrile results showed that the single pass removal efficiencies were lower for binary mixtures than for the single component experiment. In the presence of the co-pollutants, the α decreased by 20 %, 8.3 % and 46.7 % for mixtures A1, N1 and N2 respectively. For the equi-molar mixtures, acetic acid had a stronger inhibitory effect on acrylonitrile than nitrous oxide. It was also observed that the inhibition of acrylonitrile degradation was higher with increasing nitrous oxide concentrations.

Figure 46 shows the experimental results for the binary mixtures compared to single compound experiments for isoflurane. The velocity and light intensity were fixed at 1 m.s^{-1} and 4.5 mW.cm^{-2} respectively.

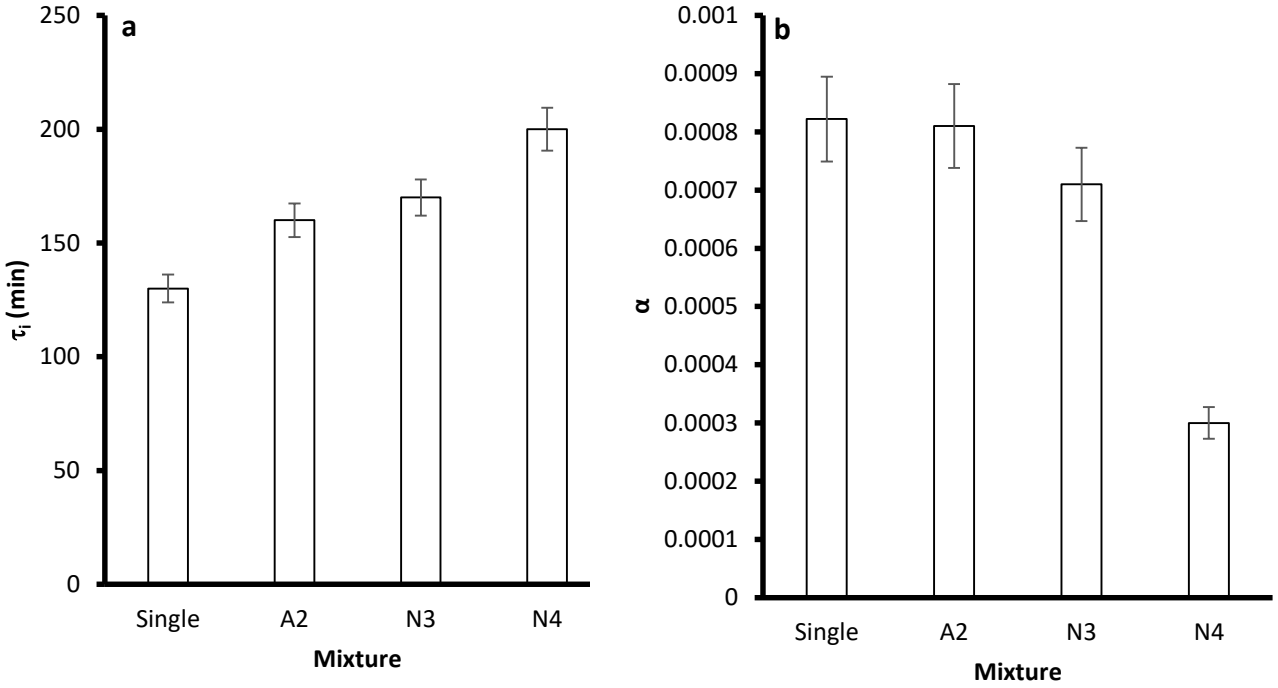

Figure 46 : Influence of presence of co-pollutants on (a) the length of the induction time (b) the single pass removal efficiency determined during isoflurane degradation (C_0 = 0.5 ppm; v = 1 m.s^{-1}; I = 4.5 mW.cm^{-2}; RH = 50%)

Isoflurane experiments showed that, in the presence of these co-pollutants the degradation of isoflurane was inhibited. The inhibitive effect is seen in the fact that the induction periods were increased whilst the removal efficiencies were decreased. The induction periods increased by 16.7 %, 24% and 46 % for mixtures A2, N3 and N4 respectively. The single-pass removal efficiencies decreased by 1%, 13% and 63% for mixtures A2, N3 and N4 respectively. Contrary to acrylonitrile, isoflurane single pass removal degradation was more negatively influenced by the presence of nitrous oxide than by acetic acid for the equi-molar experiments. The inhibition of isoflurane degradation was higher with increasing nitrous oxide concentrations.

This trend of decreasing removal efficiencies was also been reported by Chen *et al.* [53] using an equi-molar ternary mixture of 0.5 ppm toluene, ethyl acetate and ethanethiol. On the other hand, Chen *et al.* [54] observed no significant influence of the mixture effect on low concentrations (0.1 ppm) of equi-molar binary or ternary mixtures of selected compounds but observed that in a 16 VOC mixture the interference effect among the selected VOCs became quite obvious, and their removal efficiencies were significantly decreased. The inhibitive effect observed by these authors was attributed to the possible competitive adsorption for active sites by the molecules. In this study, the decrease in the degradation of

both isoflurane and acrylonitrile in the presence of the co-pollutants could also be explained by the possible competition for active sites.

Acetic acid is known to have a high adsorption affinity to TiO_2 therefore it allows it to occupy more active sites and be degraded [55] and thus may have a higher competitive adsorption ability than the target compounds. For the isoflurane-acetic acid equi-molar mixture, it seemed that the inhibitory effect was more pronounced for the first phase than for the second phase as seen in Figure 46 a and b. The induction period increases from 130 minutes in the single compound degradation to 160 minutes in the equi-molar binary degradation but α values are quite similar for both single compound (0.00082) and binary mixture (0.00081) experiments. Since acetic acid has a better adsorption affinity to the photocatalyst, it prevents enough isoflurane molecules from reaching the active sites thus delays the degradation mechanism by increasing the induction period. It can be assumed however that once acetic acid is no longer present, isoflurane degradation proceeds normally that could explain why the single-pass removal efficiency for the second phase was not significantly different from that obtained during single isoflurane degradation.

The experiments performed in mixture with N_2O showed that it inhibited the degradation of both target compounds. Once the concentration of N_2O was increased its inhibitory effect on the removal of the target compounds due to competitive adsorption unto active sites was intensified further decreasing the single-pass removal efficiencies of the target compounds.

Under the experimental conditions employed in this study, it can be concluded that PCO performance during the degradation of the target pollutants could be inhibited by the presence of co-pollutants due to competitive adsorption for active sites. Additionally the higher the concentration of the co-pollutant compared to the target compound the higher the inhibition effect. The concentrations of co-pollutants present in the OR air vary depending on the activities and thus cannot be controlled. However in order to improve the PCO performance it would be recommended that several photocatalytic banks (photocatalytic media and UV lamps) are installed in the PCO unit to ensure higher removal efficiency.

III.4.6 Presence of particles (bio-aerosols)

Aside gaseous pollutants, particulate matter is another type of pollutant that is found in indoor environments. It has been shown in chapter I that surgical smoke contains particles (tissue and microbial) which could be trapped by the photocatalytic media and subsequently their presence can affect the PCO of the target compounds. Surgical smoke is known to contain particles with diameters ranging from 0.35 to 6.50 µm [56]. To simulate the presence of particles, the photocatalytic surface was loaded with rice particles at a rate of 0.002 $g.m^{-2}$. The particle diameter range was 0.25 -10.50 µm thus was a good representation of particles that could be collected on the photocatalytic media in an OR.

Figure 47 shows the results for acrylonitrile degradation in the absence and presence of particles. The velocity, light intensity and concentration were fixed at 1 $m.s^{-1}$ and 4.5 $mW.cm^{-2}$ and 2 ppm respectively. It can be observed that α decreases by 22.5 % when particles are present on the photocatalytic media.

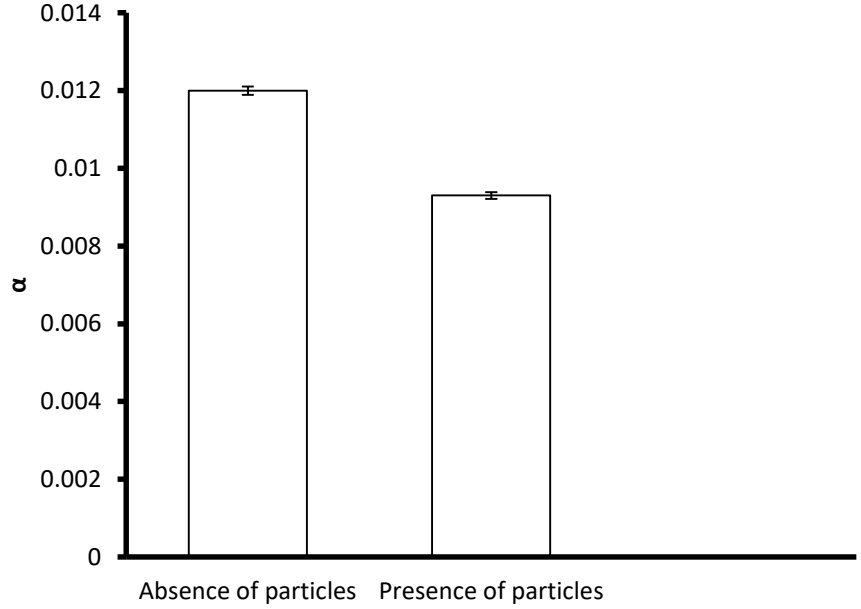

Figure 47 : Influence of the presence of particles on the single pass removal efficiency determined during acrylonitrile degradation (C_0 = 2ppm; v = 1 $m.s^{-1}$; I = 4.5 $mW.cm^{-2}$; RH = 50 %)

The results for isoflurane degradation are presented in Figure 48. For these experiments, the velocity, light intensity and concentration were fixed at 1 $m.s^{-1}$ and 4.5 $mW.cm^{-2}$ and 0.5 ppm respectively. From the figure, it can be observed that α decreases by 14.6 % whilst the induction time increases by 24.8 % when particles are present on the photocatalytic media.

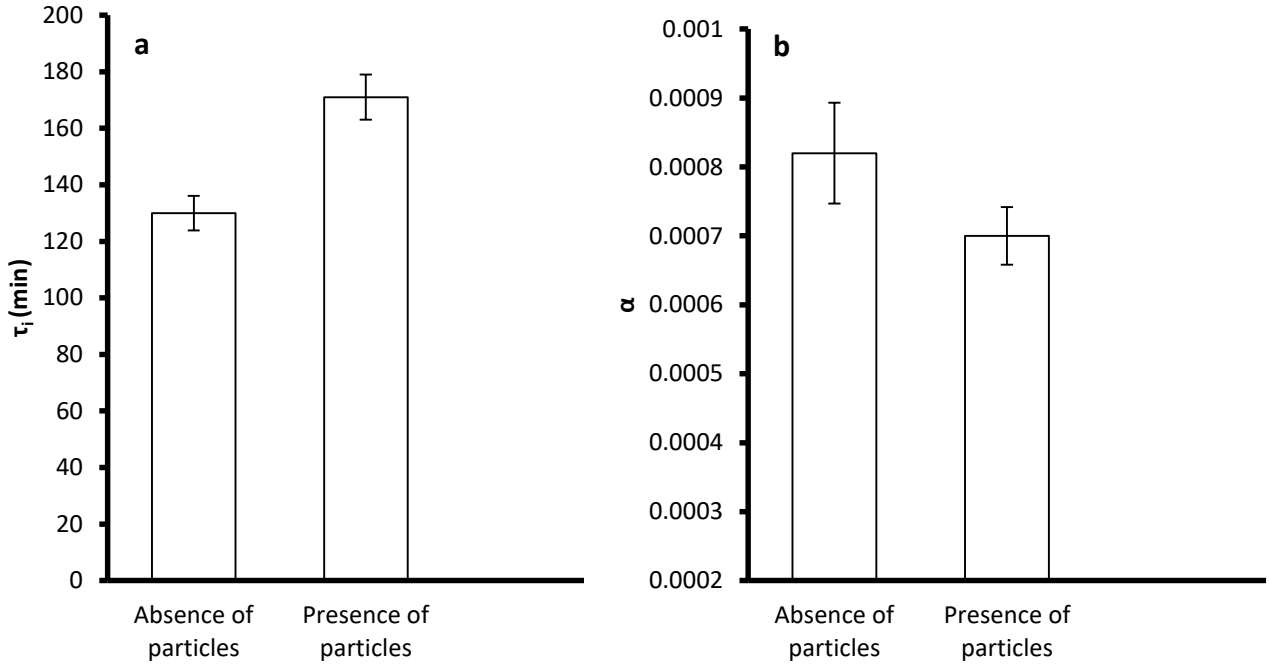

Figure 48 : Influence of the presence of particles on (a) the length of the induction time (b) the single pass removal efficiency determined during isoflurane degradation (C_0 = 0.5 ppm; v = 1 m.s^{-1}; I = 4.5 mW.cm^{-2}; RH = 50 %)

Under the experimental conditions employed, both compounds are inhibited by the presence of particles with the same order of magnitude. The trend of decreasing removal efficiencies has been reported by Park *et al.* [57]. They studied the degradation of toluene in a single-pass PCO reactor using a non woven-fabric coated with TiO_2. They observed that when air containing particles was introduced into the photocatalytic reactor, toluene removal efficiency was decreased. They explained this by two hypotheses. First, the particles could hide the active sites which could in turn block these sites for adsorption by the target compounds effectively reducing their degradation. Secondly, the particles could promote a "screening effect" thereby reducing the amount of light reaching the catalyst surface resulting in slower production of active species. Consequently, the progress of the degradation could be impeded.

In this work, the inhibition of the degradation of isoflurane and acrylonitrile could be due to the fact that the particles block the active sites preventing the molecules from adsorbing and being degraded. Secondly the particles could also screen the light intensity thereby reducing the amount of light reaching the catalyst surface. Conclusively, it would be recommended that for a PCO unit, filters should be placed upstream of the photocatalytic

media to reduce the particle load reaching the photocatalytic media in order to improve the PCO performance.

III.5 Formation of gas phase intermediates during the degradation of the target compounds

An important concern when it comes to the PCO of compounds is the formation of intermediate compounds. These intermediates can be toxic or irritating and maybe more harmful to human health than their precursors [43,58,59]. The determination of the type and levels of intermediates produced during degradation will help to characterize the performance of PCO with regards to its safety.

III.5.1 Acrylonitrile gas phase intermediate compounds

In this study, no intermediate compound was detected during the degradation of acrylonitrile irrespective of the initial concentrations studied (0.5 -10 ppm). When Krichevskaya *et al.* [52] studied the degradation of acrylonitrile inlet concentrations of 40 ppm in an annular reactor coated with Degussa (P25) TiO_2 powder, they identified carbon dioxide, water and nitrogen dioxide as the main products. However they also noticed the formation of hydrogen cyanide, a compound classified by the US EPA as an extremely toxic compound.

The inability to detect intermediates including hydrogen cyanide in this study could be explained by the fact that these compounds were probably not effectively trapped and detected by the used adsorbent cartridge sampling and GC/MS method used.

III.5.2 Isoflurane gas phase intermediate compounds

In the case of isoflurane, the intermediates that were identified in the gas phase during its degradation are listed in Table 21. Only two halogenated compounds were identified; pentafluoropropanal (C_3F_5OH) and chlorodifluoroacetaldehyde (C_2HClF_2O). The presence of the former could be evidence of the initial reaction of isoflurane with OH° to form Cl°.

$$C_3H_2ClF_5O + OH^\circ \longrightarrow \mathbf{C_3F_5OH} + Cl^\circ + H_2O$$

No other fluorinated or chlorinated compounds were identified in this study; this could probably be attributed to the fact that their concentrations could be too low to be detected by the analytical methods. Some oxygenated compounds were also detected. According to the studies of TCE reaction mechanism, it has been proposed that some chlorinated compounds are hydrolyzed into alcohols which are then transformed into aldehydes and acids before complete mineralization [14,60]. This could probably explain the presence of the oxygenated compounds during isoflurane degradation.

Under the reference experimental conditions (C_0 = 0.5 ppm; v = 1 m.s^{-1}; I = 4.5 mW.cm^{-2}) only formaldehyde and acetaldehyde were identified using HPLC. The other intermediates were identified at isoflurane concentration of 10 ppm using GC/FID. Acetaldehyde and formaldehyde were properly quantified and their concentrations were found to be lower than the European Commission indoor 8-hr exposure limits of 110 and 80 ppb respectively [61]. The concentrations of the halogenated compounds were given as isoflurane equivalents because their structures could be comparable to isoflurane. The concentrations that were calculated were relatively low as shown in Table 21. For the acids on the other hand, only their relative peak areas with respect to isoflurane peak area at 10 ppm were given. Their relative peak areas were low which means that their concentrations could also be considered low.

A major concern in PCO is the possible production of toxic (carcinogenic) intermediates. A risk assessment of the intermediates to human health can be accessed through a Health-Related Index (HRI) [62]. It is defined as:

$$\boldsymbol{HRI_i = \frac{C_i}{REL_i}} \qquad \textbf{Equation 28}$$

Where C_i is the concentration of compound i and REL_i is the recommended exposure limit of compound i. It required that the sum of all HRI not exceed the value of 1.

Formaldehyde and acetaldehyde are recognized as important inhalation toxicants by governmental agencies. They are categorized as carcinogens by the International Agency for Research on Cancer (IARC) [63]. The sum of their HRI was 0.6 at a challenge concentration of 0.5 ppm. Although their concentrations identified do not pose a significant health risk, as the challenge concentrations of isoflurane are increased the sum of HRI could possibly increase.

The acids and the halogenated compounds found in this study have not been categorized as carcinogenic and are therefore of lesser concern. Additionally, their levels produced were not high enough to pose significant risks to human health.

Compound family	Intermediate compound	Concentration (ppm)	Relative peak area	REL (ppm)	IARC carcinogenic classification
Halogenated	Pentafluoropropanal	0.0017[a]		-	-
	Chlorodifluoroacetaldehyde	0.0014[a]		-	-
Acids	Acetic acid	-	0.0016[b]	10	-
	Formic acid	-	0.0013[b]	5	-
Aldehydes	Formaldehyde	0.020		0.08	1
	Acetaldehyde	0.038		0.11	2B

Table 21 : List of reaction intermediates identified during the degradation of isoflurane (v = 1 m.s^{-1}; I = 4.5 mW.cm^{-2}; RH = 50 %)

(IARC Classification: 1: Carcinogenic to humans, 2B: possibly carcinogenic to humans)

[a]*: Isoflurane equivalent concentration*

[b]*: Relative peak area with respect to Isoflurane peak area at 10 ppm*

III.6 Mineralization rates obtained during the degradation of the target compounds

In order to completely characterize the performance of PCO and also to complete the analysis of organic intermediates produced during the degradation, it is necessary to also determine the mineralization rates. This is done by measuring the amounts of CO_2 produced and comparing this value to the amount of CO_2 which is expected to be produced when there is complete mineralization.

III.6.1 Isoflurane mineralization rates

As previously stated in chapter II, the protocol for the experiments involves a 24h homogenization period that allows the stabilization of pollutant compounds before the degradation. During this period a significant amount of CO_2 was found to enter the reactor. This entry is as a result of leaks that cannot be removed. The high CO_2 levels coupled with

the very long degradation times necessary for complete removal of isoflurane made it impossible to quantify the CO_2 formed during isoflurane degradation and subsequently information on the mineralization rates could not be provided.

III.6.2 Acrylonitrile mineralization rates

In the case of acrylonitrile, the shorter degradation times made it possible to quantify the mineralization rates. Thus, the mineralization rates were studied only for acrylonitrile by looking at the influence at different initial concentrations. Figure 49, Figure 50 and Figure 51 show the evolution of the mineralization rate and the conversion rate for different acrylonitrile concentrations.

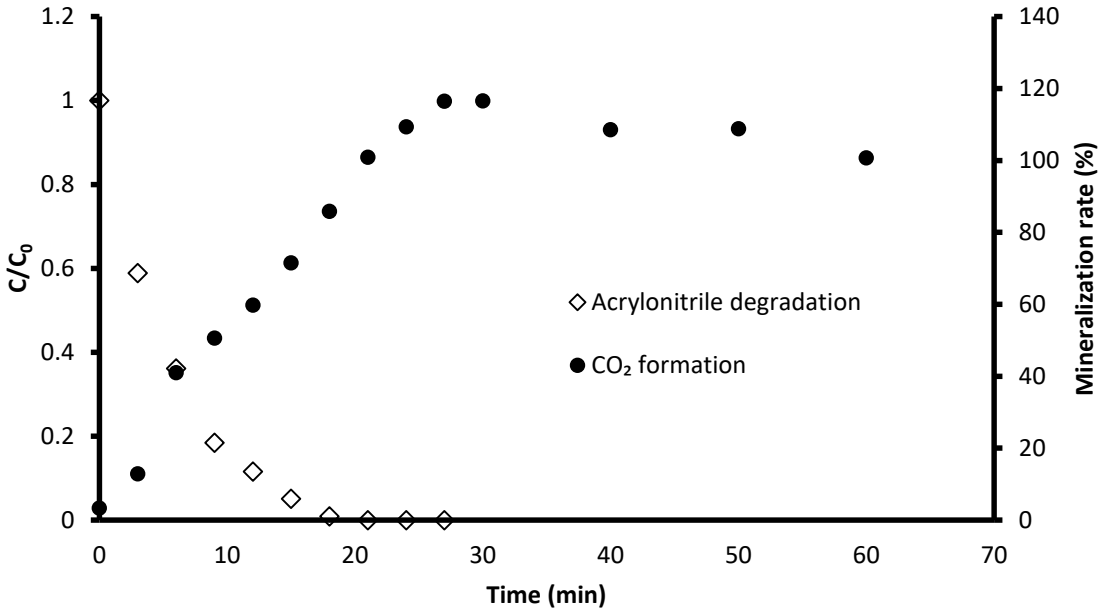

Figure 49 : Evolution of pollutant conversion and CO_2 mineralization rate during the photocatalytic oxidation of acrylonitrile (C_0 = 0.5 ppm; v = 1 m.s^{-1}; I = 4.5 mW.cm^{-2}; RH = 50%)

For all three concentrations: (i) CO_2 was formed from the beginning of the degradation and it increased until a stable value (ii) 100 % mineralization was achieved. All the eventual organic intermediates are adsorbed and oxidized into CO_2.

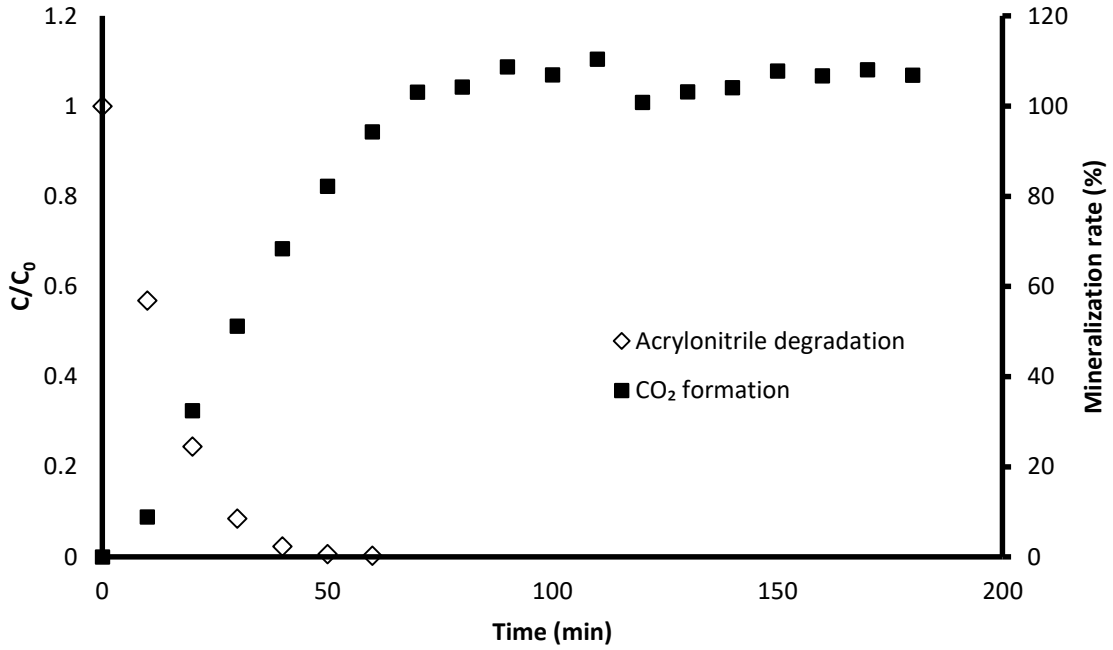

Figure 50 : Evolution of conversion and CO_2 mineralization rate during the photocatalytic oxidation of acrylonitrile (C_0 = 2 ppm; v = 1 m.s^{-1}; I = 4.5 mW.cm^{-2}; RH = 50 %)

In the case of initial concentration of 0.5 ppm and 2 ppm, 100 % mineralization was achieved almost instantaneously to 100 % conversion. However, for 10 ppm, at 100 % conversion of acrylonitrile about 70 % of the organic compounds had been transformed to CO_2. Then about 120 minutes after total removal of acrylonitrile from the gas phase, 100 % mineralization was achieved. This delay could possibly be attributed to the fact that at higher concentration of 10 ppm, higher concentrations of intermediates were formed which would require more time to be mineralized. We also observed a two step mineralization rate (Figure 51) with the first step involving the fast transformation of acrylonitrile into organic intermediate compounds which were also quickly transformed into CO_2 (0.008 ppm.min^{-1}) followed by a slower mineralization (0.003 ppm.min^{-1}) of more stable intermediates into CO_2.

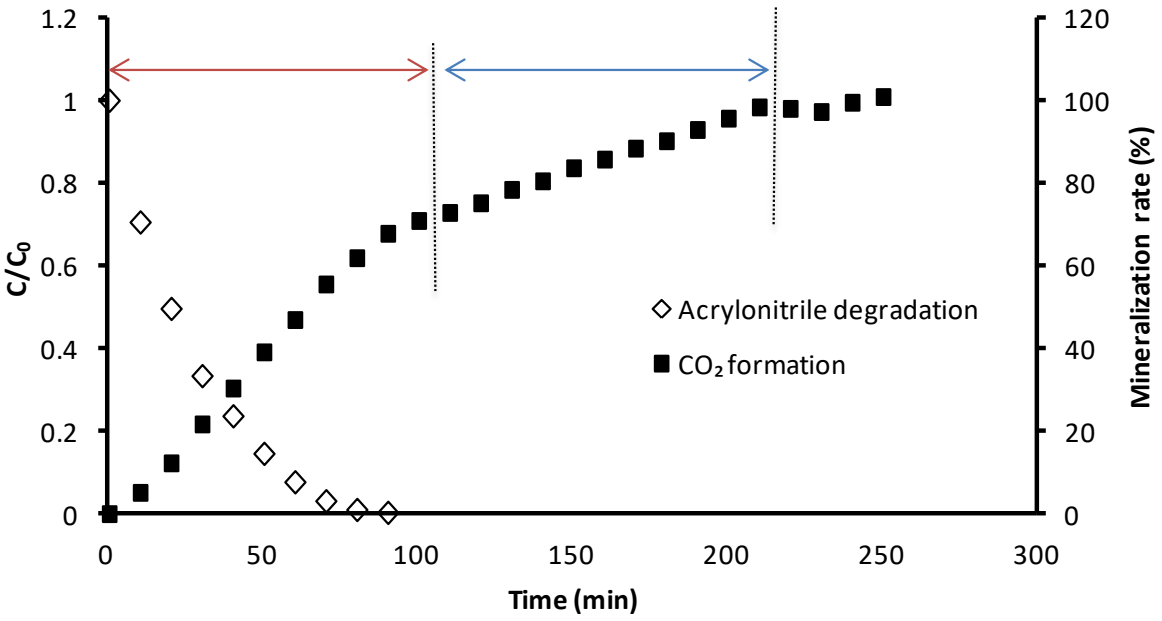

Figure 51 : Evolution of conversion and CO_2 mineralization rate during the photocatalytic oxidation of acrylonitrile (C_0 = 10 ppm; v = 1 m.s^{-1}; I = 4.5 mW.cm^{-2}; RH = 50 %), Red arrow indicates first step of mineralization whilst blue arrow indicates the second step of mineralization

To study the promptness of conversion of a compound and its reaction intermediates to CO_2, Debono *et al.* [4] suggested that the mineralization rates be plotted as a function of the conversion rates. The results are acrylonitrile conversion rate vs mineralization rates for the three concentrations studied are shown in Figure 52.

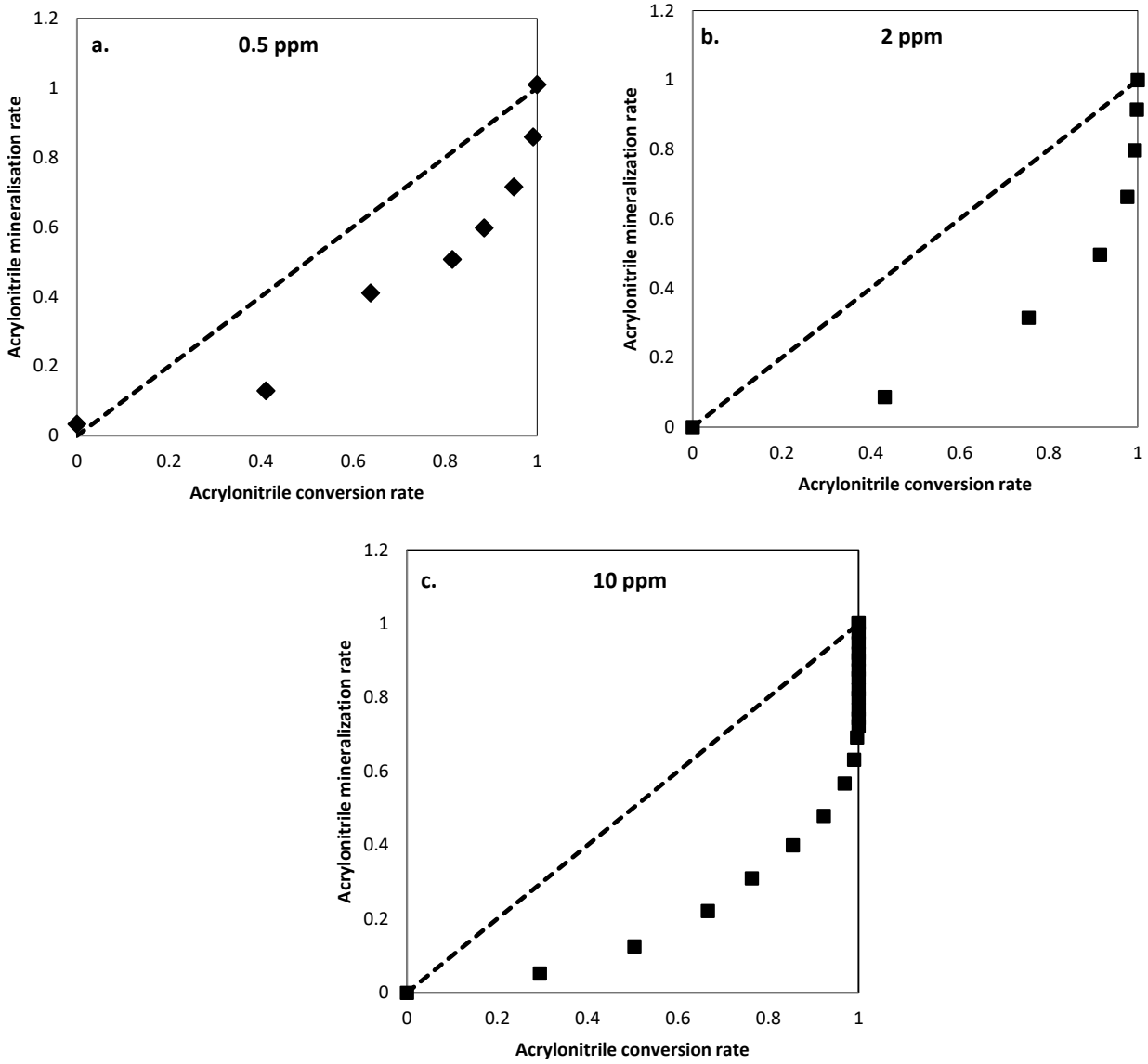

Figure 52 : Evolution of mineralization rates as a function of conversion rates during the photocatalytic oxidation of acrylonitrile at initial concentrations of (a) C_0 = 0.5 ppm (b) C_0 = 2 ppm and (c) C_0 = 10 ppm (v = 1 m.s^{-1}; I = 4.5 mW.cm^{-2}; RH = 50 %)

The dashed line represents the instantaneous conversion of the target compound into CO_2. Consequently, if acrylonitrile was instantaneously converted in CO_2 the plotted data would fit the dotted line. For all three concentrations, the results show a gap between the dotted line and the experimental data. It can also be observed that the mineralization rate at the beginning is low compared to the conversion rate but it increases until the total conversion of acrylonitrile. This gap corresponds to the fact that photocatalytic degradation of acrylonitrile involves the transient formation of reaction intermediates.

Conclusively, even though 100 % mineralization is reached at around 100 % removal for 0.5 ppm and 2 ppm, acrylonitrile is not immediately mineralized but first transformed into intermediate compounds.

Conclusion on gas phase intermediates and mineralization rates

For the acrylonitrile degradation experiments, the absence of detection of intermediates such as hydrogen cyanide that was observed by Krichevskaya *et al.* [47] does not rule out their existence. Indeed by plotting the mineralization rates as a function of the conversion rates it was shown that during the course of degradation, acrylonitrile was first converted into organic intermediate compounds which were then converted into CO_2 and any other mineral compounds. Further analysis using different and possibly more sensitive methods are recommended as these could help to identify anticipated and additional intermediates.

The intermediate compounds that were identified during isoflurane degradation include pentafluoropropanal, chlorodifluoroacetaldehyde, formaldehyde, acetaldehyde, formic acid and acetic acid. The recommended exposure levels of acetic acid (10 ppm) and formic acid (5 ppm) were higher than isoflurane (2 ppm) which implied that they could be considered less harmful than isoflurane. Additionally, their concentrations were not high enough to present a significant risk. On the other hand, the lower recommended exposure limits of acetaldehyde (0.11 ppm) and formaldehyde (0.08 ppm) implies they could be more harmful and toxic than isoflurane nevertheless their concentrations were not high enough to present a significant risk.

III.7 Effect of the change of media geometry on the degradation of target compounds

For the same reactor volume, the performance of the degradation can be increased by modifying the media geometry such that it (i) has a high surface area to allow for more active sites (ii) allows a better utilization of the light and (iii) could allow a longer contact time between the reactants and the photocatalyst [64].

Destaillats *et al*. [24] studied the degradation of seven VOCs using plane media geometry and a pleated media geometry. They observed that the single-pass removal efficiencies for all seven VOCs increased when the media geometry was changed from a

plane to a pleated configuration. They attributed the difference in performance of the two configurations to difference in (i) TiO_2 content, (ii) contact time within media and (iii) irradiance distribution within media. Unable to carry out a complete quantitative comparison to distinguish the influence of all three criteria between the experiments carried out with plane and pleated media, they used the estimated contact time to make some comparisons. They explained that improvement in PCO performance when the pleated configuration was used compared to the plane configuration was due to the fact that the pleated media reduced the velocity of pollutants in the media which consequently increased the residence time and extended the contact time of pollutants in the photocatalytic media.

Frédéric Batault [65] in his PhD studied the influence of plane and pleated geometry on the degradation of toluene. Similarly to Destaillats *et al*. [24], he observed that the degradation efficiencies were better for the pleated media geometry than for the plane media geometry. He explained that the increase in the degradation efficiency when the pleated media was used could be attributed to the global increase in contact time. However he explained that from a geometric approach, the photocatalytic media was considered as a homogeneous permeable material and so it could be assumed that the velocity field remained the same in both media geometries and that the streamlines were parallel in both geometries. He explained further that due to the angle between the pleated media and the direction of the flow, the path length (e) crossed within the media was longer in the pleated media than in the plane media as shown in Figure 53. The path length could be between e and 4e with e being the thickness of the media. Consequently the increase in contact time for the pleated media was as a result of the increase in path length and not a result of the decrease in the velocity.

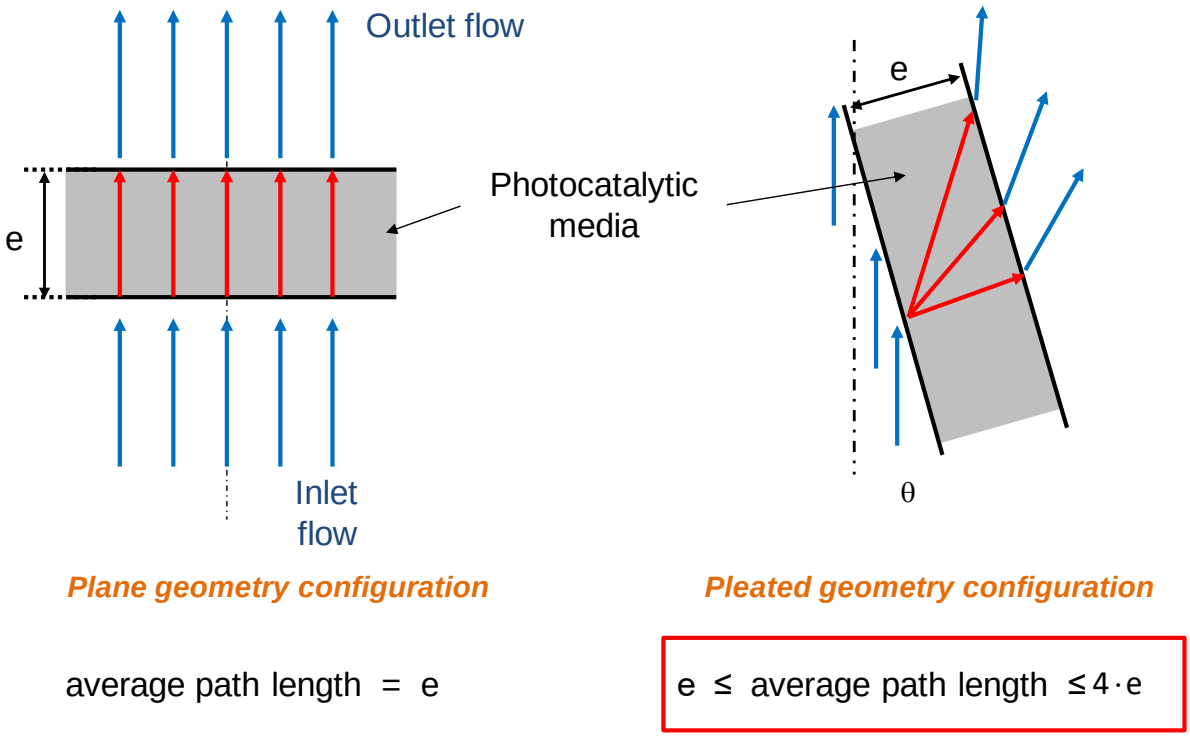

Figure 53 : Possible different path lengths between the plane and pleated media geometries according to Batault [65]

In this work, to study the influence that the change in media geometry had on the degradation of the target compounds, experiments were carried out with a pleated media configuration and the results compared to reference experiments carried out with the plane media configuration. For the plane configuration, the media is placed perpendicularly to the flow whilst the lamps are placed horizontally to media. The pleated configuration consists of the photocatalytic media is folded into four pleats creating two triangles at 60° and the lamps are placed vertically within the triangles. Figure 54 shows a schematic representation of the two configurations.

The experimental goal was to highlight the possible influence of the contact time and thus the pleated experiments were carried out at a similar flow rate, average light intensity and initial concentration as for the plane experiments. To ensure that the average light intensity received on the pleated media was the same as the plane media, numerical simulations were used and will be detailed in chapter IV. The pleated configuration experiments were carried out three times to ensure the repeatability of the experiments.

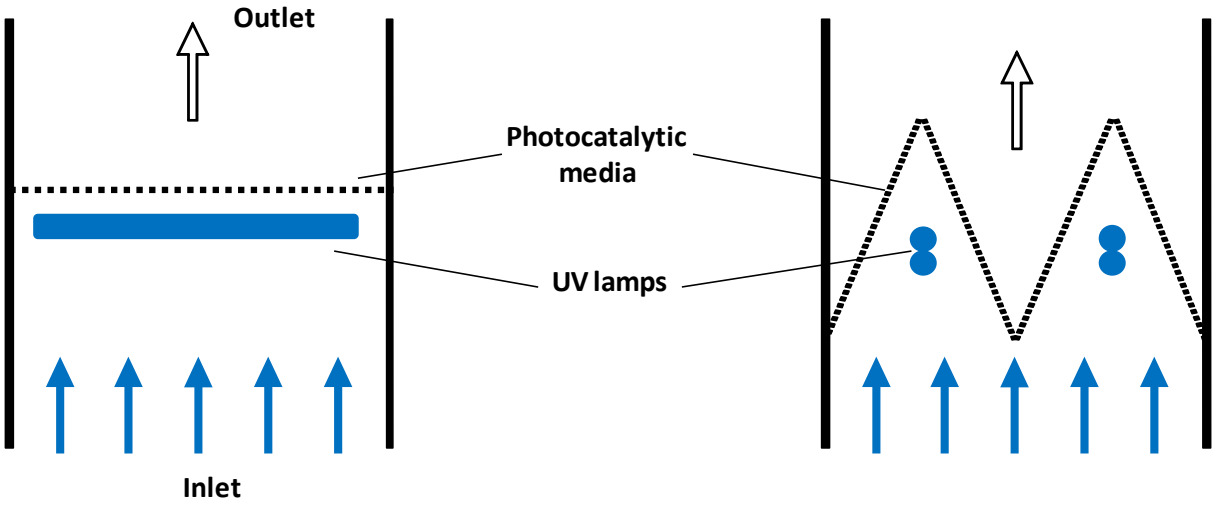

Figure 54 : Representation of plane and pleated media configurations installed in the multi-pass reactor

Figure 55 shows the single-pass removal efficiency of acrylonitrile with the plane geometry and pleated geometry. It can be observed that the single-pass removal efficiencies increased form (12.08 ± 0.11) x 10^{-3} for the plane media to (27.42 ± 0.74) x 10^{-3} for the pleated media.

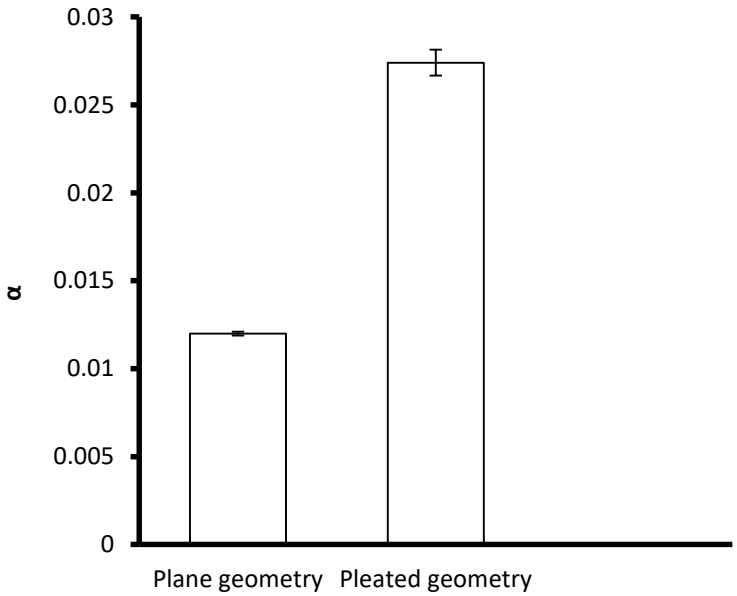

Figure 55 : Influence of the media geometry on the single pass removal efficiency determined during acrylonitrile degradation (C_0 = 2ppm; v = 1 m.s^{-1}; I = 4.5 mW.cm^{-2}; RH = 50 %)

Figure 56 shows the single pass removal efficiency and induction periods of isoflurane with the plane geometry and pleated geometry. It can be observed that the single-pass

removal efficiencies increased from $(8.2 \pm 0.8)*10^{-4}$ for the plane media to $(18.5 \pm 0.6)*10^{-4}$ for the pleated media whilst the induction periods were decreased from 137 ± 6 minutes for the plane media to 35 ± 9 minutes for the pleated media.

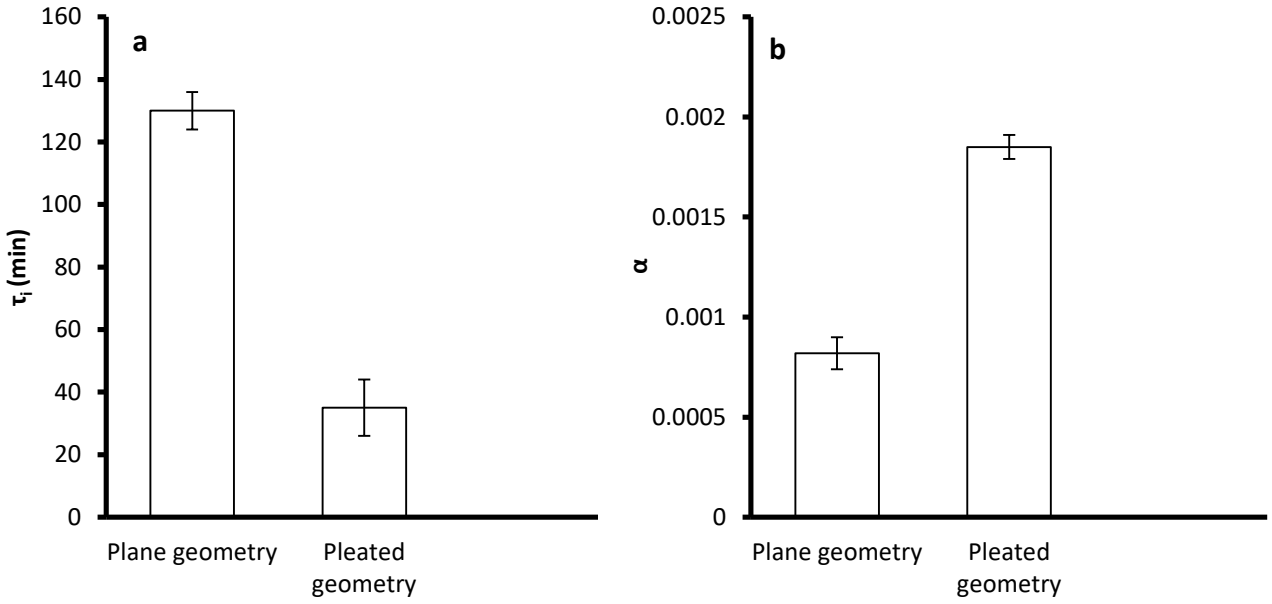

Figure 56 : Influence of the media geometry on (a) the length of the induction time (b) the single pass removal efficiency determined during isoflurane degradation (C_0 = 0.5 ppm; v = 1 m.s^{-1}; I = 4.5 mW.cm^{-2}; RH = 50 %)

It is evident in Figure 55 and Figure 56 that the pleated media geometry improves the PCO performance. This is in accordance with what Destaillats *et al*. [24] and Batault [65] observed. Three main reasons may account for this efficiency increase: (i) an increase in the surface area translates to an increase in the amount of catalyst/active sites available for pollutant removal (ii) increase in the contact time between pollutants and media, (iii) better distribution of light intensity.

To eliminate the effect of the increase in catalyst quantity due to increase in media area, the removal efficiencies obtained for both configurations were divided by their respective surface areas. The results are shown in Table 22. It can be observed that the surface corrected values of the single-pass removal efficiency (α/S) for the pleated media is 27 % higher than that of the plane media. This means that there is an increase in the efficiency not only due to the increase in catalyst quantity but probably also due to the increase in contact time and possibly the better distribution of irradiance within the media.

		Acrylonitrile	Isoflurane
Geometry	**S (m^2)**	**α/S (m^{-2})**	**α/S (m^{-2})**
Plane	0.040	0.300 ± 0.003	0.020 ± 0.002
Pleated	0.072	0.381 ± 0.010	0.026 ± 0.003

Table 22 : Surface corrected single-pass removal efficiencies of acrylonitrile and isoflurane calculated for the plane and pleated configurations

It is assumed that the contact time between the pollutants and the photocatalytic media is different in the two geometries in that it is globally increased in the pleated geometry. As previously discussed, Destaillats *et al*. [24] state that the increase in contact time is as a result of the decreasing velocity of pollutants whilst for Batault [65], the increase in the contact time is as a result of the longer path length travelled by the pollutants. Additionally, for the same average light intensity received on the photocatalytic media (plane and pleated), a modification of the irradiance distribution can also have an influence on the global efficiency of the PCO. These parameters are difficult to measure or confirm experimentally, therefore numerical simulations can be used to provide some information to be able to better connect the increase in efficiency to the change in geometry.

III.8 Conclusions on the photocatalytic degradation of acrylonitrile and isoflurane

The aim of this chapter was to show the influence that the air velocity, light intensity, the change in media geometry, initial pollutant concentration, presence of chemical co-pollutants, presence of particles (bioaerosols) and relative humidity had on the performance of photocatalytic oxidation in removing acrylonitrile and isoflurane. The results were necessary to help to extend the existing knowledge of their influence on PCO onto isoflurane and acrylonitrile in real OR conditions and to help give recommendations to improve the efficiency of the system.

In the first part, experiments were performed with the plane media configuration where media with a square section was placed perpendicular to the flow. These experiments aimed to highlight the influence of the operating parameters on the degradation of the target compounds. The experiments brought into evidence the fact that the nature of the pollutant influenced the performance of the process. In this study, acrylonitrile was degraded faster than

isoflurane due to the fact that the latter was a halogenated molecule which made it more difficult to degrade. The degradation profiles showed that acrylonitrile followed a mono-exponential decay, whilst isoflurane degradation proceeded in two distinct phases. A first phase where the degradation is slow and not very efficient attributed to possible isoflurane reactions with OH° and a second phase where the degradation accelerated due to a possible chain reaction mechanism of Cl°. This second phase of degradation is represented by a first-order decay.

A model developed by Dumont and Héquet was utilized to enable the calculation of one performance indicator (single-pass removal efficiency) for acrylonitrile and two performance indicators (induction period and single-pass removal efficiency) for isoflurane. The degradation efficiency was then accessed by studying the influence of the operating parameters on these indicators. It was observed that, although acrylonitrile and isoflurane belonged to different chemical classes, the operating parameters had a similar influence on their degradation.

Decreasing the air velocity resulted in longer one-pass contact time which then led to shorter induction periods and higher removal efficiencies. UV-C light was used as the light source for the experiments and results showed a decrease in induction period and increase in the single-pass removal efficiencies at higher average light intensities. The relationship between light intensity and removal efficiency was seen to follow a half-order regime for both compounds. This means that, for the range of light intensities studied, the electron-hole recombination was dominant. In this regime, further increment in the light intensity would not significantly improve the removal efficiencies but would only impose unnecessary energy costs. Higher initial concentrations of acrylonitrile and isoflurane led to a decrease in their degradation efficiencies attributed to saturation of the media and the competition for limited active sites.

Due to competitive adsorption for active sites an increase in relative humidity inhibited the degradation of both target compounds. The presence of other gaseous pollutants also inhibited the degradation of the target compounds again due to competition for adsorption unto active sites. It was also shown that the presence of particles on the photocatalytic media surface could block active sites and also cause a screening effect which in turn decreased the degradation efficiencies of the target compounds.

The intermediate compounds that were identified during the degradation of isoflurane include pentafluoropropanal, chlorodifluoroacetaldehyde, formaldehyde, acetaldehyde, formic acid and acetic acid. Their concentrations were not found to be high enough to present a significant risk. In the case of acrylonitrile, no organic intermediates were identified because the sampling and analytical methods were probably not suitable enough for them to be effectively trapped and detected. The study of the mineralization rates however showed that at low concentrations, 100 % mineralization was achieved almost instantaneously to 100 % degradation but at higher concentrations more time was needed to achieve 100 % mineralization. It was also observed that even though for low concentrations 100 % mineralization was achieved quite soon after 100 % degradation of acrylonitrile, the conversion to CO_2 was not instantaneous. Acrylonitrile was first transformed to intermediates which were then mineralized to CO_2. It would be recommended that further analysis using different and possibly more sensitive methods are employed to identify anticipated and additional intermediates.

Under the reference experimental conditions for acrylonitrile **(**C_0 = 2ppm; v = 1 m.s^{-1}; I = 4.5 mW.cm^{-2}; RH = 50 %) and isoflurane (C_0 = 0.5 ppm; v = 1 m.s^{-1}; I = 4.5 mW.cm^{-2}; RH = 50 %), the single-pass removal efficiencies were calculated as 1.2 % and 0.08 % for acrylonitrile and isoflurane respectively. These values were quite low and PCO performance would not be very efficient. According to the parametric evaluation, to improve the PCO performance in removing acrylonitrile and isoflurane it would be recommended to work at low velocities as this would improve the contact time between the pollutants and active species. Higher light intensities would generally give better performance but according to the range studied light intensity beyond 5 mW.cm^{-2} would only cause much more energy waste instead of much more degradation of VOCs. PCO performance would also be improved at low relative humidity however since the recommended RH levels in the OR is between 30 and 60 %, it would be recommended not operate beyond 60 %. The introduction of filters upstream the photocatalytic media would also be necessary to reduce the particle load received on the media. The PCO performance would also be better at low pollutant concentrations. However, due to the fact that the concentrations of pollutants (target and co-pollutants) vary over time, the use of multiple photocatalytic banks would help to maximize removal efficiencies of pollutants. This would also be beneficial in reducing concentrations of intermediates and keeping them at levels that would not pose health risks.

Another way of improving the PCO performance could also be to increase the developed surface of the media by changing the media geometry. The second part therefore allowed the study of the degradation of the target compounds (acrylonitrile and isoflurane) in a pleated media configuration. The configuration consisted of the photocatalytic media folded into four pleats creating two triangles at 60° and the lamps placed vertically within the triangles. Under similar experimental conditions as for the plane configuration, the efficiencies (α) were increased to 2.7 % and 0.19 % for acrylonitrile and isoflurane respectively. By increasing the surface area of the media, the removal efficiencies were increased because it was assumed the amount of catalyst was increased, the contact time was higher and the distribution of light intensity was optimized. To eliminate the influence of the increase in the amount of catalyst, the surface corrected single-pass removal efficiencies were calculated. The results showed that the pleated media configuration improved the degradation by 27 % compared to the plane which was attributed to higher contact time and better irradiance distribution.

To better understand the role of the media geometry in improving the removal efficiencies numerical simulations would be required to study the behavior of air flow and light irradiance in the photocatalytic reactor for both configurations. The results are discussed in chapter IV of this manuscript.

III.9 References

[1] O. Debono, F. Thévenet, P. Gravejat, V. Héquet, C. Raillard, L. Lecoq, N. Locoge, Toluene photocatalytic oxidation at ppbv levels: Kinetic investigation and carbon balance determination, Appl. Catal. B Environ. 106 (2011) 600–608. doi:10.1016/J.APCATB.2011.06.021.

[2] O. Debono, F. Thévenet, P. Gravejat, V. Héquet, C. Raillard, L. Le Coq, N. Locoge, Gas phase photocatalytic oxidation of decane at ppb levels: Removal kinetics, reaction intermediates and carbon mass balance, J. Photochem. Photobiol. A Chem. 258 (2013) 17–29. doi:10.1016/J.JPHOTOCHEM.2013.02.022.

[3] V. Héquet, C. Raillard, O. Debono, F. Thévenet, N. Locoge, L. Le Coq, Photocatalytic oxidation of VOCs at ppb level using a closed-loop reactor: The mixture effect, Appl. Catal. B Environ. 226 (2018) 473–486. doi:10.1016/j.apcatb.2017.12.041.

[4] O. Debono, V. Héquet, L. Le Coq, N. Locoge, F. Thévenet, VOC ternary mixture effect on ppb level photocatalytic oxidation: Removal kinetic, reaction intermediates and mineralization, Appl. Catal. B Environ. 218 (2017) 359–369. doi:10.1016/j.apcatb.2017.06.070.

[5] H. Nishikiori, M. Furukawa, T. Fujii, Degradation of trichloroethylene using highly adsorptive allophane–TiO_2 nanocomposite, Appl. Catal. B Environ. 102 (2011) 470–474. doi:10.1016/j.apcatb.2010.12.028.

[6] Z. Guo-Min, C. Zhen-Xing, X. Min, Q. Xian-Qing, Study on the gas-phase photolytic and photocatalytic oxidation of trichloroethylene, J. Photochem. Photobiol. A Chem. 161 (2003) 51–56. doi:10.1016/S1010-6030(03)00271-5.

[7] M. Hegedüs, A. Dombi, Comparative study of heterogeneous photocatalytic decomposition of tetrachloroethene and trichloroethene in the gas phase, Appl. Catal. A Gen. 271 (2004) 177–184. doi:10.1016/j.apcata.2004.02.057.

[8] S.-K. Joung, T. Amemiya, M. Murabayashi, K. Itoh, Mechanistic studies of the photocatalytic oxidation of trichloroethylene with visible-light-driven N-doped TiO_2 photocatalysts, Chemistry. 12 (2006) 5526–5534. doi:10.1002/chem.200501020.

[9] N. Fukami, M. Yosida, B.-D. Lee, K. Taku, M. Hosomi, Photocatalytic degradation of gaseous perchloroethylene: products and pathway, Chemosphere. 42 (2001) 345–350. doi:10.1016/S0045-6535(00)00140-5.

[10] M. Hegedűs, A. Dombi, I. Kiricsi, Photocatalytic decomposition of tetrachloroethylene in the gas phase with titanium dioxide as catalyst, React. Kinet. Catal. Lett. 74 (2001) 209–215. doi:10.1023/A:1017968507589.

[11] V. Héquet, C. Raillard, O. Debono, F. Thévenet, N. Locoge, L. Le Coq, Photocatalytic oxidation of VOCs at ppb level using a closed-loop reactor: the mixture effect, Appl. Catal. B Environ. (2017). doi:10.1016/j.apcatb.2017.12.041.

[12] G. Li Puma, I. Salvadó-Estivill, T.N. Obee, S.O. Hay, Kinetics rate model of the photocatalytic oxidation of trichloroethylene in air over TiO_2 thin films, Sep. Purif. Technol. 67 (2009) 226–232. doi:10.1016/J.SEPPUR.2009.03.011.

[13] M.R. Nimlos, W.A. Jacoby, D.M. Blake, T.A. Milne, Direct mass spectrometric studies of the destruction of hazardous wastes. 2. Gas-phase photocatalytic oxidation of trichloroethylene over titanium oxide: products and mechanisms, Environ. Sci. Technol. 27 (1993) 732–740. doi:10.1021/es00041a018.

[14] P.B. Amama, K. Itoh, M. Murabayashi, Gas-phase photocatalytic degradation of trichloroethylene on pretreated TiO2, Appl. Catal. B Environ. 37 (2002) 321–330. doi:10.1016/S0926-3373(02)00010-3.

[15] A.T. Hodgson, H. Destaillats, D.P. Sullivan, W.J. Fisk, Performance of ultraviolet

photocatalytic oxidation for indoor air cleaning applications, Indoor Air. 17 (2007) 305–316. doi:10.1111/j.1600-0668.2007.00479.x.

[16] W. Chen, J.J. Zhang, Z. Zhibin, Performance of Air Cleaners for Removing Multi-Volatile Organic Compounds in Indoor Air, ASHRAE Trans. 111 (2005) 1101–1114.

[17] National Center for Biotechnology Information, Acrylonitrile, PubChem Compd. Database. (n.d.). https://pubchem.ncbi.nlm.nih.gov/compound/7855 (accessed July 31, 2018).

[18] National Center for Biotechnology Information, Isoflurane, PubChem Compd. Database. (n.d.). https://pubchem.ncbi.nlm.nih.gov/compound/isoflurane#section=Top (accessed July 31, 2018).

[19] E. Dumont, V. Héquet, Determination of the Clean Air Delivery Rate (CADR) of Photocatalytic Oxidation (PCO) Purifiers for Indoor Air Pollutants Using a Closed-Loop Reactor. Part I: Theoretical Considerations, Molecules. 22 (2017). doi:10.3390/molecules22030407.

[20] V. Héquet, F. Batault, C. Raillard, F. Thévenet, L. Le Coq, E. Dumont, Determination of the Clean Air Delivery Rate (CADR) of Photocatalytic Oxidation (PCO) Purifiers for Indoor Air Pollutants Using a Closed-Loop Reactor. Part II: Experimental Results, Molecules. 22 (2017). doi:10.3390/molecules22030408.

[21] A.H. Mamaghani, F. Haghighat, C.-S.S. Lee, Photocatalytic oxidation technology for indoor environment air purification: The state-of-the-art, Appl. Catal. B Environ. 203 (2017) 247–269. doi:10.1016/J.APCATB.2016.10.037.

[22] K.-H. Wang, H.-H. Tsai, Y.-H. Hsieh, The kinetics of photocatalytic degradation of trichloroethylene in gas phase over TiO_2 supported on glass bead, Appl. Catal. B Environ. 17 (1998) 313–320. doi:10.1016/S0926-3373(97)00099-4.

[23] H. Yu, K. Zhang, C. Rossi, Experimental Study of the Photocatalytic Degradation of Formaldehyde in Indoor Air using a Nano-particulate Titanium Dioxide Photocatalyst, Indoor Built Environ. 16 (2007) 529–537. doi:10.1177/1420326X07083513.

[24] H. Destaillats, M. Sleiman, D.P. Sullivan, C. Jacquiod, J. Sablayrolles, L. Molins, Key parameters influencing the performance of photocatalytic oxidation (PCO) air purification under realistic indoor conditions, Appl. Catal. B Environ. 128 (2012) 159–170. doi:10.1016/j.apcatb.2012.03.014.

[25] N. Quici, M.L. Vera, H. Choi, G.L. Puma, D.D. Dionysiou, M.I. Litter, H. Destaillats, Effect of key parameters on the photocatalytic oxidation of toluene at low concentrations in air under 254+185nm UV irradiation, Appl. Catal. B Environ. 95 (2010) 312–319. doi:10.1016/j.apcatb.2010.01.009.

[26] L. Zhong, F. Haghighat, P. Blondeau, J. Kozinski, Modeling and physical interpretation of photocatalytic oxidation efficiency in indoor air applications, Build. Environ. 45 (2010) 2689–2697.

[27] L. Yang, A. Cai, C. Luo, Z. Liu, W. Shangguan, T. Xi, Performance analysis of a novel TiO_2-coated foam-nickel PCO air purifier in HVAC systems, Sep. Purif. Technol. 68 (2009) 232–237. doi:10.1016/J.SEPPUR.2009.05.008.

[28] T.N. Obee, Photooxidation of Sub-Parts-per-Million Toluene and Formaldehyde Levels on Titania Using a Glass-Plate Reactor, Environ. Sci. Technol. 30 (1996) 3578–3584. doi:10.1021/es9602713.

[29] F. Batault, V. Héquet, C. Raillard, F. Thévenet, N. Locoge, L. Le Coq, How chemical and physical mechanisms enable the influence of the operating conditions in a photocatalytic indoor air treatment device to be modeled, Chem. Eng. J. 307 (2017) 766–775. doi:10.1016/j.cej.2016.08.118.

[30] A. Ginestet, D. Pugnet, J. Rowley, K. Bull, H. Yeomans, Development of a new photocatalytic oxidation air filter for aircraft cabin, Indoor Air. 15 (2005) 326–334.

doi:10.1111/j.1600-0668.2005.00369.x.

[31] C.-S. Lee, L. Zhong, F. Haghighat, C. Coulthrust, A. Bahloul, Evaluation of Ozone Removal Performance of Ultraviolet Photocatalytic Oxidation Air Cleaning Systems, in: ASHRAE Annu. Conf., Atlanta, 2016.

[32] J. Zhao, X. Yang, Photocatalytic oxidation for indoor air purification: a literature review, Build. Environ. 38 (2003) 645–654. doi:10.1016/S0360-1323(02)00212-3.

[33] J.-M. Herrmann, Heterogeneous photocatalysis: State of the art and present applications, Top. Catal. 34 (2005) 49–65. doi:10.1007/s11244-005-3788-2.

[34] D.F. Ollis, E. Pelizzetti, N. Serpone, Photocatalyzed destruction of water contaminants, Environ. Sci. Technol. 25 (1991) 1522–1529. doi:10.1021/es00021a001.

[35] T.-H. Lim, S.-D. Kim, Photocatalytic degradation of trichloroethylene over TiO_2/SiO_2 in an annulus fluidized bed reactor, Korean J. Chem. Eng. 19 (2002) 1072–1077. doi:10.1007/BF02707235.

[36] W. Wang, Y. Ku, Photocatalytic degradation of gaseous benzene in air streams by using an optical fiber photoreactor, J. Photochem. Photobiol. A Chem. 159 (2003) 47–59. doi:10.1016/S1010-6030(03)00111-4.

[37] C. Raillard, A. Maudhuit, V. Héquet, L. Le Coq, J. Sablayrolles, L. Molins, Use of experimental designs to establish a kinetic law for a gas phase photocatalytic process, Int. J. Chem. React. Eng. 12 (2014) 113. doi:10.1515/ijcre-2014-0012.

[38] J. Mo, Y. Zhang, Q. Xu, R. Yang, Effect of TiO_2/adsorbent hybrid photocatalysts for toluene decomposition in gas phase, J. Hazard. Mater. 168 (2009) 276–281. doi:10.1016/J.JHAZMAT.2009.02.033.

[39] F.V.S.S. Lopes, R.A.R.R. Monteiro, A.M.T.T. Silva, G. V. Silva, J.L. Faria, A.M. Mendes, V.J.P.P. Vilar, R.A.R.R. Boaventura, Insights into UV-TiO2 photocatalytic degradation of PCE for air decontamination systems, Chem. Eng. J. (2012) 244–257.

[40] A.H. Mamaghani, F. Haghighat, C.-S. Lee, Photocatalytic degradation of VOCs on various commercial titanium dioxides: Impact of operating parameters on removal efficiency and by-products generation, Build. Environ. (2018). doi:10.1016/j.buildenv.2018.05.002.

[41] L. Zhong, F. Haghighat, C.-S. Lee, N. Lakdawala, Performance of ultraviolet photocatalytic oxidation for indoor air applications: Systematic experimental evaluation, J. Hazard. Mater. 261 (2013) 130–138.

[42] M. Jafarikojour, M. Sohrabi, S.J. Royaee, A. Hassanvand, Evaluation and Optimization of a Novel Immobilized Photoreactor for the Degradation of Gaseous Toluene, CLEAN - Soil, Air, Water. 43 (2015) 662–670. doi:10.1002/clen.201300985.

[43] J. Mo, Y. Zhang, Q. Xu, J.J. Lamson, R. Zhao, Photocatalytic purification of volatile organic compounds in indoor air: A literature review, Atmos. Environ. 43 (2009) 2229–2246.

[44] T. Tytgat, B. Hauchecorne, A.M. Abakumov, M. Smits, S.W. Verbruggen, S. Lenaerts, Photocatalytic process optimisation for ethylene oxidation, Chem. Eng. J. 209 (2012) 494–500. doi:10.1016/J.CEJ.2012.08.032.

[45] J. Mo, Y. Zhang, Q. Xu, Effect of water vapor on the by-products and decomposition rate of ppb-level toluene by photocatalytic oxidation, Appl. Catal. B Environ. 132–133 (2013) 212–218. doi:10.1016/J.APCATB.2012.12.001.

[46] AFNOR, NF S90-351 - Health care institutions - Controlled environment areas - Requirements for airborne contamination control, (2013). https://www.boutique.afnor.org/norme/nf-s90-351/etablissements-de-sante-zones-a-environnement-maitrise-exigences-relatives-a-la-maitrise-de-la-contamination-aeroportee/article/809391/fa168416 (accessed April 18, 2018).

[47] ASHRAE, ASHRAE 170-2017-Ventilation of Health Care Facilities, (2017).

https://www.techstreet.com/ashrae/standards/ashrae-170-2017?product_id=1999079&ashrae_auth_token=12ce7b1d-2e2e-472b-b689-8065208f2e36 (accessed April 18, 2018).

[48] C.A. Balaras, E. Dascalaki, A. Gaglia, HVAC and indoor thermal conditions in hospital operating rooms, Energy Build. 39 (2007) 454–470. doi:10.1016/j.enbuild.2006.09.004.

[49] C. Raillard, V. Héquet, P. Le Cloirec, J. Legrand, Kinetic study of ketones photocatalytic oxidation in gas phase using TiO_2-containing paper: effect of water vapor, J. Photochem. Photobiol. A Chem. 163 (2004) 425–431.

[50] L. Zhang, W.A. Anderson, S. Sawell, C. Moralejo, Mechanistic analysis on the influence of humidity on photocatalytic decomposition of gas-phase chlorobenzene, Chemosphere. 68 (2007) 546–553. doi:10.1016/J.CHEMOSPHERE.2006.12.056.

[51] D. Vildozo, R. Portela, C. Ferronato, J.-M. Chovelon, Photocatalytic oxidation of 2-propanol/toluene binary mixtures at indoor air concentration levels, Appl. Catal. B Environ. 107 (2011) 347–354. doi:10.1016/J.APCATB.2011.07.035.

[52] M. Krichevskaya, S. Jõks, A. Kachina, S. Preis, Gas-phase photocatalytic oxidation of acrylonitrile, Photochem. Photobiol. Sci. 8 (2009) 600. doi:10.1039/b817063k.

[53] J. Chen, G. Li, Z. He, T. An, Adsorption and degradation of model volatile organic compounds by a combined titania–montmorillonite–silica photocatalyst, J. Hazard. Mater. 190 (2011) 416–423. doi:10.1016/j.jhazmat.2011.03.064.

[54] W. Chen, J. Zhang, Z. Zhang, UV-PCO device for indoor VOCs removal: Investigation on multiple compounds effect, in: Indoor Air, 2005.

[55] F. Batault, F. Thevenet, V. Hequet, C. Raillard, L. Le Coq, N. Locoge, Acetaldehyde and acetic acid adsorption on TiO2 under dry and humid conditions, Chem. Eng. J. 264 (2015) 197–210. doi:10.1016/J.CEJ.2014.10.089.

[56] K.J. Weld, S. Dryer, C.D. Ames, K. Cho, C. Hogan, M. Lee, P. Biswas, J. Landman, Analysis of Surgical Smoke Produced by Various Energy-Based Instruments and Effect on Laparoscopic Visibility, J. Endourol. 21 (2007) 347–351. doi:10.1089/end.2006.9994.

[57] O. Park, C.S. Kim, H.H. Cho, Development of a photoreactive fabric filter for simultaneous removal of VOCs and fine particles, Korean J. Chem. Eng. 23 (2006) 194–198. doi:10.1007/BF02705715.

[58] L. Lin, Y. Chai, B. Zhao, W. Wei, D. He, B. He, Q. Tang, Photocatalytic oxidation for degradation of VOCs, Open J. Inorg. Chem. 03 (2013) 14–25. doi:10.4236/ojic.2013.31003.

[59] O. Debono, Oxydation photocatalytique de composés organiques volatils et suivi de leurs intermédiaires réactionnels : étude en réacteurs statique et dynamique à des concentrations typiques de l'air intérieur, Nantes, Ecole des Mines, 2011.

[60] K.-H. Wang, J.-M. Jehng, Y.-H. Hsieh, C.-Y. Chang, The reaction pathway for the heterogeneous photocatalysis of trichloroethylene in gas phase, J. Hazard. Mater. 90 (2002) 63–75. doi:10.1016/S0304-3894(01)00331-4.

[61] K. Koistinen, D. Kotzias, S. Kephalopoulos, C. Schlitt, P. Carrer, M. Jantunen, S. Kirchner, J. McLaughlin, L. Mølhave, E.O. Fernandes, B. Seifert, The INDEX project: executive summary of a European Union project on indoor air pollutants, Allergy. 63 (2008) 810–819. doi:10.1111/j.1398-9995.2008.01740.x.

[62] J. Mo, Y. Zhang, Q. Xu, Y. Zhu, J.J. Lamson, R. Zhao, Determination and risk assessment of by-products resulting from photocatalytic oxidation of toluene, Appl. Catal. B Environ. 89 (2009) 570–576. doi:10.1016/J.APCATB.2009.01.015.

[63] IARC, IARC Monographs on the Evaluation of carcinogenic risks to humans Classifications, (n.d.). http://monographs.iarc.fr/ENG/Classification/ (accessed April

29, 2018).
[64] M. Birnie, S. Riffat, M. Gillott, Photocatalytic reactors: design for effective air purification, Int. J. Low Carbon Technol. 1 (n.d.).
[65] F. Batault, Influence de l'adsorption et des paramètres opératoires sur le traitement photocatalytique de composés organiques volatils en mélange dans les conditions de l'air intérieur, Lille 1, 2014.

CHAPTER IV:
CFD AS A TOOL TO UNDERSTAND THE PERFORMANCE OF PHOTOCATALYTIC REACTORS

IV.1 Introduction

In Chapter III, it was shown that change in the media geometry from plane to pleated increased the degradation efficiency of the target compounds. It was assumed that this increase was as a result of an increase in contact time and better irradiation distribution. However, being able to experimentally predict the behavior of some operational parameters (i.e., fluid velocity and UV irradiance) globally and locally and also being able to accurately measure local values of these operational parameters is sometimes difficult depending on the configuration of the used photocatalytic reactor [1]. An effective approach to solve this issue is through the use of Computational Fluid Dynamics (CFD).

CFD can be defined as the science of predicting fluid flow, heat transfer, mass transfer, chemical reactions, and related phenomena by solving the mathematical equations that govern these processes using numerical algorithms [2,3]. There are several commercial design packages or software that exist to solve the governing equations that can produce accurate and reliable simulation of the physico-chemical processes. These include Ansys (CFX and Fluent), COMSOL, Abaquis and PHEONIX. The solvers usually make use of the finite volume method. This is a method in which the geometry (calculation domain) of interest is divided or discretized, into a number of computational cells. Discretization is the method of approximating the differential equations by a system of algebraic equations for the variables at some set of discrete locations in space and time. The discrete locations are referred to as grid or mesh. Once the grid has been created, boundary conditions need to be specified. For the inlet, parameters such as pressure, velocity, mass flow, and temperature may be specified. Temperature, UV-irradiance, wall shear rates, or heat fluxes may be set at walls. For the outlet, pressure or flow-rate splits may be fixed at outlets. The component material properties, such as density, viscosity, diffusion coefficient, UV-absorbance and heat capacity, need to be also prescribed. With the grid created, the boundary conditions and physical properties defined, the calculations can be performed. A CFD code is used to solve the appropriate conservation equations for all grid cells using an iterative procedure [4].

CFD is becoming more and more popular to investigate photocatalytic reactors for air treatment [5]. It allows for comprehensive analysis of photocatalytic reactor through the simulation of fluid dynamics, species mass transport, chemical reaction kinetics, and irradiance

distribution. It is also a cost effective approach as it helps to reduce the number of experiments necessary to predict the behavior of a process.

Mohseni and Taghipour [6] used experimental and CFD modeling to investigate the flow field and the photocatalytic degradation of vinyl chloride in an annular reactor and reported good agreement of conversion values between the model to experimental results. Castrillion and de Lasa [7] used CFD to simulate the flow field in a photo-CREC reactor. The simulation gave them information about the flow field within the reactor and by optimizing the design they were able to uniformize mass flow and contact time distributions within the reactor. Salvado-Estivill *et al*. [8] modeled the degradation of trichloroethylene in a single- pass flat plate photocatalytic reactor by combining CFD modeling of the fluid flow in the reactor with radiation field modeling and photocatalytic reaction kinetics. A comparison of the model prediction with the experimental results yielded good agreement [8]. Chong *et al.* [9] modeled flow field, radiation and kinetics of toluene and formaldehyde through a porous monolith photocatalytic reactor. The simulation gave them information about the local flow field and light intensity profile. They also observed a good agreement between model predictions and experimental values for conversion profiles. Wang *et al.* [10] conducted a CFD simulation to enable them describe the local UV flux within a porous monolith channel. They also investigated the monolith to lamp spacing and the number of lamps to achieve the optimal configuration that would provide higher formaldehyde conversion yields. Verbruggen *et al.* [11] presented the use of computational fluid dynamics (CFD) for accurately determining the adsorption parameters of acetaldehyde on photocatalytic fiber filter material, integrated in a continuous flow glass tube reactor. CFD allowed them to extract precise, intrinsic adsorption parameters for situations in which analytical analysis would otherwise fail. Roegiers *et al.* [12] developed a CFD model which coupled radiation field modeling with reaction kinetics and fluid dynamics in order to simulate the degradation of acetaldehyde in a multi-tube glass photoreactor. They reported a good agreement between model predictions and experimental values for acetaldehyde conversion profiles. A summary of the information from these authors is presented in Table 23.

Reactor	Pollutant	CFD software	Objectives	Reference
Annular flow reactor	Vinyl chloride	Fluent 6.0	Investigation of flow field and kinetic reaction	Mohseni and Taghipour [6]
Photo-CREC reactor	-	CFX-5.7.1	Investigation of flow field	Castrillion and de Lasa [7]
Flat plate reactor	Trichloroethylene	Fluent 6.2	Investigation of flow field, radiation field and kinetic reaction	Salvado-Estivill *et al*. [8]
Monolith photocatalytic reactor	Toluene and formaldehyde	Fluent	Investigation of flow field, radiation field and kinetic reaction	Chong *et al.* [9]
Monolith photocatalytic reactor	Formaldehyde	Fluent	Investigation of radiation field and reaction kinetic	Wang *et al.* [10]
Glass tube reactor	Acetaldehyde	Comsol Multiphysics v.4.4.	Determination of adsorption parameters	Verbruggen *et al.*[11]
Multi-tube glass reactor	Acetaldehyde	Comsol Multiphysics v5.3	Investigation of flow field, radiation field and kinetic reaction	Roegiers *et al.* [12]

Table 23 : Summary of different uses of CFD in PCO as found in the literature

In this work numerical simulations by CFD are conducted to better understand the influence of the change of media geometry on the efficiency in terms of the air flow and light irradiance. The objectives of this part are:

- Evaluate the behavior of the air flow and the irradiance in the reactor and in and on the media,
- Determine average velocity, contact time and average irradiance in and on the media.

IV.2 CFD Methodology

Ansys Workbench 14.5 was used for all the simulation work. In Ansys, the simulation process is carried out in three main stages using different tools in each stage:

- pre-processing: creation of geometry and generation of meshing using Design modeler and Ansys meshing respectively,
- processing: definition of physical phenomena to be assessed and specification of appropriate boundary conditions based on the finite volume method using CFX and Fluent codes,
- post processing: the graphical visualization of results and exportation of simulation outputs using CFD-Post.

IV.2.1 Geometry definition

The first step in the process is the creation of the computational domain or the system geometry. It is necessary to identify which regions the governing equations will have to be solved and the physical limits for which the boundary conditions are set. The computational domain in this work was the photocatalytic module of the multi-pass laboratory reactor. As previously described in chapter II, it is an 0.8 m x 0.2 m x 0.2 m stainless steel box that houses the immobilized monolith photocatalyst and the lamps. The porous media consists of TiO_2 immobilized on SiO_2 support with an average thickness of 0.0175 m. The photocatalytic media is irradiated by two low-pressure Phillips TUV PL-L 18W, which emit light at a peak wavelength of 254 nm (UVC).

For the plane media configuration (Figure 57), the photocatalytic media has a surface area of 0.04 m^2. The media is placed perpendicularly to the flow whilst the lamps are placed horizontally to the media and are also 3 cm away from the media surface.

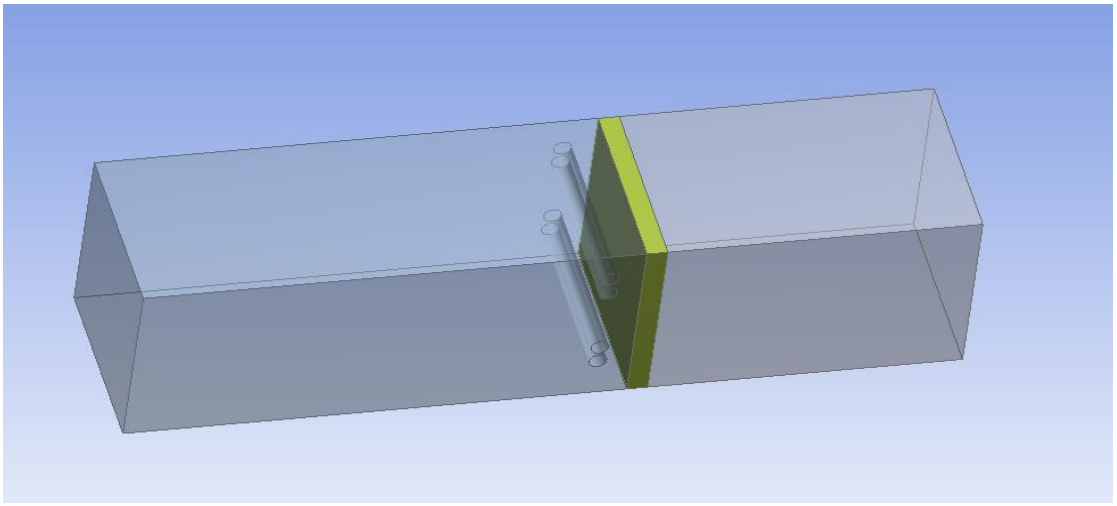

Figure 57 : Geometry definition of plane configuration using ANSYS Design modeler

The pleated configuration consists of the photocatalytic media folded into four pleats creating two triangles at 60° with a surface area of 0.072 m^2. The lamps are placed vertically within the triangles. The lamps were also placed 3 cm from the middle of the media pleats. The geometry designed with Ansys design modeler is shown in Figure 58. In both geometries, the media has an average thickness of 0.0175 m.

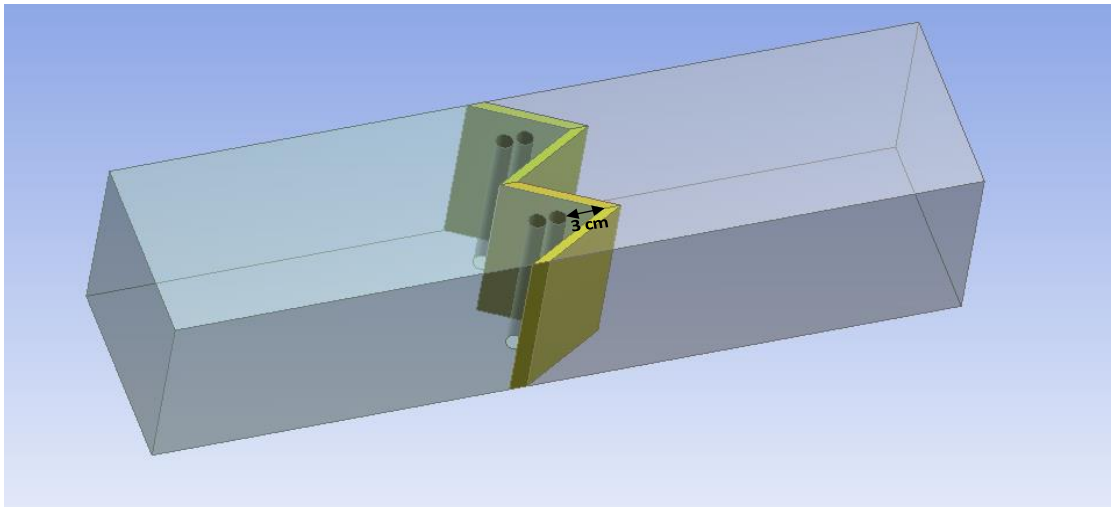

Figure 58 : Geometry definition of pleated configuration using ANSYS Design modeler

IV.2.2 Meshing

Once the geometry has been created, it is then divided into a number of control volumes that do not overlap each other called cells or elements where the governing equations are solved.

The meshing process is important as it affects the accuracy of the CFD results and the solving time. A fine mesh better captures the qualities of the flow and other governing equations included in the model. In fact, the higher the number of elements, the better the solution accuracy. However, the number of elements directly influences the computational time thus the higher the number of elements, the higher the computational time. It is therefore necessary to identify the case-specific optimal mesh that could guarantee the mesh-independence of results as well as sustainable computational requirements.

The type of mesh structure or topology used depends on the geometry. There are basically three types of mesh topologies which are: structured, unstructured and block. As described by Tu *et al*. [13]:

- Structured mesh: the edges of the cells forms continuous meshing lines that follow a uniform pattern thus improving the connectivity between adjacent cells. The use of structured mesh is more convenient for simple geometries. They are usually quadrilaterals (2D) or hexahedral (3D).

- Unstructured mesh: the cells do not have a particular order, that is, cells are allowed to assemble freely and cannot be directly identified by their indexes. They are usually triangles (2D) or tetrahedrons (3D). They are especially useful when dealing with non-standard or complex geometries. The disadvantage of this type of meshing is that calculation might require more computational power as neighboring cells are not well defined and more complex solution algorithms might be required.

- Block meshes: This structure consists of structured and unstructured cells. In this type of meshing, a certain part of the domain volume is meshed in a specific manner, i.e. structured mesh while other parts are meshed in a manner which accommodates better the specific geometry i.e. unstructured mesh. In this manner, simple geometries within the

domain volume can be solved easier with less computational resources, while the resources are focusing on more complex geometries within the domain.

In this work, the block structure was used as shown in Figure 59. The geometry was discretized in 503123 structured and unstructured volume cells which were high enough to give mesh-independent results. Structured hexahedral meshing was applied to the media and the fluid region after the media but unstructured tetrahedral meshing applied to fluid region before the media in which the lamps are found to account for the complexities around the lamps.

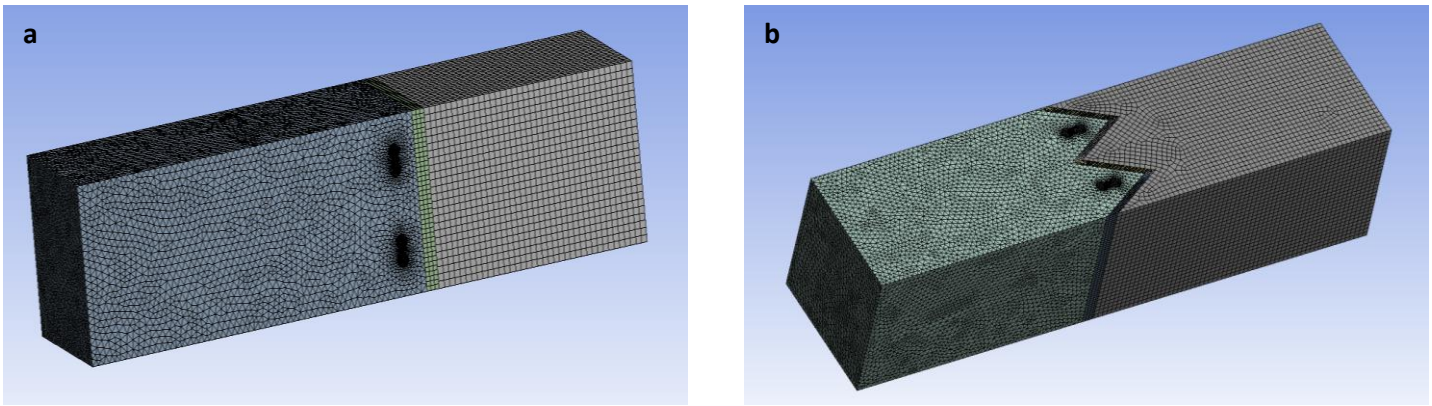

Figure 59 : (a) Plane geometry meshing (b) pleated geometry meshing

Mesh independence tests were carried out by running the calculation at three different mesh sizes. Table 24 shows the average velocity and irradiance on media surface of the plane configuration for the different mesh sizes. It can be seen that the values were quite similar. 503123 was chosen because it provided better capture of the flow and irradiance qualities at a reasonable computational time.

Mesh Size	Average velocity ($m.s^{-1}$)	Average irradiance ($W.m^{-2}$)
138974	1.11	100.17
348599	1.13	100.36
503123	1.14	100.44

Table 24 : Influence of the mesh size on the average velocity and irradiance on the media surface

IV.2.3 Model development

The computational model is divided into two parts. The first part deals with the solution of the flow characteristics (fluid dynamics modeling) within the module and the second part deals with the calculation of the UV irradiance distribution (radiation field modeling).

IV.2.3.1 Fluid dynamics modeling

In order to investigate the flow field in the photocatalytic module, the governing equations of fluid dynamics, which mathematically represent the conservation of mass and momentum, are solved. The conservation of mass is achieved by solving the classical continuity equation. For the conservation of momentum, since the flow is in the turbulent regime, the Reynolds-Averaged Navier Stokes (RANS) equation is solved. However since the reactor also contains a porous region which is the photocatalytic media, the equations are modified to account for the porosity of the media. The modified continuity and the momentum equations are given below as Equation 29 and Equation 30 respectively [10,14].

$$\frac{\partial(\varepsilon)\rho}{\partial t} + \nabla(\varepsilon\rho\vec{v}) = 0 \qquad \textbf{Equation 29}$$

$$\frac{\partial(\varepsilon\rho\vec{v})}{\partial t} + \nabla(\varepsilon\rho\vec{v}\vec{v}) = -\varepsilon\nabla p + \nabla\varepsilon\rho g + \nabla\varepsilon\tau + S_M \qquad \textbf{Equation 30}$$

where ρ, v, τ ,g, p *and* ε are the density of the fluid, the velocity of the fluid, stress tensor, gravity, pressure and porosity of the media respectively. S_M is the momentum sink term which accounts for the loss of momentum or pressure drop due to an obstacle which in this case is the media. It is given by the modified Darcy law previously described in Chapter II of this manuscript and is given again in Equation 31 as:

$$S_M = \frac{\mu}{k}v + \frac{1}{2}C\rho v^2 \qquad \textbf{Equation 31}$$

where k is the permeability, C is the inertial resistance factor.

In turbulent flow modeling, one of the main challenges is to close the governing equation by modeling the Reynolds stress tensor in Equation 30. Generally, for most engineering flow modeling applications, this so-called closure problem is solved by introducing a turbulence

model [14]. Several turbulence models have been proposed but no turbulence model is universally accepted to be superior for all conditions. Proper turbulence models need to be selected according to the problem under consideration. In this work, the standard k-ε turbulence model which is the most widely used for photocatalytic reactors [5] is employed.

In this work, the fluid dynamics package CFX was used to carry out the simulations. The geometry was characterized by two zones, the fluid (air) and the porous (media) zones. The following assumptions were then made in the mathematical model: a) the flow is at steady state and turbulent and b) the fluid (air) is incompressible and isothermal with constant physical properties. The media was assumed to be a porous body with porosity of 0.875, permeability is of 1.45 $x10^{-8}$ m^2 and an inertial resistance factor is of 823 m^{-1}.These characteristics were stated in chapter II of this manuscript.

For the boundary conditions, the velocity of 1 $m.s^{-1}$ at the inlet was considered. A pressure-outlet boundary condition of 1 atm was also fixed. To solve the equations, the first order high resolution scheme was chosen.

IV.2.3.2 Radiation field modeling

To model the irradiance distribution within the reactor the radiative transport equation (RTE) needs to be solved. Due to its trajectory through a medium the light will experience absorption, out-scattering and in-scattering as shown in Figure 60.

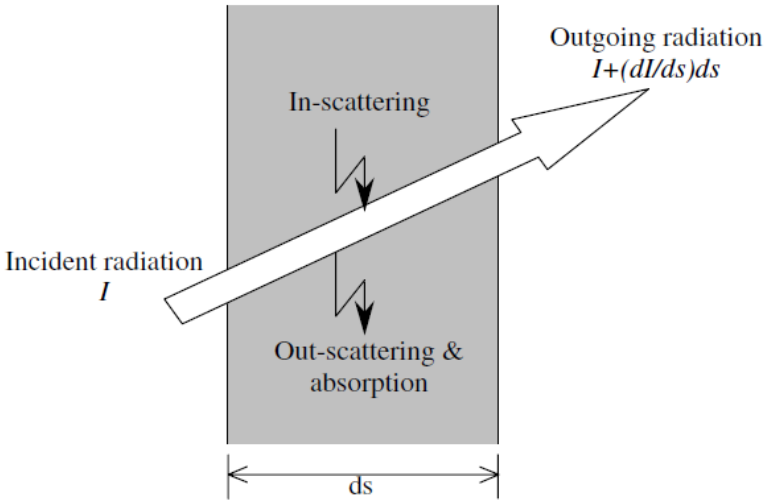

Figure 60 : Path of a light ray in a medium [15]

The RTE is an integro-differential equation which describes the photonic rays with their corresponding energy loss due to absorption and out-scattering and gain due to in-scattering. It describes the movement of a bundle of light rays travelling in a direction s having a solid angle Ω, intensity I and wavelength λ. The generic form of the equation is given in Equation 32 as [14]:

$$\frac{dI_\lambda(s\Omega)}{ds} + a_\lambda I_\lambda(s\Omega) + \sigma_\lambda I_\lambda(s\Omega) = a_\lambda n^2 \frac{\sigma_{SB} T^4}{\pi} + \frac{\sigma_s}{4\pi} \int_0^{4\pi} I_\lambda(s'\Omega)\phi(s'.s)\, d\Omega' \qquad \textbf{Equation 32}$$

where :
s = direction
s' = scattering direction
a = absorption coefficient
n = refractive index
σ = scattering coefficient
σ_{SB} = Stefan-Boltzmann constant (5.67×10^{-8} W.m^{-2}K^{-4})
I = light intensity which depends on solid angle, direction and wavelength
T = local temperature
Φ = phase function
Ω = solid angle
Ω' = scattering solid angle

The first term on the left represents the radiance change along the direction s of photon. The second term on the left represents the loss of photons due to absorption. The third term accounts for loss due to out-scattering. The second term on the right hand side accounts for a

gain in energy due to in-scattering. And Φ (s'.s) is a phase function describing the incident radiation from all other directions.

In this work, the radiation field modeling was done using the Ansys Fluent solver. The solver provides five models that allow the RTE to be solved. These are Discrete Transfer Radiation Model (DTRM), P-1 Radiation Model, Rosseland Radiation Model, Surface-to-Surface (S2S) Radiation Model, and Discrete Ordinates (DO) Radiation Model [16].

The numerical resolution of the RTE was carried out using the DO Radiation Model because it is only this model that allows the definition of the optical processes considering different wavelengths, as well as to include the effect of dispersion, absorption and the emission of radiation by volumes and surfaces. It is the most rigorous method that is valid for the whole range of optical thicknesses, and allows the solution of radiation transport through semitransparent walls. It is a popular choice for photocatalytic reactor applications [15]. In the DO model, the radiation field is divided into a number of discrete directions and the RTE is written and solved separately for each of the directions [15]. One of the disadvantages however of using the DO model is the ray effect where radiation is caused to concentrate along the discrete directions. It results in the appearance of star-like contours which create a doubt about the intensity of the light. Thus although the average irradiation in the domain area might remain the same, the distribution of the irradiation will vary. An example is shown in Figure 61a.

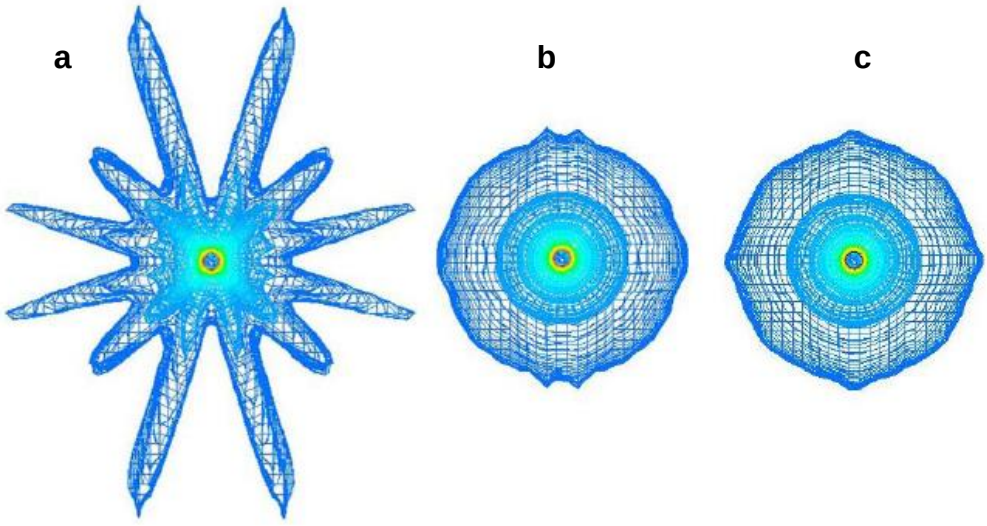

Figure 61 : (a) Ray effect seen when angular discretization is 3x3; Ray effect disappears when angular discretization is increased to (b) 10x10 and (c) 15x15 [17]

To solve this problem, angular discretization is done. When using the DO Model, the spatial discretization of the computational region is taken directly from the mesh grid topology. However, the directional discretization for the RTE needs to be explicitly specified using an angular discretization. The angular discretization is defined by the angles Theta (θ) and Phi (ϕ), and is required as a user input in the solver. The more the angular divisions for discretization, the better the irradiation will be distributed within the control volume as shown in Figure 61b and Figure 61c. However, when the number of cells is also high, the computational time may become excessive, and a balance must be found between the number of cells and the angular discretization. In this study an angular discretization of 10x10 was used because it is enough to overcome the ray effect [18].

Within the photocatalytic reactor, the lamp is the only source of radiation emission thus the radiation emission from all other sources is neglected. This enables the simplification of the computational model by avoiding the coupling of the radiation balance with the overall energy balance of the system. The simulations were therefore done by inactivating the first term on the right hand side in Equation 32 by setting a value of 1 K (minimum allowed in Fluent) in all regions of the model except the lamp.

Emission from the lamp is usually defined as a boundary condition using a lamp emission model. In a review by Pareek *et al*. [15] they described that the lamp emission modeling could be carried out in three ways :

- Line source modeling: this model depicts the lamp as an emitting line and is useful when the lamp diameter is relatively small in comparison with the reactor diameter.
- Surface source modeling: this model assumes that all the radiation emission occurs at the surface of the lamp and depicts the model as a surface.
- Volume source modeling: for this model emission is from both the surface and also the interior volume of the lamp.

Figure 62 shows a schematic representation of all three models. For our purpose the surface source model was used.

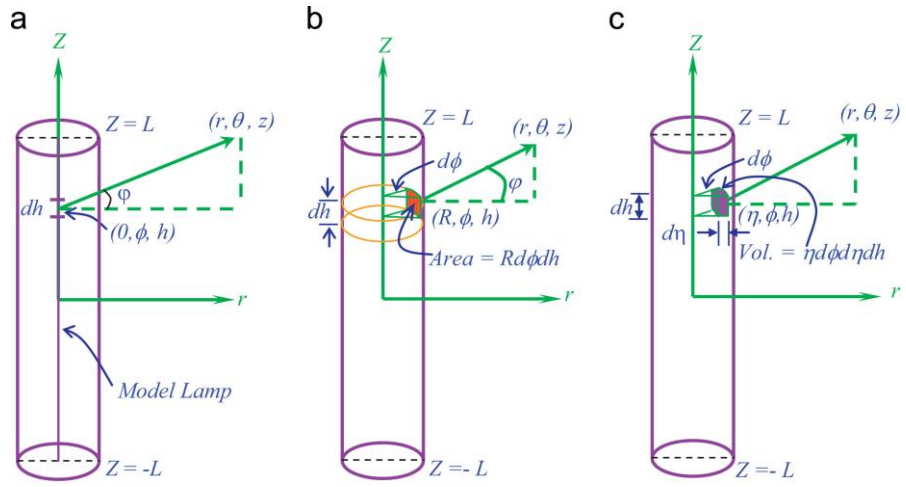

Figure 62 : Schematic representation of lamp emission models (a) line source model (b) surface source model (c) volume source model [15]

In an immobilized system like the one that is used in this work there is a gradual loss of light due to absorption through the photocatalytic media. As stated in the literature [5,9] for immobilized systems, the scattering and reflection are assumed to be negligible. Therefore within the photocatalytic media, Equation 32 is reduced to:

$$\frac{dI_\lambda(s\Omega)}{ds} + a_\lambda I_\lambda(s\Omega) = 0 \qquad \textbf{Equation 33}$$

The absorption coefficient (a) is therefore a necessary user input. It is related to the UV-Transmittance (UVT) by the Beer-Lambert Law which is given as:

$$UVT = \exp(-ax) \qquad \textbf{Equation 34}$$

where *x (m) is* the path length travelled by the light inside the photocatalytic media.

Using the UVT of 0.6% obtained in chapter II of this manuscript, the absorption coefficient is calculated as 292 m^{-1}.

To carry out the simulations, the following assumptions were made: (a) gas-phase absorption, scattering and reflection of the light is negligible, (b) the photocatalytic media was adiabatic and non-conducting, (c) TiO_2 particles are evenly distributed in the photocatalytic

media, (d) the light intensity of the lamps does not vary with time for the duration of the experiments.

The following boundary conditions were also employed: (a) the lamp surfaces were modeled as diffuse semitransparent monochromatic walls with external surface irradiation. (b) reactor walls were defined as diffusely reflecting opaque stainless walls with a reflectivity of 0.15. The second order upwind method was used to solve the RTE.

IV.2.4 Convergence criteria

The resolution of the governing equations in Ansys is an iterative process thus values change from one iteration to the next. If this change is significant then that means that a solution has not been reached. To monitor the convergence, the value of residuals is used. The residuals represent the absolute error in the solution of a particular variable. In general, the residual must decrease as the number of iterations increases or it could stabilize at a certain value [16].

In this work, the convergence was ensured by imposing a residual value of 10^{-6} for continuity and momentum and 10^{-4} for incident radiation. It took 1130 iterations and 6 hours to achieve convergence for fluid dynamic modeling whilst it took 1100 iterations and about 14 hours to achieve convergence for radiation field modeling.

IV.2.5 Results and discussion

The simulation results are discussed first for the fluid dynamic modeling and then for the radiation field modeling.

IV.2.5.1 Fluid dynamics modeling

The aim of this section was to be able to describe the behavior of the flow in the reactor and in the media and to be able to determine the contact time within the media. The results for the plane configuration are first discussed then those of the pleated configuration will be discussed.

Plane configuration

The inlet velocity was set to 1 $m.s^{-1}$ and Figure 63 shows the results for the flow distribution from the inlet to the outlet of the photocatalytic module along a plane. From the figure, it is observed that the flow is homogeneous from the inlet until it encounters the lamps where the flow is obliged to move around the lamps. This change in course presented by the lamps, causes zones of higher velocity above and beneath the lamps and zones of lower velocity behind the lamps. However, once inside the media, the flow homogenizes again and remains homogeneous when it exits the media and subsequently the reactor.

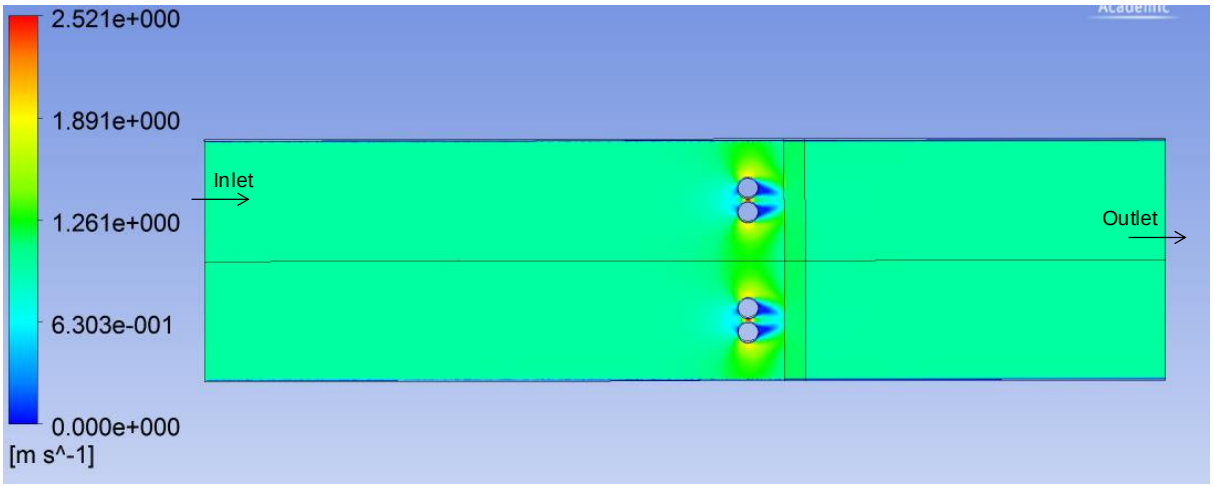

Figure 63 : Velocity contour showing flow behavior through the reactor in the plane configuration

Due to the fact that the lamps are quite close to the media (3 cm), this behavior of having zones that have higher and lower velocities compared to the inlet velocities is replicated on the surface of the media. This is shown in Figure 64. The range of velocities on the surface of the media is 0.90 - 1.39 $m.s^{-1}$. Once inside the media, the flow becomes quite homogeneous as shown in Figure 65. The range at this distance is 1.12 -1.15 $m.s^{-1}$. The flow is still homogeneous when it exits the media as shown in Figure 66 and has a range of 0.98 - 1.00 $m.s^{-1}$.

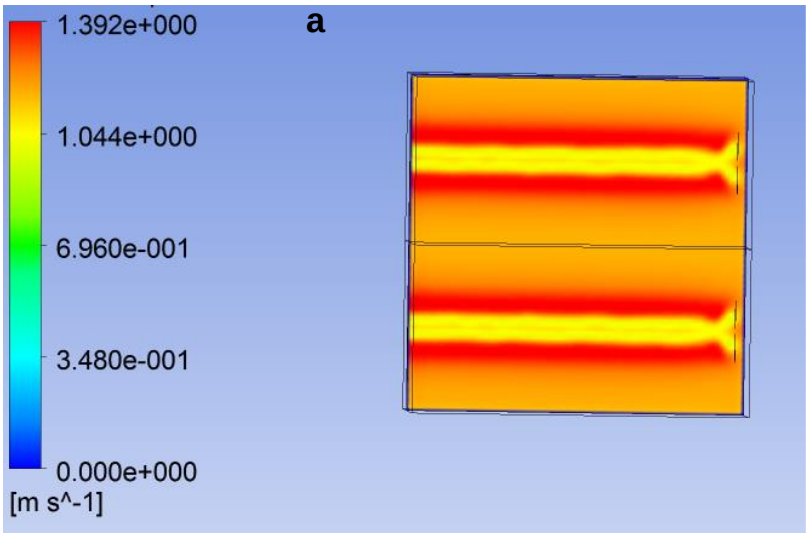

Figure 64 : Velocity contour showing flow behavior on the surface of the photocatalytic media for the plane configuration

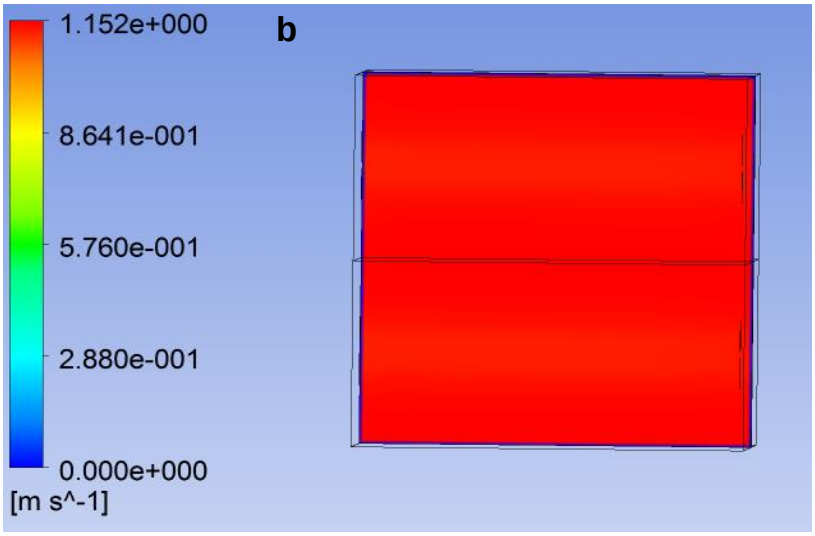

Figure 65 : Velocity contour showing flow behavior 8mm distance in media for the plane configuration

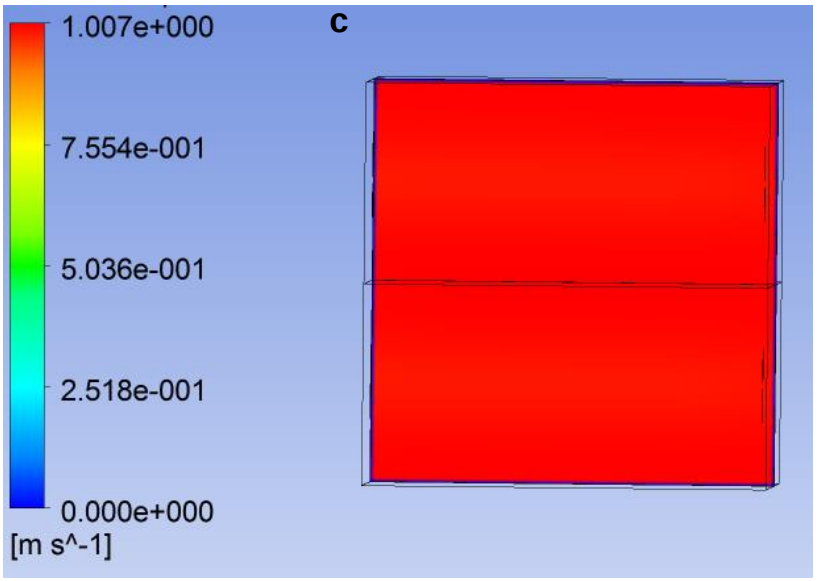

Figure 66 : Velocity contour showing flow behavior on the outlet of the media for the plane configuration

The streamlines were then studied and the results are shown in Figure 67. It shows that the flow is parallel with some small recirculation zones behind the lamps but these are not significant enough to affect entire flow. The streamlines within the media showed that the flow was orthogonal as it moved through the media.

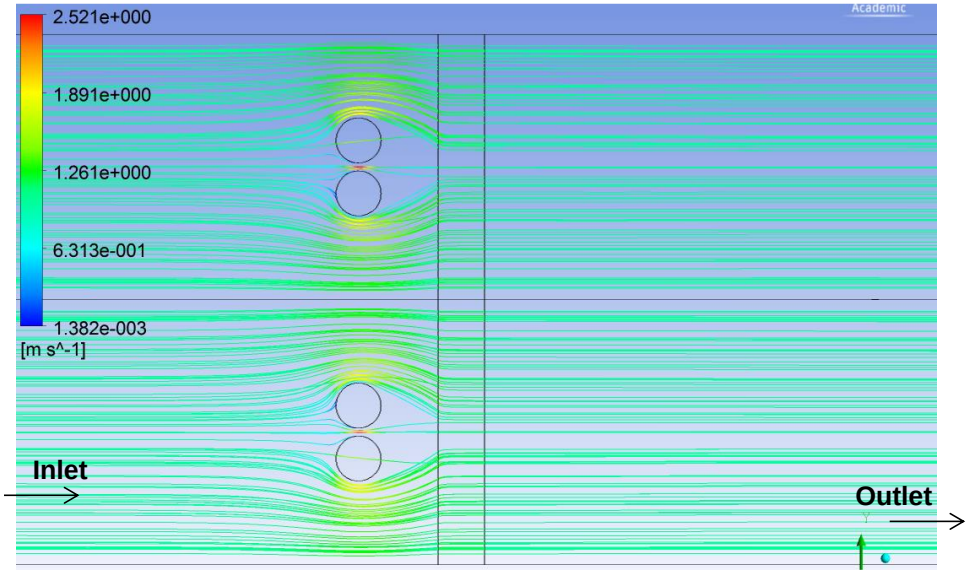

Figure 67 : Streamlines through the photocatalytic module in plane media configuration

To verify the simulation results, the velocity distribution along the height of the reactor at a distance of 8 cm on the x-axis and 6 cm before the media surface was measured experimentally. A Veloport 20 portable air velocity meter was placed in the reactor and the velocity at several distances along the height of the reactor was recorded. As observed in Figure 68, the simulated and experimental results were quite similar signaling that the simulation was quite representative of what was occurring in real conditions.

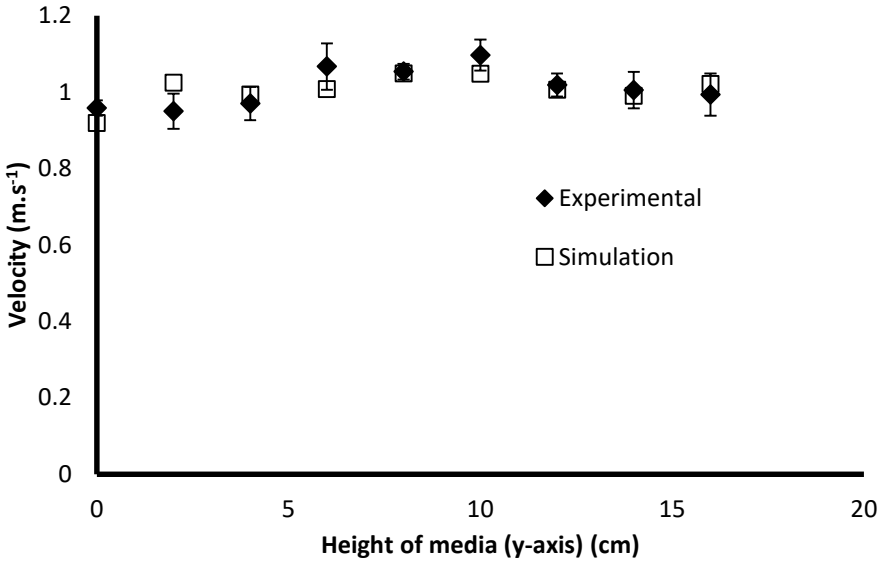

Figure 68 : Comparison between simulated and experimental velocity values along the height of reactor at a distance of 6 cm before media.

The average velocity that is received on the media surface and also within the media is calculated to be 1.14 $m.s^{-1}$. This value is about 14 % higher than the inlet velocity of 1 $m.s^{-1}$. For fluid flow through a porous medium, the superficial velocity (v_0) is the flow rate Q ($m^3.s^{-1}$) divided by the cross-sectional area A (m^2). In our case, the presence of SiO_2 fibers and TiO_2 particles within the photocatalytic media reduces the area available for fluid flow i.e. to conserve fluid continuity with the entering superficial flow, the fluid has to move through a smaller area; hence the velocity within the photocatalytic media (v) is greater than that of the superficial velocity. The interstitial velocity (v) is related to the superficial velocity by the following expression [5]:

$$v = \frac{v_0}{\varepsilon} \qquad \textbf{Equation 35}$$

where ε is the porosity.

In knowing the local average velocity within the media and the path length, the contact time (τ) was then calculated as 15.3 ms using the equation:

$$\tau = \frac{e}{v}$$ **Equation 36**

Where *e* is the path length which is equal to the thickness of the media (m) and *v* is the average true velocity in media ($m.s^{-1}$).

Pleated configuration

The behavior of the flow as it moves across the photocatalytic module for the pleated configuration at an inlet velocity of $1m.s^{-1}$ is shown in Figure 69. Similarly to the plane configuration, the flow in the pleated configuration is homogeneous until it encounters the lamps. At this point, the presence of the lamps and the pleats causes the flow to lose its homogeneity. Additionally, as a result of the influence of the presence of the pleats, the flow exiting the media is quite heterogeneous.

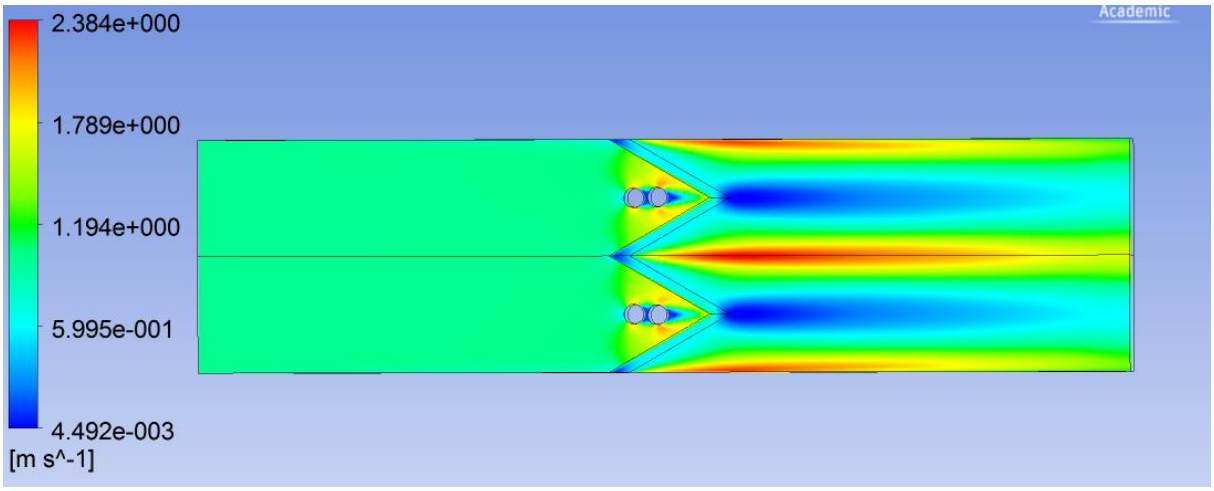

Figure 69 : Velocity contour showing flow behavior through the reactor in the pleated configuration

Figure 70 shows the velocity profile received on the media surface. It can be observed that the flow was heterogeneously distributed on the surface with the maximum velocities at the regions surrounding the pleat joints. The range on the surface was found to be 0.07 - 2.03 $m.s^{-1}$. Unlike the plane configuration, the flow did not homogenize within the media as shown in Figure 71. The range was found to be 0.17- 0.72 $m.s^{-1}$. At the exit of the media the minimum velocities were found at the pleat joints as shown in Figure 72 and the range of velocities for the entire surface was 0.0098 - 0.7 $m.s^{-1}$.

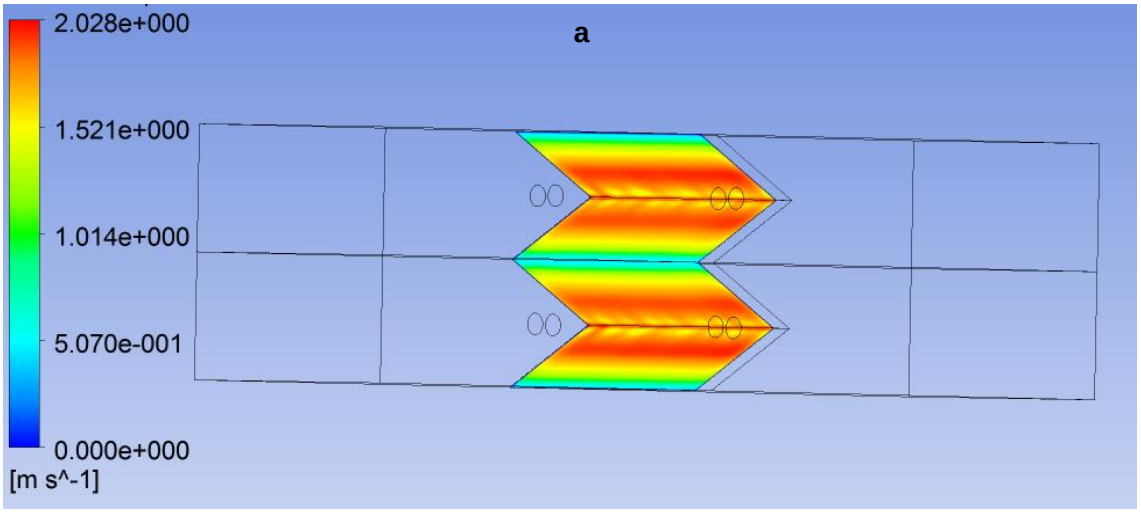

Figure 70 : Velocity contour showing flow behavior on the surface of the photocatalytic media for the pleated configuration

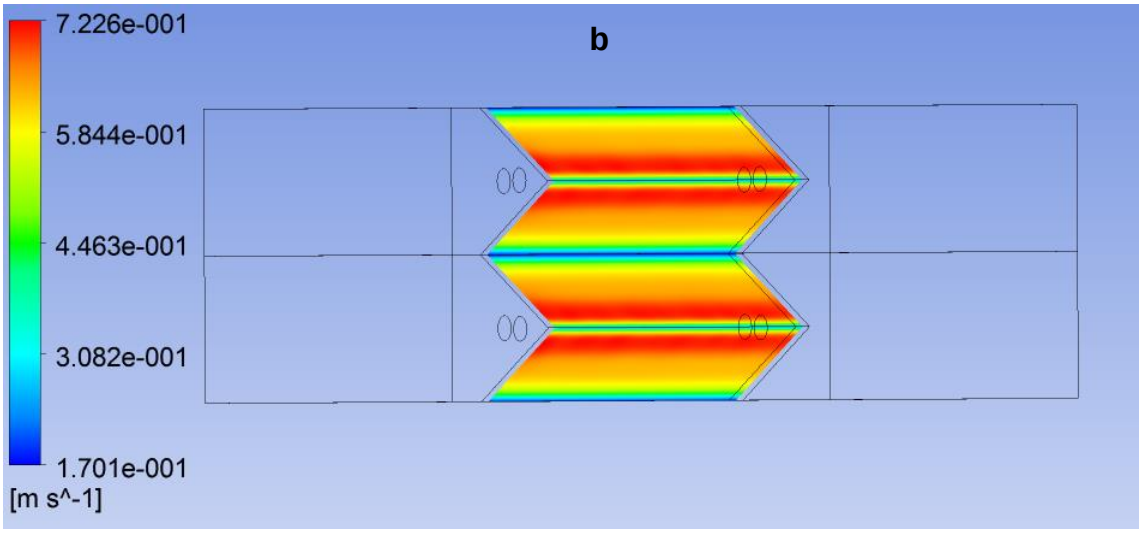

Figure 71 : Velocity contour showing flow behavior 8 mm distance in media for the pleated configuration

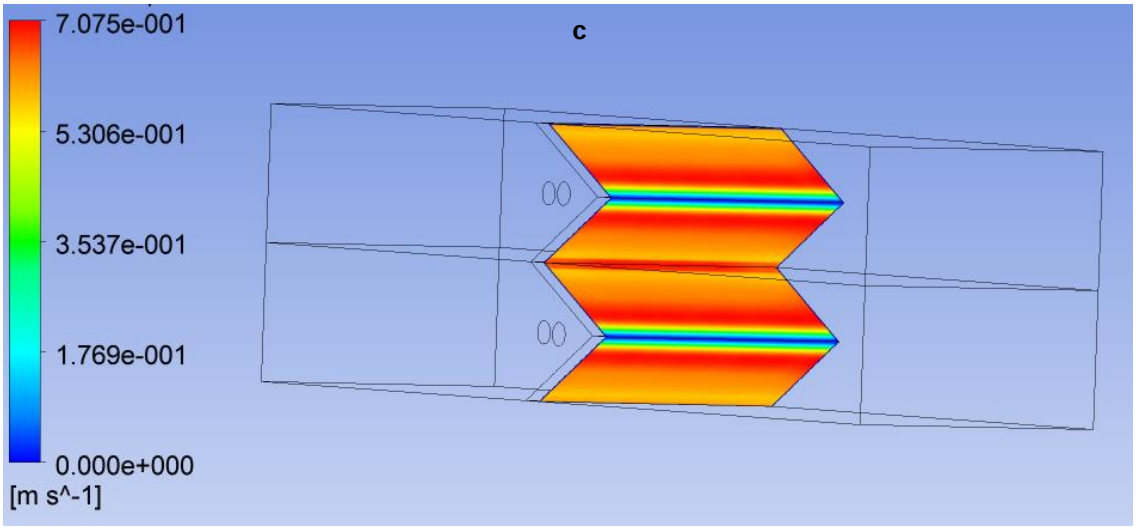

Figure 72 : Velocity contour showing flow behavior on the outlet of the media for the pleated configuration

The streamlines showed that the flow is parallel but once it enters the media becomes orthogonal as shown in Figure 73. A closer look at the media shows that the flow enters perpendicularly into the media but at a distance of about 3 mm within the media the flow becomes orthogonal and remains orthogonal at the exit of the media. This meant that the local distance travelled within the media could be assumed to be equal to the thickness of the media.

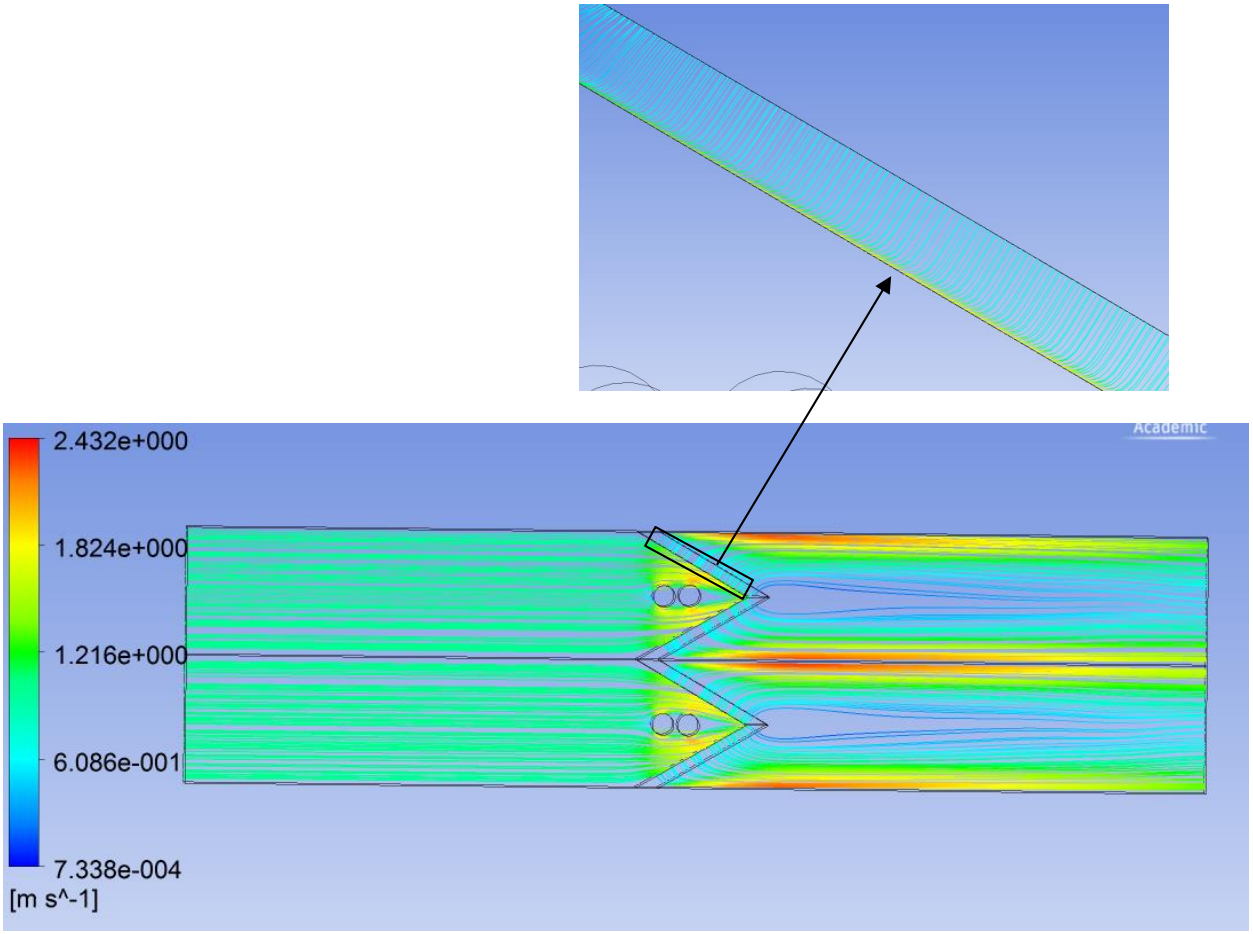

Figure 73 : Streamlines through the photocatalytic module and media in pleated media configuration

At the inlet surface of the media, the average velocity received is about 1.5 $m.s^{-1}$ and is 32 % higher than what is received averagely by the plane configuration. This increase could probably be explained by the fact that presence of the pleats creates a canal effect (which means that area reduces) such that the velocity increases in order to maintain the same flow-rate. However once inside the media the increase in the surface area causes the velocity to be reduced to an average of about 0.65 $m.s^{-1}$ which is about 43 % lower than the average velocity within plane configuration. Since the distance travelled (path length) was equivalent to the thickness of the media, the contact time within the pleated media is calculated as 26.9 ms.

Conclusions on the fluid dynamics simulation

The flow behavior in the reactor for both media configurations was studied. The results showed that the flow distribution received on the surface of the media was heterogeneous for both configurations but even more heterogeneous for the pleated media than for the plane media. The flow becomes homogenous within the plane media but remains heterogeneous in the pleated media.

The quantitative information on the flow behavior for both geometries is summarized in Table 25. The average velocity received on the media surface was 32 % higher on the pleated media than the plane due to the canal effect caused by the presence of the pleats. However the average velocity within the media was 43 % lower in the pleated due to the increase in surface area. The contact time was calculated based on the average local velocities within the media and the distance travelled within the media. It was found to be 76 % higher for the pleated than for the plane media geometry.

Media Geometry	Inlet velocity ($m.s^{-1}$)	Average velocity on media surface ($m.s^{-1}$)	Average velocity within media ($m.s^{-1}$)	Contact time (ms)
Plane	1	1.14	1.14	15.3
Pleated	1	1.50	0.65	26.9

Table 25 : Results obtained from the hydrodynamic simulation of plane and pleated geometries

IV.2.5.2 Radiation field modeling

The objective of this section is to evaluate and compare the distribution of irradiance received within the reactor and media for the two geometry configurations. The simulation results are discussed first for the plane configuration then for the pleated configuration.

Plane configuration

The irradiation behavior through the reactor was firstly studied. Figure 74 shows the irradiance contour through the reactor. It can be seen that the irradiance was the highest around the lamps but rapidly decays as the distance from the lamps increases. This is attributed to the effect of geometric attenuation which is explained as the reduction in the radiation quantity due to the distance between the point of interest and the source and excludes absorption by any matter present.

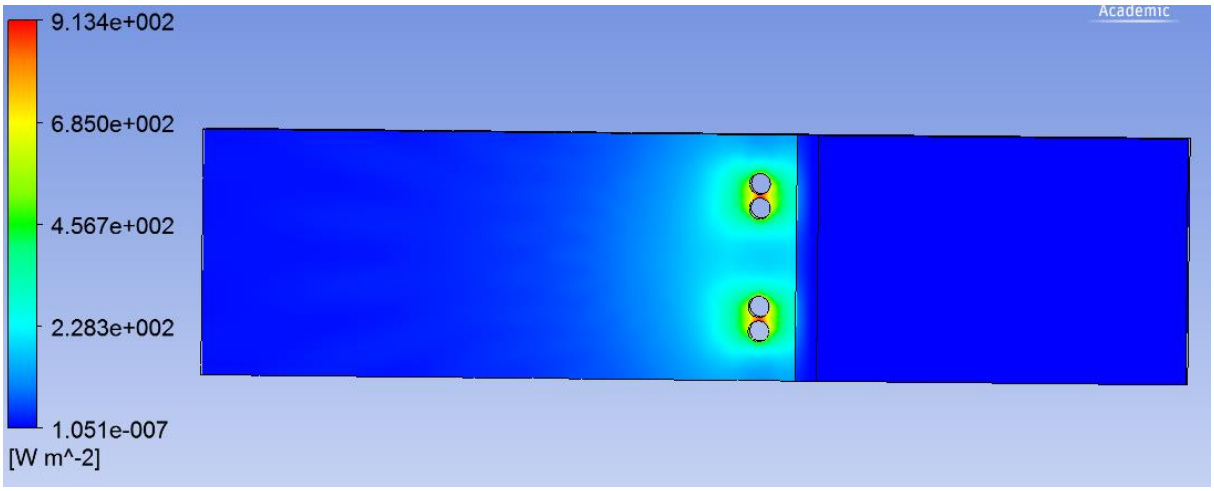

Figure 74 : Irradiance contours showing irradiance distribution through reactor for plane media configuration

The irradiance distribution on the surface of the media was also investigated of which the results are shown in Figure 75. The irradiance was not homogeneously distributed on the surface, it was highest in the areas found directly behind the lamps but as the distance from the lamps was increased, the light irradiance decreased.

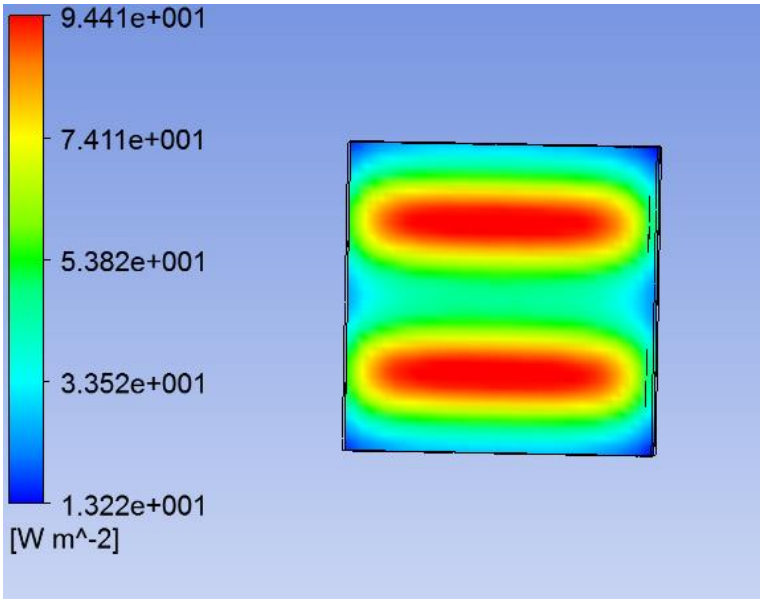

Figure 75 : Irradiance distribution on the plane media surface for the simulation measurements

This behavior was similar to what was observed from the experimental measurements as shown in Figure 76.

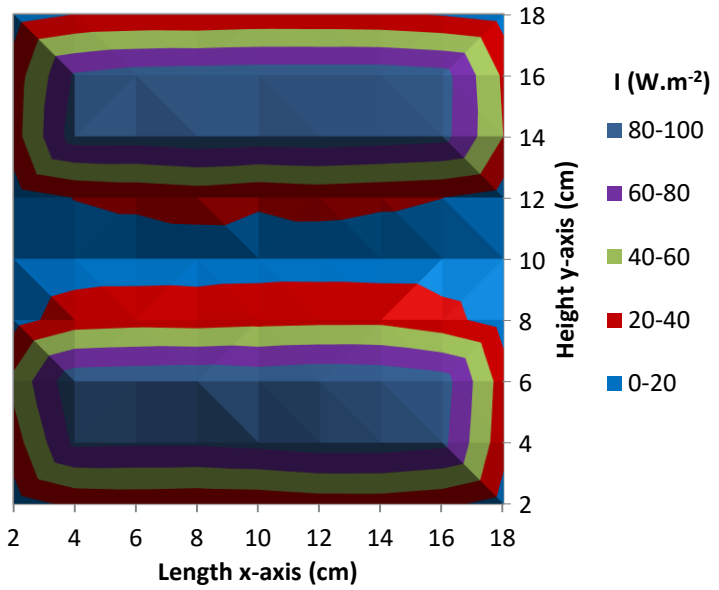

Figure 76 : Irradiance distribution on the plane media surface for the experimental measurements

The emissive power of the lamps is a necessary input parameter that helps to attain the desired results during the simulation. It is not known and has to be set with reference experimental measurements. Thus to verify the accuracy of the simulation results, the emissive power of the lamps was iteratively changed until the irradiance values that were experimentally measured along the height of the media surface at a distance of 10 cm on the x-axis matched the simulation values. The results are presented in Figure 77.

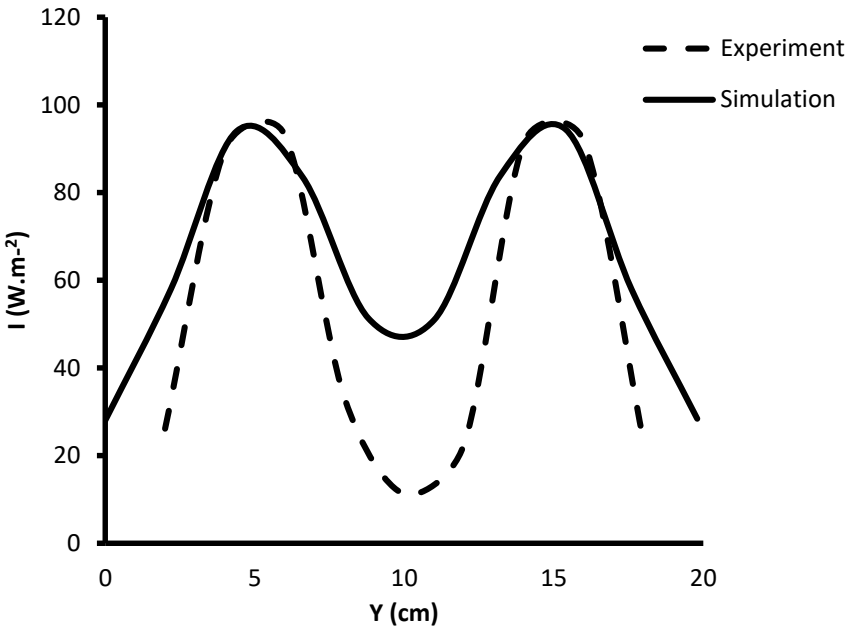

Figure 77 : Comparison between simulated and experimental irradiance values along the height of the plane media at a distance of 10 cm along the media length (y-axis)

It can be observed that the irradiance values increase up to a point then decrease and start to increase again. The highest irradiance values represent the areas on the media directly behind the lamp whilst the lowest values represent the area between the two lamps. From the graph, it is seen that the simulation values were quite similar to the experimental values at highest values or in areas directly behind the lamp. However for the values that represented the region between the two lamps, the simulation values were higher than what was measured experimentally. This difference between the simulated and experimental values could be attributed to the influence of the sensor that was used for the experimental measurements.

The Lambert cosine law of incidence is one of the laws of illumination which states that the irradiance received by a surface varies proportionally to the cosine of the incident angle (the angle θ between the direction of the incident light and the surface normal) [19]. It is given as:

$$E = \frac{I \cos\theta}{d^2} \qquad \textbf{Equation 37}$$

where E is the irradiance received by surface, I is the light intensity from the source, θ is the incident angle and d is the distance from the source.

If a detector receives irradiance from a distant source the amount of this flux will decrease with the cosine of incident angle and is called the cosine response. For a radiometer to accurately measure irradiance, it is necessary that it preserve this ideal cosine response. UV radiometers are therefore developed to replicate this ideal cosine response. However some of these radiometers may have angular responses that deviate from the ideal cosine response [20–22]. When the sensor is located directly in line with the light source a more accurate reading is obtained but once the angle of incidence is increased the error between the ideal cosine response and the detector reading increases and the sensor underestimates the irradiance that is received at that point [23,24].

Consequently, it could be assumed that Ansys gives a more accurate representation of what is received in this region between the lamps than the detector. Therefore, the average irradiance received on the surface obtained by the simulation was 60 $W.m^{-2}$ which is 33 % more than what was calculated experimentally (45 $W.m^{-2}$).

With the simulation it was also possible to calculate the average irradiance within the media volume and this value is given as 21.5 $W.m^{-2}$.

Pleated configuration

For the pleated configuration, when the lamp emissive power was maintained at the same level as for the plane configuration, the average irradiance received on the surface was calculated as 100 $W.m^{-2}$. This clearly brought into light the fact that at similar lamp emissive power, light intensity was better utilized in the pleated configuration than for the plane. This is because, in the

plane configuration, the distance between the lamp and the media at any distance is 3 cm but the distance between the pleats and the lamp differed with the closest point being at 1.4 cm.

However, since the experimental goal was to highlight the possible influence of the contact time, the emissive power in the simulation was changed until the average irradiance received on the pleated media surface was similar to that received on the plane media surface (60 $W.m^{-2}$).

Once this was done, the irradiance distribution was then studied. Figure 78 shows the irradiance distribution within the reactor. The results presented show that similarly to the plane configuration the irradiance was highest around the lamps and decreased as the distance from the lamps increased due to the effect of geometric attenuation.

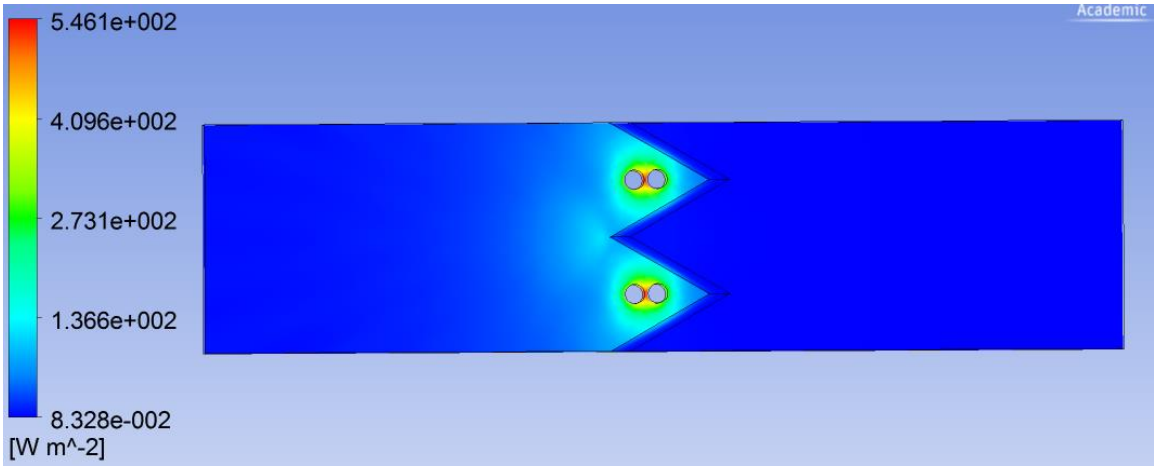

Figure 78 : Irradiance contours showing irradiance distribution through reactor for pleated media configuration

The distribution received on the surface of the media was also studied. First of all, Figure 79 shows that the irradiance was not homogeneously distributed on the surface and secondly that the highest irradiance was found in the areas directly behind the lamps and decreased as the distance from the lamps increased. It was also observed that the region around pleat joints was the lowest illuminated region. A trend that was replicated through the media as shown in Figure 80 and Figure 81.

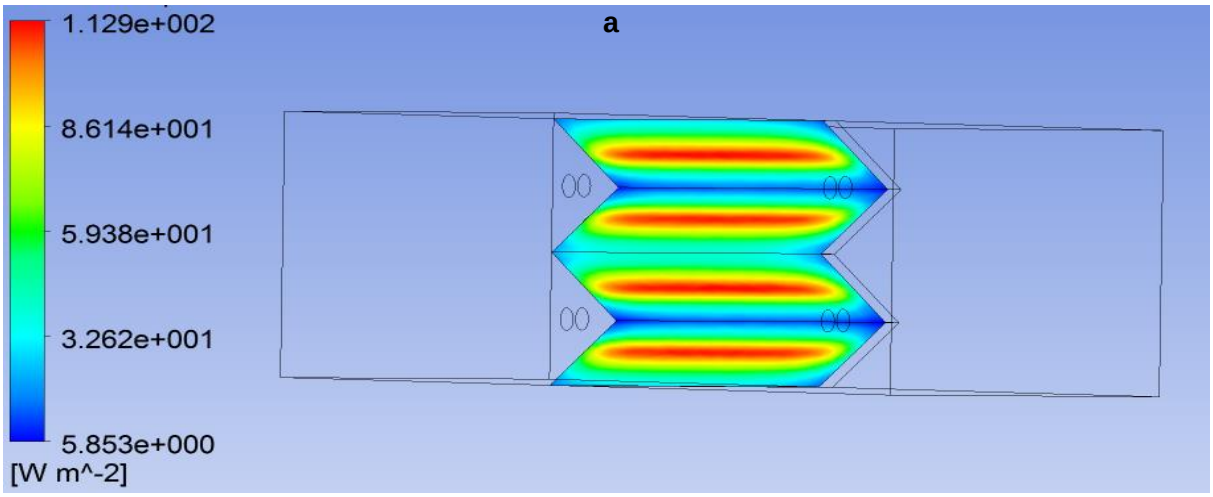

Figure 79 : Irradiance contour showing behavior on the surface of the photocatalytic media for the pleated configuration

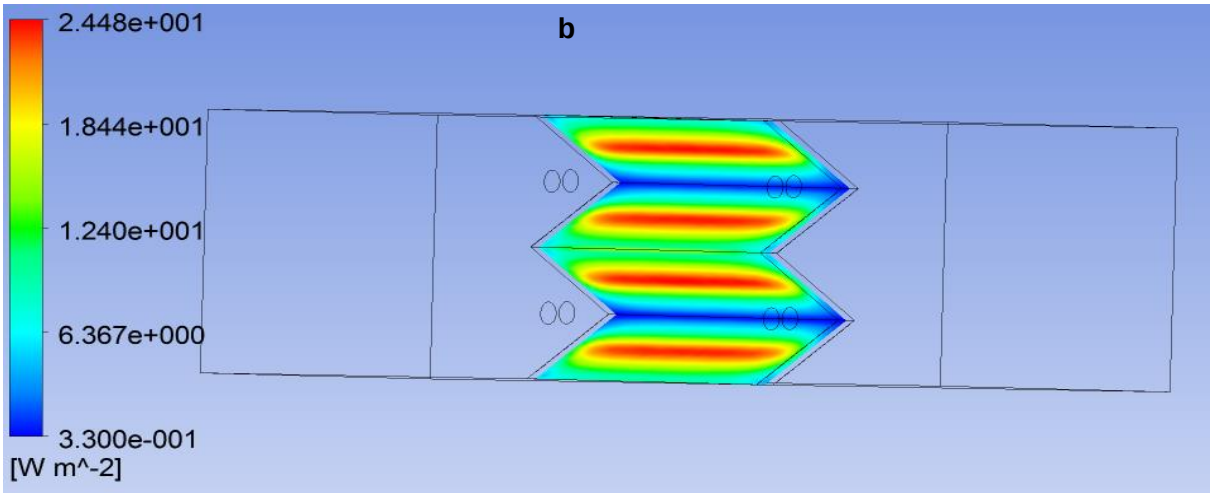

Figure 80 : Irradiance contour showing behavior 8 mm distance in media for the pleated configuration

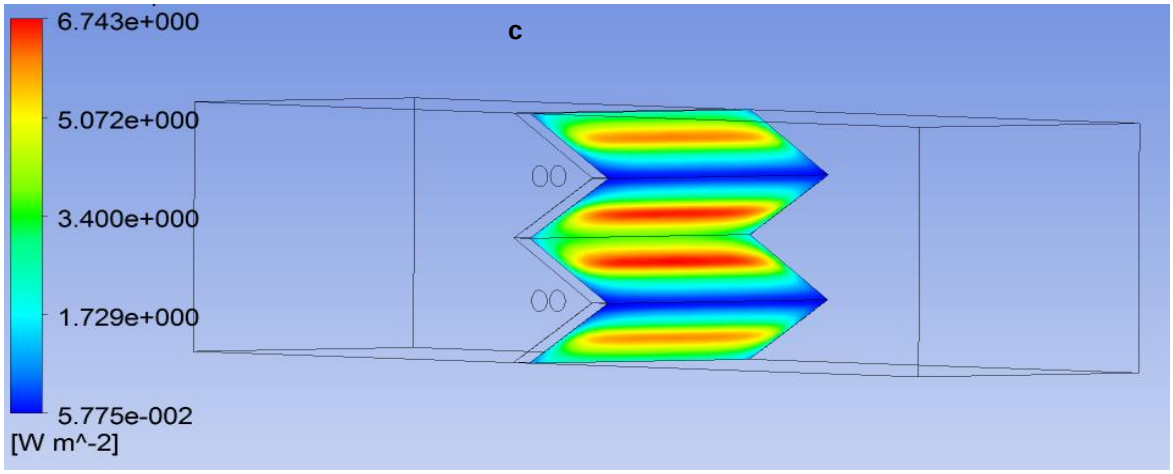

Figure 81 : Irradiance contour showing behavior at the outlet of the media for the pleated configuration

As stated in chapter II, the desired average irradiance on the surface of the media is obtained by controlling the power of the lamp using a variable voltage supply. Thus in order to obtain an average intensity on the pleated media surface that was similar to that of the plane media for the experiments, the variable voltage was adjusted until the highest experimental value corresponded to the highest simulated value. For the simulation, the measurements were taken from across the length of the media at a distance of 10 cm on the height for only one pleat. The highest value was taken as the reference value because this was the value directly in line with the lamp and the plane media results showed that the measurements were most accurate when the sensor was directly in line with the light.

The decision was also taken to verify the simulation results only on one pleat due to the difficulty to experimentally measure the irradiance on the entire surface of the pleated media as was done for the plane. The result of the comparison between the simulated and experimental values is shown in Figure 82. Here it was observed that the experimental and simulated values are quite similar. This could be probably explained by the fact that the angle created by the pleats led to a decrease in incident angles which subsequently led to a decrease in the measurements error.

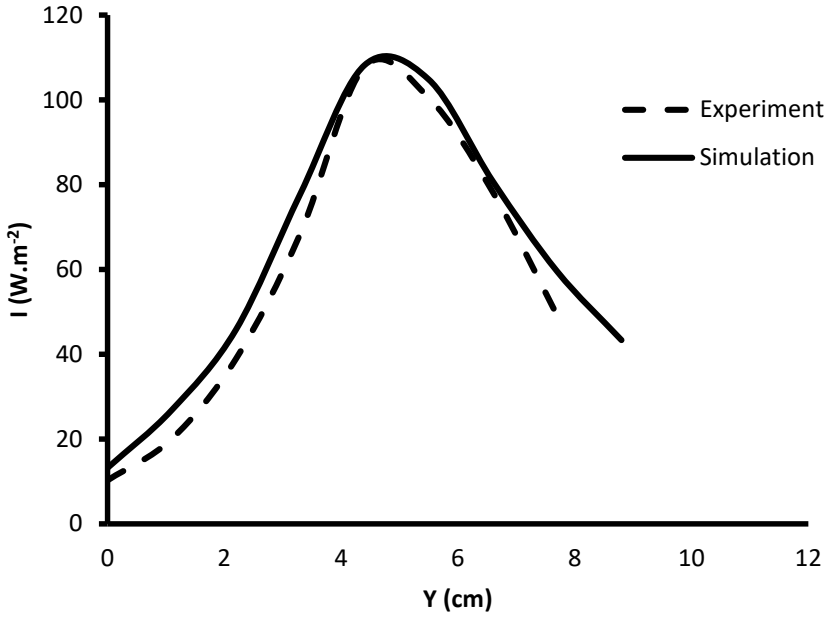

Figure 82 : Comparison between simulated and experimental irradiance values along the length of the one pleat at a distance of 10 cm along the media height

IV.2.5.2.1 Light distribution within the photocatalytic media

Monolith reactors are known to offer low-pressure drop and high catalyst surface area however the light intensity is known to quickly decline through the monoliths [25,26]. Figure 82 shows the irradiance profile through the photocatalytic media for both configurations. The irradiance is highest at the media inlet but decreases sharply to 23 % at 50 % distance within the media for both configurations. At 85 % media distance it drops below 1 % for the plane media and 3 % for the pleated configuration. Beyond this distance the media is not sufficiently illuminated and is subjected to operate under dark conditions.

Wang *et al*.[10] found similar results when they simulated the irradiance profile through a cordierite ceramic monolithic media with a thickness of 25.4 mm. In plotting a graph of the dimensionless UV flux to distance they found that at a distance of 3.2 mm the UV light intensity decreased to 30 % of the incoming flux and to 1 % at a distance of 9.5 mm.

These results suggest that a shorter media width would be preferable to reduce the dark zones or the provision of lamps on both sides of the photocatalytic media to allow a better utilization of the media.

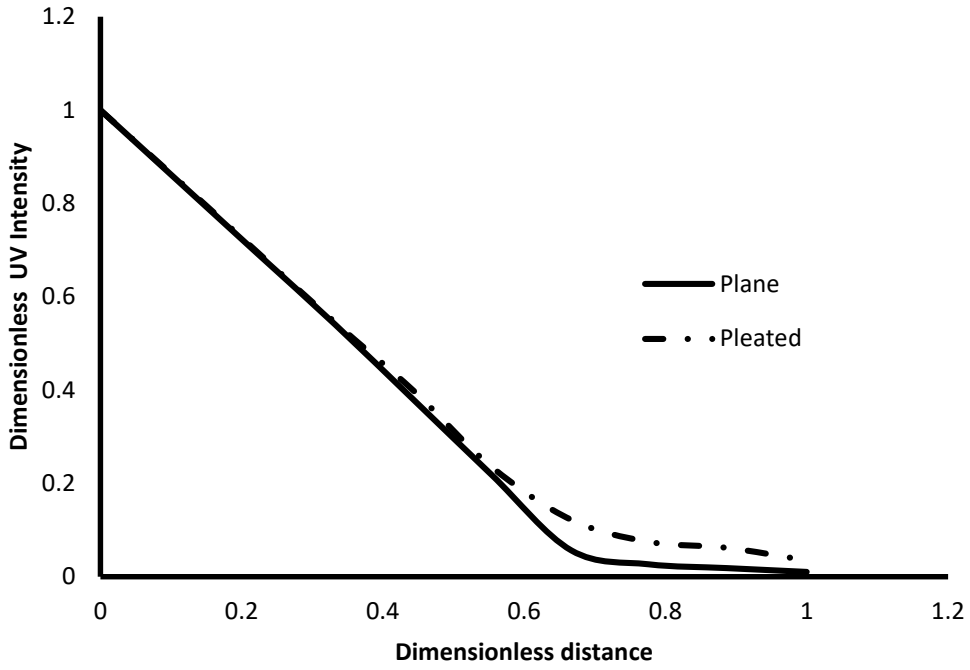

Figure 83 : Irradiance profile within photocatalytic media for plane and pleated configurations

Conclusion on radiation field modeling

The light distribution in the reactor was studied for plane and pleated configurations. For both configurations, the irradiance was highest around the lamps and decreased rapidly when the distance to the lamps was increased due to geometric attenuation. The study of the media surface showed that the radiation was highest in the regions directly behind the lamps and decreased as the distance to the lamps was increased. The average irradiance received on the surface and within the media was calculated at around 60 and 22 $W.m^{-2}$ respectively for both media geometries as shown in Table 26.

Media Geometry	Average irradiance on media surface ($W.m^{-2}$)	Average irradiance within media volume ($W.m^{-2}$)
Plane	60.3	21.5
Pleated	60.3	22.3

Table 26 : Simulation results for radiation modeling of photocatalytic module

It was also observed that even though the average light intensity received at the inlet of the media and within the media was similar for both media, the distribution of irradiance was different and that the light intensity was more heterogeneous (bigger range in values) in the pleated than in the plane. Table 27 shows the range in values depending on location in media.

Variable	Geometry	Media inlet	8 mm in media	Media outlet
Irradiance ($W.m^{-2}$)	**Plane**	13.22 – 94.41	4.38 – 33.47	0.06 -1.03
	Pleated	5.80 -112.90	0.33 -24.50	0.05 – 6.74

Table 27 : Range of irradiance on different sections within the media

Simulation results also showed that for both media geometry there were regions where the irradiation was quiet low. It could be assumed that the degradation in these regions would be less effective. For the plane media geometry, the lowest irradiated regions were the corners of the media irrespective of the location (inlet, 8 mm within media and outlet) in the media. In the case of the pleated media, the lowest illuminated region was the region around pleat joints. Depending on the location in the media the irradiance changed. Therefore using a criterion range of 0.06 $W.m^{-2}$ to 13 $W.m^{-2}$, it represented 1.5 % of the total surface of the plane media and 18 % of the total pleated media surface.

A study of the irradiance profile within the media also showed that the irradiance decreased rapidly to about 23 % halfway into the media and that beyond 85 % distance the media was subjected to operate under near dark conditions.

IV.3 Confirmation of experimental results

In chapter III, the single-pass removal efficiencies (α) for acrylonitrile and isoflurane were calculated as 0.012 and 0.00082 respectively for the plane media and 0.027 and 0.00185 for the pleated media. In order to eliminate the possible influence of the increase in the amount of TiO_2 when the media is changed from plane to pleated, the single-pass removal efficiencies were corrected by dividing by the surface areas. In so doing, the surface corrected single-pass removal efficiencies (α/m^2) were found to be 27 % higher for the pleated geometry than for the plane geometry. Quantitative results are presented in Table 28.

		Acrylonitrile		Isoflurane	
Geometry	**S (m^2)**	**α**	**α/S (m^{-2})**	**α**	**α/S (m^{-2})**
Plane	0.040	0.01203 ± 0.00011	0.300 ± 0.003	0.00082 ± 0.00008	0.020 ± 0.002
Pleated	0.072	0.02742 ± 0.00074	0.38 ± 0.01	0.00185 ± 0.00006	0.026 ± 0.003

Table 28 : Single-pass removal efficiencies (α) of acrylonitrile and isoflurane calculated for the plane and pleated configurations and the surface areas (S) for each configuration

The simulations however showed a 76 % increase in contact time by using the pleated media geometry. Thus under ideal conditions it is expected that the surface corrected single-pass removal efficiencies (α/m^2) obtained from the experiments would be similar to this number but the experiments showed a much lower improvement of 27 %. Two hypotheses could be proposed to explain this performance:

(i) It was observed that the lowest region of illumination where the media would be operating under near dark conditions and would not be very effective represented 18% of the total media surface compared to the 1.5 % in the plane media. This subsequently meant that effective surface of the pleated media was further decreased. If the surface corrected single-pass removal efficiencies (α/m^2) is calculated considering the new "efficient surface" for both plane and pleated media, it was observed that they were 48 % higher for the pleated geometry than for the plane geometry. Quantitative results are presented in Table 29.

	Acrylonitrile			Isoflurane	
Geometry	**S' (m^2)**	**α**	**α/S' (m^{-2})**	**α**	**α/S' (m^{-2})**
Plane	0.039	0.01203 ± 0.00011	0.308 ± 0.003	0.00082 ± 0.00008	0.021 ± 0.002
Pleated	0.059	0.02742 ± 0.00074	0.46 ± 0.01	0.00185 ± 0.00006	0.031 ± 0.003

Table 29 : Surface corrected single-pass removal efficiencies (α/m^{-2}) of acrylonitrile and isoflurane calculated for the plane and pleated configurations and the corrected surface areas (S') for each configuration

(ii) It was also shown in the simulation that the flow and irradiance distribution within the pleated geometry was more heterogeneous (bigger range in values) than the plane geometry (Table 30). This means that even though the global average velocity was decreased and the contact time was higher within the pleated media, the higher level of heterogeneity could explain why the α values were lower than expected for the pleated configuration.

Variable	Geometry	Media inlet	8 mm in media	Media outlet
Velocity ($m.s^{-1}$)	**Plane**	0.9 - 1.39	1.12 -1.15	0.98 - 1.0
	Pleated	0.07 - 2.03	0.17 - 0.72	0.0098 - 0.7
Irradiance ($W.m^{-2}$)	**Plane**	13.22 – 94.41	4.38 – 33.47	0.06 -1.03
	Pleated	5.80 -112.90	0.33 -24.50	0.05 – 6.74

Table 30 : Range of velocities and irradiance on different sections within the media

Conclusively, the use of pleated media geometry improves the degradation efficiency by decreasing the velocity of pollutants within the media and consequently increasing the contact time between the pollutants and the media. However, the more heterogeneous distribution of the velocity in the pleated media counteracts the influence of the contact time. Additionally, even though the average light intensity on the media is the same for both media, the more heterogeneous distribution in the pleated geometry also partially hinders the effect of increase in contact time.

The CFD model that was presented in the previous sections was useful for predicting the contact time and average irradiance and distribution of irradiance in the media, parameters that are important to the efficiency of a single-pass system. The results showed that simulations could be useful in designing configurations that could improve the efficiency of commercial systems.

IV.4 Application of CFD modeling to a commercial system to help improve degradation efficiency

The knowledge that was obtained from simulating the experimental setup was employed to design a preliminary pleated geometry system to improve the efficiency of a commercial photocatalytic system.

In this work, the commercial photocatalytic system that is studied is the Room DOPair. It is a mobile unit which aims to purify and decontaminate air in hospital risk areas. It is produced by ATA medical, a French company that has expertise in providing air treatment solutions to various sectors including the medical sector. The unit utilizes filtration and photocatalytic oxidation as cleaning techniques. The air is pre filtered first using a G4 filter to remove any coarse dust particles (≥ 10 μm), then it passes through a M7 filter to remove fine dust particles (≥ 1 μm). The filtered air then passes through a photocatalytic unit where organic compounds are degraded and microorganisms are destroyed. Finally, it passes through a HEPA (H14) filter with an efficiency of 99.995 % most penetrating particle size (MPPS) to remove any remaining particles [27].

For the simulation, the geometry that was chosen was the photocatalytic module represented by the green section as shown in Figure 84. The current configuration of the module consists of two plane photocatalytic media each with a surface of 0.235 m^2 and irradiated by two Philips TUV PL-L 95W UVC lamps. In the photocatalytic module, the air first passes through a plane photocatalytic media, encounters the lamps upon exit from the first media then passes through a second media before finally exiting the photocatalytic module. For the proposed configuration, the plane media are replaced by two pleated media each made up of four pleats creating two triangles at 120°.

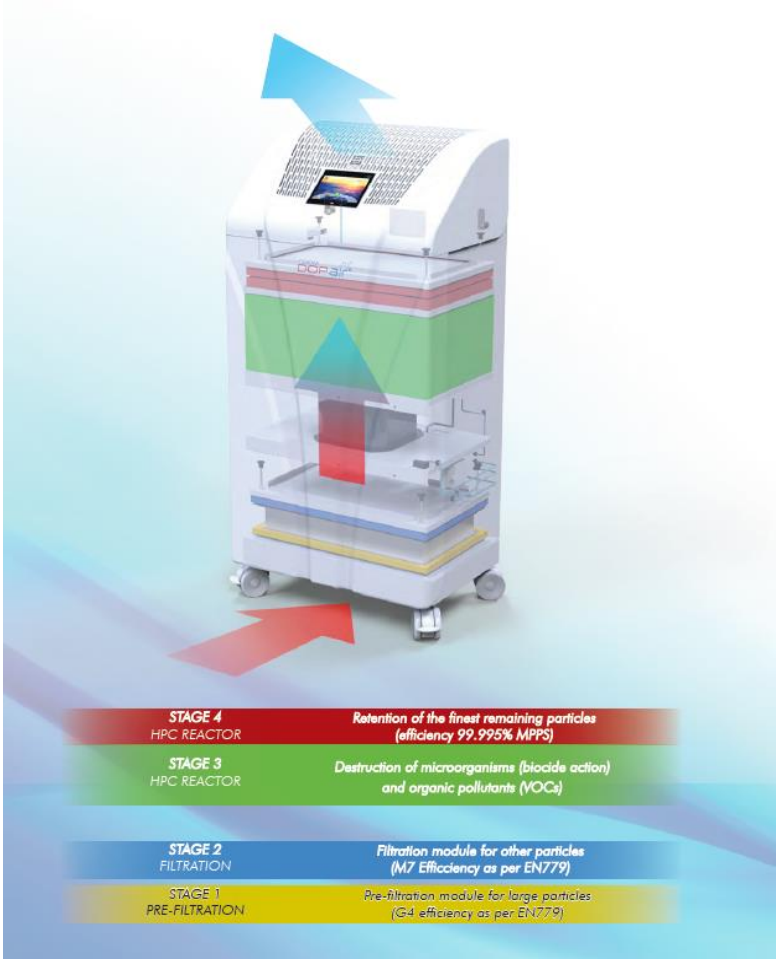

Figure 84 : Representation of Room DOPair showing the air flow and the various air cleaning stages [27]

The surface for each media was calculated as 0.275 m^2. The geometries of both configurations as designed with Ansys design modeler are shown in Figure 85.

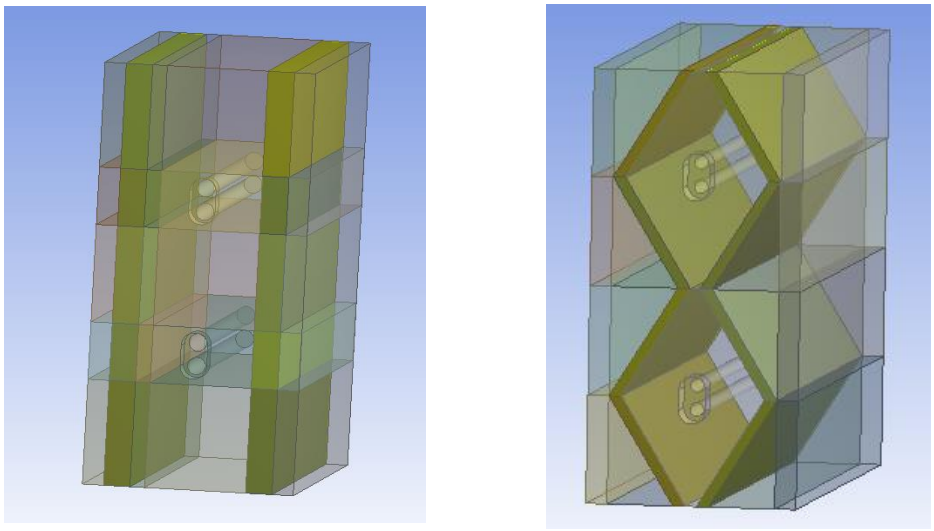

Figure 85 : (a) Current plane media geometry (b) Proposed pleated media geometry

The study of the behavior of the flow through the module for both configurations showed that the flow was homogenous at the inlet and in the first media but lost its homogeneity when it encountered the lamps consequently leading to a replication of the heterogeneity on the surface of the second media. The results for plane configuration are shown in Figure 86 and 87 whilst those for the pleated configuration are shown in Figure 88 and 89.

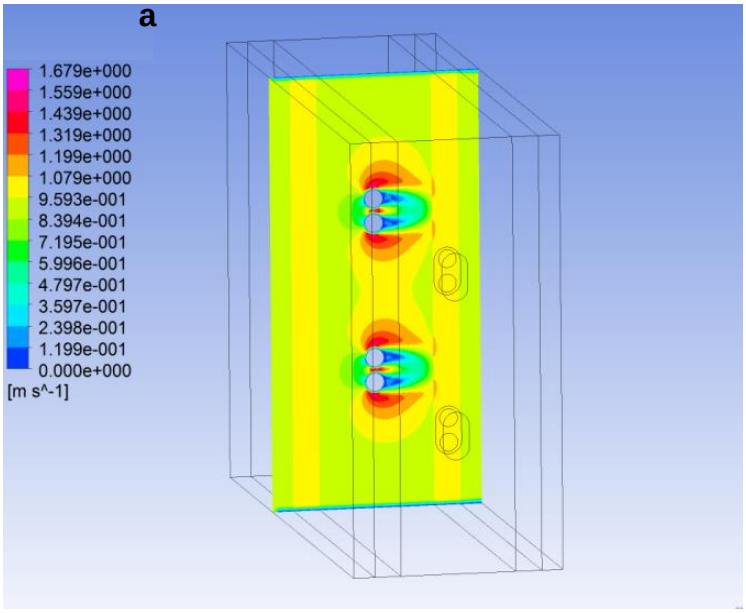

Figure 86 : Flow distribution through the module for the plane configuration of Room DOPair

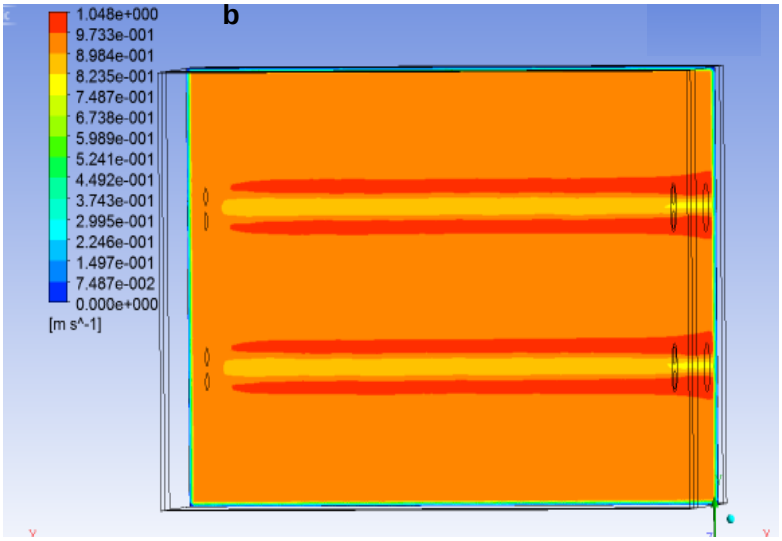

Figure 87 : Flow distribution on the downstream media surface for the plane configuration of Room DOPair

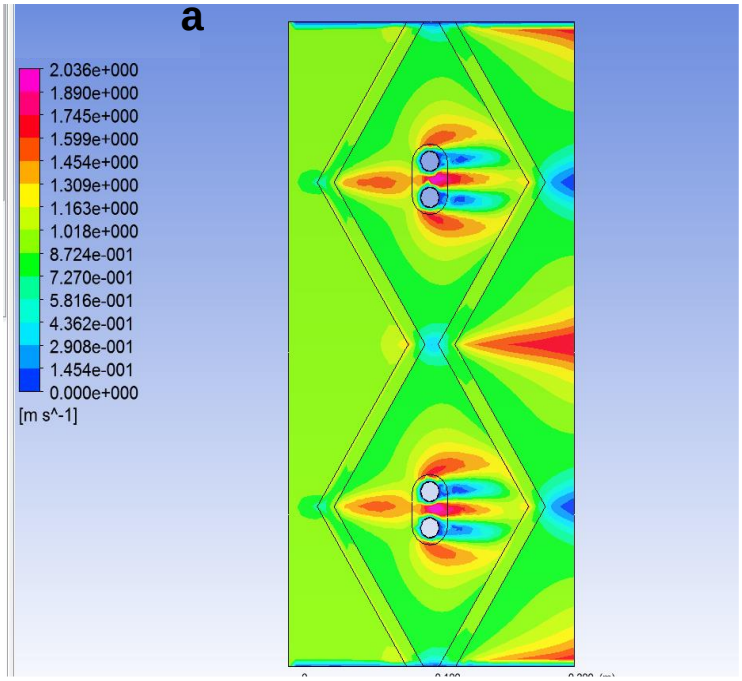

Figure 88 : Flow distribution through the module for the pleated configuration of Room DOPair

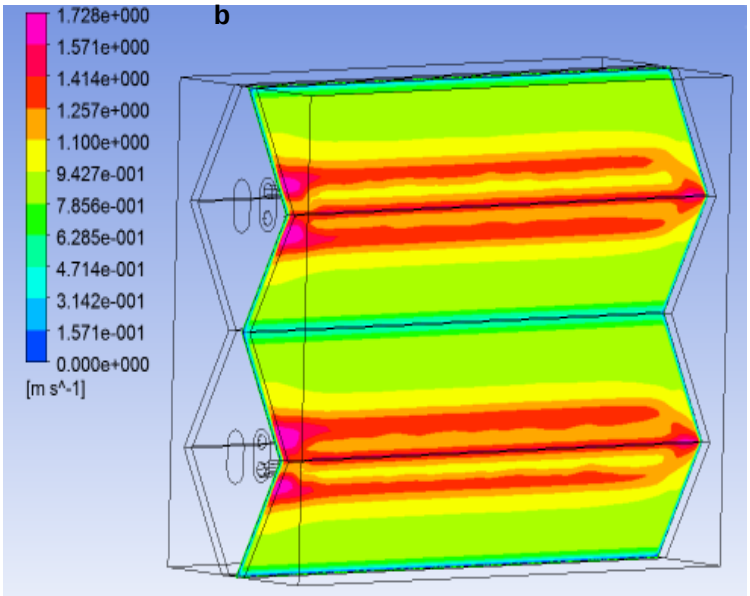

Figure 89 : Flow distribution on the downstream media surface for the pleated configuration of Room DOPair

The quantitative results presented in Table 31 showed that the pleated configurations had a lower average velocity in the media which translated to a higher contact time. The use of the pleated configuration led to a 19 % increase in the contact time.

Geometry	Inlet Velocity ($m.s^{-1}$)	Average on media surface ($m.s^{-1}$)	Average in media ($m.s^{-1}$)	Contact time (ms)
Plane	0.90	1.03	1.03	17.8
Pleated	0.90	0.98	0.87	21.1

Table 31 : Velocities and contact time obtained from the fluid dynamic simulation of plane and pleated geometries for the Room DOPair device

The irradiance distribution within the reactor and also on the surface of the media was simulated and results are presented in Figure 90 and Figure 91 for the plane and the pleated configurations respectively. For both configurations, the distribution through the module showed that the irradiance was highest around the lamps and decreased as the distance from the lamps increased due to the effect of geometric attenuation.

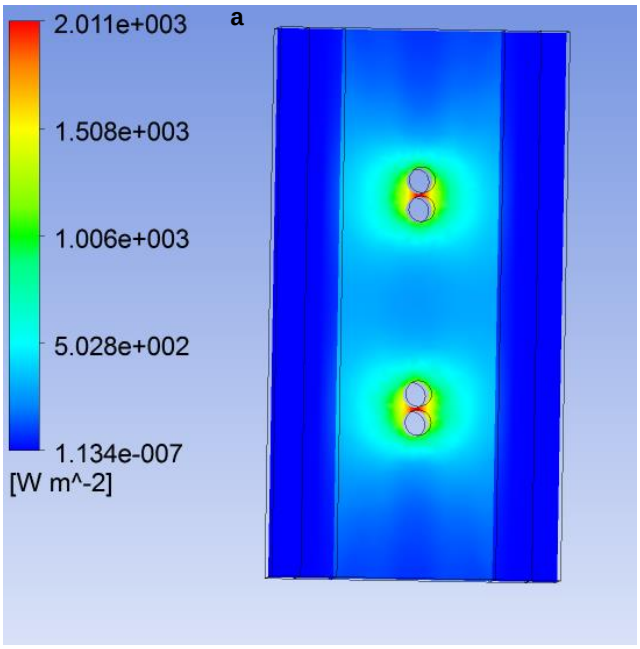

Figure 90 : Irradiance profile through the module for the plane configuration of Room DOPair

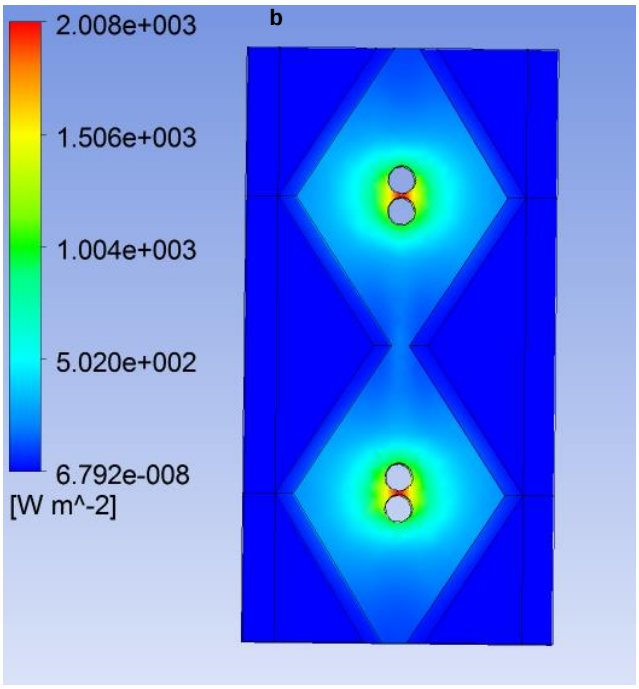

Figure 91: **Irradiance profile through the module for the pleated configuration of Room DOPair**

The study of the irradiance profile on the surface of both media for both configurations showed that the highest illumination was found on the regions directly behind the lamps. And

that the irradiation received on the media surface decreased when the distance from the lamp was increased. The results are shown in Figure 92 for the plane configuration and Figure 93 for the pleated configuration

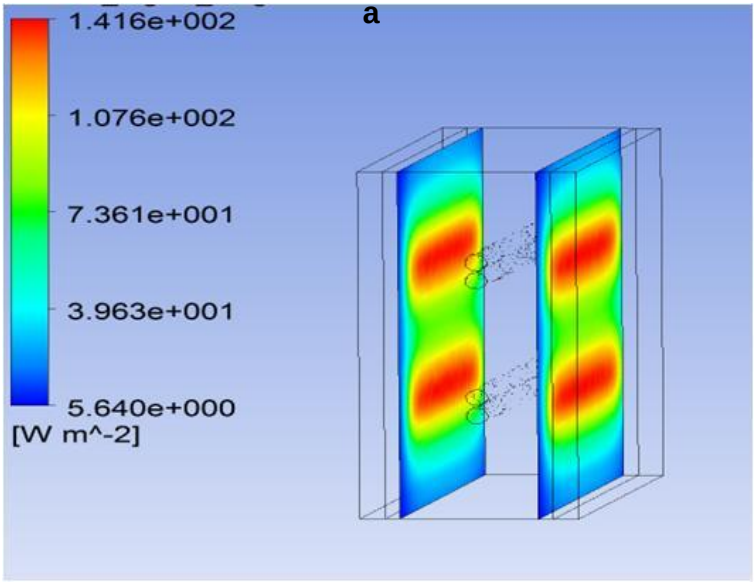

Figure 92 : Irradiance profile on media surface for the plane configuration of Room DOPair

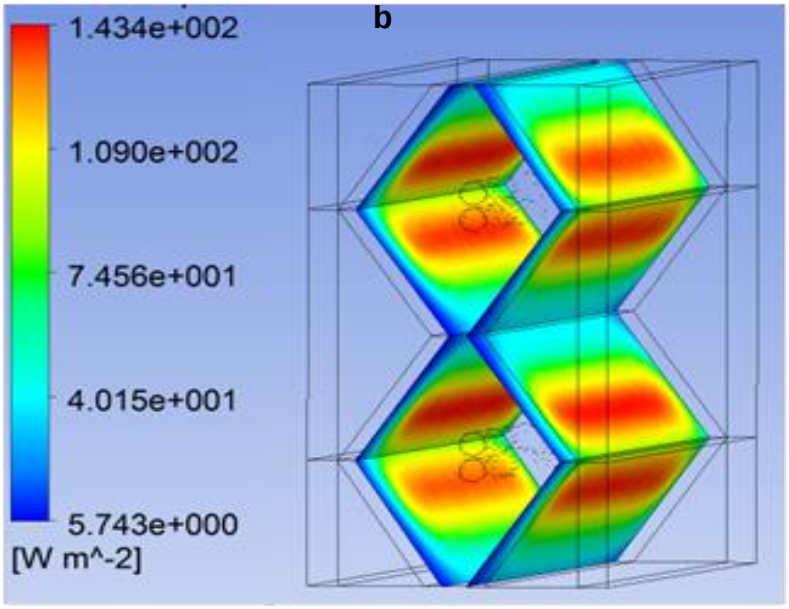

Figure 93 : Irradiance profile on media surface for the pleated configuration of Room DOPair

The average irradiance that was received on both media surface was higher for the pleated media than for the plane media. There was also a 12 % increase in the average irradiance received in the pleated media compared to the plane media. These results are summarized in Table 32.

Geometry	Average on media surface ($W.m^{-2}$)	Average in media volume ($W.m^{-2}$)
Plane	74	44
Pleated	83	51

Table 32 : Irradiance obtained from the radiation field simulation of plane and pleated geometries for Room DOPair

Conclusively for Room DOPair, the simulations enabled us to confirm that the pleated geometry would allow an improvement in the degradation efficiency because (i) higher amount of catalyst (ii) lower average velocities within media translated to higher contact time in the media (iii) better utilization of light due to the higher average irradiance.

IV.5 Conclusions on the use of CFD as a tool to understand the performance of the photocatalytic reactor

The modeling of fluid dynamics and radiation in the photocatalytic module of the multi-pass laboratory closed loop reactor was conducted in this chapter. The simulations were done for both plane and pleated media geometry to be able to bring into evidence the influence of the change in geometry on the flow and radiation distribution within the reactor as a whole and specifically within the media.

CFD simulations of the fluid dynamics in the experimental set-up indicated that within the media the flow was more heterogeneous in the pleated geometry than in the plane. Also due to the canal effect created by the pleats the average velocity received on the surface of the media was higher by 32 % for the pleated media than for the plane. However due to the increase in the surface area of the pleated configuration, the average velocity in the media was 43 % lower which led to a 76 % increase in the contact time.

For the radiation simulation, it brought into light the possible deviation of the radiometer from the ideal cosine response which led to the probable underestimation of the irradiance received on the media at the region in between the two lamps. Due to the fact that the experimental aim was to highlight the possible influence of the contact time, the CFD model enabled an approximate fixing of the variable voltage supply in the experimental set-up to have similar average irradiance on the pleated media surface and within the media as for the plane media geometry. The simulations also showed a rapid decrease of irradiance within the media, a problem that is common to monolith systems. For both configurations, the irradiance decreased to about 23 % halfway into the media and the media would be operating under near dark conditions beyond 85 % distance the media. Consequently a shorter width of the media would be preferable for photocatalytic degradation. CFD could be useful to help predict the thickness that would reduce the dark zones for better utilization of media.

A comparison of the percentage improvement in contact time obtained from the simulation when the pleated geometry is used to the experimental improvement of the surface corrected single-pass removal efficiency (α/m^2) was done. It was found that the efficiency for the pleated geometry is not increased as much as expected when considering the increase in the contact time. Based on the study of the irradiance and flow profiles in the media, two hypotheses were proposed to explain this; firstly, the effective surface of the pleated media was reduced due to the presence of a significant dark zone (18 %) around the pleat joints and secondly higher level of heterogeneity of the velocity and irradiance distribution could lead to a reduction in the expected global efficiency of the pleated configuration.

The CFD approach that was developed and used for the experimental set-up was applied to a commercial unit to help investigate the improvement in the system by proposing a pleated configuration. Although experimental confirmation could not be done, the simulations showed that by only changing the configuration of the pleats the degradation efficiency of the system could be improved because there was an increase in the contact time and the average irradiance received in the media.

CFD simulations helped to highlight important behavior with respect to flow and the irradiance in a photocatalytic unit and could be useful to help investigate configurations that

could improve the contact time and irradiance but also better homogeneity of these variables in the media.

IV.6 References

[1] J. Taranto, D. Frochot, P. Pichat, Modeling and optimizing irradiance on planar, folded, and honeycomb shapes to maximize photocatalytic air purification, Catal. Today. 122 (2007) 66–77. doi:10.1016/J.CATTOD.2007.01.031.

[2] V. V. Ranade, Computational Flow Modeling for Chemical Reactor Engineering., Elsevier, 2001.

[3] A. Bakker, A. Haidari, Fluids/Solids Handling, (2001). http://lib3.dss.go.th/fulltext/Journal/Chemical Engineering Progress/no.3/2001v97n3p45-53.pdf (accessed March 4, 2018).

[4] H.K. Versteeg, An Introduction to Computational Fluid Dynamics: The Finite Volume Method, Pearson Prentice Hall, 2007.

[5] Y. Boyjoo, M. Ang, V. Pareek, Some aspects of photocatalytic reactor modeling using computational fluid dynamics, Chem. Eng. Sci. 101 (2013) 764–784. doi:10.1016/j.ces.2013.06.035.

[6] M. Mohseni, F. Taghipour, Experimental and CFD analysis of photocatalytic gas phase vinyl chloride (VC) oxidation, Chem. Eng. Sci. 59 (2004) 1601–1609. doi:10.1016/j.ces.2004.01.017.

[7] S. Romero-Vargas Castrillón, H. Ibrahim, H. de Lasa, Flow field investigation in a photocatalytic reactor for air treatment (Photo-CREC–air), Chem. Eng. Sci. 61 (2006) 3343–3361. doi:10.1016/J.CES.2005.11.039.

[8] I. Salvadó-Estivill, D.M. Hargreaves, G.L. Puma, Evaluation of the intrinsic photocatalytic oxidation kinetics of indoor air pollutants., Environ. Sci. Technol. 41 (2007) 2028–35.

[9] S. Chong, S. Wang, M. Tadé, H.M. Ang, V. Pareek, Simulations of photodegradation of toluene and formaldehyde in a monolith reactor using computational fluid dynamics, AIChE J. 57 (2011) 724–734. doi:10.1002/aic.12295.

[10] X. Wang, X. Tan, T. Yu, Modeling of Formaldehyde Photocatalytic Degradation in a Honeycomb Monolith Reactor Using Computational Fluid Dynamics, Ind. Eng. Chem. Res. 53 (2014) 18402–18410. doi:10.1021/ie5016427.

[11] S.W. Verbruggen, M. Keulemans, J. van Walsem, T. Tytgat, S. Lenaerts, S. Denys, CFD modeling of transient adsorption/desorption behavior in a gas phase photocatalytic fiber reactor, Chem. Eng. J. 292 (2016) 42–50. doi:10.1016/J.CEJ.2016.02.014.

[12] J. Roegiers, J. van Walsem, S. Denys, CFD- and radiation field modeling of a gas phase photocatalytic multi-tube reactor, Chem. Eng. J. 338 (2018) 287–299. doi:10.1016/J.CEJ.2018.01.047.

[13] J. Tu, G.H. Yeoh, C. Liu, Computational fluid dynamics : a practical approach, Elsevier/Butterworth-Heinemann, 2013.

[14] Ansys Inc., Ansys CFX Solver Modeling Guide, 14.5, Canonsburg, 2013.

[15] V. Pareek, S. Chong, M. Tadé, A.A. Adesina, Light intensity distribution in heterogenous photocatalytic reactors, Asia-Pacific J. Chem. Eng. 3 (2008) 171–201. doi:10.1002/apj.129.

[16] Ansys Inc., Ansys Fluent 14.0: Theory Guide, 2011.

[17] A.J. Cortes Capetillo, Computational Fluid Dynamic Modeling of In-duct UV Air Sterilisation Systems., University of Leeds, 2015.

[18] C. Casado, J. Marugán, R. Timmers, M. Muñoz, R. van Grieken, Comprehensive

multiphysics modeling of photocatalytic processes by computational fluid dynamics based on intrinsic kinetic parameters determined in a differential photoreactor, Chem. Eng. J. 310 (2017) 368–380. doi:10.1016/J.CEJ.2016.07.081.

[19] R. McCluney, Introduction to radiometry and photometry, Artech House, 1994.

[20] T.C. Larason, C.L. Cromer, Sources of Error in UV Radiation Measurements., J. Res. Natl. Inst. Stand. Technol. 106 (2001) 649–56. doi:10.6028/jres.106.030.

[21] J.J. Michalsky, L.C. Harrison, W.E. Berkheiser, Cosine response characteristics of some radiometric and photometric sensors, Sol. Energy. 54 (1995) 397–402. doi:10.1016/0038-092X(95)00017-L.

[22] G. Zibordi, B. Bulgarelli, Effects of cosine error in irradiance measurements from field ocean color radiometers, Appl. Opt. 46 (2007) 5529. doi:10.1364/AO.46.005529.

[23] U. Feister, R. Grewe, K. Gericke, A method for correction of cosine errors in measurements of spectral UV irradiance, Sol. Energy. 60 (1997) 313–332. doi:10.1016/S0038-092X(97)00030-3.

[24] L.Â. Berni, W.A. Vilela, A.F. Beloto, F.O. de Sena, System for measuring the angular response of radiometers, in: M.F.P.C. Martins Costa (Ed.), International Society for Optics and Photonics, 2013: p. 87852F. doi:10.1117/12.2019888.

[25] Y. Boyjoo, H. Sun, J. Liu, V.K. Pareek, S. Wang, A review on photocatalysis for air treatment: From catalyst development to reactor design, Chem. Eng. J. 310 (2017) 537–559. doi:10.1016/J.CEJ.2016.06.090.

[26] M.L. Sauer, D.F. Ollis, Acetone Oxidation in a Photocatalytic Monolith Reactor, J. Catal. 149 (1994) 81–91. doi:10.1006/JCAT.1994.1274.

[27] ATA Medical, MOBILE AIR DECONTAMINATION UNITS | ATA Medical, (n.d.). http://ata-medical.com/en/products-2/ (accessed February 1, 2018).

GENERAL CONCLUSIONS

Hospitals are contaminated with several chemical pollutants due to the variety of activities that are performed there. Continuous exposure of hospital occupants to these pollutants leads to undesirable effects on their health. Major concern when it comes to IAQ has been with respect to reducing the microbial contamination. Consequently, indoor air treatment devices that use techniques such as photocatalytic oxidation are mostly implemented to reduce microbial load. However since chemical pollutants are also present in the indoor air in hospitals it is necessary to evaluate the fate of these compounds when they pass through a PCO treatment unit. The aim of this PhD was therefore to evaluate the efficiency of PCO devices in removing some specific chemical pollutants found in hospitals and subsequently to investigate whether PCO is a safe technology for the occupants of the hospital.

In the first chapter, a literature review was done to provide a state of the art on the chemical pollutants that were present in the hospital and that could be interesting for study. The choice of the target compounds was limited to the OR. In the OR, the air is polluted with anesthetic gases, surgical smoke and sterilants. Based on this, two target pollutants isoflurane and acrylonitrile were chosen. These two compounds were generally selected because they belong to two of the main pollutants types that are found in ORs; anesthetic gases (isoflurane) and surgical smoke (acrylonitrile). They also belonged to two different chemical families which would also allow the evaluation of the behavior of two different compounds to degradation by PCO. Additionally, they are complex compounds and thus could potentially be important sources of intermediates. Then PCO was discussed with a specific focus on the influence of parameters on the efficiency of PCO and performance indicators of which some were retained for this study. The experimental objectives of this PhD work were then defined as :

1. Perform a parametric evaluation on the degradation of isoflurane and acrylonitrile by studying the influence of air velocity, light intensity, the change in media geometry, initial pollutant concentration, presence of chemical co-pollutants, presence of particles (bioaerosols) and relative humidity on their degradation efficiencies.

2. Evaluate the safety of the use of PCO for the degradation of isoflurane and acrylonitrile through the identification of possible intermediates formed during their degradation.

After having defined the experimental objectives, the materials and methods that would be utilized were then described in the second chapter. The experiments were carried out in a 420-L closed-loop reactor operating in multi-pass mode. The reactor is equipped with a variable speed fan that controlled the flow of air and allowed a flow rate from 28 to 300 $Nm^3.h^{-1}$. A tranquilization chamber where a honeycomb is installed enables a homogeneous flow distribution and allows for the injection and sampling of isoflurane. The photocatalytic media and the lamps were housed in the photocatalytic module. The media was irradiated with two 18-W UVC fluorescent tubes (Phillips PL-L series). During the degradation, samples were collected onto CarboPack B and DNPH cartridges and were analyzed using TD/GC/MS/FID and HPLC respectively. The photocatalytic media that was used was a commercial one produced by Saint-Gobain Quartz (QUARTZEL®). It consisted of SiO_2 fibers coated with TiO_2 deposited through a sol-gel method and pressed into a felt. A characterization of the media was done and quantitative information on properties like porosity and UV transmittance were determined to serve as inputs during the numerical simulation. In order to extract the performance indicators that would allow the evaluation of the influence of the parameters on the degradation of PCO, a model developed by Dumont and Héquet would be used and thus was also described.

In the third chapter, a study of the degradation profiles of acrylonitrile and isoflurane showed that acrylonitrile was degraded faster than isoflurane: the latter is a halogenated molecule and it is more difficult to degrade. It was also observed that acrylonitrile followed an apparent first order degradation whilst isoflurane showed a two phase degradation. A first phase where the degradation is slow and not very efficient attributed to possible isoflurane reactions with OH° and a second phase where the degradation accelerated due to a possible chain reaction mechanism involving Cl°. This second phase of degradation is represented by a first-order decay. The model developed by Dumont and Héquet was applied to the experimental degradation points of both pollutants and allowed the calculation of one indicator (single-pass removal efficiency) for acrylonitrile and two indicators (induction period and single-pass removal efficiency) for isoflurane. Then, the influence of the air velocity, light intensity, the change in media geometry, initial pollutant concentration, presence of chemical co-pollutants, presence of particles (bioaerosols) and relative humidity had on the performance of photocatalytic oxidation in removing acrylonitrile and isoflurane was presented. The results showed that parameters had a similar influence on both compounds when they were varied. Decreasing the air velocity resulted in longer one-pass contact time

which then led to shorter induction periods and higher removal efficiencies. Increasing the light intensity led to a decrease in induction period and increase in the single-pass removal efficiencies at higher average light intensities. The relationship between light intensity and removal efficiency was seen to follow a half-order regime for both compounds. This meant that for the range of studied light intensities, the electron-hole recombination was dominant. In this regime, further increment in the light intensity would not significantly improve the removal efficiencies but would only impose unnecessary energy costs. Higher initial concentrations of acrylonitrile and isoflurane led to a decrease in their degradation efficiencies attributed to competition for limited active sites. Due to competitive adsorption for active sites an increase in relative humidity inhibited the degradation of both target compounds. The presence of other gaseous pollutants also inhibited the degradation of the target compounds again due to competition for adsorption unto active sites. It was also shown that the presence of particles on the photocatalytic media surface could block active sites and may also cause a screening effect which in turn decreased the degradation efficiencies of the target compounds. The results of the parametric evaluation showed that in order to improve the PCO performance in removing acrylonitrile and isoflurane it would be recommended to work at low velocities as this would improve the contact time between the pollutants and active species. Higher light intensities would generally give better performance but according to the range studied light intensity beyond 5 $mW.cm^{-2}$ would only cause much more energy waste instead of much more degradation of VOCs. PCO performance would also be improved at low relative humidity however since the recommended RH levels in the OR is between 30 and 60 %, it would be recommended not operate beyond 60 %. The introduction of filters upstream the photocatalytic media would also be necessary to reduce the particle load received on the media. The PCO performance would also be better at low pollutant concentrations. However, due to the fact that the concentrations of pollutants (target and co-pollutants) vary over time, the use of multiple photocatalytic banks would help to maximize removal efficiencies of pollutants. This would also be beneficial in reducing concentrations of intermediates and keeping them at levels that would not pose health risks. The intermediate compounds that were identified during the degradation of isoflurane include pentafluoropropanal, chlorodifluoroacetaldehyde, formaldehyde, acetaldehyde, formic acid and acetic acid. Their concentrations were not found to be high enough to present a significant risk. In the case of acrylonitrile, no organic intermediates were identified however a study of the mineralization rate versus conversion rate showed that acrylonitrile was first transformed to intermediates which were then mineralized to CO_2. It was therefore concluded that the

sampling and analytical methods were probably not suitable enough for them to be effectively trapped and detected. Finally, the influence of the change in media geometry was also studied. Experiments at reference conditions for both acrylonitrile and isoflurane were carried out with a plane media configuration and pleated media configuration. The experimental objective here was to highlight the possible influence of the contact time thus the average light intensity received on the media was kept constant for both media configurations. The results showed that the degradation efficiencies for both compounds were 2.3 times higher for the pleated configuration than for the plane configuration. This increase was attributed to an increase in the amount of catalyst; longer contact time between pollutant and media and better irradiance distribution. To eliminate the influence of the increase in the amount of catalyst, the surface corrected single-pass removal efficiencies were corrected by dividing the values by the respective surface areas of the plane and pleated configurations. The results showed that the pleated media configuration improved the degradation by 27 % compared to the plane which was attributed to higher contact time and better irradiance distribution. In the literature, at least two authors were in agreement with the fact that the contact time was increased in the pleated media but one was of the view that it was due to a decrease in the velocity whilst the other was of the view that the path length was increased. Both of these are difficult to evaluate experimentally. Additionally, even though the light intensity received was the same for both media, the distribution of irradiance on and within the media could also influence the efficiency. In order to better understand the role of the media geometry in improving the removal efficiencies numerical simulations would be required to study the behavior of air flow and light irradiance in the photocatalytic reactor for both configurations.

In chapter four, numerical simulations of fluid dynamics and radiation field were performed on both plane and pleated media geometries using ANSYS 14.5. The results showed that the path length travelled by the air within the media was equal to the media thickness which was the same for both plane and pleated media configurations. However, the velocity was 43 % lower in the pleated media than in the plane media. Consequently the contact time would be longer in the pleated than in the plane media. By calculating the contact time as the path length (thickness of the media) divided by the local velocity within the media, it was found that the contact time was increased by 76 % for the pleated media. It was also observed that the irradiance distribution was more heterogeneous on the pleated media than on the plane media. A comparison of the percentage improvement in contact time obtained from the simulation when the pleated geometry is used to the experimental improvement of

the surface corrected single-pass removal efficiency (α/m^2) showed that the experimental value was lower than the expected value given by the simulation. Based on the study of the irradiance and flow profiles in the media, two hypotheses could be proposed to explain this; firstly, the effective surface of the pleated media was reduced due to the presence of a significant dark zone (18 %) around the pleat joints and secondly higher level of heterogeneity of the velocity and irradiance distribution could hinder the effect of the contact time and lead to a reduction in the expected global efficiency of the pleated configuration.

In conclusion, PCO could be used as a treatment technique to improve air quality in the OR as the results show that it can degrade OR pollutants like isoflurane and acrylonitrile. This work could contribute to extending the existing knowledge of the influence of parameters on PCO unto two compounds that have never been studied (isoflurane) or rarely studied (acrylonitrile) in the literature. It has been evidenced that adjusting the operating parameters is useful to improve the PCO performance. However as also shown, a single-pass is not enough to remove a substantial amount of these pollutants from the incoming air. It would be recommended that for a treatment device, several photocatalytic banks are used in order to maximize the removal of the target pollutants as well as their intermediates. Media geometry like the pleated one will also further improve the removal efficiency of pollutants as they can provide more catalyst amount and higher contact time. Additionally, CFD is a useful tool to highlight the behavior of flow and irradiance in a photocatalytic media.

Based on the results of this PhD several perspectives can be envisaged. These perspectives can be classified under several categories.

Firstly to continue to improve the efficiency and safety of the use of a photocatalytic system in an OR:

a. It would be necessary to investigate the PCO performance for a system that has a series of photocatalytic media and lamps. In so doing, it will help to provide answers firstly on how much the removal efficiencies of pollutants are improved and secondly what influence it would have on the intermediates found at the outlet of the treatment device.

b. Studies should be done on the effect of the combination of several air treatment techniques like filtration and adsorption with PCO on the removal efficiency of

pollutants. As indoor air contains particles which have been shown to decrease the efficiency of PCO the use of pre-treatment techniques like filtration could improve efficiency. Introducing adsorption downstream of the photocatalytic step could be useful in capturing the intermediates that are produced during the photocatalytic degradation.

c. The safety of PCO process is important in completely characterizing the efficiency of PCO and the safety can be evaluated by identifying and quantifying the intermediates that are formed during degradation. Further work should be done on the identification and quantification of intermediate compounds using more sensitive sampling and analytical processes.

Secondly, by developing a more rigorous model that couples fluid dynamics with radiation field modeling and kinetic reaction modeling, CFD could be used to design, optimize and predict the degradation efficiency of the photocatalytic system. The use of CFD modeling would also provide some economic benefits as the reactor can be easily modified to optimize the hydrodynamics and irradiance of the system without requiring different reactor setups and experiments to determine the most efficient geometry.

Thirdly, once the system has been designed to include other air treatment techniques like filtration and adsorption, it would be necessary to evaluate its performance in a real case in order to validate the design and efficiency.

UNIVERSITE BRETAGNE SCIENCES LOIRE POUR L'INGENIEUR

IMT Atlantique
Bretagne-Pays de la Loire
École Mines-Télécom

Title : Evaluation of the performance of photocatalytic systems for the treatment of indoor air in medical environments

Keywords : Indoor air treatment, Photocatalytic oxidation, Operating room, Isoflurane, Acrylonitrile, Computational fluid dynamics

Abstract : Photocatalytic oxidation (PCO) is an advanced air cleaning technology that is used as a means to improve air quality in indoor environments and could potentially be used in the operating rooms (OR). In hospitals, operating rooms (ORs) are very demanding in terms of the indoor air quality (IAQ) and require systems that minimize the concentrations of pollutants. In this work, the fate of two OR pollutants acrylonitrile (chemical found in surgical smoke) and isoflurane (anesthetic gas) when they go through a PCO device was investigated. Firstly, a parametric evaluation on the degradation of isoflurane and acrylonitrile by studying the influence of air velocity, light intensity, the change in media geometry, initial pollutant concentration, presence of chemical co-pollutants, presence of particles (bioaerosols) and relative humidity on their degradation efficiencies is performed. Secondly the safety of the use of PCO for the degradation of isoflurane and acrylonitrile through the identification of possible intermediates formed during their degradation is evaluated. The experiments were conducted in a closed loop reactor which has been designed to study low concentration air pollutants and has also been recently modeled. Finally, to better understand how the change in media geometry influenced the degradation efficiency, simulations with ANSYS 14.5 were performed and discussed.

Titre : Evaluation de la performance des systèmes photocatalytiques pour le traitement de l'air intérieur en milieu médical

Mots clés : Traitement de l'air intérieur, Oxydation photocatalytique, Salle d'opération, Isoflurane, Acrylonitrile, Simulations de dynamique des fluides computationnelle

Résumé : La photocatalyse est une technologie d'oxydation avancée qui peut être utilisée pour améliorer la qualité de l'air dans les environnements intérieurs et pourrait être mise en œuvre dans les milieux médicaux. Dans les hôpitaux, les salles d'opération sont très exigeantes en matière de qualité de l'air intérieur et nécessitent des systèmes qui minimisent les concentrations des polluants générés par les différentes activités. Dans ce travail, le devenir de deux polluants spécifiques des blocs opératoires, l'acrylonitrile (produit chimique trouvé dans la fumée chirurgicale) et l'isoflurane (gaz anesthésique) lorsqu'ils passent dans un dispositif de traitement d'air photocatalytique est étudié. Tout d'abord, une évaluation paramétrique de la dégradation de l'isoflurane et de l'acrylonitrile en étudiant l'influence de la vitesse de l'air, de l'intensité lumineuse, de la géométrie du média photocatalytique, de la concentration initiale en polluants, de la présence de co-polluants chimiques, de la présence de particules et l'humidité relative sur leur efficacité de dégradation est réalisée. En second lieu, l'innocuité de l'utilisation de ce procédé pour la dégradation de l'isoflurane et de l'acrylonitrile par l'identification des éventuels intermédiaires formés au cours de leur dégradation est étudiée. Les expériences sont menées dans un réacteur dynamique en boucle fermée conçu pour étudier les polluants à faibles concentrations.Enfin, pour mieux comprendre comment le changement de géométrie du média photocatalytique influence l'efficacité de la dégradation, des simulations avec ANSYS 14.5 sont effectuées et discutées au regard des résultats expérimentaux.